Studying physical and biological aspects of coastal suspended particulate matter (SPM) dynamics using a novel distribution-based flocculation (DBFloc) model

Von der Fakultät für Mathematik und Naturwissenschaften
der Carl von Ossietzky Universität Oldenburg
zur Erlangung des Grades und Titels eines Doktors der Naturwissenschaften
– Dr. rer. nat. –
angenommene Dissertation
von

Jöran März

geboren am 18. Juli 1978 in Bad Soden-Salmünster

Erste Gutachterin:	Prof. Dr. Ulrike Feudel
Zweiter Gutachter:	Prof. Dr. Kai W. Wirtz

Tag der Disputation: 20.12.2010

CARL VON OSSIETZKY universität OLDENBURG
INSTITUT FÜR CHEMIE UND BIOLOGIE DES MEERES (ICBM)

Die vorliegende Doktorarbeit wurde in der Zeit von Oktober 2006 bis November 2010 am Institut für Chemie und Biologie des Meeres der Carl von Ossietzky Universität Oldenburg in der Arbeitsgruppe Theoretische Physik / Komplexe Systeme angefertigt.

Diese Arbeit wurde von der Deutschen Forschungsgemeinschaft (DFG) im Rahmen der Forschergruppe FOR 432 BioGeoChemie des Watts sowie durch den Deutschen Akademischen Auslandsdienst (DAAD) gefördert.

meiner Familie

Twenty years from now you will be more disappointed by the things that you didn't do than by the ones you did do. So throw off the bowlines. Sail away from the safe harbor. Catch the trade winds in your sails. Explore. Dream. Discover.

Mark Twain

Summary

Modeling of suspended particulate matter (SPM) dynamics is essential to provide knowledge of sediment budgets and understanding of biogeochemical cycles in coastal waters. Among SPM, cohesive sediments are mainly transported in aggregates / flocs that are accompanied with a variety of particulate components of organic origin and trace metals. Environmental changes of biological and physical nature affect aggregate size, structure, shape, composition and determine thus the floc density and transport behavior on different timescales. For example, the tidally varying hydrodynamic regime is an important driver for aggregation and fragmentation (flocculation) processes, while a seasonally varying primary productivity can change the composition and thus related floc characteristics.

Even recent spatial models for cohesive sediment transport rarely include a process-based description of flocculation processes owing to high computational costs of flocculation models. The latter is mainly due to the usage of several size classes to represent the floc size distribution. This also prevents needed attempts to depict the intricate coupling between biological and flocculation processes. In order to bridge this gap, a distribution-based model for flocculation processes (DBFloc) is proposed here that is saving computational resources. It introduces only one more additional variable (the mean size of aggregates) to bulk concentration-based models to account for flocculation processes.

Within the scope of this thesis, the DBFloc model is successfully compared to a typically used size class-based (SCB) model, and both models to experimentally derived laboratory data. The mean size dynamics of natural flocs under changing hydrodynamical conditions observed in an agitated suspension has been reliably reproduced by both models. Even the modeled distributions of both, the DBFloc and the SCB model, are very similar.

The DBFloc model has been further applied to the backbarrier basin of Spiekeroog Island. Integrating the processes of resuspension, deposition and tidal exchange, it has been used to investigate seasonal shifts of biological influences on SPM concentration and size dynamics. The

resulting parameter sets reflect *i)* a stronger shear resistence against erosion, and *ii)* a weaker aggregate structure in summer compared to winter. Both results likely can be related to seasonally changing primary productivity, as microphytobenthic release of extracellular polymeric substances (EPS) tend to stabilize the sediment. Further, the incorporation of such algae excretions into aggregates potentially change the floc structure towards a more loose nature, reflected by a smaller fractal dimension of flocs in the summer parameter set.

Within this thesis, several applications of the DBFloc model are elaborated. Among them, its coupling to a 1D vertical hydrodynamical model is derived. The DBFloc model in a 1D framework is investigated with respect to results of a SCB model. The typically observed tidally and lunarly changing SPM concentration and size dynamics realized by the DBFloc model is promising for its further applications. However, small differences appear between the SCB and the DBFloc model that need further investigations, also in comparison with observations.

Based on the 1D coupled DBFloc model, a potential role of aggregates for dissolved organic matter (DOM) concentration changes on a tidal time scale is indicated by calculated potential release rates of DOM from particles into the water column. Moreover, the mean advantage or disadvantage for aggregate-associated cells has been examined under the assumption that only a potential increase of DOM flux towards the cell due to intra-floc flow is relevant. Estimated conservatively, it can be shown that an increase of potential uptake capability can take place for an aggregate-associated cell relative to a cell in the ambient water that experiences shear. This, however, strongly depends on the hydrodynamical regime that drives the SPM dynamics.

To conclude, the distribution-based flocculation model proposed in this thesis is an appropriate potential candidate to bridge the gap between cohesive sediment transport and ecosystem models by being computationally inexpensive, while being able to reproduce typical features of SPM concentration and size dynamics under changing hydrodynamical conditions. It is further applicable for biogeochemically relevant processes due to clear interfaces for potential model extensions.

Zusammenfassung

Die Modellierung der Dynamik von Schwebstoffen (SPM) ist essenziell, um ein verbessertes Verständnis von Sedimentbudgets und von biogeochemischen Flüssen in Küstengewässern zu erlangen. Ein wesentlicher Anteil von Schwebstoffen sind cohäsive Sedimente, die in Form von Aggregaten transportiert werden. Diese enthalten darüber hinaus eine Vielzahl an partikulären organischen Komponenten sowie Spurenmetallen. Umwelteinflüsse biologischer und physikalischer Art beeinflussen die Aggregatgröße, -struktur, -form und -zusammensetzung und bestimmen dadurch die Aggregatdichte und entsprechend das Transportverhalten auf verschiedensten Zeitskalen. Beispielsweise ist ein tidal veränderliches hydrodynamisches Regime eine wesentliche Treibkraft für Aggregations- und Fragmentationsprozesse (Flockulationsprozesse), während sich eine saisonale Entwicklung der Primärproduktion auf die Zusammensetzung und damit auf Aggregatcharakteristika auswirken kann.

Prozessbasierte Flockulationsmodelle sind aufgrund der Nutzung einer Vielzahl an Größenklassen äußerst rechenzeitaufwendig, weswegen entsprechende Module selbst in aktuell angewandten Sedimenttransportmodellen nur selten implementiert sind. Notwendige Modellstudien zur komplexen Interaktion zwischen Flockulations- und biologischen Prozessen werden dadurch ebenfalls erschwert. Um solche Untersuchungen in Zukunft zu erleichtern, wird in dieser Arbeit ein verteilungsbasiertes Flockulationsmodell (DBFloc) vorgestellt. Nur eine weitere Variable wird darin über die SPM-Konzentration hinaus eingeführt: der mittlere Radius der Aggergate. Entsprechend recheneffektiv ist das Modell.

Im Rahmen dieser Arbeit wurde das DBFloc Modell erfolgreich mit einem typischerweise genutzten größenklassenbasierten (SCB) Modell verglichen. Beide Modelle zeigten das gleiche Verhalten der Aggregatverteilung unter veränderlichen hydrodynamischen Bedingungen sowie eine sehr gute Übereinstimmung mit der mittleren Aggregatgrößendynamik gegenüber experimentell erhaltenen Labordaten.

Mit Einführung weiterer Prozesse wie Resuspension, Deposition und tidalem Austausch von SPM wurde das DBFloc Modell auf das Spiekerooger Rückseitenwatt angewandt. Saisonale Veränderungen biologischer

Einflüsse auf die Konzentrations- und Größendynamik des SPM wurden untersucht. Die resultierenden Parameterwerte zeigen eine höhere Sedimentstabilität gegen Erosion und eine losere Struktur der Aggregate im Sommer verglichen mit der Wintersituation. Beide Ergebnisse können mit einer saisonal veränderlichen Primärproduktion in Verbindung gebracht werden. Zahlreiche Studien zeigen eine Stabilisierung des Sediments durch extrazelluläre polymere Substanzen (EPS), die unter anderem von Phytobenthos ausgeschieden werden. Es ist ebenso wahrscheinlich, dass EPS zur lockeren Struktur von Aggregaten beitragen können, was sich im Modell in Form einer geringeren fraktalen Dimension der Aggregate im Sommer als im Winter widerspiegelt.

Mehrere potenzielle Anwendungen des DBFloc Modells wurden in der Arbeit vorangetrieben. Eine Kopplung des DBFloc Modells an ein 1D vertikales hydrodynamisches Modell wurde erzielt und dessen Ergebnisse mit denen eines SCB Modell verglichen. Die qualitativ gute Reproduktion typischer beobachtbarer tidaler und lunarer Muster der SPM-Konzentrations- und Größendynamik sind vielversprechend für weitere Anwendungen des Modells.

Basierend auf dem gekoppelten DBFloc Modell konnte anhand potenzieller Freisetzungsraten von gelösten organischen Substanzen (DOM) gezeigt werden, dass Aggregate für die tidale Variabilität von DOM eine wichtige Rolle spielen können. Darüber hinaus wurde der Vor- oder Nachteil aggregatassoziierter Bakterien gegenüber frei im Umgebungswasser suspendierten Zellen untersucht. Es wurde gezeigt, dass aggregatassoziierte Bakterien eine leichte Erhöhung der potenziellen DOM-Aufnahmerate aufgrund von Advektion innerhalb der Aggregate erfahren können. Dies ist jedoch stark abhängig vom hydrodynamischen Regime und der entsprechenden SPM-Dynamik.

Zusammenfassend wird deutlich, dass das DBFloc Modell potenziell geeignet ist, als Brückenschlag zwischen Sedimentdynamik- und Ökosystemmodellen Anwendung zu finden. Es leistet eine effektive Beschreibung typischer Charakteristika der SPM Konzentrations- und Größendynamik unter hydrodynamisch variablen Bedingungen. Durch eine klare Modellstruktur wird eine potenzielle Erweiterung um biogeochemische Prozesse deutlich vereinfacht.

List of Publications

Manuscripts

Joeran Maerz, Kai Wirtz (2009)[1] *Resolving physically and biologically driven suspended particulate matter dynamics in a tidal basin with a distribution-based model.* Estuarine, Coastal and Shelf Science 84 (1), 128 - 138

Joeran Maerz, Romaric Verney, Kai Wirtz and Ulrike Feudel (2010)[2] *Modeling flocculation processes: intercomparison of a size class-based model and a distribution-based model.* Special Issue INTERCOH 2007 in Continental Shelf Research doi:10.1016/j.csr.2010.05.011

Jens Zahnow, **Joeran Maerz** and Ulrike Feudel (submitted)[3] *Particle-based modelling of aggregation and fragmentation processes in chaotic advection: Fractal aggregates.* Submitted to Physica D

Presentations on international meetings

Joeran Maerz, Romaric Verney, Ulrike Feudel (2010) *Intercomparison of aggregation models for turbid coastal systems and a potential link to ecosystem modeling.* Trends in Complex Systems. Workshop on Living Organisms in Flows:

[1] Joeran Maerz: Model development, implementation and study, draft of the manuscript; Kai Wirtz: Model development, revision of the mansucript

[2] Joeran Maerz: Draft of the manuscript, work with the distribution-based model; Romaric Verney: Revision of the manuscript, work with the size class-based model; Kai Wirtz: Revision of the manuscript; Ulrike Feudel: Revision of the manuscript

[3] Jens Zahnow: Draft of the manuscript, model development, implementation and study; Joeran Maerz: Co-development of the model, revision of the manuscript; Ulrike Feudel: Revision of the manuscript

From Small-scale Turbulence to Geophysical Flows. Palma de Mallorca / Spain. **Poster**

Joeran Maerz, Kai Wirtz and Ulrike Feudel (2009) *Resolving size dynamics of suspended particulate matter (SPM) by using a distribution-based model.* Final symposium on BioGeoChemistry of Tidal Flats. Delmenhorst / Germany. **Oral presentation**

Joeran Maerz, Mirko Lunau and Ulrike Feudel (2009) *Studying the impact of bacteria on suspended particulate matter transport properties under different hydrodynamical conditions.* American Society of Limnology and Oceanography (ASLO) Aquatic Sciences Meeting. Nice / France. **Oral presentation**

Joeran Maerz, Ulrike Feudel and Mirko Lunau (2008) *Interplay of hydrodynamics and microbes determines the transport behaviour of marine aggregates: a case study.* Dynamics of Inertial Particles: From Oceanic to Atmospheric Particles (DIPOAP) 2008. Dresden / Germany. **Poster and short oral presentation**

Joeran Maerz, Ulrike Feudel and Mirko Lunau (2008) *Do microbes mediate flocculation processes of suspended particulate matter?* Summer Meeting of the American Society of Limnology and Oceanography (ASLO) 2008. St. Johns / Canada. **Poster**

Joeran Maerz, Martin Mierzejewski, Tobias Bockhorst, Ulrike Feudel and Mirko Lunau (2007) *Microbially mediated aggregation of suspended particulate matter.* 9$^{\text{th}}$ International Conference on Nearshore Estuarine Cohesive Sediment Transport Processes (INTERCOH) 2007. Brest / France. **Oral presentation**

Romaric Verney, **Joeran Maerz** and Ulrike Feudel (2007) *Modelling flocculation processes: intercomparison of a size class-based model and a distribution-based model.* 9$^{\text{th}}$ International Conference on Nearshore Estuarine Cohesive Sediment Transport Processes (INTERCOH) 2007. Brest / France. **Oral presentation by Romaric Verney**

Joeran Maerz, Ulrike Feudel and Kai Wirtz (2006) *Using a distribution-based modeling approach to understand aggregate dynamics in coastal waters.* International Workshop On Marine Aggregates (IWOMA) 2006. Bremen / Germany. **Poster and its short oral presentation**

Joeran Maerz, Ulrike Feudel and Kai Wirtz (2006) *How do physics and biology control the dynamics of suspended aggregates in coastal waters?* Summer Meeting of the American Society of Limnology and Oceanography (ASLO) 2006. Victoria / Canada. **Poster**

Joeran Maerz, Ulrike Feudel and Kai Wirtz (2006) *What controls the dynamics of suspended matter aggregates in coastal waters?* 9^{th} International Estuarine Biogeochemistry Symposium (IEBS) 2006. Warnemünde / Germany. **Poster**

Joeran Maerz, Ulrike Feudel and Kai Wirtz (2005) *Understanding aggregate dynamics in turbulent shallow waters using a new modelling approach.* Summer Meeting of the American Society of Limnology and Oceanography (ASLO) 2005. Santiago de Compostela / Spain. **Poster**

Contents

Summary xi

Zusammenfassung xiii

List of Publications xv

Abbreviations xxxv

Mathematical Symbols xxxvii

Roman symbols and description xxxvii

Greek symbols and description xli

1 Introduction 1

1.1 Marine snow and its functions in the oceans 2

1.1.1 Precursor formation and their role in aggregation processes 3

1.1.2 Mechanisms leading to aggregation and fragmentation . . 5

1.1.3 Significance of biological processes for aggregate transformation 6

Bacterial interactions with marine snow 6

Zooplankton, microbes and their role in the vertical flux 8

1.1.4 Trace chemical transport and mineralic particle scavenging by marine snow 9

1.2 Aggregates in coastal waters 12

1.2.1 Why studying suspended particulate matter (SPM) dynamics? 13

1.2.2 How to measure SPM concentration and aggregate distributions? 14

1.2.3 SPM dynamics in coastal and estuarine waters with an emphasis on the Wadden Sea – processes, mechanisms and effects . . . 16
1.2.4 Potential feedback mechanisms of biological processes on SPM transport in coastal waters . . . 20
1.2.5 Modeling SPM dynamics . . . 23
1.3 Thesis outline . . . 26

2 Model description **31**
2.1 Sediment transport models . . . 31
2.2 The fractal concept for aggregates . . . 33
2.3 Fragmentation and aggregation . . . 34
2.4 Distribution-based flocculation model . . . 36
2.4.1 A general introduction to the moment closure approach . 37
2.4.2 Formulation of the aggregation models . . . 40
Formulation for aggregation due to shear . . . 42
Formulation for aggregation due to differential settling . 47
2.4.3 Fragmentation . . . 52
2.5 Coupling the flocculation model with other processes . . . 53
2.5.1 Settling and deposition . . . 54
2.5.2 Resuspension / erosion . . . 58

3 Publications **61**
3.1 Modeling flocculation processes: intercomparison of a size class-based model and a distribution-based model . . . 63
3.1.1 Introduction . . . 64
3.1.2 Description of the two models . . . 65
Size class-based model . . . 66
Distribution-based model . . . 69
3.1.3 Results . . . 71
Validation data . . . 72
Model and data comparison . . . 73
Sensitivity analysis . . . 78
3.1.4 Discussion . . . 82

3.1.5 Conclusion . . . 86
3.2 Resolving physically and biologically driven suspended particulate matter dynamics in a tidal basin with a distribution-based model . . . 89
3.2.1 Introduction . . . 90
3.2.2 Methods . . . 93
Model derivation . . . 93
Physical forcing by tidal currents . . . 98
Model validation . . . 99
Winter and summer parametrization . . . 100
Model analysis . . . 101
3.2.3 Results . . . 101
Aggregate number frequency distribution . . . 103
Winter situation . . . 104
Summer compared to winter situation . . . 105
Sensitivity analysis . . . 108
3.2.4 Discussion . . . 110
Model properties . . . 112
3.2.5 Conclusion . . . 114
3.2.6 Appendix: Aggregation . . . 115

4 Potential applications of the novel flocculation model 119
4.1 The distribution-based model in a 1D vertical water column . . . 120
4.1.1 Vertical transport processes in the 1DV SiAM model developed at IFREMER . . . 120
4.1.2 Representation of the SPM transport in the SiAM model 121
4.1.3 The spatially explicit distribution-based SPM model . . . 121
4.1.4 Sinking . . . 123
4.1.5 Turbulent diffusion . . . 124
4.1.6 Erosion / Resuspension . . . 125
4.1.7 Deposition . . . 126
4.1.8 Comparison of the SCB and the DB model in a water column . . . 127
4.1.9 Sensitivity of the DB model in a water column . . . 130

4.2 Fluxes to and from particles – a link to microbial processes . . . 139
4.2.1 Mass transfer from or towards a spherical particle 140
Characterization of the hydrodynamic regime 141
Relevant Sherwood numbers for specific hydrodynamic regimes 144
4.2.2 Variabilities in the hydrodynamic regime and resulting SPM dynamics as an explanation for inter-tidal variability of DOM 145
4.2.3 Mean effect of turbulence and sinking of aggregates on bacterial substrate uptake capability 152
Intra-floc flow rates 152
Uptake of substrate by a single cell in a sheared fluid and under laminar flow 156
Relative uptake capability of particle-attached bacteria . 160
Calculating the relative uptake capability based on the DB model and SiAM 162
4.2.4 Mean potential uptake capability under changing hydrodynamic conditions in a 1D water column 164
Mean potential uptake capability due to sinking of particles 164
Mean potential uptake capability due to shear around particles 165
Tidal mean potential uptake capability 165
4.3 Discussion of the potential applications 169
4.3.1 SiAM coupling and the comparison to the SCB model . . 169
4.3.2 DOM fluxes and mean relative potential uptake capabilities 171

5 Discussion & Conclusions **177**
5.1 Physical and biological implications 178
5.2 Model properties 187
5.3 Conclusion 196

6 Outlook & Future research perspectives **199**

A Supplementary material **203**
A.1 Change of the average size due to erosion and deposition in 0D . 205
A.1.1 Deposition 205
A.1.2 Erosion / Resuspension 206
A.2 Rectilinear aggregation kernels for shear and differential settling 207
A.3 Aggregation due to shear: the K_γ function 209
A.4 Aggregation due to differential settling: the K_v function 217
A.5 Numerical implementation of the DB model in the SiAM model 221
A.5.1 Turbulent diffusion 222
A.5.2 Sinking 223
A.5.3 Erosion / Resuspension 224
A.5.4 Deposition 224
A.5.5 Representation of vertical transport for the change of the average radius 225

Bibliography **227**

Curriculum Vitae **255**

Danksagung **258**

Le dernière mot **259**

List of Figures

2.1 Number distribution, aggregate weight and resultant concentration distribution 43

2.2 The relative concentration change (according to Eq. (2.37)) for typical values that can be found in coastal areas (apart from $\alpha = 1$ that has been chosen for simplicity). 45

2.3 Underlying assumptions for the rectilinear and the curvilinear kernel for differential sinking (re-drawn after Jackson and Lochmann, 1993). The curvilinear kernel takes the displacement of the smaller particle due to the flow field around the larger particle into account while the rectilinear kernel does not. Stokes flow is present when the particles' Reynolds number is $Re < 1$ (see also Sec. 4.2). 48

2.4 The mean density of flocs calculated from Eq. (2.61) with $D_\mathrm{p} = 4\,\mu\mathrm{m}$, $\rho_\mathrm{p} = 2.6\,\mathrm{g\,cm^{-3}}$ and $\rho = 1.0\,\mathrm{g\,cm^{-3}}$ for different, but in their value observable $\langle r \rangle$ and d_f. 51

2.5 The appearing term for the mean sinking velocity derived in Eq. (2.67). 55

2.6 Comparison between the directly (Eq. (2.70); blue line) and the distribution-based derived formulation for deposition (Eq. (2.71); red line) for different fractal dimensions ($h = 8\,\mathrm{m}$, $\mu = 0.01\,\mathrm{g\,cm^{-1}\,s^{-1}}$, $D_\mathrm{p} = 4\,\mu\mathrm{m}$, $\rho_\mathrm{p} = 2.6\,\mathrm{g\,cm^{-3}}$). 57

3.1 Aggregation of flocs of mass m_i and m_j into mass $m_i + m_j$ and subsequent distribution into the nearest size classes by using a mass-weighted interpolation. V_i and ρ_i are the volume and the effective density of a floc in size class i, respectively. 68

3.2 Mean floc size variation during a simulated tidal cycle: comparison between laboratory measurements and models results. Note that the mean diameter of the observed flocs might be overestimated due to limitations of the camera system. SCB: size class-based and DB: distribution-based model. 75

3.3 Normalized concentration in % of the experimentally derived distribution (EXP), size class-based model (SCB) and distribution-based model (DB). Note that both models fail for the time 6 h $< t \leq$7 h as settling is not taken into account in the model comparison. 76

3.4 Normalized concentration in % of the experimentally derived distribution (EXP), size class-based (SCB) and distribution-based (DB) model for different times (t). 77

3.5 Mean settling velocity for experimentally observed particles, size class-based model (SCB) and distribution-based model (DB) calculated by Eqs. (3.21) (data, SCB model) and (3.22) (DB model). Note that both models fail for the time 6 h $< t \leq$7 h as the models do not account for changes in the size distribution by settling. 78

3.6 Left: Time evolution of the mean floc diameter as simulated by the distribution-based (DB) and the size-class based (SCB) model. Right: Floc size distribution computed by both models at simulation start and after 20 min (indicated by open circles in the left panel). Notice that only the term of aggregation is taken into account with the same initial distribution and the same parameter set used in the comparison with data (see Tab. 3.1). . 80

3.7 Sensitivity of both models to initial conditions. SCB: size class-based model; DB: distribution-based model. 81

3.8 Sensitivity of both models to changed fractal dimension compared to the reference runs. SCB: size class-based model; DB: distribution-based model. 82

3.9 Sensitivity of both models to variations in collision efficiency compared to the reference runs. SCB: size class-based model; DB: distribution-based model. 83

3.10 Growth rates for the mean radius of the DB model. A) Different α and f_b pairs for the same steady state ($\langle r \rangle^* = 100\,\mu m$). The correspondent α:f_b values are: $0.04 : 2801\,s^{1/2} \cdot m^{-2}$, $0.11 : 7701\,s^{0.5} \cdot m^{-2}$, $0.18 : 12602\,s^{0.5} \cdot m^{-2}$, $0.25 : 17503\,s^{0.5} \cdot m^{-2}$, and $0.32 : 22404\,s^{0.5} \cdot m^{-2}$. B) The same α and f_b pair as for the reference run, but using different shear values. 88

3.11 Geographic location (53° 45′ N, 7° 45′ W) within the German Bight, intertidal physiography, and anchor positions of two sampling campaigns on 17./18.2.2003 and 22./23.7.2003 conducted by Lunau et al. (2006) 91

3.12 Observed and simulated average radius $\langle r \rangle$ changing over time in a stirred tank system. Data from experiments for a range of different turbulent shear rates originate from Flesch et al. (1999). 103

3.13 Aggregate number frequency distribution (per cubic volume and size class bin width) in different tidal situations in February 2003 (winter) and July 2003 (summer) (Lunau et al., 2006) and datafits to better illustrate the exponential decrease of aggregate numbers. 104

3.14 Observed average ECR in February 2003 (winter) and July (summer) during two tides in the back-barrier basin of Spiekeroog island (diamonds) compared to the simulation (continuous line) 106

3.15 Observed (diamonds) and simulated (line) suspended matter concentrations in the back-barrier basin of Spiekeroog island during two tides in February 2003 (winter; upper panel) and July 2003 (summer; lower panel) 107

3.16 Mean settling velocity of the modified runs compared to the reference run a) February and b) July. 109

4.1 Reference run: Shear rate, sediment budget in the water column, SPM concentration of the SCB an the DB model, their ratio, the mean diameter of the SCB and DB model and their ratio. . . . 133

4.2 Reference run: Shear rate, sediment budget in the water column, SPM concentration of the SCB an the DB model, their ratio, the mean diameter of the SCB and DB model and their ratio. . . . 134

4.3 Ratios for SPM concentration and mean floc size of the DB model between the reference run and the sensitivity run with $\alpha - 10\,\%$. . . . 135

4.4 Ratios for SPM concentration and mean floc size of the DB model between the reference run and the sensitivity run with $\alpha + 10\,\%$. . . . 135

4.5 Ratios for SPM concentration and mean floc size of the DB model between the reference run and the sensitivity run with $f_\mathrm{b} - 10\,\%$. . . . 136

4.6 Ratios for SPM concentration and mean floc size of the DB model between the reference run and the sensitivity run with $f_\mathrm{b} + 10\,\%$. . . . 136

4.7 Ratios for SPM concentration and mean floc size of the DB model between the reference run and the sensitivity run with $d_f - 10\,\%$. . . . 137

4.8 Ratios for SPM concentration and mean floc size of the DB model between the reference run and the sensitivity run with $d_f + 10\,\%$. . . . 137

4.9 Ratios for SPM concentration and mean floc size of the DB model between the reference run and the sensitivity run with $r_\mathrm{b} - 10\,\%$. . . . 138

4.10 Ratios for SPM concentration and mean floc size of the DB model between the reference run and the sensitivity run with $r_\mathrm{b} + 10\,\%$. . . . 138

4.11 The Péclet number for turbulent shear is estimated using Eq. (4.26) and the Péclet number for sinking is estimated using the definition $Pé = (U\,r)/D$ (see e. g. Karp-Boss et al., 1996), where the characteristic velocity U is here the sinking velocity of a particle calculated by using Eq. (2.52). 141
4.12 Reynolds number (Eq. (4.27)) based on the settling velocity for fractal particles (refer to Eq. (2.52)) with the given parameter values. 142
4.13 Sherwood numbers for shear listed in Tab. 4.2. The figure inlet shows the detail for very small particles. 145
4.14 Sherwood numbers as listed in Tab. 4.2 for sinking particles. The figure inlet shows the detail for very small particles. Note that for some Sherwood numbers, limitations were not given in the respective, citet literature (see Tab. 4.2). 146
4.15 Estimated fluxes for a molecular diffusion coefficient of the substance of $D = 1 \cdot 10^{-5}\,\mathrm{cm^2\,s^{-1}}$ for sinking particles. 148
4.16 Estimated fluxes for a molecular diffusion coefficient of the substance of $D = 1 \cdot 10^{-5}\,\mathrm{cm^2\,s^{-1}}$ for particles experiencing shear. . 148
4.17 Estimated fluxes for a molecular diffusion coefficient of the substance of $D = 1 \cdot 10^{-5}\,\mathrm{cm^2\,s^{-1}}$ for particles experiencing shear and sinking. 149
4.18 Estimated fluxes for a molecular diffusion coefficient of the substance of $D = 1 \cdot 10^{-7}\,\mathrm{cm^2\,s^{-1}}$ for sinking particles. 149
4.19 Estimated fluxes for a molecular diffusion coefficient of the substance of $D = 1 \cdot 10^{-7}\,\mathrm{cm^2\,s^{-1}}$ for particles experiencing shear. . 150
4.20 Estimated fluxes for a molecular diffusion coefficient of the substance of $D = 1 \cdot 10^{-7}\,\mathrm{cm^2\,s^{-1}}$ for particles experiencing shear and sinking. 150
4.21 Floc permeability as calculated from Eq. (4.44) and (4.42) using $r_\mathrm{p} = 2\,\mu\mathrm{m}$. 155
4.22 Intra-floc velocity due to sinking of an aggregate (Eq. (4.37)) with $D_\mathrm{p} = 4\,\mu\mathrm{m}$, $\rho_\mathrm{p} = 2.6\,\mathrm{g\,cm^{-3}}$, $\rho = 1\,\mathrm{g\,cm^{-3}}$, $\mu = 0.01\,\mathrm{g\,cm^{-1}\,s^{-1}}$ and $g = 981\,\mathrm{cm\,s^{-2}}$ used to calculate the sinking velocity according to Eq. (2.52). 156

4.23 E_0 as tabulated in Adler (1981) and the fitting function used for the calculations. Note that tabulated E_0 values from Adler (1981) were only taken into account for $\xi_1 \geq 2$ for the fitting function as this is the relevant range of occuring values (see also Fig. 4.24). 157

4.24 The dimensionless value $\xi_1 = r/\sqrt{\lambda}$ for various fractal dimensions and radii for $D_\mathrm{p} = 4\,\mu\mathrm{m}$. Note the critical value $\xi_{1,c}$ for intra-floc flow due to laminar shear. Note moreover that ξ_1 is larger than two in the plotted region even for $d_f = 1.6$ so that the simplified relation for E_0, found in Fig. 4.23, holds. $d_f = 1.6$ is a small value compared to fractal dimension measured in coastal waters (in coastal waters: $d_f \approx 2$, e. g. Dyer and Manning, 1999; Kranenburg, 1994). 158

4.25 Intra-floc velocity due to shear (here $\gamma = 1$) calculated using Eq. (4.46) with $D_\mathrm{p} = 4\,\mu\mathrm{m}$. 159

4.26 $\langle\chi_\mathrm{v}\rangle$ for a molecular diffusion coefficient $D = 1 \cdot 10^{-5}\,\mathrm{cm^2\,s^{-1}}$. Calculation based on the reference run of the DB model in Sec. 4.1.8. 166

4.27 $\langle\chi_\mathrm{v}\rangle$ for a molecular diffusion coefficient $D = 1 \cdot 10^{-7}\,\mathrm{cm^2\,s^{-1}}$. Calculation based on the reference run of the DB model in Sec. 4.1.8. 167

4.28 $\langle\chi_\gamma\rangle$ for a molecular diffusion coefficient $D = 1 \cdot 10^{-5}\,\mathrm{cm^2\,s^{-1}}$. Calculation based on the reference run of the DB model in Sec. 4.1.8. 167

4.29 $\langle\chi_\gamma\rangle$ for sheared particles and a molecular diffusion coefficient $D = 1 \cdot 10^{-7}\,\mathrm{cm^2\,s^{-1}}$. Calculation based on the reference run of the DB model in Sec. 4.1.8. 168

4.30 Tidal mean $\langle\chi_\mathrm{v}\rangle$ and $\langle\chi_\gamma\rangle$ for molecular diffusion coefficients of $D = 1 \cdot 10^{-5}\,\mathrm{cm^2\,s^{-1}}$ and $D = 1 \cdot 10^{-7}\,\mathrm{cm^2\,s^{-1}}$. Calculation based on the reference run of the DB model in Sec. 4.1.8. 168

5.1 Schematical visualization of the internal mass redistribution effect in the distribution-based (DB) compared to the size class-based (SCB) model. Loss and gain means losses and gains due to internal mass redistribution compared to the SCB model. In the latter, such redistribution cannot occur due to a more variable shape of the distribution. 191

A.1 The rectilinear kernel for aggregation due to differential settling $\rho_p = 2.6\,g\,cm^{-3}$, $\rho = 1.0\,g\,cm^{-3}$, $\mu = 0.01\,g\,cm^{-1}\,s^{-1}$ $D_p = 4\,\mu m$, $d_f = 2$. 207
A.2 The rectilinear kernel for aggregation due to shear $\gamma = 1$. 208
A.3 A comparison of the K_γ functions for *i)* the rectilinear and the curvilinear kernel, and *ii)* for the two different possibilities to start the model derivation violating the mass conservation in the first step of integration. 212
A.4 A comparison of the K_γ funtions of *i)* the rectilinear kernel under different orders of closures, and *ii)* the different versions. . 213
A.5 A comparison of the K_γ funtions of *i)* the curvilinear kernel under different orders of closures, and *ii)* the different versions. 214
A.6 The different K_γ functions for rectilinear aggregation due to shear and their possible approximation. 215
A.7 The different K_γ functions for curvilinear aggregation due to shear and their possible approximation. 216
A.8 A comparison of the K_v funtions of the curvilinear kernel for aggregation due to differential settling for the different versions. 218
A.9 A comparison of the analytically correct derived change (Eq. (A.20)) of the $\langle r \rangle$ due to differential settling and the general form (Eq. (A.21)), both based on v1, the curvilinear kernel and a 4th order closure, for $d_f = 2$. The (typical) parameter values are: $D_p = 4\,\mu m$, $\alpha = 0.05$, $g = 9.81\,m\,s^{-2}$, $\rho = 1\,g\,cm^{-3}$, $\rho_p = 2.6\,g\,cm^{-3}$, $C = 50\,mg\,L^{-1}$ and $\mu = 0.0102\,cm^2\,s^{-1}$ 219
A.10 The different K_γ functions for curvilinear aggregation due to differential sinking and their possible approximation. 220
A.11 Grid in the SiAM 1D vertical model. 221

List of Tables

3.1 Parameter (P) set for the reference runs. In case of the break-up factor f_b and the collision efficiency α values are given as DB/SCB values. 73
3.2 State variables, auxiliary and forcing variables 102
3.3 List of model parameters with values for the winter (Feb.) and the summer (July) situation 102

4.1 Parameter values for the comparison between the SCB and the DB model and its sensitivity study (with variations of the parameters by $\pm 10\,\%$) in a 1D vertical application to the SiAM model (no value means no variation). The parameter values of the SCB model are choosen according to Sec. 3.1. 128
4.2 Sherwood numbers Sh for shear (based on $Pé = r^2\,\gamma/D$) and sinking (based on $Pé = r\,v_s/D$, $Re = v_s\,r/\nu$ and $Sc = Pé/Re = \nu/D$) and references 151
4.3 Parameter values for the calculations of the relative potential uptake capability. 164

A.1 $K_\gamma(d_f)$ functions 211
A.2 $K_v(d_f)$ functions 217

Abbreviations

ADCP	Acoustic Doppler Current Profiler
ADV	Acoustic Doppler Velocimeter
C	Carbon
COM	Colloidal Organic Matter
CO_2	Carbon Dioxide
DB	Distribution-Based (model)
DCAA	Dissolved Combined Amino Acids
DFAA	Dissolved Free Amino Acids
DOC	Dissolved Organic Carbon
DOM	Dissolved Organic Matter
DW	Dry Weight
EPS	Extracellular Polymeric Substances
LISST	Laser *In Situ* Scattering and Transmissiometry
MST	Multispectral Transmissiometer
NIOZ	Netherlands Institute for Sea Research (Texel)
NPP	Net Primary Production
PCAA	Particulate Combinded Amino Acids
POC	Particulate Organic Carbon
POM	Particulate Organic Matter
RCI	Relative Contribution Index
SCB	Size Class-Based (model)
SiAM	Simulation d'Advection Multivariable
SPM	Suspended Particulate Matter
TEP	Transparent Exopolymer Particles
^{234}Th	Thorium isotope 234

TKE	Turbulent Kinetic Energy
^{238}U	Uranium isotope 238
UN	United Nations
wt-%	Weight percent (weight/weight)

Mathematical Symbols

Roman symbols and description*

a_e	empirical factor for the sediment concentration dependency of erosion
A_h	horizontal eddy diffusivity
A_v	vertical eddy diffusivity
B	bacteria per mass suspended particulate matter
b	power of the shear dependency of the break-up
b_e	empirical power of the sediment concentration dependency of erosion
$B_{\gamma,i}$	fragmentation kernel due to shear
$\dot{C}$	time derivative of the total concentration
C	total concentration (mass per volume)
$\dot{C}_i$	time derivative of the concentration in size class i
C_i	suspended particulate matter concentration in size class i
C_i'	normalized floc mass in class i
C_∞	a background concentration of a substance
$\dot{C}(m)$	change of mass concentration of particles with mass m
$C(m)$	mass concentration of particles with mass m
C_o	external suspended particulate matter concentration
C_p	a concentration of a substance on a particle
$C(r)$	mass-concentration of particles with radius r
C_sed	SPM concentration in the sediment in the SiAM model
D	floc diameter, in Sec. 4.2 the molecular diffusion coefficient
d_f	fractal dimension of an aggregate

$D_{\max}$	maximum diameter used in the size class-based model
D_{p}	primary particle diameter
E_0	function of ξ_1 as tabulated by Adler (1981)
E_{B}	cell surface fraction that contains transport enzymes for a substance
E_{w}	time-dependent water exchange rate
f	coriolis parameter
f_{b}	break-up factor
$F_{\mathrm{D},i,k}$	distribution function for fragmented flocs
F_{dep}	deposition flux of suspended particulate matter
$F_{\mathrm{dep},r}$	deposition flux of suspended particulate matter of radius r
F_i	a flux term (also F_x in Sec. 3.2)
F_{res}	resuspension/erosion flux of suspended particulate matter
F_{tidex}	suspended particulate matter flux due to tidal exchange
G	laminar shear
g	gravitational accelaration constant ($g = 9.81\,\mathrm{m\,s^{-2}}$)
h	water depth
I	collision frequency kernel
i	an index for a size class
I_γ	collision frequency due to shear
I_{D}	collision frequency due to diffusion
$I_{i,j}$	collision frequency for two particles in classes i and j
I_v	collision frequency due to differential settling
J	flux of a substance
j	an index for a size class
J_{c}	flux of a substance towards a cell
J_{T}	total flux of substance from or to a distribution of particles
$J_{\mathrm{T},\gamma}$	total flux of substance from or to a distribution of particles due to shear
$J_{\mathrm{T,v}}$	total flux of substance from or to a distribution of particles due to sinking of particles
k	an index for a size class
K_γ	higher order collecting function for shear-induced aggregation

K_v	higher order collecting function for aggregation due to differential settling
l	function of ξ_1 as derived by Adler (1981)
L_c	characteristic length scale
m	mass of an aggregate
M_0	erosion rate at twice the critical bottom shear stress
m_∞	infinite aggregate mass
m_i	mass of an aggregate of class i
N	number of used discrete size classes in the size class-based model
n	number of aggregates
N_0	value where the number distribution crosses the y-axis
N_c	number of cells on an aggregate
n_i	number of aggregates in class i
$n(m)$	number of particles with mass m
n_p	number of primary particles in an aggregate
$n(r)$	number of particles of radius r
N_t	total number of particle-associated bacterial cells
N_v	vertical eddy viscosity
p_atm	atmospheric pressure
$Pé$	Péclet number
q	power of the radius dependency of the break-up
$\langle r \rangle$	concentration-weighted average radius of the particle distribution
r	radius of an aggregate
$R_{\mathrm{agg}\gamma}$	change of the average radius by aggregation due to shear
R_aggv	change of the average radius by aggregation due to differential settling
r_b	average radius of the eroded/resuspended particles
R_break	change of the average radius by shear-induced break-up
r_c	radius of a cell
RCI	relative contribution index
R_dep	change of the average radius by deposition
Re	Reynolds number
r_f^*	drainage radius of an aggregate

r_∞	infinitive radius
R_i	a process that changes the average radius
r_i	radius of an aggregate in size class i
$r_{\min}$	detection limit of the camera system
$\langle r \rangle_N$	number-weighted average radius
r_o	average radius of external, incoming aggregates
r_p	radius of the primary particle ($r_\mathrm{p} = D_\mathrm{p}/2$)
R_res	change of the average radius by resuspension/erosion
R_tidex	change of the average radius by tidal exchange
S	function of ξ_1 as derived by Adler (1981)
Sc	Schmidt number ($Sc = Pé/Re = \nu/D$)
Sh	Sherwood number
Sh_γ	Sherwood number for a cell in suspension experiencing shear
Sh_p	Sherwood number for a particle (either for shear or for sinking)
$Sh_{\mathrm{p},\gamma}$	Sherwood number for an aggregate experiencing shear
Sh_u	Sherwood number for a cell experiencing flow through an aggregate
T	function of ξ_1 as derived by Adler (1981)
t	time
TKE	turbulent kinetic energy
U	a characteristic velocity
u	velocity component in direction x
u_f	intra-floc velocity (can be either generated by sinking or shear)
$u_{\mathrm{f},\gamma}$	intra-floc velocity due to shear
$u_{\mathrm{f,v}}$	intra-floc velocity due to sinking
u_*	friction velocity
$\mathbf{v}$	velocity vector: $\mathbf{v} = (u, v, w)$
v	velocity component in direction y
$V_{\mathrm{f,t}}$	total solid and interstitial volume of aggregates in a unit water volume
V_p	spherical volume of a primary particle
$V_{\mathrm{p,t}}$	total solid volume of aggregates in a unit water volume
$V(r)$	volume of an aggregate of radius r
$\langle v_\mathrm{s} \rangle$	mean settling velocity of particles

$v_{\mathrm{s},i}$	settling velocity of particles in size class i
$v_{\mathrm{s}}(r)$	settling velocity of an aggregate of radius r
V_{t}	total volume of aggregates in a distribution
w	velocity component in direction z
w_0	radius-weight relation factor $w_0 = 2^{d_f}\,\rho_{\mathrm{p}}\,\pi\,D_{\mathrm{p}}^{3-d_f}/6$
w_i	weight of an aggregate in class i
$w(r)$	weight of an aggregate of radius r
$\mathbf{x}$	vectorial description of a spatial position ($\mathbf{x} = (x, y, z)$)
x	longitudinal direction
y	latitudinal direction
y'	closing factor
y_γ	closing factor for shear-induced aggregation
z	vertical direction
z_0	bottom bed roughness

Greek symbols and description*

α	collision efficiency ("stickiness")
$\alpha_{i,j}$	collision efficiency for two particles in classes i and j
β	slope of the particle number distribution
γ	turbulent shear
$\Gamma(x)$	gamma function defined as $\Gamma(x+1) = \int_0^\infty \exp(-t)\,t^x\,\mathrm{d}t$
δr^2	variance of the concentration distribution
δr^4	fourth moment of the concentration distribution
$\Delta\rho$	excess floc density ($\Delta\rho = \rho_{\mathrm{f}} - \rho$)
ΔR_i	bin width of size class i
ϵ	turbulent kinetic energy dissipation rate
ζ	sea level elevation
η	Kolmogorov length scale ($\eta = (\nu^3/\epsilon)^{1/4}$)

η_b	Batchelor length scale ($\eta_\mathrm{b} = (\nu\, D^2/\epsilon)^{1/4}$)
ϵ_v	a constant for deposition calculation in SiAM
κ	von Kármán constant ($\kappa = 0.4$)
λ	permeability of a floc
μ	dynamic viscosity
$\hat{\mu}$	relative growth rate
$\langle\hat{\mu}\rangle$	average relative growth rate
$\hat{\mu}_{\mathrm{agg}\gamma}$	relative growth rate for aggregation due to shear
$\hat{\mu}_i$	relative growth rate in class i
μ_up	uptake rate by microbial cells on an aggregate
$\mu_\mathrm{up,d}$	uptake rate by microbial cell on an aggregate under purely diffusive conditions
ν	kinematic viscosity
ξ_1	dimensionless value given as $\xi_1 = r/\lambda^{1/2}$
$\langle\rho\rangle$	mean effective density of particles
ρ	density of water
ρ_f	effective density of a floc
ρ_p	density of a primary particle
σ	sigma coordinate
τ	bottom shear stress
τ_D	time scale for diffusion ($\tau_\mathrm{D} = \frac{L_\mathrm{c}^2}{D}$)
τ_c	critical bottom shear stress for erosion
$\tau_\mathrm{c,e}$	critical bottom shear stress for erosion calculated by $\tau_\mathrm{c,e} = a_\mathrm{e}\, C_\mathrm{sed}^{b_\mathrm{e}}$
$\tau_\mathrm{c,v}$	critical bottom shear stress for deposition
ϕ	porosity of an aggregate
Φ_a	Thiele modulus for advection
Φ_d	Thiele modulus for diffusion
$\langle\chi\rangle$	mean potential relative uptake capability of a particle-attached cell
χ_a	potential relative uptake capability of a particle-attached cell due advective flow
χ_d	potential relative uptake capability of a particle-attached cell due to diffusion

$\langle\chi_\gamma\rangle$ mean potential relative uptake capability of particle-attached cell due to aggregates' experiencing shear

$\langle\chi_v\rangle$ mean potential relative uptake capability of a particle-attached cell due to sinking of aggregates

---

* Note that some few symbols are not listed here which become clear in the context of the text.

Chapter 1

Introduction

Earth is called a "blue planet" as from a global perspective, oceans cover more than 70 % of the earth's surface. In the photic zone of the oceans, photosynthetically active primary producers convert carbon dioxide and inorganic nutrients to biomass. This biomass forms the basis for the marine food web. In turn, dead organisms and excretions ('detritus') get remineralized in the microbial loop that allows for nutrient cycling through the food web. Therefore, knowledge about transport and fate of organic matter is essential to understand the functioning of the marine ecosystem. One fraction of organic matter is particulate organic matter (POM)[1]. It consists of and forms aggregates called marine snow[2] that range over several orders of magnitudes in size (from a few microns to sometimes even meters like e. g. in the Adriatic Sea, described by Herndl and Peduzzi, 1988).

More general, the formation of organic aggregates, sometimes in combination with mineralic/sediment particles, is ubiquitous in aquatic environments ranging from lakes, rivers, coastal waters to the open ocean (Alldredge and Gotschalk, 1988; Bungartz and Wanner, 2004; Lunau et al., 2006; von Wachenfeldt, 2008). For a better understanding of their role in aquatic systems, it is

[1]There are two other operationally – by retention size of filters – defined fractions: Dissolved Organic Matter (DOM <0.2 µm) and Colloidal Organic Matter (0.2 µm < COM < 0.45 µm; Simon et al., 2002).

[2]For simplicity, the differentiation into marine snow (>500 µm), microaggregates (1-500 µm), and submicron particles (<1 µm) will not be used explicitly in the introduction (for operational size ranges see e. g. Simon et al., 2002).

therefore necessary not only to carry out field and experimental studies, but also to develop mechanistic models to describe aggregate dynamics. In the present thesis, a model for aggregation and (some) related processes is presented, aiming for *i)* insights into their particular relevance in and the biological influence on sediment dynamics, and *ii)* a better representation of aggregate dynamics in future coupled ecosystem-sediment transport models. Therefore, the model is designed to effectively describe the temporal and spatial aggregate dynamics emphasizing on coastal waters. However, much fieldwork has been carried out in open oceans to enlighten the role of biological processes that are most likely also involved in coastal aggregate dynamics. An overview on marine snow will therefore be given to provide a background on relevant processes for the formation and fate of aggregates, followed by a section focussing on specific coastal aspects.

1.1 Marine snow and its functions in the oceans

The formation and fate of marine snow are of high complexity, and thus, still not conclusively understood in detail. Apart from scientific interest, there is a large need to investigate mechanisms leading to formation and decomposition of aggregates, as marine snow transports carbon to the deep sea (Lee et al., 2004), and therefore forms a driving force for the carbon dioxide reduction in the atmosphere. Hence, aggregates play an important role in the marine carbon cycle and are therefore necessarily to be considered in the perspective of global warming. Investigating the role of aggregates in marine ecosystems facilitates a better understanding of the system itself and furthermore provides essential information to predict the future climate on earth. In addition, enhanced knowledge about the processes influencing the flux towards the sea floor will improve the reconstruction of the paleo-climate on earth from sediment cores.

When following aggregates from their formation to their decomposition or sedimentation, a complex picture evolves. Primarily in the surface waters, particles are produced/formed which can settle through the water column undergoing physical and biogeochemical transformation processes until either the dissolution or the sedimentation of particles occur.

1.1.1 Precursor formation and their role in aggregation processes

Phytoplankton, but also bacteria are producing extracellular polymeric substances (EPS, e. g. Decho, 1990; Passow, 2002b; Bhaskar and Bhosle, 2005)[3]. EPS are generally heteropolymers composed of mainly polysaccharides with a wide variety of simple sugars (e. g. Hoagland et al., 1993), but also proteins, nucleic acids and lipids (Lee et al., 2004). For a review on EPS, and its roles in the ocean, refer e. g. to Decho (1990) or Bhaskar and Bhosle (2005). While EPS range in structure from being loose, dissolved slimes to tight capsules surrounding the cell, a subtype of EPS, the transparent exopolymer particles (TEP) exist as individual particles (Alldredge et al., 1993). Those are operationally defined as particles formed from acid polysaccharides (Passow, 2002c, also refer to this publication for a review on TEP). The production of TEP can be regarded as dependent on many factors such as e. g. the species (Claquin et al., 2008), the stage of their life cycle (Kahl et al., 2008), the environmental conditions like the nutrition state, etc. For example, Schartau et al. (2007) have shown in a model study that there exist two dominant modes of organic carbon exudation by phytoplankton: carbon overconsumption and exudation above Redfield ratio during the growth phase, and excessive carbon release under nutrient limited conditions.

Indeed, a diverse, large pool of small organic molecules (ca. 1-1000 nm, Verdugo et al., 2004) exists in form of dissolved organic matter (DOM) which constitutes with $700{\cdot}10^{15}$ g carbon (Verdugo et al., 2004) about 28 % of the total organic carbon in the oceans[4]. This DOM originates from excretions and the breakdown of bio-macro-molecules of organisms. DOM generation allows the recycling of nutrients through the food web either by photosynthetic up-take or bacterial production via transfer to higher organisms like protists and zooplankton (Verdugo et al., 2004). Verdugo et al. emphasize that such biologically mediated cycling between the dissolved and particulate organic

[3] Various authors use different terms, e. g. Decho (2000): Extracellular polymeric secretions; Passow (2002c): exopolymeric substances.

[4] The total oceanic reservoir of carbon (inorganic and organic) is ca. $40\,000{\cdot}10^{15}$ g carbon, of which $2\,500{\cdot}10^{15}$ g carbon is organic (refer to Zimov et al., 2006).

matter is critical, on a large scale, to the transfer and fate of nutrients because only particles can sink to selectively transport bioactive elements from the lighted surface waters into the ocean's depth. This *biological pump* removes climatically active elements, such as carbon, from direct contact with the atmosphere. In addition to this biologically mediated cycling, biopolymers in this DOM pool can spontaneously assemble into microscopic polymer gels in seawater (Chin et al., 1998)[5]. Generally, gels can have a complex physical and chemical nature (Tanaka, 1992). "Small changes in ambient pH, ionic concentration, or temperature can trigger extensive and abrupt phase transitions in gels" like EPS/TEP, "which can radically change their size, density, dielectric properties, chemical reactivities, and permeabilities, and hence, their potential interactions with enzymes and living organisms" (Tanaka, 1992; Verdugo et al., 2004).

Those nano- and microgels eventually grow further by continued collision and annealing (Wells and Goldberg, 1994; Kepkay, 1994), forming larger macrogels and gel-like particles, such as TEP (Alldredge et al., 1993; Passow, 2002a,b). And hence, by bridging the DOM and POM phase, provide precursors for the formation of larger aggregates. This is supported e. g. by a comprehensive experimental and modeling study of Logan et al. (1995) revealing a primarily by TEP concentration controlled aggregate formation that followed blooms of mucous-producing diatoms. This might be either due to higher collision frequencies by a provided "background particle" concentration (e. g. Kahl et al., 2008), and/or due to an increased stickiness ("collision efficiency") of the formed aggregates (Kiørboe and Hansen, 1993; Dam and Drapeau, 1995). However, Jackson (1995b) concluded that it will be difficult to understand how TEP interact with algal particles until one knows more about the details of their generation and interaction with other particles which is crucial to develop a comprehensive theory of (algal) coagulation.

Remarkably, Azetsu-Scott and Passow (2004) reported that TEP particles have a density of $0.7 - 0.84\,\mathrm{g\,cm^{-3}}$ which is well below the density of water. But owing to aggregation with particles of other sources like bacterial and phy-

[5] Brownian motion and annealing are the processes involved in this "spontaneous" assembling.

toplankton cells, larvacean houses, radiolaria, foraminifera, and other organic and inorganic material (e. g. Hansen et al., 1996; Serra and Logan, 1999; Lee et al., 2004; Passow, 2004, and others), TEP nonetheless enhances the settling velocity compared to the single particles (De La Rocha and Passow, 2007), maybe also by clogging up pores in aggregates that reduces the drag (Ploug et al., 2002). The aggregation results in particles of different composition that again can undergo processes of aggregation. Hence, a "cascade" from smallest soluble molecules (DOM) to colloids and large particles (POM) like marine snow can occur and is present in the ocean.

1.1.2 Mechanisms leading to aggregation and fragmentation

Three main physical mechanisms are assumed to be involved in the formation of aggregates: *i)* Brownian motion, *ii)* aggregation due to shear, and *iii)* aggregation due to differential settling. McCave (1984) pointed out that Brownian motion is only relevant for particles of diameter <1 µm. By contrast, the two other mechanisms are so far suggested to be more relevant for larger particles (McCave, 1984), while physical considerations of e. g. Davoudi and Schumacher (2006) for the stretching and alignment of polymers in a turbulent flow also lead to the hypothesis that shear might be more relevant than thought for the aggregation of small 'particles' like polymers. Davoudi and Schumacher (2006) showed an alignment of stretched polymers to the shear which might enhance their contact rate. This could be, in particular, a possible shear-driven mechanism of TEP generation from polymer fibrils that are secreted by algae and bacteria. Shear is most often present in the upper water column where wind stress generates shear either by waves or by wind driven currents. It can either be laminar or – most often – turbulent and enhances the aggregation process by an increased collision frequency. However, shear can also lead to fragmentation of marine snow (e. g. Ruiz and Izquierdo, 1997). Turbulent kinetic energy (TKE) leading to turbulent shear via its dissipation is mainly produced at the ocean surface. The production of TKE increases approximately with the cube of the wind speed and decreases approximately linear with depth (Kiørboe et al., 1990). While shear thus mainly appears at

the surface of the ocean, aggregation due to differential settling takes place throughout the whole water column and is only dependent on the relative speed to each other and the size of the particles. It is therefore obvious that the relative importance of the aggregation and fragmentation processes can vary in space and time.

1.1.3 Significance of biological processes for aggregate transformation

The evolution of the aggregate distribution and the aggregates' composition in the oceans is not only dependent on physical processes, but is also, apart from the source of particles, coupled to biological processes taking place throughout the water column. As aggregates and, in particular, the polymer gels are an important micro-environment for bacteria, archaea and protists (Azam and Malfatti, 2007, refer to this publication as a comprehensive review on the microbial structuring of marine ecosystems), those organisms alter the chemical composition of the particles and may influence their hydraulic and/or chemical behavior. For example, bacteria can inhibit, as well as enhance, the aggregation state of the pelagic system by reducing the stickiness with hydrolases or increasing it by mucus production (Azam and Smith, 1991; Smith et al., 1992).

Bacterial interactions with marine snow

In particular for bacteria, aggregates are an important niche as the settling of aggregates leads to an increase in available oxygen from the surrounding water due to a decreased diffusive boundary layer. Ploug and Grossart (2000), for example, reported a 5-10-fold increased bacterial production when aggregates are kept in suspension during incubations compared to static conditions where they are allowed to settle down to the bottom of the experimental vessel. Additionally, aggregates themselves serve as an important food source. This can lead to a more than 2000-fold higher microbial density on aggregates than in the surrounding water, observed by Ploug et al. (1999) on marine snow from surface waters of Southern California Bight. Moreover, bacteria chemotactically sense, follow and take advantage of the organic solute plume behind settling aggregates (e. g. Jackson, 1989; Azam and Long, 2001; Fenchel, 2002;

Visser and Jackson, 2004) which results from extracellular enzymatic activity of attached bacteria (e. g. Ziervogel and Arnosti, 2008). Kiørboe and Jackson (2001) emphasize that plumes in the wake of sinking particles may provide important growth habitats for free bacteria and account for a significant proportion of water column bacterial production (up to 50 %, Azam and Malfatti, 2007) at typical concentrations of marine snow aggregates.

The high bacterial density on aggregates again provides a food source for protists like e. g. flagellates (Kiørboe, 2003). The attachment of bacteria on aggregates, and hence, their decomposition, seems to be strongly related to the settling velocity of the aggregates. Goutx et al. (2007) reported for the northwestern Mediterranean Sea (in 200 m depth) a correlation between the degradation state of the aggregates and the particles' settling velocities which were dependent on the initial composition. Fast settling aggregates ($>230\,\mathrm{m\,d^{-1}}$) showed biomarkers for fresh undecomposed material and a slow total degradation rate, whereas slow settling particles were characterized by a decomposed state and higher total degradation rate. Hence, it is likely that bacteria were better able to colonize on slow settling than on fast settling aggregates which has again implications for the vertical carbon flux. Goutx et al. (2007) also reported that the decomposition of aggregates leads to a homogenization in their chemical composition reflecting the process of loss through enzymatic hydrolysis of source compounds. Generally, the process of bacterial particle decomposition appears to consist of a mass loss (Stemmann et al., 2004a). During the process of decomposition, bacteria, and the present protists consume oxygen which can lead to oxygen depletion or even anoxic micro-zones in the aggregate itself (Ploug et al., 1997). As a larger effect, this oxygen consumption by bacteria and other organisms on particles (and in the surrounding water) fosters the evolution of oxygen minimum zones in upwelling regions where a high primary productivity occurs, or suboxic[6] and even anoxic zones in stratified areas of the oceans like in the Black and Baltic Sea.

[6] $O_2 \leq 5\,\mu M$; Murray et al. (1989)

Zooplankton, microbes and their role in the vertical flux

Not only bacteria use aggregates as a food source, but also zooplankton does. Shanks and Walters (1997) certainly reported a weak association of adult holoplanktic calanoid and cyclopoid copepods with marine snow, but by contrast, a concentration on aggregates of their nauplii, harpacticoid copepods, nematodes, bivalve and gastropod veligers, and foraminiferans compared to the surrounding water. Indeed, the behavior of organisms and their concentration on particles suggest that marine snow is an important pelagic component for a variety of both holoplanktonic[7] and meroplanktonic[8] zooplankton (Shanks and Walters, 1997). Higher organisms thus impact the aggregate composition by various processes, but even protozoa appear to cause a size reduction of aggregates during the process of decomposition (Stemmann et al., 2004a).

As shown in laboratory studies, macro-zooplankton, in particular *Euphausia pacifica*, a common euphausiid, not only ingest marine snow, but also fragment it by either entrainment and direct impact with the beating pleopods or by eddies generated during swimming (Dilling and Alldredge, 2000). This process of fragmentation is discussed to induce a night-daily alteration of the aggregates in the upper water column (<100 m) off Southern California due to the daily migration of zooplankton species like euphausiids (Graham et al. (2000), and further supported by Dilling and Alldredge (2000)). The fragmentation by macro-zooplankton not only links animal behavior and geochemical cycles and potentially impacts food web structure, but might be an ubiquious process of considerable magnitude throughout the ocean (Dilling and Alldredge, 2000).

In particular copepods excrete faecal pellets that are part of the POM pool, but have different characteristics than e. g. aggregates composed of diatoms (Kilps et al., 1994), in particular the fractal dimension. This influences the excess density and the settling velocity of particles, and hence, the vertical flux. The process of aggregation and utilization of aggregates by zooplankton can even lead to competetive effects as shown in a model study by Jackson (2001) using the Fasham et al. (1990) model extended by coagulation processes. After a modeled spring bloom, aggregation of diatoms increased their

[7] These organisms live in all life stages in the pelagic environment.

[8] These organisms only live in some life stages in the pelagic environment.

settling velocity and thus reduced the available food for zooplankton by settling out of surface waters. Additionally, particles grew larger than the optimal ingestion size. By contrast, low aggregation lead to a larger zooplankton population after the bloom. Contrarywise, in the sense of vertical flux, aggregation and zooplankton feeding/fecal pellet production are not purely competetive processes removing algae, but can also interact to increase the vertical fluxes (Jackson, 2001). By investigating results of a field study in the northwestern Mediterranean Sea with a model (Stemmann et al., 2004a), Stemmann et al. (2004b) showed that the oberved stop of high flux of large particles in the upper midwater zone requires the mesozooplankton to feed preferentially on large settling particles using remote detection, totally ingesting the particles. Even high microbial degradation activity alone does not remove enough large particles to explain the observations. By contrast, below 500 m depth, the microbial activity becomes more important because zooplankton becomes less frequent.

1.1.4 Trace chemical transport and mineralic particle scavenging by marine snow

Particle-reactive trace chemicals, like e. g. some metals, are often used to measure vertical fluxes impacted by the above mentioned biological and aggregation processes. Hence, knowledge about their behavior with respect to marine snow, and also to the particles' changing composition due to biological activity, is needed to better gain insights into the biological pump. Especially EPS (Decho, 1990), and in particular TEP (e. g. for Thorium ^{234}Th; Guo et al., 2002; Azetsu-Scott and Niven, 2005), play a prominent role as adhesive substance for particle-reactive chemicals. For example, Azetsu-Scott and Niven (2005) reported for the Badford Basin, Nova Scotia (Canada), a positive correlation between the TEP concentration at the surface layer (<5 cm) and the ^{234}Th : ^{238}U activity ratio. Moreover, a simultaneous enrichment of both ^{234}Th and TEP in the surface water through upward transport of TEP indicated that the TEP dynamics in the upper ocean play an important role for the accumulation of ^{234}Th (which then might sink down due to TEP enhanced aggregation and subsequent particle sinking). Suggesting a new pathway of

TEP and associated particle-reactive elements, this accumulation needs to be considered when estimating the strength of the biological pump using ^{234}Th (Azetsu-Scott and Niven, 2005).

In contrast to ^{234}Th, aluminium is primarily associated to clay particles or at least with apparently nonbiogenic, silicon-containing particles (Deuser et al., 1983). These mineralic particles (to which clays, coccoliths, diatom fragments, foraminifera, and radiolaria contribute; Passow and De La Rocha, 2006), can either aggregate with or be scavenged by sinking marine snow due to its porous nature. For example, Ploug et al. (2002) measured fluid velocities through diatom aggregates ranging from 5 to 40 µm s^{-1}. These mineralic particles are in discussion to enhance the settling velocity by ballasting the particles and/or prevent marine snow from decomposition (Deuser et al., 1983; Hedges et al., 2001; Armstrong et al., 2002; Hamm, 2002; Passow, 2004; Passow and De La Rocha, 2006; De La Rocha and Passow, 2007, and others), while it is questionable whether the POM flux controls the mineralic flux or vice versa. Deuser et al. (1983) already found a quite close relationship between the POM export from surface waters to depth with aluminium, but no relationship of aluminium input and the annual primary productivity cycle. This suggests a POM determined mineralic flux. However, Armstrong et al. (2002), Klaas and Archer (2002) and others support the opposite, followed on by a discussion of this "ballast hypothesis" by Passow (2004) suggesting a carrying capacity of POM for mineral particles of biogenic and lithogenic origin of about 3 - 7 wt-%.

Lab experiments with phytoplankton-detritus derived aggregates and a suspension of clay or calcium carbonate of different concentrations in rolling tanks carried out by Passow and De La Rocha (2006) support the conclusions of Passow (2004) suggesting that the POC flux determines the flux of minerals to the deep sea and not the other way around. Passow and De La Rocha (2006) found aggregates to be very effective in scavenging suspended mineral particles, and moreover that the incorporation of minerals into organic aggregates can diminish aggregate size (and thus alter the settling velocity). The experiments showed for higher concentrations of mineralic particles (10.000 µg L^{-1} and 50.000 µg L^{-1} for illite, and 37.000 µg L^{-1} for calcium carbonate) a sharp increase (compared to the experiments with lower concentrations) of remaining

microaggregate numbers in the final stage. The saturation of organic material with mineralic particles seemed to occur with 0.03 µg carbon (C) μg^{-1} dry weight (DW) and 0.02 µg C μg^{-1} DW for calcium carbonate and illite, respectively. This is a bit below, but still close to the value of 5 wt-% organic carbon observed by Armstrong et al. (2002) in sediment trap material (below 1800 m). However, these large concentrations of small negligibly-sinking mineralic particles in the mesopelagic and bathypelagic[9] likely leading to such constant POC/DW ratios await quantification (Passow and De La Rocha, 2006) to further support the saturation hypothesis. It is important to emphasize that the suspended mineral concentrations used in the experiments ranged from 7 µg L^{-1} to 50.000 µg L^{-1}, where the latter is representative for more turbid systems, such as estuaries or the North Sea (Passow and De La Rocha, 2006).

Most of the above described processes can occur simultanuously, and again can change and modify the transport behaviour of aggregates. Furthermore, the decomposition of aggregates and the accompanying release of nutrients, mono- and oligomers change the environment for the surrounding organisms that again might affect the aggregates. A complex interplay between physical, chemical and biological processes is thus involved in the formation, transport and fate of marine snow.

Eventually, only between 5 % and 25 % (Martin et al., 1987; Buessler, 1998) of the total oceanic net primary production (NPP: 48.5 Pg C a^{-1}; Field et al., 1998) is exported from the euphotic zone, and only about $1 - 3$ % reaches the deep sea and sediments (De La Rocha and Passow, 2007), but nevertheless constitutes an important food source for the benthic community, and thus only approximately 0.1 % of the global net primary production is ultimately preserved in marine sediments (Hedges, 1992). Hence, it follows that most of the POM gets decomposed and respired on the way down, but quantitative estimates of carbon fluxes in the deep ocean are still prone to errors as analyzed by Burd et al. (2010).

[9] 200 – 1000 m and 1000 – 4000 m depth, respectively

1.2 Aggregates in coastal waters

Compared to the open ocean, coastal waters are highly dynamic systems as they are mainly rich in nutrients and show therefore a high primary productivity. They account for about 30 % of the total marine primary production (14.4 Gt C a^{-1} of 44.7 – 50.2 Gt C a^{-1}, Longhurst et al., 1995). When looking at aggregates in coastal waters, they differ in their composition compared to open ocean particles of surface waters that originate more than 80 % from biological sources (e. g. Herndl, 1988, based on dry weigth, thus not taking into account inorganic material of biological origin). By contrast, coastal aggregates consist, in terms of weight, up to 95 % of small mineral particles and have a total organic matter content of typically 6 – 11 % (reported for coastal waters of the North Sea by Joerdel et al., 2004). The mineral particles in aggregates are most often smaller than 8 µm and are in discussion to represent the cohesive part of the sediment pool (approx. 7 phi[10]; Chang et al., 2006b). Especially in modeling studies, these single cohesive sediment particles are often refered to as "primary particles"[11]. Larger particles like sand grains and even parts of the mud fraction[12] are mainly transported solely (Chang et al., 2006b), but especially the sand fraction needs high hydrodynamical energies to be transported. The total load in the water is refered to as suspended particulate matter (SPM) which is by operational definition larger than 0.45 µm (e. g. Simon et al., 2002) and contains both POM and particulate inorganic matter. Furthermore, it should be noted that studies carried out in coastal waters often refer to aggregates by using the terminology of 'flocs' reflecting

[10] phi $= -\log_2$(particle size (mm))

[11] Definitions/terms used throughout this work:

particle	:	can mean → primary particles or → aggregates / → flocs
primary particle	:	a single particle that is the basic unit of an aggregate (can be organic or inorganic)
aggregate	:	a particle that consists of a number of primary particles (the term aggregate is mainly used in open ocean studies)
floc	:	is an aggregate, but the term is often used in coastal studies dealing with aggregates that mainly consists of sediment particles

[12] Mud is defined as (Chang et al., 2006a): grain sizes below 63 µm that can be subdivided into clays (< 2 µm) and silts (2 µm – 63 µm).

a more physical point of view (e. g. Manning and Dyer, 1999; Van der Lee, 2000)[13]. Within this thesis, both expressions will be used synonymously in the following.

1.2.1 Why studying suspended particulate matter (SPM) dynamics?

Far from scientific interest, adopting the engineering and managing point of view, SPM transport is an important factor to be considered in the planning and assessing of harbour and port building, but also for coastal preservation and protection. Human activities in such areas that have an important natural function can easily lead to conflicts, and facing the fact that over 50 % of the world's population are living in the coastal zone (Haslett, 2000, p. 149)[14], the management of such coastal systems requires a knowledge about both the natural function of these environments, and the potential of these areas to human use, based on the assessment of the systems 'resilience' (de Jonge, 2000). Thus, a knowledge about structure and functioning and the temporal fluctuations within a natural system have to be based on solid scientific information about physical and biological structure, the physical and ecological functioning and operating geo-chemical processes (de Jonge, 2000).

Keeping this more general statement in mind, it is evident that scientists are highly demanded and encouraged to understand SPM transport and its effects on and interplay with the environment. As suspended sediments are always coated with (Eisma et al., 1991a) and related to organic matter, their fate also influences the fate of POM in the coastal environment and thus, through the nutrient recycling in the microbial loop, the primary productivity. Moreover, particle-reactive contaminants are highly associated with SPM, in particular its fine sediment fraction (e. g. Milligan and Loring, 1997), whose dynamics should be understood to better predict the contaminants' fate. As mainly the fine sediment fraction *i)* aggregate with POM and, moreover, *ii)* provides reactive surfaces, it turns out that flocs play a prominent role for the

[13] Van Straaten and Kuenen (1957) and others use the terminology of 'flakes' or 'floccules'.

[14] within 200 km of the coast, see also: UN Atlas of the Oceans (30.09.2009): http://www.oceansatlas.com

transport of POM and particle-reactive chemicals. It is therefore necessary to understand aggregate dynamics to gain insights into the coastal ecosystem and the budgets of various particulate components transported in such flocs. This is even true for various dissolved components due to the bridging between the DOM and POM phase by physical and biological processes described in Sec. 1.1.

1.2.2 How to measure SPM concentration and aggregate distributions?

To use data from experimental studies for model validation, at least a rough knowledge about differences, capabilities, advantages and drawbacks of the sampling methods involved is helpful to interpret the obtained data. Therefore, it is within the scope of this section to give a general, but not detailed overview on measurement techniques that are widely used and recognized to be useful in studies dealing with SPM.

A classical way to measure bulk concentration of SPM is the filtration of a water sample through preweighed and precombusted glass fibre filters of 0.45 µm pore size with a subsequent de-ionized water washing step to remove excess salt. This method was used to obtain the SPM bulk concentration data used for the model validation in Sec. 3.2. With this technique, after freezing and drying, the total SPM concentration as dry weight (DW), but also, after ashing, the inorganic and the POM fraction can be determined (see e. g. Mikkelson, 2002; Dellwig et al., 2007). However, such compounds like TEP can escape this procedure as they can, due to their gel-like nature, partly be sucked through the filter pores, although they are larger than the average filter retention size.

Another technique is the estimation of SPM concentration by using the acoustic doppler current profiler (ADCP; see e. g. Santamarina Cuneo and Flemming, 2000) or acoustic doppler velocimeter (ADV, see e. g. Fugate and Friedrichs, 2002). An advantage is the possibility of high frequent measurements accompanied by information of the velocity and turbulence in the water column. The main disadvantage of this method is its sensitivity to the floc characteristics like size, shape and elastic characteristics (Tessier et al.,

2007; Van Santen et al., 2007), but also to turbulence-particle interactions (Bartholomä et al., 2009).

In order to get a two-dimensional spatial distribution of SPM, satellite remote sensing data can be used which is in particular useful for the validation of sediment transport models (e. g. Pleskachevsky et al., 2005; Gemein et al., 2006). However, a high level of difficulties has to be faced when dealing with turbid coastal waters (see e. g. Gemein et al., 2006). Nevertheless, even recent attempts to estimate the particle size from satellite remote sensing data (Van der Lee et al., 2009) have been carried out.

A principle that can be applied to determine the size distribution of aggregates is laser diffraction, used e. g. in the LISST (laser *in situ* scattering and transmissiometry; Agrawal and Pottsmith, 2000). It allows not only to determine the size distribution in high frequent measurements, but also (with some instruments like e. g. LISST-ST) the settling velocity of flocs. The distributions are validated by using standard glass sphere powder. As a consequence, effects on the size distribution arising from the measuring of very light aggregate type particles are not known (Agrawal and Pottsmith, 2000). Consequently, the obtained distributions are only semi-quantitative. Especially in estuarine waters no absolute DW concentrations can be obtained, but the relative relations of the distributions to each other (Fugate and Friedrichs, 2002). Moreover, distinguishing between sediment particles and e. g. algae is not possible, but could be obtained, in principle, by camera-based systems and a subsequent (semi-automatic or automatic) image processing like e. g. used by Lunau et al. (2004); Benson and French (2007)[15]. The mean sizes of aggregates for the model validation in Sec. 3.2 were obtained by Lunau et al. (2006) by using such a camera-based system invented by Lunau et al. (2004). Another technique is the multispectral transmissiometer (MST) that measures beam attenuation coefficients to calculate various parameters like Gelbstoff, SPM and chlorophyll concentration (Badewien et al., 2009). However, especially flocculation processes affects optical measurements leading to problems for transmissiometry usage in long term monitoring (Mikkelson and Pejrup, 2000). A

[15]Within the constraints of the camera system used by Benson and French (2007) and Lunau et al. (2004, 2006), the determination of compounds by image analysis was not possible.

direct quantitative conversion between classical measurements, ADCP, ADV, MST, LISST and camera-based systems is yet not attainable, but studies of e. g. Fugate and Friedrichs (2002); Flory et al. (2004); Winter et al. (2007a); Badewien et al. (2009) help to gain insights into the operating systems and their differences. However, the structure and the constituting compounds of aggregates are of high interest, and can only be achieved by using other techniques not summarized here.

1.2.3 SPM dynamics in coastal and estuarine waters with an emphasis on the Wadden Sea – processes, mechanisms and effects

As already noted above, coastal and estuarine waters are highly dynamical systems. They are not only rich in nutrients, but are often tidally affected, and thus, strong currents can occur. Besides the tidally driven currents, various other processes lead to hydrodynamically highly variable regimes that are most often not in equilibrium (Hunt, 1986). Namely, density-driven currents occur that are induced by temperature and salinity gradients, the latter either be driven by river run-off or/and by evaporation, precipitation and groundwater discharge. Moreover, wind-generated currents and waves interact with the aforementioned processes. The resulting hydrodynamically highly variable regime is a strong driving force for sedimentological, but also ecological processes. Even when leaving the ecological implications aside and focussing on the chemico-physical effects of such variable systems on SPM transport, a complex picture arises.

Due to the strong currents, wave action and a mainly low water depth in coastal regions, spatially and temporally variable high turbulent shear and energy dissipation rates occur in such systems. A strong benthic-pelagic coupling is the consequence. Hence, erosion/resuspension and transport of sediment play an important role in coastal waters. This leads to high weight proportions of fine sediments on aggregates and, in total, to high loads of SPM in the water column (sometimes more than $10\,\mathrm{g\,L^{-1}}$ as reported for an estuary by Uncles et al., 2006). Owing to the tidal phases, a cycle of deposition, erosion/resuspension and subsequent transport and again deposition of SPM

is typical. The turbulent shear promotes *flocculation processes* that include – by definition in this thesis – *i) aggregation* and *ii) fragmentation processes* of the fine sediment fraction (cohesive sediments) and POM. These flocculation processes can alter the hydraulic characteristics of aggregates, and thus their transport behavior. For example, Jiang and Logan (1991) showed on basis of theoretical steady-state size distributions that aggregation of aquatic flocs solely by fluid shear leads to fractal dimension higher than 2.4, whereas the values for those flocs formed by differential settling ranges between 1.6 an 2.3. However, Chen and Eisma (1995) have not found any correlation of fractal dimension with environmental conditions in the Elbe estuary and the North Sea, but a general trend of estuarine flocs tending to be more fractal than the coastal flocs. By contrast, Mikkelson (2002) reported a temporal increase of fractal dimension from June to September for two sites, one situated off the coast of Fanø (North Sea) and the other in the Horsens Fjord (Baltic Sea), both in Danish waters. The author related these findings to changing turbulence conditions (induced by a windy period before the September field work) causing aggregates to break up and become restructured into more compact entities.

Especially in estuaries, the changing salinity might also be a factor that has to be considered. It is observed in west-european estuaries that the particle size is smaller at increased salinity compared to the fresh water of the rivers (Eisma et al., 1991b, study on the west european estuaries Ems, Rhine, Scheldt, Gironde and Rhône). Eisma et al. (1991a) related these observations to the mobilization of bio-polymers (polysaccharides) at the fresh-saline water contact which results in a reduction of the floc strength. However, the direct impact of salinity on flocculation ('salt flocculation') due to changes in ionic strength has come more and more into question (Eisma et al., 1991a; van Leussen, 1999, and references therein). Ecologically, the salinity gradient acts as a border for many organisms that cannot regulate the osmosis leading to e. g. lysis of phytoplankton cells. As a consequence, polymers are released that can adsorb onto the sediment particle surfaces, and thus, bridging and binding sediment particles together (van Leussen, 1999). Within the transition zone from fresh to saline water, the amount of organic compounds of terrestrial origin like lignin, phenoles, cellulose and xylose also decreases (Eisma et al., 1991b), an

observation that might also be related to aggregation and deposition processes. On a large scale, the resulting turbidity maximum is a feature of many estuaries (e. g. Uncles et al., 2006).

When focussing on the Wadden Sea along the coastline of the Netherlands, Germany and Denmark, already Postma (1954); Van Straaten and Kuenen (1957) and Postma (1961) pointed out the importance of aggregated material for the accumulation of fine grained material. They presented different hypotheses of the intricate interaction between the processes of erosion/resuspension, transport and deposition of aggregates as driving force for the accumulation of fine sediments in the Dutch Wadden Sea. Adopting the Lagrangian point of view, a specific water body transports SPM that can settle out of the water column faster on the tidal flats (at high tide) than in the deep water (at low tide). By contrast, the deposited material cannot be eroded into the same water body as the current velocity must exceed a critical value, before the material can be again resuspended. The interplay between erosion, deposition, the tidally changing current velocities and the bottom topography thus leads to a small net transport towards the shore and thus to a net accumulation of fine material.

Van Straaten and Kuenen (1957) also postulated that during storms, vast quantities of fine sediment are lost to the open sea. This postulation has been investigated in a recent study by Bartholomä et al. (2009). They found that an export towards the open sea during extreme events like storms is strongly dependent on the interaction of wind, waves and tidal phase, and thus, not every storm generates a net-export. However, according to Bartholomä et al. (2009), it is still difficult to access the quantity of such fluxes as autonomously working measurement techniques based on backscatter include a substantial amount of noise produced by the high turbulence during extreme events, especially near the surface.

The transport of sediment and its seasonal variation affects the Wadden Sea in several ways. The transport of sediment leads, on the long term, to changes of the morphology of the islands and their surrounding tidal flats. For example, the chain of the East Frisian Islands shows a net-drift towards the east (Bartholomä, 1999). Naturally, tidal channels and gullies can be shifted as well as shipping lanes. On a seasonal timescale, the proportions of

the sediment fractions are changing which has been shown by Chang et al. (2006a,b) for the backbarrier basin of Spiekeroog island. During spring and early summer, especially the proportion of the fine fraction (mud fraction) is increasing in the sediment, while in autumn and winter a depletion of this fraction occurs. Chang et al. (2006b) related these experimental findings to changing hydrodynamical conditions (induced by a higher amount of storm events in the winter season), but also to the seasonally variable influence of biological processes that enhance fine-sediment deposition and lead to bio-stabilization of the sediment. The primary production (phytoplankton and -benthos) that is accounted for such effects (see Sec. 1.2.4 below), is not only affected by the transport of POM in the aggregates (and its remineralization by microbes), but also by SPM-induced turbidity that determines the light climate (Colijn and Cadée, 2003).

The turbidity in coastal waters is strongly influenced by the strength of the benthic-pelagic coupling that even affects the microbial communities. Stevens et al. (2005) found persisting specific microbial communities as free-living, aggregate-attached and sediment surface-attached in the German Wadden Sea. However, some phylotypes either from the free-living or the sediment surface-attached community have been found on aggregates which reflects respective exchange processes. Bacteria may take advantage of a thinner diffusive boundary layer around aggregates to take up nutrients (Bergstedt et al., 2004). A higher activity of particle-attached bacteria has been indeed shown by e. g. Griffith et al. (1994) in the Chesapeake Bay, USA. By theoretical considerations, Ritzau (1996) hypothesized a stimulation of microbial activity especially in the benthic boundary layer – a region of high shear rates, which also decreases the floc boundary layer. Formerly, Logan and Hunt (1987) calculated the relative (dis-) advantage of a bacterial cell attached to a porous particle – in purely sinking state or under turbulent conditions – compared to a cell in the ambient water. Bergstedt et al. (2004) even found indications for a generally enhanced respiration activity of bacteria due to turbulence for a culture of *E. coli*.

Especially POM and the fine, cohesive fraction of sediment which are mainly transported as aggregates, are accompanied by trace chemicals of organic and inorganic nature. Thus, flocculation processes and their effect on

the transport behavior of particles playing a role in the fate of such chemicals (e. g. Milligan and Loring, 1997; Zwolsman et al., 1997, the latter is a study on the impact of seasonal variability on cadmium, copper, and zinc). Indeed, the decrease of the usually conservative trace metal molybdenum in the water column of the back-barrier basin of Spiekeroog, German Wadden Sea, is hypothesized to be directly related to increased aggregation and subsequent deposition following the breakdown of a phytoplankton bloom in July 2005 (Dellwig et al., 2007).

To summarize this part, it is evident that the aggregation of fine sediment particles and POM is an important factor in the coupling of bio-geochemical cycles in coastal waters. However, as already broached above, biological processes, partly discussed in Sec. 1.1, can have an effect on several processes involved in sediment transport processes. Hence, an intricate feedback from physico-chemical processes involved in sediment transport, in particular flocculation processes, on biological processes and *vice versa* exists. Some possible feedback mechanisms are discussed in the following.

1.2.4 Potential feedback mechanisms of biological processes on SPM transport in coastal waters

Due to the high load of sediment compared to organic matter, the role of biological processes has often been overlooked or underestimated. But as shortly broached in the last section, biological processes are likely to affect sediment transport. In recent years, more and more attention has been therefore paid to the interaction between cohesive sediment transport, POM and biological processes. In particular in regions of higher latitudes with a pronounced seasonality, variations in primary productivity might be accompanied by a highly variable release of organic compounds like polysaccharides, which are a major constituent of EPS. This in consequence implies that the contribution of the underlying biological processes to sediment transport is highly variable.

With the validated ecological tidal model 'EcoTiM', Kohlmeier and Ebenhöh (2007) indeed showed typical seasonal patterns of algal concentrations in the back-barrier basin of Spiekeroog, German Wadden Sea. Triggered by

light, first a spring diatom bloom with a subsequent decrease of algal concentrations occurs due to silicate limitation. Growth of flagellates[16] sets in afterwards, reaching a temporal maximum followed by a decline due to zooplankton grazing. Flagellates have their annual maximum concentration in July and a third, but smaller bloom appears later in summer. Again, an in concentration smaller, but temporally longer diatom bloom occurs in late summer (compared to the spring bloom). Effectively, according to the model results, the mean annual net primary production (NPP) within the back-barrier area of Spiekeroog island is estimated to be $138\,\mathrm{mg\,C\,m^{-2}}$ whereof 55 % arises from phytoplankton. However, a spatial heterogeneity of the contribution exists, as on the tidal flats the phytobenthic production can dominate (up to 85 %) where the annual NPP locally reaches up to $250\,\mathrm{mg\,C\,m^{-2}}$.

In nature, microphytobenthos excretes EPS that is discussed to generally stabilize the sediment and the deposits by increasing the resistence against bottom shear stress (e. g. Decho, 2000; Black et al., 2002; Le Hir et al., 2007), which is a relevant measure used in sediment transport models. However, the simple relationship of EPS and the sediment stabilization is still in discussion (Stal, 2003). Not only phytobenthos is accounted to bio-stabilize cohesive sediments (up to 120 % more than the sediment stability alone), but also bacteria seem to do so. Both together even tend to better stabilize the sediment in a synergistic effect (Lundkvist et al., 2007, in a laboratory study). The influence of microphytobenthos and their excretions is not only variable on a seasonal time – and a spatial – scale, but even on tidal time scales as the organisms are known to carry out vertical migration in dependence of the tidal phase and the respective diurnal light intensity (de Brouwer and Stal, 2001). By contrast, benthic fauna tend to destabilize the sediment while a generalization – especially in a combination with microorganisms – is difficult (Black et al., 2002). Moreover, filter feeders like mussels influence the particle composition and number. Evidently, the spatial and temporal variability of these benthic processes makes it difficult to account for biological effects in sediment transport models (Le Hir et al., 2007).

[16] Both, diatoms and flaggellates are representatives for functional groups that are used in the model with respect to their trophic position, size, and function.

Not only benthic algae, but also pelagic diatoms produce extracellular substances[17]. Even more, bacterioplankton has been shown to release TEP dependent on the turbulent conditions – less turbulence leads to higher production of (small) TEP, while higher turbulence leads to less production, but larger TEP (reported for bacterial cultures originally sampled at the NIOZ[18] pier, North Sea, by Stoderegger and Herndl, 1999). Moreover, stimulating effects on aggregation processes induced by bacteria has been reported (Paerl, 1974; Biddanda, 1985; Muschenheim et al., 1989; Fukuda and Koike, 2004).

The production of EPS/TEP by phytoplankton has been shown to be dependent on temperature (Claquin et al., 2008), and nutrient stress (Underwood et al., 2004), which is often considered to be the consequence of overflow of photosynthate produced in excess of cellular requirements (Staats et al., 2000). As EPS/TEP provides precursors for aggregation and affects the stickiness of particles (see Sec. 1.1), it might also in coastal waters change flocculation processes and floc characteristics like the excess density. Indeed, Verney et al. (2009) found faster aggregation speeds and increase in aggregate size during the presence of diatom blooms in the Seine estuary (France). Moreover, Chen et al. (2005) found a changing morphology of flocs throughout the season in the Scheldt estuary: In winter, flocs are more compact, while in summer they show a fluffy, looser structure. One could relate this to a higher and lower fractal dimension, respectively, and hence, higher and lower excess density. Chen et al. (2005) did not relate their findings directly to EPS/TEP, but, more general, to the organic matter content. Such structures, where sediment particles are embedded in organic matrices, were also reported for other regions e. g. by Ayukai and Wolanski (1997) for the Fly River Plume, Papua New Guinea. Lunau et al. (2006) reported smaller aggregates in winter and larger in summer for the back-barrier of Spiekeroog island, Germany, while SPM concentrations where lower in summer than in winter which also points towards a change in morphology.

[17] Kiørboe and Hansen (1993) reported that dinoflaggelates do not produce sticky EPS like diatoms.

[18] Netherlands Institute for Sea Research, Texel

Based on observations in the southern North Sea, Jones et al. (1998) pointed out that aggregation might be under certain conditions be beneficial for diatoms: Tidal deposition/resuspension cycles allow them to stay in suspension, while the water is cleared due to aggregation with mineral particles and thus light availability increases. Such visual effects have been also observed in the Wadden Sea by Chang et al. (2006b). They reported less turbid seawater when large flocs are formed – commonly observed in summer – and more turbid waters when flocs are small – commonly observed in winter.

It is evident that the above described mechanisms are not comprehensive, but should give a brief overview of potential feedback mechanisms. However, it follows that due to the strong benthic-pelagic coupling (and thus a strong erosion and resuspension of benthic material), both, benthic and pelagic biological processes, can affect the suspended particle characteristics. Namely, those are primary particle size, density and even shape, stickiness, excess density of flocs, their size and shape, and, overall, SPM concentration. A highly variable amount of SPM, a variable composition and settling velocity, and thus transport behavior of flocs, is the consequence. Fettweis (2008) has shown for coastal waters of the southern North Sea that the relative standard deviation of the settling velocity is about 100 % calculated on basis of statistical errors attributed to field measurements. He showed that the main sources of such statistical errors are the uncertainty of primary particle and floc sizes in the case of settling velocity. As the latter is an important parameter in sediment transport modeling, Fettweis (2008) emphasized to either include these measurement uncertainties in models, or introducing floc size (settling velocity) distributions in sediment transport models. Therefore, within the next section, a brief overview of modeling approaches and recent developments in SPM modeling is given.

1.2.5 Modeling SPM dynamics

As a new modeling approach of flocculation processes will be presented in this thesis, a short overview on SPM models will be given with a focus on aggregation/fragmentation models and their implementation in SPM transport models.

In the past, box models[19] were used to calculate annual sediment budgets (e. g. Postma, 1981). With an increasing availability of computational resources, 1-dimensional (1D) (e. g. Winterwerp, 2002), 2D (Pleskachevsky et al., 2005) and 3D models (e. g. Gemein et al., 2006; Burchard et al., 2004; Stanev et al., 2007) are in usage to study sediment transport processes on the basis of hydrodynamic transport equations. Most of these models are based on a theoretical description that does not explicitly resolve changing suspended cohesive sediment characteristics like size, excess density etc. In the past, however, flocculation effects on the settling velocity are represented by using several hydraulic size classes (e. g. Lee et al., 2007) or parameterizations e. g. in dependence on the total SPM concentration (e. g. Gemein et al., 2006). Amongst others, statistical models were also developed based on field measurements (e. g. Manning and Dyer, 2007). Nevertheless, frameworks were proposed by e. g. McCave (1984) to include flocculation processes explicitly.

With an ongoing research on flocculation processes in aquatic systems, process-based aggregation models were used to trace changes in the phytoplankton concentration and its effect on carbon transport and cycling of nutrients in pelagic environments (e. g. Jackson, 1990; Riebesell and Wolf-Gladrow, 1992; Jackson, 1995a; Burd and Jackson, 1997; Ruiz, 1997; Jackson, 2001, and others) or to test and improve aggregation formulations (Hill et al., 1992). But also a few models explicitly dealing with sediment flocculation processes were proposed (e. g. McCave, 1984). Most models had no spatial resolution, and were thus zero-dimensional (0D). Within these studies, often several hundred distinct size classes are used that interact according the originally by von Smoluchowski (1916, 1917) developed equation for aggregation, who proposed this coagulation equation for colloid particles. The interactions of size classes are calculated on basis of kernels that describe the collision frequency between particles of different (but also equal) size. The three mechanisms of aggregation: Brownian motion, aggregation due to shear and due to differen-

[19] In this context, a box model discretizes the space in two or more boxes that are connected via exchange processes, for example a tidal basin would be one box and the adjacent part of the North Sea another, and both are connected via a flow representing tidal currents.

tial settling[20] can be represented by such kernels[21]. Moreover, attempts have been made to model the break-up of aggregates due to shear e. g. by Ruiz and Izquierdo (1997) who solved the equation earlier proposed by McCave (1984) by introducing a specific function for the break-up rate.

However, only few attemps had been made to use such models in spatially resolved models (e. g. Lick et al., 1992; Lee et al., 2002a; Boyd and Stevens, 2002; Stemmann et al., 2004a,b; Bungartz and Wanner, 2004). This might be due to high computational costs. Therefore, simplified descriptions based on the Smoluchowski equation had been developed for phytoplankton aggregation (e. g. Jackson, 1990; Kiørboe et al., 1990; Kriest and Evans, 1999, 2000, the latter a distribution-based model on basis of a power law aggregate distribution), but also for cohesive sediments (Winterwerp, 1998), the latter also introducing fractal theory for flocs described by e. g. Kranenburg (1994); Jackson (1995a); Logan (1999). First efforts to couple such process-based explicit flocculation models with hydrodynamic models were made e. g. by Winterwerp (2002) who studied cohesive sediment dynamics in a 1D framework on the basis of his previously in 1998 published model for the change of a characteristic diameter of flocs due to shear-induced aggregation and fragmentation.

However, the above mentioned models are mainly either applied to a pelagic environment without sediment interactions or to cohesive sediment transport processes without taking into account biologial processes (apart from parameter estimations). Like in Lee et al. (2002b), a recent model by Krivtsov et al. (2008) uses the (modeled) dynamics of SPM to study its influence on a complex marine food web based on ERSEM (European Regional Seas Ecosystem Model), but did not take into account any feedback mechanisms.

[20] Kernels for aggregation due to Brownian motion and aggregation due to differential settling were presented by e. g. Friedlander (1957); Pruppacher and Klett (1980) and the kernel for shear-induced aggregation originally by Saffman and Turner (1956), however, several other kernels (based on other assumptions) are available, see e. g. Jackson and Lochmann (1993) like e. g. for filter feeders (Humphries, 2009).

[21] when disregarding effects that can appear due to the inertia of particles, where further kernel development is needed.

1.3 Thesis outline

In the last decade, it clearly turned out that the 'feedback loops' of biological processes on SPM transport are relevant. Thus, when investigating coastal ecosystems either for scientific interest or for engineering planning and assessment, it is important and useful to take both, ecological *and* sedimentological aspects into account. This favours the conclusion that a coupling of ecosystem modeling approaches and sediment transport modules with hydrodynamic models is useful to step forward in scientific understanding of the complex interplay of SPM transport and biological processes. In order to account for biotic effects on sediment dynamics in models, it is necessary to bridge the world of on the one hand ecosystem models and on the other hand sediment transport models. For this reason, powerful modeling tools need to be developed that meet specific demands. Besides a well process-based description, such models should be also computationally effective.

With respect to the here presented thesis, aggregates are an essential part of the coupling of cohesive sediment transport and many biological processes such as primary productivity and microbial activity, sketched in Sec. 1.1 and 1.2. Therefore, a novel flocculation model is proposed in this thesis. It is a process-based model and aims

- to reduce the complexity of classical size class-based flocculation models,
- to be easily coupled to existing sediment transport and ecosystem models,
- to account for an underlying, in coastal waters observable aggregate distribution,
- and to be computationally effective.

Based on the aforementioned roles of aggregates in the ocean described in Sec. 1.1 and 1.2, specific requirements for such an aggregation/fragmentation model can be deduced.

Besides the fundamental processes of aggregation, fragmentation, sinking, deposition and resuspension, bio-geochemical processes should be easily introduced into a model dealing with flocculation processes. This would improve

recent coupling attemps shortly touched on in Sec. 1.2.5. The DOM generation and subsequent precursor formation in form of TEP and EPS excretion (see Sec. 1.1.1) needs the resolution of small scale processes on microscopic scales. A flocculation model should nevertheless be able to represent the prominent role of EPS/TEP in aggregation/fragmentation processes. The often seasonally variable production of marine gels by algae and bacteria and their incorporation into – in coastal waters – cohesive sediment flocs[22] influence the aggregate morphology, size, density and stickiness (refer to Sec. 1.1.1 and 1.2.4). This should be ideally incorporated. Similarily, the consideration of subsequent effects on flocculation processes (Sec. 1.1.2) in dependence on hydrodynamic conditions would be favorable.

Microbial activity on aggregates, their consequential successive decomposition, weight loss and changing chemical reactivity (refer to Sec. 1.1.3 and 1.2.4) should be easy to address and incorporate in specific applications. The same is true for zooplankton and -benthos feeding on aggregates. But also the role of aggregates for biological processes is important to represent sufficiently. For example, the changing size distribution is important in order to deduce a variable turbidity and thus light absorption from the model as turbidity influences photosynthesis of algae. Also for the fate of aggregates, the floc size distribution has been acknowledged to be important (Fettweis, 2008). This is therefore also true for the transport and fate of particle-reactive chemicals (Sec. 1.1.4 and 1.2.3).

Facing many of the demands for a flocculation model, a novel aggregation model will be presented in this thesis. Earlier model developments on aggregation have either used several size classes (e. g. Jackson, 1990) to represent the size distribution or assumed only one specific size of aggregates (Winterwerp, 1998). The first is advantageous to follow the evolution of a size distribution while it is computationally expensive. By contrast, following only a specific size of aggregates is computationally effective, but unfavorable when needing any information about the size distribution. Trying to bridge these approaches, the here presented novel distribution-based model allows to easily represent

[22] or vice versa – paying more attention to the findings of Passow and De La Rocha (2006): the embedding of sediment grains into gel matrices

and recalculate the distribution from the mean size of aggregates that is the basic state variable characterizing the total SPM concentration. Additionally, it is computionally effective and incorporates such essential factors like the stickiness, primary particle size, and floc density. The latter is represented by using the fractal dimension concept for aggregates that relates mass, density and floc size to each other. By doing so, influences of biological factors like e. g. TEP can, in principle, be accounted for. However, it is out of the scope of this thesis to establish explicit dynamical model descriptions for – in reality variable – parameters like the fractal dimension or stickiness that are influenced by biological process as briefly revisited in Sec. 1.2.4. Nevertheless, the model can be used to enlighten the contribution of biological to flocculation processes as can be seen in Sec. 3.2.

The structure of the thesis is as follows:

- In Chap. 2, underlying assumptions for the flocculation model are presented and the model is derived. Furthermore, its possible coupling to fundamental processes like deposition and resuspension of SPM is realized in 0D.

- In Sec. 3.1 an intercomparison between a classical size class-based (SCB) and the here presented novel distribution-based (DB) flocculation model has been carried out. Both models are also validated and intercompared with experimentally derived laboratory data obtained by Verney et al. (2009, 2010). The dynamics of the mean size and the size distribution have been investigated by using the flocculation models based on shear-induced aggregation and fragmentation (Maerz et al., 2010). In Sec. 3.2 the novel flocculation model has been extended by aggregation due to differential settling, deposition and resuspension in combination with a dynamic model for the change of the total concentration of SPM in a water column. In a 0D version, it has been applied to the backbarrier basin of Spiekeroog island to enlighten the influence of biological processes on SPM dynamics (Maerz and Wirtz, 2009). A parameter variation has been carried out to detect seasonal shifts of the relative contribution of the driving processes and parameters that are influenced by biological processes.

- In Chap. 4, the novel distribution-based flocculation model is coupled to a 1D vertical turbulence model. In Sec. 4.1.8, it is compared to a size class-based model. A validation with experimental data is still lacking, but it is at least plausible that the size class-based model can give an indication about the ongoing SPM concentration and size dynamics as a very similar model has been successfully applied to laboratory experiments by Xu et al. (2008). Moreover, both models show qualitatively reasonable SPM concentration and size dynamics as observed typically in tidally affected areas by e. g. Jago et al. (2006); Bartholomä et al. (2009). In Sec. 4.2.2 the role of changing hydrodynamical conditions on DOM flux from aggregates into the water is investigated to gain insights into the potential role of flocs for tidally varying DOM concentrations. In Sec. 4.2 the model has been used to identify possible benefits for particle-attached bacteria due to turbulence and particle sinking. Therefore, the analysis of Logan and Hunt (1987) has been adopted and applied to the specific assumptions made for the here proposed flocculation model.

- The biological processes that influence SPM concentration and size dynamics are comprehensively discussed in Chap. 5. Furthermore, possible conclusions from the in Chap. 4 proposed future applications are drawn and dicussed. The novel flocculation model is also discussed especially regarding its advantages and disadvantages with respect to classically used SCB models. Afterwards a conclusion is given.

- Finally, a short outlook is given in Chap. 6.

Chapter 2

Model description

This chapter is structured in three parts. In the first part, a short introduction to sediment transport models for SPM dynamics will be given to embed the here presented flocculation model in a broader context. Then, the concept of the fractal-like description for the structure of cohesive sediment flocs is introduced and the classical approach for aggregation of von Smoluchowski (1916, 1917) is presented. Finally, a newly developed model is derived to resolve processes related to SPM dynamics. In particular, a 0D distribution-based model for aggregation is proposed and combined with the processes of fragmentation, deposition, resuspension and tidal exchange due to currents.

Sec. 3.2 is mainly based on this model and discusses biological influences on aggregate size and SPM dynamics (published in Maerz and Wirtz, 2009). In the second publication (Sec. 3.1; Maerz et al., 2010) the distribution-based (DB) model for aggregation and fragmentation due to shear is compared with a size class-based (SCB) flocculation model.

2.1 Sediment transport models

Usually the three-dimensional hydrostatic equations of motion with the Boussinesq approximation and the eddy viscosity assumption are used to describe geophysical coastal sea and ocean dynamics (e. g. Haidvogel and Beckmann, 1999; Burchard et al., 2004, and references therein). The numerical solution of those equations is then used as driving force for sediment transport modules.

This can be implemented with or without any feedback of the sediment load on the motion of the water (for some feedback mechanisms see e. g. Toorman, 2003). In general, one has to account for a wide range of size fractions of sediment in those models. Many sediment models therefore use more than one size class to describe the spatial and temporal evolution of the sediment distribution (e. g. Stanev et al., 2007; Warner et al., 2008). The transport of a specific sediment size class C_i (or any other concentration) is often formulated as follows

$$\frac{\partial C_i}{\partial t} + \underbrace{u\frac{\partial C_i}{\partial x} + v\frac{\partial C_i}{\partial y} + w\frac{\partial C_i}{\partial z}}_{\text{advection}} + \underbrace{\frac{\partial (v_{\mathrm{s},i} C_i)}{\partial z}}_{\text{settling}} = \underbrace{\frac{\partial}{\partial x} A_\mathrm{h} \frac{\partial C_i}{\partial x} + \frac{\partial}{\partial y} A_\mathrm{h} \frac{\partial C_i}{\partial y} + \frac{\partial}{\partial z} A_\mathrm{v} \frac{\partial C_i}{\partial z}}_{\text{turbulent diffusion}} + \text{sources} - \text{sinks} \quad . \tag{2.1}$$

Here, $\mathbf{v} = (u, v, w)$ is the velocity vector where u, v and w are the velocity components into the x, y and z direction, respectively. Furthermore, $v_{\mathrm{s},i}$ is the settling velocity of the specific size class, and A_h and A_v are the horizontal and the vertical eddy diffusivity coefficients, respectively. Sources are erosion or resuspension of sediment from the seafloor, but also processes that change the internal size distribution of the sediment, namely aggregation and fragmentation. Deposition of sediment acts as a sink, but, again, also do the processes of aggregation and fragmentation. Those internal processes are relevant for cohesive sediments, whereas larger particles ($>$ ca. 8 µm; Chang et al., 2006b) like sand do not form conglomerates.

When neglecting inertial effects of the particles, it is easier to determine the transport behaviour – the settling velocity – for a single grain of a specific size compared to a particle formed by aggregation of cohesive sediment primary particles, particulate and colloidal organic matter (POM and COM, respectively). Although several aggregates might have the same size, they can have different densities and morphologies, and hence, settle with different velocities which is due to their inhomogeneous composition and their different forming past.

The complexity of the problem is challenging many scientists scince several decades, and there is still a lack of knowledge about related pocesses and their mathematical representation in models.

2.2 The fractal concept for aggregates

When doing a literature survey on aggregate morphology, it attracts attention that natural particles are often refered to as "amorphous" (which means "without structure"; e. g. Leppard et al., 1996) or "porous" (e. g. Alldredge and Gotschalk, 1988), but also as "fractal objects" (which is a structural description for a particle; e. g. Kranenburg, 1994; Logan, 1999). These contradictionary descriptions of the aggregate' morphology *i)* point again towards the complicated nature of the problem, and *ii)* give rise to the assessment that the in the following described concept of fractality is more a powerful tool to mathematically describe, and to relate size and density of a particle to each other, than giving a perfect description of its natural morphology. Nevertheless, as aggregates results from collision of primary particles and small aggregates, the scaling relationship between their size and density often appears to be a power law at least for wide size ranges. Thus, a fractal-like description can be regarded as suitable. However, it is important to keep in mind that such a description can function as a parameterization of unknown influences of e. g. POM in sediment transport models.

For cohesive sediment particles, the fractal concept has been introduced by Kranenburg (1994). It relates the floc of diameter D to its density ρ_f via the fractal dimension d_f and the constituent primary particles of diameter D_p of the aggregate. Following Kranenburg (1994), the number of primary particles n_p in an aggregate is

$$n_\mathrm{p} \propto \left(\frac{D}{D_\mathrm{p}}\right)^{d_f} \quad . \tag{2.2}$$

Considering a uniform suspension of n aggregates in a unit water volume, the solid volume in the aggregates is given by $V_\mathrm{p,t} = n\, n_\mathrm{p}\, V_\mathrm{p}$. The volume of a

primary particle is $V_\mathrm{p} \propto D_\mathrm{p}^3$. Therefore, using Eq. (2.2),

$$n \propto \frac{V_\mathrm{p,t}}{n\, D_\mathrm{p}^3} = \frac{V_\mathrm{p,t}}{D^{d_f}\, D_\mathrm{p}^{3-d_f}} \tag{2.3}$$

As the volume of a floc is $V \propto D^3$, the total aggregate volume in the suspension (including the interstitial water) $V_\mathrm{f,t}$ is

$$V_\mathrm{f,t} \propto n\, D^3 = \frac{V_\mathrm{p,t}}{D^{d_f}\, D_\mathrm{p}^{3-d_f}}\, D^3 = V_\mathrm{p,t} \left(\frac{D}{D_\mathrm{p}}\right)^{3-d_f} \tag{2.4}$$

From mass conservation it follows

$$\rho_\mathrm{f}\, V_\mathrm{f,t} = \rho_\mathrm{p}\, V_\mathrm{p,t} + \rho\, (V_\mathrm{f,t} - V_\mathrm{p,t}) \quad , \tag{2.5}$$

where ρ is the density of the fluid. Therefore, a relationship between the primary particle size and density ρ_p, the floc diameter and the fractal dimension can be found where $\Delta\rho$ is, by definition of Kranenburg (1994), the excess floc density

$$\boxed{\Delta\rho = (\rho_\mathrm{f} - \rho) = (\rho_\mathrm{p} - \rho) \left(\frac{D_\mathrm{p}}{D}\right)^{3-d_f} \quad .} \tag{2.6}$$

2.3 Fragmentation and aggregation

In common with the process of aggregation, fragmentation[1] of aggregates internally alters the floc size distribution. Within this thesis, the expression of *flocculation* refers to both aggregation and fragmentation processes. Fragmentation can occur in different ways:

i) Erosion-like fragmentation, where small pieces of the aggregate are eroded from the outer layer of the floc. This process has been related to either the size of the aggregates (when they are smaller than the Kolmogorov microscale, which can be calculated by $\eta = (\nu^3/\epsilon)^{1/4}$ with ν

[1] The terms *fragmentation* and *break-up* are used synonymously here.

being the kinematic viscosity and ϵ is the energy dissipation rate), or to the strength of the aggregates: more compact flocs are more likely to undergo erosion (Thomas et al., 1999, and references therein)

ii) Rain drop-like break-up[2], where the aggregate is fractured into (several) smaller fragments (e. g. observable during turbulence inducing grid experiments of A. Alldredge, pers. communication).

Furthermore, zooplankton can break up aggregates during their feeding on them (in particular *Euphausia pacifica*; Dilling and Alldredge, 2000) and biological processes of disaggregation, such as animal grazing, appear even more likely to mediate the size spectrum of SPM in the open ocean than break-up due to fluid motion (Alldredge et al., 1990).

All detailed process-based models for aggregation base upon the size class-based (SCB) Smoluchowski equation (von Smoluchowski, 1916, 1917) that describes the net gain or loss of particles in a size class n_k with a given diameter and mass m_k due to aggregation processes

$$\frac{\mathrm{d}}{\mathrm{d}\,t}\,n_k(m_k) = \underbrace{\frac{1}{2}\sum_{i+j=k}\alpha_{i,j}\,n_i(m_i)\,n_j(m_j)\,I_{i,j}(m_i,m_j)}_{\text{gain due to aggregation into size class } k} \underbrace{-\,n_k(m_k)\sum_{i}^{N}\alpha_{i,k}\,n_i(m_i)\,I_{i,k}(m_i,m_k)}_{\text{loss due to aggregation out of size class } k}\quad . \tag{2.7}$$

In this form, the function α describes the collision efficiency of aggregates and has a range of $\alpha = ([0,1])$. The often as stickiness refered function α is still not understood, although there have been a few attempts to access insights into the role of e. g. algae and transparent exopolymeric particles (TEP) in the determination of its value (e. g. Kiørboe et al., 1990, 1994; Kiørboe and Hansen, 1993; Ackleh et al., 1995; Dam and Drapeau, 1995; Kahl et al., 2008). Hence, in models for aquatic systems, α is used as a parameter or, more recently, as a time series (but also independent of the aggregate size by Kahl et al., 2008). The

[2]For a review on drop fragmentation and fragmentation processes, see Villermaux (2007).

function I describes the collision frequency. Generally, three main processes can be distinguished that determine the collision frequency, in particular the kernel for Brownian motion I_{D}, aggregation due to shear I_γ and differential settling I_v. Therefore, the collision frequency can be written as a sum of all these processes

$$I = I_{\mathrm{D}} + I_\gamma + I_v \quad . \tag{2.8}$$

In the context of microaggregates and macroaggregates, Brownian motion is often neglected in modeling SPM dynamics, as it is only relevant for particles smaller than one micrometer (McCave, 1984). By using the generally used simplification of the stickiness α, Eq. (2.7) can be written in an integral form (see e. g. Jackson, 1995a)

$$\begin{aligned} \frac{\mathrm{d}}{\mathrm{d}\,t}\, n(m) \;\; = \;\; & \frac{1}{2}\,\alpha \int_0^m n(m')\, n(m-m')\, I(m', m-m')\, \mathrm{d}m' \\ & - \alpha\, n(m) \int_0^{m_\infty} n(m')\, I(m, m')\, \mathrm{d}m' \quad , \end{aligned} \tag{2.9}$$

where $\lim_{m_\infty} = \infty$. The formulation has been developed by assuming homogenuous aggregates regardless of particles of different sources, etc.

In general, most models representing aggregation describe the change of the particle distribution by using several distinct size classes (e. g. McCave, 1984; Jackson, 1990; Hill, 1992; Riebesell and Wolf-Gladrow, 1992; Dam and Drapeau, 1995; Logan et al., 1995; Ruiz, 1997; Stemmann et al., 2004a; Verney et al., 2010). For technical details of the implementation of the size class-based Smoluchowsky equation see e. g. Prakash et al. (2003); Verney et al. (2010).

2.4 Distribution-based flocculation model

In order to reduce the complexity of traditional size class-based aggregation models, a distribution-based model is proposed here that follows the moments of a given distribution, in particular the mass concentration distribution of aggregates, to reproduce the tidal variability of the distribution and hence the mean settling velocity of aggregates. The latter is one of the main key properties to understand the transport of SPM as it essentially determines the

deposition rate. The distribution-based model has been developed by using the moment closure approach of Wirtz and Eckhardt (1996)[3]. Basically, the model couples two components: The change of the total mass concentration that is formulated in a traditional way, and, as a new approach, the change of the average radius to unravel the variability of the SPM size distribution and hence the deposition rate. In the following, a short introduction to the general idea of the moment closure, presented by Wirtz and Eckhardt (1996), will be given. Subsequently, this concept will be applied for deriving a simplified model of processes relevant to changes of the floc size distribution.

2.4.1 A general introduction to the moment closure approach

In the following, we stick to the outline of this thesis and explain the moment closure approach on basis of terms relevant in SPM dynamics. However, the moment closure approach of Wirtz and Eckhardt is not restricted to applications in SPM dynamics. In fact, it is a general formulation and was formerly used e. g. to model phytoplankton succession (Wirtz and Eckhardt, 1996).

The total mass concentration C is given by

$$C = \sum_i C_i \, \Delta R_i \quad , \tag{2.10}$$

where C_i is the mass concentration density given by the SPM mass per volume and bin width ΔR_i in each size class i. Therefore, a quantity of the mass concentration, in particular the mass concentration-weighted average radius of the particle distribution $\langle r \rangle$, can be represented by

$$\langle r \rangle = \sum_i r_i \, \frac{C_i \, \Delta R_i}{C} \quad , \tag{2.11}$$

where r_i is the radius in size class i. As in general both the concentration and

[3] A recent revisiting of the moment closure approach can be found in Merico et al. (2009).

$\langle r \rangle$ can change in time, a derivative of Eq. (2.11) with respect to time leads to

$$\frac{\mathrm{d}}{\mathrm{d}\,t}\langle r \rangle = \sum_i r_i \frac{\dot{C}_i\,\Delta R_i}{C} - \frac{\dot{C}}{C}\sum_i r_i \frac{C_i\,\Delta R_i}{C} \quad , \tag{2.12}$$

where $\dot{C}_i$ and $\dot{C}$ are the time derivatives of the concentration in each size class and in total, respectively. The change of the concentration in each size class can be expressed as

$$\dot{C}_i = \hat{\mu}_i(r_i, E, \ldots) \cdot C_i \quad , \tag{2.13}$$

where $\hat{\mu}$ represents the relative growth rate that is dependent on specific quantities. Here, these quantities are in particular the radius of the size class r_i and environmental conditions E that are relevant as forcings in the model e. g. the turbulent shear rate, the tidally changing water depth, etc. Hence, the change of the quantity $\langle r \rangle$ (Eq. (2.12)) can also be expressed by

$$\frac{\mathrm{d}}{\mathrm{d}\,t}\langle r \rangle = \langle r \cdot \hat{\mu} \rangle - \langle r \rangle \cdot \langle \hat{\mu} \rangle \quad . \tag{2.14}$$

It is obvious that the change of the average radius is identically to the cross-correlation between the radius and the relative growth rate. This relation is also known as Fisher-Eigen dynamics, and hence, a correlation between the relative growth rate and the radius would lead to high changes of the average radius.

By expanding the relative growth rate $\hat{\mu}_i$ in a Taylor-series around $\langle r \rangle$ and using a moment closure leads to (see Wirtz and Eckhardt, 1996)

$$\boxed{\frac{\mathrm{d}}{\mathrm{d}\,t}\langle r \rangle \simeq \delta r^2 \cdot \frac{\mathrm{d}\,\hat{\mu}(\langle r \rangle)}{\mathrm{d}\,r}} \tag{2.15}$$

that is exact for a Gaussian concentration distribution. Temporal changes of $\langle r \rangle$ follow a local gradient of $\hat{\mu}$ and the rate of change is proportional to the gradient itself. A proportionality factor appears which is given by the variance δr^2 of the distribution. In principle, as only in a first approximation the variance is constant, a gradient dynamics for the variance can also be formulated (see below).

In general, the change of the total concentration can be expressed as

$$\dot{C} = \langle \hat{\mu} \rangle \cdot C \quad , \tag{2.16}$$

where $\langle \hat{\mu} \rangle$ is the average relative growth rate. When expanding the average relative growth rate around $\langle r \rangle$ in a Taylor-series[4] under the assumption of a Gaussian distribution (and hence neglect higher orders than the second one), Eq. (2.16) can be approximated by (see Wirtz, 1998, for details)

$$\dot{C} \approx \left(\hat{\mu}(\langle r \rangle) + \frac{1}{2} \delta r^2 \cdot \frac{\mathrm{d}^2 \, \hat{\mu}(\langle r \rangle)}{\mathrm{d} \, r^2} \right) \cdot C \quad . \tag{2.17}$$

As can be seen in Eq. (2.17), an additive correction term for the relative growth rate appears to approximate the mean relative growth rate $\langle \hat{\mu} \rangle$. This correction accounts for the contributions of higher moments to the mean relative growth rate. Here, for a Gaussian distribution, it is the second moment. But, in principle, this Taylor series has not to be cut off after the second order and other moments can appear. For this reason, a derivation for the change of the variance, based on the relative growth rate at the average of the quantity $\hat{\mu}(\langle r \rangle)$, has to take these corrections into account, and thus leads to (see Wirtz, 1998, for details)

$$\frac{\mathrm{d}}{\mathrm{d} \, t} \delta r^2 = \frac{3}{2} \delta r^4 \cdot \frac{\mathrm{d}^2 \, \hat{\mu}(\langle r \rangle)}{\mathrm{d} \, r^2} \quad , \tag{2.18}$$

again under the assumption of a Gaussian distribution. This relationship, in which the fourth moment of the distribution δr^4 occurs, will not be used in the following derivation of the flocculation model. The particular underlying distribution function that is used in the aggregation model, leads to a direct functional dependency of the variance on $\langle r \rangle$. However, as this might be not always the case, it is useful to note the possible derivation for the change of the variance *i)* to give a more comprehensive view on the moment closure approach and *ii)* to show its capability for a diversity of applications.

[4] where the first moment is always zero for the average

2.4.2 Formulation of the aggregation models

In the following, a more detailed description of the derivation of the models for aggregation due to shear and differential settling will be given than has been done in the publications (see Chap. 3). In order to do so, the main underlying assumptions are summarized in the part below.

As the moment closure approach, introduced in Sec. 2.4.1, was developed for mass distributions, the Smoluchowski equation (Eq. (2.9)) has to be rewritten for the concentration $C(m)$ of aggregates with mass m

$$\begin{aligned}\frac{\mathrm{d}}{\mathrm{d}\,t}\,C(m) &= \frac{1}{2}\,\alpha\,m\int_0^m n(m')\,n(m-m')\,I(m',m-m')\,\mathrm{d}m' \\ &\quad -\alpha\,C(m)\int_0^{m_\infty} n(m')\,I(m,m')\,\mathrm{d}m' \quad . \end{aligned} \tag{2.19}$$

Furthermore, the relative growth rate $\hat{\mu}$, defined by

$$\hat{\mu} = \frac{\dot{C}(m)}{C(m)} \quad , \tag{2.20}$$

is needed to apply the moment closure approach developed by Wirtz and Eckhardt (1996). This leads to

$$\begin{aligned}\hat{\mu} &= \frac{\alpha}{2\,n(m)}\int_0^m n(m')\,n(m-m')\,I(m',m-m')\,\mathrm{d}m' \\ &\quad -\alpha\int_0^{m_\infty} n(m')\,I(m,m')\,\mathrm{d}m' \quad . \end{aligned} \tag{2.21}$$

As it is not possible to integrate neither the Smoluchowski equation Eq. (2.9) for aggregation nore Eq. (2.21) in a general way, an assumption for the underlying aggregate number distribution is necessary.

In the next steps, such a function has to be chosen and, furthermore, tested whether it is possible to solve the integrals in Eq. (2.21) for the given function. In the here presented case, it is not possible to do so with the used function (see below) directly. For this reason, a further treatment is chosen to simplify the problem. Eq. (2.21) is written in such a way that the aggregate number distributions $n(m)$ becomes directly $n(r)$, and hence dependent on the floc

radius r by using exceptionally in this step the relation $m = r$

$$\hat{\mu} = \frac{\alpha}{2\,n(r)} \int_0^r n(r')\,n(r-r')\,I(r', r-r')\,\mathrm{d}r' - \alpha \int_0^{r\infty} n(r')\,I(r, r')\,\mathrm{d}r' \quad . \tag{2.22}$$

Hence, mass conservation is not fulfilled anymore. But this will be ensured afterwards (see below).

As the model is mainly developed for the German Wadden Sea, in particular the backbarrier basin of Spiekeroog island, an exponential aggregate number distribution $n(r)$ is chosen in agreement with data published by Lunau et al. (2006, see also Fig. 3.13 on page 104)

$$\boxed{n(r) = N_0 \exp(-\beta r) \quad .} \tag{2.23}$$

N_0 gives the value, where the number distribution crosses the y-axis and β is the slope of the distribution (see also Fig. 2.1). Furthermore, the aggregate radius r denotes the radius of a floc with a given fractal dimension d_f and hence, it is not the radius of a massive sphere. The fractal theory for aggregates, proposed by Logan (1999) and Kranenburg (1994) that is already introduced in Sec. 2.2, is applied for the solid mass of an aggregate $w(r)$ of radius r

$$w(r) = w_0\, r^{d_f} \quad , \tag{2.24}$$

where $w_0 = 2^{d_f}\,\rho_\mathrm{p}\,\pi\,D_\mathrm{p}^{3-d_f}/6$ is a radius-weight relation factor originating from the fractal scaling relationship. It is composed of the diameter of the primary particles D_p and their density ρ_p. For simplicitly, the lower borders of Eq. (2.19) and the in the following derived concentration distribution has has not been adapted to the fractal scaling approach (this would imply: $\int_0^x$ becomes $\int_{D_\mathrm{p}/2}^x$). Admittedly, this can introduce some small complications in further model applications as in Sec. 4.2. Ongoing from this, the aggregate mass distribution can be written as

$$C(r) = n(r) \cdot w(r) \quad , \tag{2.25}$$

and hence the total concentration C is given by

$$C = \int_0^\infty n(r)\, w(r)\, \mathrm{d}r \quad . \tag{2.26}$$

Its average radius can be calculated by

$$\langle r \rangle = \frac{\int_0^\infty r \cdot n(r)\, w(r)\, \mathrm{d}r}{\int_0^\infty n(r)\, w(r)\, \mathrm{d}r} \tag{2.27}$$

that yields by usage of the Gamma function, defined as

$$\Gamma(x+1) = \int_0^\infty \exp(-t)\, t^x\, \mathrm{d}t \quad , \tag{2.28}$$

a relation between the average radius of the concentration distribution $\langle r \rangle$, the slope of the number distribution β and the fractal dimension d_f of the particles

$$\langle r \rangle = \frac{d_f + 1}{\beta} \quad . \tag{2.29}$$

Furthermore, a relation between the variance of the concentration distribution δr^2, the fractal dimension and the average radius can be found

$$\delta r^2 = \frac{\langle r \rangle^2}{d_f + 1} \quad . \tag{2.30}$$

With this set of equations described above, it is now possible to solve the integrals in Eq. (2.22) for different types of aggregation processes. In the following, first, the formulation for aggregation due to shear will be derived, and second, for aggregation due to differential settling (for further calculations regarding the different kernels see also App. A.3 and A.4).

Formulation for aggregation due to shear

For aggregation due to shear, either the rectilinear kernel

$$I_\gamma(r, r') = 1.3\, \gamma\, (r + r')^3 \tag{2.31}$$

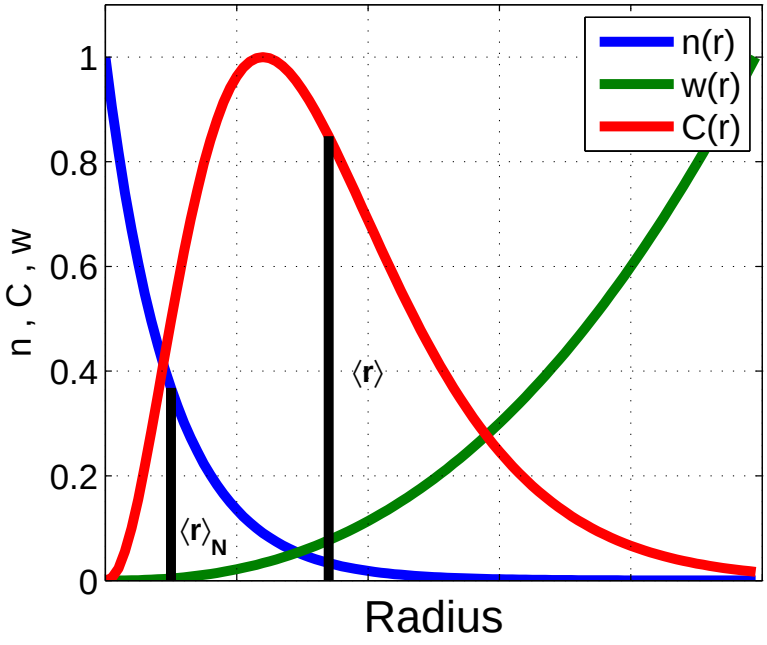

Figure 2.1: An exemplary aggregate number distribution $n(r)$, weight of the aggregates $w(r)$ and the resulting concentration distribution $C(r)$ - all normalized to 1. Additionally, the number-weighted average radius $\langle r \rangle_{\mathrm{N}}$ and the mass-weighted radius $\langle r \rangle$ are shown. The latter is used in the flocculation model.

or the curvilinear kernel

$$I_\gamma(r, r') \;=\; 10\,\gamma\,(r + r')^2\,r \tag{2.32}$$

(Jackson and Lochmann, 1993) can be used. Further kernels for non-spherical particles are described by e. g. (Jackson and Lochmann, 1993). Both, the recti- and curvilinear kernel, describe the collision frequency between two spheres, but assume different types of interaction between them determined by hydraulic properties of the interacting particles. The underlying assumption for the rectilinear kernel is the limit of a totally porous sphere where the area of a circle given by the radii of the particles is taken into account for the calculation of the interaction. In the case of the curvilinear kernel, a solid sphere

is assumed, and hence, the water displaced by the particle pushes the other particle away for some amount. Therefore, these kernels can be regarded as boundaries for the interaction range of spherical particles that can appear in any system[5]. In the following, the curvilinear kernel is used to describe how to apply the moment closure approach of Wirtz and Eckhardt (1996) on the Smoluchowski equation.

Ongoing from Eq. (2.22)

$$\begin{aligned}\hat{\mu} &= \frac{\alpha}{2\,N_0\,\exp(-\beta r)} \\ &\quad \cdot \int_0^r N_0\,\exp(-\beta r')\,N_0 \exp(-\beta(r-r'))\,10\,\gamma\,(r'+(r-r'))^2\,(r-r')\,\mathrm{d}r' \\ &\quad - \alpha \int_0^{r_\infty} N_0\,\exp(-\beta r')\,10\,\gamma\,(r'+r)^2\,r\,\mathrm{d}r' \end{aligned} \tag{2.33}$$

the integrals can be solved which leads to

$$\begin{aligned}\hat{\mu} &= \frac{5}{2}\,\alpha\,N_0\,\gamma\,r^4 \\ &\quad - \frac{10\,\alpha\,N_0\,\gamma\,r}{\beta^3} \\ &\quad \cdot \Bigg(- \exp\left(-\beta r_\infty\right) \cdot \left(\beta^2\,r^2 + 2\,\beta\,r + 2 \; + 2\,\beta^2\,r_\infty\,r + 2\,\beta\,r_\infty + r_\infty^2\,\beta^2\right) \\ &\qquad + \beta^2\,r^2 + 2\,\beta\,r + 2\Bigg) \quad . \end{aligned} \tag{2.34}$$

With the assumption of a decreasing particle number with (without limit) increasing radius

$$r_\infty \;\rightarrow\; \infty \quad , \tag{2.35}$$

$$\beta \;>\; 0 \quad , \tag{2.36}$$

[5] disregarding the ongoing research on the development for kernels that take inertial effects of particles into account (see e. g. Sundaram and Collins, 1997; Xue et al., 2008; Ayala et al., 2008a,b).

it follows for the relative mass change due to aggregation

$$\hat{\mu} = \frac{5\,\alpha\,N_0\,\gamma\,r}{2\,\beta^3}\left(\beta^3\,r^3 - 4\,\beta^2\,r^2 - 8\,\beta\,r - 8\right) \quad . \tag{2.37}$$

In Fig. 2.2, the relative concentration changes according to Eq. (2.37) in dependence on $\langle r \rangle$ and d_f are shown. It is obvious that the relative growth rate

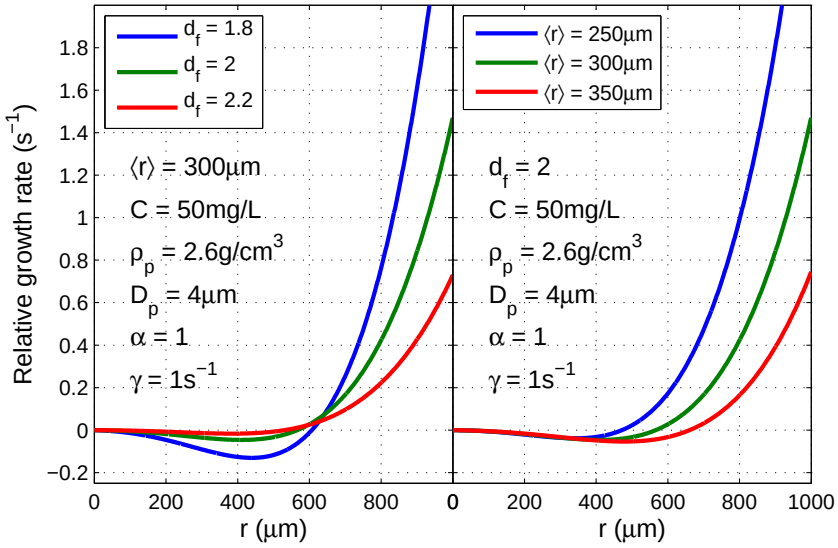

Figure 2.2: The relative concentration change (according to Eq. (2.37)) for typical values that can be found in coastal areas (apart from $\alpha = 1$ that has been chosen for simplicity).

changes with the radius r of the aggregates. There is a loss of concentration for smaller particles (aggregating into larger particles) and a thus a gain of larger flocs. The lower the fractal dimension, the higher the gain of larger flocs while a change of $\langle r \rangle$ mainly shifts the turning point from negative to positve changing rates. It is not possible to use the relative growth rate of Eq. (2.37) directly in Eq. (2.15), as this would lead to a negative change of the average radius due to shear aggregation which is not in agreement with the process of aggregation. Therefore, following Eq. (2.17) in Sec. 2.4.1, a Taylor expansion of second order for the mean relative growth rate $\langle \hat{\mu}(\langle r \rangle) \rangle$ is used

$$\langle \hat{\mu}(\langle r \rangle) \rangle \;\approx\; \hat{\mu}(\langle r \rangle) + \underbrace{y'\,\delta r^2}_{y_\gamma} \cdot \frac{\partial^2}{\partial\, r^2}\,\hat{\mu}(\langle r \rangle) \;=\; 0 \quad . \tag{2.38}$$

For mass conservation, the mean relative growth rate must fulfill the condition to be zero as the process of aggregation does not change the total concentration. In the context of Eq. (2.17), y' would be $y' = 0.5$. Instead, a factor y_γ is introduced that collects higher moments of the distribution. y_γ can easily be assessed by

$$y_\gamma = -\frac{\hat{\mu}}{\frac{\partial^2}{\partial r^2}\hat{\mu}} \quad . \tag{2.39}$$

In order to solve this equation, the derivatives of the relative growth rate have to be calculated

$$\frac{\partial}{\partial r}\hat{\mu}(r) = \frac{10\,\alpha\,N_0\,\gamma}{\beta^3}\left(\beta^3 r^3 - 3\,\beta^2 r^2 - 4\,\beta r - 2\right) \tag{2.40}$$

$$\frac{\partial^2}{\partial r^2}\hat{\mu}(r) = \frac{10\,\alpha\,N_0\,\gamma}{\beta^2}\left(3\,\beta^2 r^2 - 6\,\beta r - 4\right) \tag{2.41}$$

$$\frac{\partial^3}{\partial r^3}\hat{\mu}(r) = \frac{60\,\alpha\,N_0\,\gamma}{\beta}\left(\beta r - 1\right) \quad . \tag{2.42}$$

By using Eq. (2.37) and (2.41) for $r = \langle r \rangle$ together with Eq. (2.29) in Eq. (2.39), the moment collecting factor becomes a polynomial of d_f and $\langle r \rangle$

$$y_\gamma = -\frac{1}{4}\langle r \rangle^2 \cdot \frac{d_f^3 - d_f^2 - 13\,d_f - 19}{(d_f + 1)\cdot(3\,d_f^2 - 7)} \quad . \tag{2.43}$$

Now, one can calculate the change of the average radius due to shear aggregation by using the gradient dynamics of Eq. (2.15). For this, the mean relative growth rate in combination with the factor found in Eq. (2.43) are used in Eq. (2.15)

$$\frac{\mathrm{d}}{\mathrm{d}\,t}\langle r \rangle\bigg|_{\mathrm{agg}\gamma} = \delta r^2 \cdot \frac{\partial}{\partial r}\left(\hat{\mu}(r = \langle r \rangle) + y_\gamma \frac{\partial^2}{\partial r^2}\hat{\mu}(r = \langle r \rangle)\right) \quad . \tag{2.44}$$

In order to further simplify this equation after insertion of the relevant derivatives of the relative growth rate (Eq. (2.40) and (2.42)), N_0 can be expressed in terms of the total concentration C by using and re-arranging Eq. (2.26)

$$N_0 = \frac{C\,(d_f + 1)^{d_f + 1}}{w_0\,\langle r \rangle^{d_f + 1}\,\Gamma(d_f + 1)} \quad . \tag{2.45}$$

Finally, one receives for the change of the average radius by aggregation due to shear based on the assumption of the curvilinear kernel

$$\boxed{\left.\frac{\mathrm{d}}{\mathrm{d}\,t}\,\langle r\rangle\right|_{\mathrm{agg}\gamma} = \alpha\,\gamma\,K_\gamma(d_f)\,\frac{C}{w_0}\,\langle r\rangle^{4-d_f} \quad .} \tag{2.46}$$

K_γ is a function of the fractal dimension that collects higher orders

$$K_\gamma(d_f) = \frac{5\,(d_f+1)^{d_f-2}}{(3\,d_f^2-7)\,\Gamma(d_f+2)}\,(3\,d_f^5-14\,d_f^3+48\,d_f^2+155\,d_f+112) \quad . \tag{2.47}$$

Further information on and the approximation of the function K_γ can be found in App. A.3 that are discussed in 5.2.

Formulation for aggregation due to differential settling

Like for aggregation due to shear, two different kernels are used in literature (e. g. Jackson and Lochmann, 1993) to describe the collision frequency of spherical particles due to differential settling. The underlying assumptions for each kernel are shown in Fig. 2.3, where either the flow around the larger particle is considered (the curvilinear case) or not (the rectilinear case) leading to a smaller and a larger capture cross section, respectively.

The rectilinear kernel for aggregation due to differential settling is given by

$$I_v(r,r') = \pi\,(r+r')^2\,|v_\mathrm{s}(r)-v_\mathrm{s}(r')| \quad , \tag{2.48}$$

and the curvilinear kernel by

$$I_v(r,r') = \frac{1}{2}\,\pi\,r^2\,|v_\mathrm{s}(r)-v_\mathrm{s}(r')| \quad . \tag{2.49}$$

In order to solve the integrals of Eq. (2.22), the settling velocity v_s of an aggregate has do be defined to be used in the kernels. The settling velocity of suspended particles can be described by the Stokes law

$$v_\mathrm{s}(D) = \frac{1}{18\,\mu}\,(\rho_\mathrm{f}-\rho)\,g\,D^2 \quad , \tag{2.50}$$

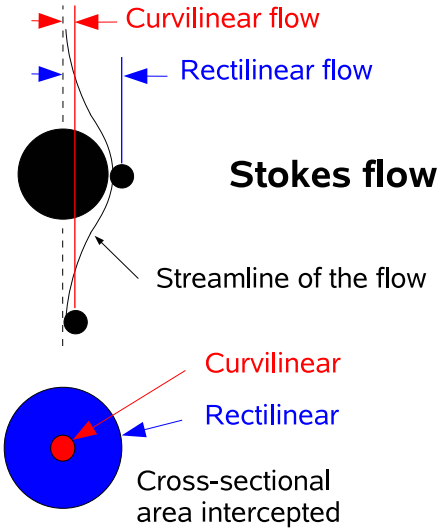

Figure 2.3: Underlying assumptions for the rectilinear and the curvilinear kernel for differential sinking (re-drawn after Jackson and Lochmann, 1993). The curvilinear kernel takes the displacement of the smaller particle due to the flow field around the larger particle into account while the rectilinear kernel does not. Stokes flow is present when the particles' Reynolds number is $Re < 1$ (see also Sec. 4.2).

where μ is the dynamic viscosity, g is the gravitational accelaration constant ρ_f and ρ are the density of the floc (of diameter D), and the water, respectively. As the model is developed for aggregates treated as fractal objects according to Kranenburg (1994, see also Sec. 2.2), the aggregate density

$$\rho_\mathrm{f} = (\rho_\mathrm{p} - \rho) \left(\frac{D_\mathrm{p}}{D}\right)^{3-d_f} + \rho \tag{2.51}$$

can be expressed as a relation between the diameter of the primary particles D_p, their density ρ_p and the fractal dimension of the aggregate. When inserting

ρ_f into Eq. (2.50), one receives a settling velocity for fractal aggregates

$$v_\mathrm{s}(r) \;=\; \frac{2^{d_f-1}}{18\,\mu}\,(\rho_\mathrm{p}-\rho)\,g\,D_\mathrm{p}^{3-d_f}\,r^{d_f-1} \quad . \tag{2.52}$$

In this work, only the curvilinear kernel for aggregation due to differential settling is used to develop a formulation for the change of the average radius due to this process. Starting again from Eq. (2.22)

$$\begin{aligned}\hat{\mu} \;=\; & \frac{\alpha}{2\,N_0\,\exp(-\beta\,r)}\int_0^r N_0\,\exp(-\beta\,r')\,N_0\,\exp(-\beta\,(r-r')) \\ & \qquad \cdot\,\frac{1}{2}\,\pi\,(r-r')^2\,\left|v_\mathrm{s}(r-r')-v_\mathrm{s}(r')\right|\,\mathrm{d}r' \\ & -\alpha\int_0^{r_\infty} N_0\,\exp(-\beta\,r')\,\frac{1}{2}\,\pi\,r^2\,\left|v_\mathrm{s}(r)-v_\mathrm{s}(r')\right|\,\mathrm{d}r' \quad ,\end{aligned} \tag{2.53}$$

One would not be able to integrate this equation generally by using as settling velocity the fractal approach derived in Eq. (2.52). The solution of the integrals is only possible for a given fractal dimension. For this reason, another treatment is chosen to derive a general solution for aggregation due to differential settling that is analytically incorrect. First, Eq. (2.53) will be solved for a non-fractal sphere and hence, with the classical Stokes settling velocity. Secondly, a mean effective density $\langle\rho_\mathrm{f}\rangle$ is calculated and introduced in the solution of Eq. (2.53) as density for the aggregates. As mentioned above, this treatment is analytically incorrect, but i) gives a possibility to introduce a general dependency of the aggregation due to different settling on the fractal dimension in a reasonable form (the more looser the aggregate is, the less is the effective density) and ii) is totally valid in the limit of $\lim_{d_f\to 3}$ because $\lim_{d_f\to 3}\langle\rho_\mathrm{f}\rangle = \rho_\mathrm{p}$ (see Eq. (2.61) below).

Eq. (2.53) is treated similar to the derivation of the formulation for aggregation due to shear. By distinguishing between the cases $r > r'$ and $r < r'$ the integrals can be splitted in two parts with different lower and upper boundaries. After this treatment, the integrals can be solved. Again, the assumption of

$$r_\infty \;\to\; \infty \quad , \tag{2.54}$$

$$\beta \;>\; 0 \tag{2.55}$$

is used to simplify the relative growth rate that leads to

$$\hat{\mu} = F \left(\frac{3}{32} r^5 - \frac{r^2 \left(\beta^2 r^2 - 2 + 4 \exp(-\beta r) + 4 \beta r \exp(-\beta r)\right)}{\beta^3} \right) \tag{2.56}$$

with

$$F = \frac{1}{2} \alpha N_0 \pi \frac{2}{9 \mu} (\rho_\mathrm{f} - \rho) g \quad . \tag{2.57}$$

As the second order closure would lead to a negative change of the $\langle r \rangle$ (which is physically not realistic), a fourth order closure is chosen to treat this problem. One receives for the change of the average radius due to differential settling with a curvilinear kernel under the assumption of Stokes settling

$$\boxed{\frac{\mathrm{d}}{\mathrm{d}\, t} \langle r \rangle \Big|_{\mathrm{aggv}} = \alpha \pi K_\mathrm{v} \frac{C}{w_0} \frac{(\rho_\mathrm{f} - \rho)}{\mu} \langle r \rangle^{5 - d_f} \quad ,} \tag{2.58}$$

where K_v is given by

$$\begin{aligned} K_\mathrm{v} \quad = \quad & \frac{(d_f + 1)^{d_f - 2}}{216\, \Gamma(d_f + 2)} \\ & \cdot \left(\sum_{i=0}^{4} b_i\, d_f^i + \exp(-d_f - 1) \sum_{i=0}^{7} c_i\, d_f^i + \exp(-2 d_f - 2) \sum_{i=0}^{4} d_i\, d_f^i \right) \\ & \cdot \left(-45\, d_f + 51 + \exp(-d_f - 1) \sum_{i=0}^{3} e_i\, d_f^i \right)^{-1} \end{aligned} \tag{2.59}$$

with: $b_0 = -24615$, $b_1 = -12465$, $b_2 = 6174$ $b_3 = 675$, $b_4 = -405$, $c_0 = -34236$, $c_1 = -137496$, $c_2 = -74376$, $c_3 = 40164$, $c_4 = 10020$, $c_5 = -3216$, $c_6 = -96$, $c_7 = 36$, $d_0 = -21504$, $d_1 = -75776$, $d_2 = -25600$, $d_3 = 7168$, $d_4 = 3072$, $e_0 = 96$, $e_1 = 144$, $e_2 = -128$, $e_3 = 16$. More information as well as their approximation and discussion on K_v are presented in App. A.4 and Sec. 5.2, respectively.

For an aggregate with a fractal dimension of $d_f = 3$, the effective density ρ_f should be equal to the density of the primary particles ρ_p. But for aggregates of fractal dimensions smaller than $d_f = 3$, the effective density decreases rapidly with decreasing fractal dimensions. Hence, the settling velocity decreases and therefore the aggregation probability due to differential settling. To consider

this relationship, the effective density ρ_f is now calculated as a mass-weighted mean effective density $\langle\rho_\mathrm{f}\rangle$ (see also Eq. (2.51))

$$\langle\rho_\mathrm{f}\rangle = \frac{\int_0^\infty n(r)\, w(r)\, \rho_\mathrm{f}(r, d_f)\, \mathrm{d}r}{\int_0^\infty n(r)\, w(r)\, \mathrm{d}r} \quad , \tag{2.60}$$

and hence

$$\boxed{\langle\rho_\mathrm{f}\rangle = \frac{\frac{1}{8}\,(d_f+1)^{3-d_f}\, D_\mathrm{p}^{3-d_f}\, 2^{d_f}\, \Gamma(2\,d_f-2)\,(\rho_\mathrm{p}-\rho)}{\langle r\rangle^{3-d_f}\,\Gamma(1+d_f)} + \rho \quad .} \tag{2.61}$$

This equation results in an effective density of $\rho_\mathrm{f} = \rho_\mathrm{p}$ for a fractal dimension of $d_f = 3$ and $\langle r\rangle \geq D_\mathrm{p}/2$. The mean density for different fractal dimensions and $\langle r\rangle$ is shown in Fig. 2.4. By using this relation as effective density in

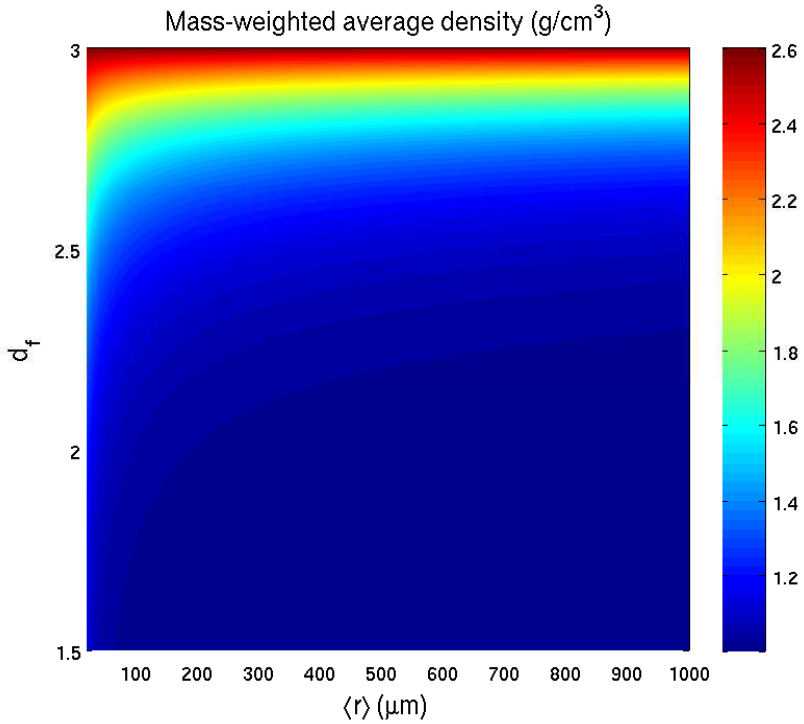

Figure 2.4: The mean density of flocs calculated from Eq. (2.61) with $D_\mathrm{p} = 4\,\mu\mathrm{m}$, $\rho_\mathrm{p} = 2.6\,\mathrm{g\,cm^{-3}}$ and $\rho = 1.0\,\mathrm{g\,cm^{-3}}$ for different, but in their value observable $\langle r\rangle$ and d_f.

Eq. (2.58) one yields

$$\boxed{\left.\frac{\mathrm{d}}{\mathrm{d}\,t}\,\langle r\rangle\right|_{\mathrm{aggv}} = \alpha\,\pi\,K_{\mathrm{v}}\,\frac{C}{w_0}\,\frac{(\langle\rho_{\mathrm{f}}\rangle-\rho)}{\mu}\,\langle r\rangle^{5-d_f}} \qquad (2.62)$$

as relationship for the change of the average radius due to differential settling. Owing to the dependency of $\langle\rho_{\mathrm{f}}\rangle$ on $\langle r\rangle$, the change of $\langle r\rangle$ by aggregation due to differential settling is always

$$\left.\frac{\mathrm{d}}{\mathrm{d}\,t}\,\langle r\rangle\right|_{\mathrm{aggv}} \propto \langle r\rangle^2 \quad , \qquad (2.63)$$

which is in the power higher than the aggregation due to shear, when $d_f > 2$. In sum, the change of $\langle r\rangle$ due to aggregation by differential settling depends not only on the $\langle r\rangle$, but especially also on the density difference between the flocs and the ambient water. The higher the density of flocs compared to the fluid, the higher is the sinking velocity. This also leads to a higher discrepancy of sinking velocities between smaller and larger flocs which results in a higher collision frequency and thus faster growth of flocs.

For a further discussion about the treatment, please refer to Sec. 5.2.

2.4.3 Fragmentation

A main task of this thesis was to derive a practicable model to describe flocculation processes. As there are only little information about the fragmentation process (Stemmann et al., 2004a), a simplification of the model of Winterwerp (1998) was chosen to depict the process of fragmentation. Therefore, the change of the $\langle r\rangle$ due to fragmentation is given by

$$\boxed{\left.\frac{\mathrm{d}}{\mathrm{d}\,t}\,\langle r\rangle\right|_{\mathrm{break}} = f_{\mathrm{b}}\,\gamma^b\,\langle r\rangle^q \quad , \qquad (2.64)}$$

where f_{b} is a specific factor for break-up, and b and q are the powers for the shear and radius dependency, respectively. The power for the shear was set to $b = 1.5$, which is in a good agreement with several experimental studies (e. g. Flesch et al., 1999) and dimensional analysis (Winterwerp, 1998). Furthermore,

in agreement with the simplified model of Winterwerp (1998), the power for the radius was set to $q = 3$.

The set of equations for aggregation and fragmentation due to shear was used to investigate the distribution-based model in comparison to a size class-based model and experimental data. This work is described in Sec. 3.1 and gives a better understanding of the underlying equations and their behaviour.

In the following paragraphs, a description is given for the coupling of the flocculation model to other processes that are relevant in SPM dynamics used in Sec. 3.2.

2.5 Coupling the flocculation model with other processes

From the elaborations above, a dynamical description for the change of average aggregate size due to flocculation processes was found. Indeed, these are only one, but an important part of SPM size dynamics. Also sedimentation affects the average size of aggregates. Resulting from settling, deposition takes place. Resuspension and lateral transport processes can also alter the aggregate distribution, and hence, the mean size of flocs. These processes will be derived in the following with respect to the change of the average size. However, some more specific processes like e. g. the evolution of fluffy layers (Winterwerp, 2002) and their consolidation (for modeling approaches of consolidation see e. g. de Boer et al., 2007) are not revisited.

In this section, derivations of differential equations for the above mentioned processes are proposed for a 0D framework. They are used in the publication in Sec. 3.2 (Maerz and Wirtz, 2009). Such a simple 0D set of ordinary differential equations possesses the opportunity to perform an extensive parameter variation to assess how biological processes may influence the SPM dynamics. This gives hints for the importance of biological processes on the influenced parameters and the models' outcomes. However, as a spatial representation of SPM dynamics is desirable, in Sec. 4.1 the DB model is explicitly coupled

to the 1D vertical hydrodynamical model SiAM (developed by Le Hir et al., 2001). The coupling of the DB model in terms of partial differential equations is described in detail in Sec. 4.1. This is due to the need of further assumptions for the dynamic transport of such a property as the $\langle r \rangle$ that cannot be described as easy as for variables like e. g. the SPM concentration. In Sec. 4.1 the DB model is compared to a size class-based (SCB) model run whose parameter set is based on its 0D application in Sec. 3.1 (published in Maerz et al., 2010).

2.5.1 Settling and deposition

As already described above, and in agreement with Stokes' law, the size and the density of aggregates determine the settling velocity of flocs and therefore the vertical flux of SPM and its deposition. In contrast to a size class-based model, where the settling velocity can be derived for each single size class by using

$$v_\mathrm{s}(r) = \frac{2^{d_f-1}}{18\,\mu}\,(\rho_\mathrm{p}-\rho)\,g\,D_\mathrm{p}^{3-d_f}\,r^{d_f-1} \tag{2.65}$$

(refer for derivation to Eq. (2.52)), a mean settling velocity has to be derived to calculate the total vertical flux. A relation can be found for the mass-weighted mean settling velocity again under the assumption of an exponential number distribution and a fractal behaviour of aggregates

$$\langle v_\mathrm{s} \rangle = \frac{\int_0^\infty n(r)\,w(r)\,v_\mathrm{s}(r)\,\mathrm{d}r}{\int_0^\infty n(r)\,w(r)\,\mathrm{d}r} \quad , \tag{2.66}$$

which leads after some elaborations to

$$\boxed{\langle v_\mathrm{s} \rangle = \frac{2^{d_f-1}}{18\,\mu}\,(\rho_\mathrm{p}-\rho)\,g\,D_\mathrm{p}^{3-d_f}\,\langle r \rangle^{d_f-1} \cdot \frac{2^{2\,d_f-1}\,(d_f+1)^{1-d_f}\,\Gamma(d_f+\frac{1}{2})}{d_f\,\sqrt{\pi}}} \quad . \tag{2.67}$$

In comparison to Eq. (2.65), it is obvious that a new term occurs. The mean settling velocity therefore cannot necessarily directly derived by using $r = \langle r \rangle$ in Eq. (2.65), refer also to Fig. 2.5. The new term reflects the different contributions of aggregate sizes to the mean sinking velocity. While smaller flocs

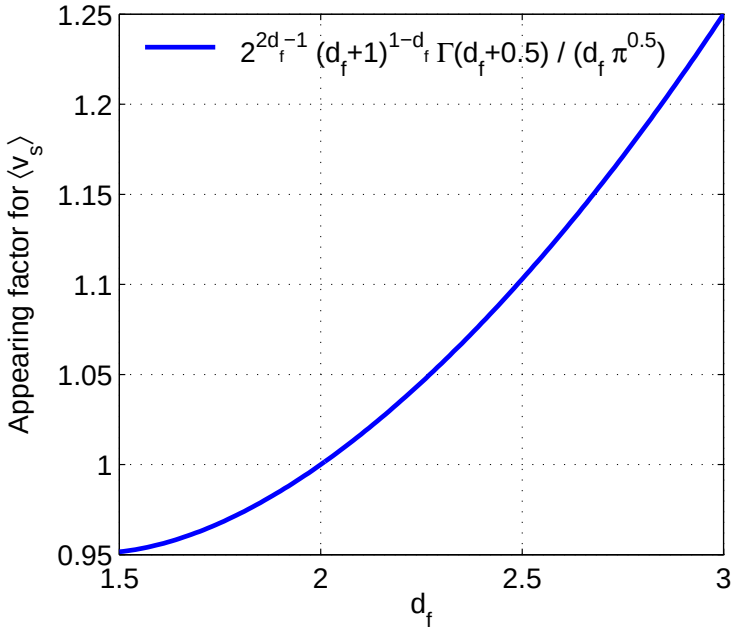

Figure 2.5: The appearing term for the mean sinking velocity derived in Eq. (2.67).

sink slowlier than large flocs, they are more numerous. The contribution to $\langle v_\mathrm{s} \rangle$ of flocs smaller or larger than $\langle r \rangle$ therefore varies with the underlying distribution that is linked to d_f. The new term hence accounts for the distributational contribution to the mean settling velocity. For fractal dimensions unequal two, the term has to be considered. This is especially true for large fractal dimensions.

In earlier works, the deposition flux F_dep was considered as a function of the bottom shear stress τ and its critical value for deposition τ_c according to Krone (1962)

$$F_\mathrm{dep} = \langle v_\mathrm{s} \rangle \, C \left(1 - \frac{\tau}{\tau_\mathrm{c}} \right) \quad . \tag{2.68}$$

In recent publications (e. g. Winterwerp, 2007; Sanford, 2008), the deposition has been found or calculated as beeing independent of any critical shear stress for deposition. However, this is still a matter of debate (Ha and Maa, 2009). Here, in a 0D framework under an assumption of a homogeneously mixed water column, the change of the total concentration due to deposition is considered

by

$$F_{\mathrm{dep}} = \frac{C\,\langle v_{\mathrm{s}}\rangle}{h} \tag{2.69}$$

according to Winterwerp (2007) where h is the water depth. Due to the dependence of $\langle v_{\mathrm{s}}\rangle$ on $\langle r\rangle$, flocculation processes affect the vertical fluxes of SPM. A more realistic representation of the deposition flux in spatial applications can either be achieved by an explicit vertical representation of a water column (as introduced in Sec. 4.1) or, when thinking about a vertically integrated approach by e. g. Pleskachevsky et al. (2005), by taking vertical SPM distributions implicitly into account.

Larger particles settle faster than smaller ones. Therefore, the mean size of the aggregates also changes with settling and deposition. Based on Eq. (2.69), one can either use Eq. (2.12) or Eq. (2.15) to derive a formulation for the change of the average radius by deposition. In the first case it yields (see also App. A.1)

$$\left.\frac{\mathrm{d}}{\mathrm{d}\,t}\langle r\rangle\right|_{\mathrm{dep}} = \frac{F\,\langle r\rangle^{d_f}}{h}\,\frac{2^{2\,d_f-1}\,\Gamma(d_f+1)}{d_f\,\sqrt{\pi}}\cdot\frac{d_f-1}{(d_f+1)^{d_f}}\quad, \tag{2.70}$$

and in the second case it is

$$\left.\frac{\mathrm{d}}{\mathrm{d}\,t}\langle r\rangle\right|_{\mathrm{dep}} = \frac{d_f-1}{d_f+1}\,\frac{F\,\langle r\rangle^{d_f}}{h}\quad, \tag{2.71}$$

where $F = 2^{d_f-1}\,(\rho_{\mathrm{p}}-\rho)\,g\,D_{\mathrm{p}}^{3-d_f}\,/\,(18\,\mu)$. Comparing both approaches for typical fractal dimensions (see Fig. 2.6), it is obvious that the distribution-based approach is close or even exact compared to the directly derived change due to deposition by using Eq. (2.12). It shows that the distribution-based approach is capable to well reproduce the deposition dynamics[6].

[6]When taking into account that the fractal description of an aggregate is also only an approximation, it is most likely that a modified shape or composition of such an aggregate would lead to much higher deviations from the directly derived fluxes than the deviation due to the gradient dynamics approach.

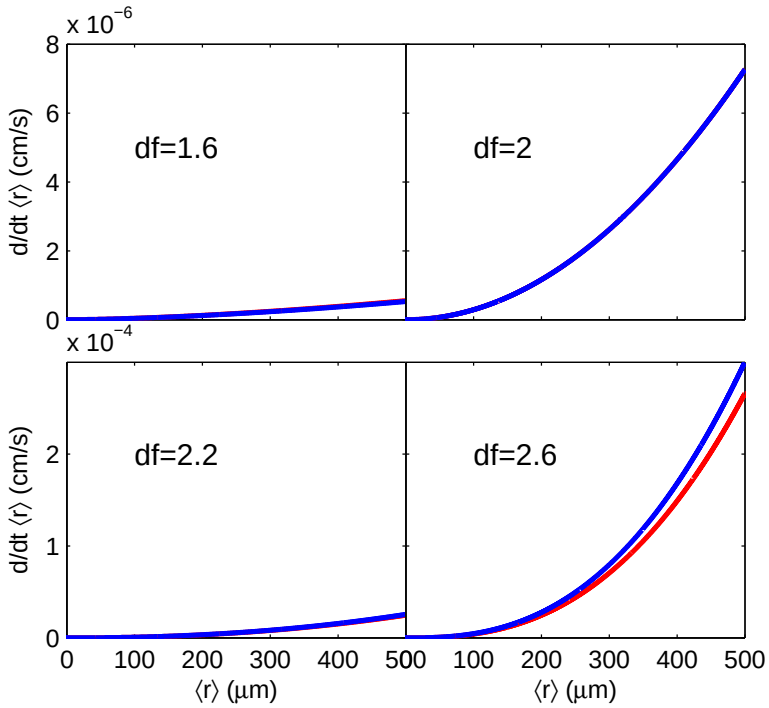

Figure 2.6: Comparison between the directly (Eq. (2.70); blue line) and the distribution-based derived formulation for deposition (Eq. (2.71); red line) for different fractal dimensions ($h = 8\,\mathrm{m}$, $\mu = 0.01\,\mathrm{g\,cm^{-1}\,s^{-1}}$, $D_\mathrm{p} = 4\,\mu\mathrm{m}$, $\rho_\mathrm{p} = 2.6\,\mathrm{g\,cm^{-3}}$).

2.5.2 Resuspension / erosion

The antagonistic process to deposition, described in the last section, is the resuspension / erosion of sediment from the sea floor. These processes are strongly dependent on the bottom shear stress, but are also determined by several factors like the consolidation state of the sediment, the grain size distribution in the sediment that might lead to armouring (cf. e. g. to Lee et al., 2007), but also to biological processes that either stabilize or destabilize the sediment. It is observed that the phytobenthos and microbial biofilms tend to stabilize the sediment, whereas benthic fauna tend to destabilize the sediment (Black et al., 2002).

In the present work, a common formulation in sediment transport models (e. g. used in Stanev et al., 2007) is used to describe the processes of resuspension and erosion (Partheniades, 1984)

$$F_{\mathrm{res}} = \frac{M_0}{h}\left(\frac{\tau}{\tau_{\mathrm{c}}} - 1\right) \quad , \tag{2.72}$$

where M_0 is the erosion rate at twice the critical bottom shear stress.

Particles that are eroded from the sediment can have different distributions and densities compared to the particles in the water column. In the present study, due to lack of knowledge about the most likely different composition and structure of eroded aggregates, it is only accounted for a different mean size. Under this assumption, Eq. (2.12) on page 38 can be used in combination with Eq. (2.72) to yield (see also App. A.1)

$$\left.\frac{\mathrm{d}}{\mathrm{d}\,t}\langle r\rangle\right|_{\mathrm{res}} = \frac{M_0}{C\,h}\left(\frac{\tau}{\tau_{\mathrm{c}}} - 1\right)(r_{\mathrm{b}} - \langle r\rangle) \tag{2.73}$$

as a description for the change of the $\langle r\rangle$ due to erosion of particles with a mean radius r_{b} into a homogeneously mixed water column of depth h.

In the following chapter, the model will be applied to

- carry out a comparison with a size class-based flocculation model, and
- SPM size dynamics in the tidal basin of Spiekeroog Island to verify seasonal changes in parameters related to biological influences.

Chapter 3

Publications

3.1 Modeling flocculation processes: intercomparison of a size class-based model and a distribution-based model

Joeran Maerz[1], Romaric Verney[2], Kai Wirtz[3] and Ulrike Feudel[1]

Published in Continental Shelf Research
Special Issue INTERCOH Proceedings 2007[4]

Abstract

Modeling suspended particulate matter (SPM) dynamics is essential to calculate sediment transport budgets and to provide relevant knowledge for the understanding of biogeochemical cycles in coastal waters. Natural flocs are characterized by their size, shape, structure and density that determine their settling velocity and therefore their vertical as well as horizontal transport. During transport, several processes, in particular aggregation and fragmentation, alter these particle properties. In the present study, we compare two different 0 D modeling approaches for flocculation processes, a *size class-based* (SCB) model and a *distribution-based* (DB) model that follows the first moment of the particle distribution function. The study leads to an improved understanding of both models, which aim to better resolve SPM dynamics in spatial and ecosystem models in the near future. Both models are validated using data from laboratory experiments. The time evolution of the particle dynamics subjected to tidal forcing is represented equally well by both models, in particular in terms of i) the mean diameter, ii) the computed mean settling velocity and iii) the particle size distribution. A sensitivity study revealed low sensitivity to changes in the collision efficiency and initial conditions, but a high sensitivity with respect to the particles' fractal dimension. The latter is an incitation to enhance the knowledge on processes related to changes of fractal dimension in order to further improve SPM transport models. The limitations of both models are discussed. The model intercomparison revealed that the SCB model is useful for studies focussing on the time evolution of floc distributions, especially under highly variable conditions. By contrast, the DB model is more suitable for studies dealing with larger spatial scales and, moreover, with coupled marine physical-biogeochemical systems, as it is computationally very effective.

---

[1]Institute for Chemistry and Biology of the Marine Environment (ICBM), University of Oldenburg, Oldenburg, Germany

[2]Ifremer, Hydrodynamics and Sediment Dynamics laboratory (DYNECO/PHYSED), BP 70, 29280 Plouzané, France

[3]Institute for Coastal Research, GKSS Research Center, Geesthacht, Germany

[4]We acknowledge the DFG for funding of the Research Group BioGeoChemistry of Tidal Flats (FOR 432) and the DAAD/PROCOPE for travel support.

3.1.1 Introduction

Modeling suspended particulate matter (SPM) dynamics is essential to calculate sediment transport budgets. Furthermore, SPM models provide knowledge on turbidity, on the fate of both particulate organic and inorganic matter, and on particle-reactive chemicals that are relevant quantities for modeling and understanding marine ecosystems.

Natural flocs (or similar: aggregates, particles) are composed of clay, silt and particulate organic matter. They can be characterized by their size, shape, structure (fractal dimension) and density. These properties determine the settling velocity and hence the vertical and lateral transport. Flocs in suspension experience various processes like aggregation, fragmentation, repacking, remineralization, deposition, and eventually subsequent resuspension. Hence, their properties can dynamically change with time. Ideally, these changes and their effects on floc settling velocity should be represented in sediment transport models.

So far, sediment transport models mainly consider semi-empirical relationships between settling velocity and environmental variables, e. g. SPM concentration, shear rate or salinity (developed by e. g. Krone, 1962; Van Leussen, 1994; Manning and Dyer, 1999, 2007). These relationships were obtained from field or laboratory measurements. Therefore, they are not necessarily applicable elsewhere.

In order to represent the processes of aggregation and fragmentation more realistically, various models have been developed on the basis of the Smoluchowski equation (von Smoluchowski, 1917) assuming a spatially well-mixed environment (zero-dimensional (0D) model). Most of these models only consider changes in size, whereas a few of them also consider a size dependent changing fractal dimension (Maggi et al., 2007; Son and Hsu, 2008).

In general, there are two possibilities to represent the size distribution of particles in models. In *size class-based* (SCB) models the floc distribution is represented in terms of size classes (e. g. McAnally and Mehta, 2002; Maggi et al., 2007; Verney et al., 2010) or only their central moments (Prat and Ducoste, 2006). Other approaches use a characteristic diameter (Son and Hsu, 2008; Winterwerp, 1998; Winterwerp et al., 2006) while Maerz and Wirtz

(2009) use the average floc size of a continuous floc size distribution function leading to *distribution-based* (DB) models.

All of these models can be potentially included in SPM transport models. But only a few applications were achieved in a 1 D vertical model (Krishnappan and Marsalek, 2002; Winterwerp, 2002) and in a 2 D model (Krishnappan, 1991). This might have several reasons, e. g. limitations due to computational costs, increasing model complexity, difficulty of parametrization and the so far little understanding of processes changing aggregates' properties like fractal dimension, size and density. Models using a characteristic diameter or an average radius need less computational time than models that explicitly resolve a number of size classes. For this reason, they might be more appropriate for a coupling to a 3 D transport model. However, DB models use some approximations and thus, it is an open question, how well they reflect the dynamics of the whole floc distribution compared to SCB models. In order to point out assets and drawbacks of the two different modeling approaches the present study focuses on an intercomparison of a SCB and a DB model. Both models are validated with the same data set from a laboratory experiment. This provides a better understanding of both models, which aim to resolve SPM size dynamics in both higher dimensional SPM transport and marine ecosystem models in the near future.

3.1.2 Description of the two models

Both 0 D models (SCB and DB) represent the processes of aggregation (using the Smoluchowski equation) and fragmentation due to shear.

The size class-based (SCB) model, developed by Verney et al. (2010) represents the floc distribution in terms of distinct size classes. By contrast, the distribution-based (DB) model, developed by Maerz and Wirtz (2009), uses an underlying continuous distribution function and only follows the average radius. Therefore it aims for reducing model complexity. In the following, the common features of the two models are described.

Both aggregation models are based on the formulation of von Smoluchowski (1917) that is given by

$$\frac{\mathrm{d}\, n(m)}{\mathrm{d}\, t} = \frac{1}{2} \int_0^m \alpha(m-m', m')\, n(m-m') \cdot n(m')\, I(m-m', m')\, \mathrm{d}m' - n(m) \int_0^\infty \alpha(m, m')\, n(m') \cdot I(m, m')\, \mathrm{d}m' \tag{3.1}$$

where the first term of the right hand side is the gain of particles n of mass m by aggregation of smaller particles $n(m-m')$ and $n(m')$ with the collision efficiency α and the collision frequency I. The second term describes the loss of particles due to aggregation with other particles. For simplification, in both models we assume a size-independent collision efficiency. Furthermore we focus on the aggregation due to turbulent shear $\gamma = (\epsilon/\nu)^{1/2}$ (ϵ being the turbulent energy dissipation rate and ν being the kinematic viscosity of the fluid) using the rectilinear approach for the collision frequency, here written for particles in classes i and j with radii r_i and r_j, respectively

$$I_{\gamma,i,j} = 1.3\, \gamma\, (r_i + r_j)^3\,. \tag{3.2}$$

Aggregation due to differential settling is believed to be less relevant compared to shear-induced aggregation (Lick et al., 1993) and Brownian motion is only relevant for particles $< 1\,\mu\mathrm{m}$ (McCave, 1984). We hence neglect these processes of aggregation. In order to simulate the fragmentation of particles, a simplified fragmentation kernel (with f_b being a fragmentation factor) is used for a particle of diameter D_i:

$$B_{\gamma,i} = f_\mathrm{b}\, \gamma^{1.5}\, D_i^2\,, \tag{3.3}$$

that is close to the formulation proposed by Winterwerp (1998). The detailed implementation of both, the aggregation and the fragmentation kernel, in the two flocculation models are described in Sec. 3.1.2 and 3.1.2.

Size class-based model

The size class-based (SCB) model, developed to reproduce the flocculation and fragmentation processes, is briefly described hereafter, but an extended

description can be found in Verney et al. (2010). The SCB model is based on the population equation system originally proposed by von Smoluchowski (1917) that describes the floc population in N discrete size classes. Here, each of the used N (=15) classes corresponds to a specific particle size (and hence a related mass). They are logarithmically distributed starting from the primary particle diameter $D_\mathrm{p} = 4\,\mu\mathrm{m}$ to the maximum floc size $D_\mathrm{max} = 1500\,\mu\mathrm{m}$ by using the following relation:

$$D_i = D_\mathrm{p}^{1+\frac{i-1}{N-1}\cdot\left(\frac{\log_{10}(D_\mathrm{max})}{\log_{10}(D_\mathrm{p})}-1\right)} \tag{3.4}$$

where D_i is the floc diameter in size class i. In order to reduce the number of size classes required to realistically reproduce flocculation processes, an interpolated aggregation scheme is applied to represent the particle distribution. Each size class represents specific characteristics like floc size and mass. Newly formed flocs that have a mass and size in-between those classes are distributed in the two neighbour classes by using a mass-weighted linear interpolation (Prakash et al., 2003; Xu et al., 2008). Mass conservation is ensured by the conversion of the redistributed mass into the related number of aggregates of the class specific mass by using the below described fractal concept (see Fig. 3.1 and for a more detailed description Verney et al., 2010). This allows to use a much smaller number of size classes compared to the number of potentially newly formed floc sizes, and therefore reduces the computation time. The fractal behaviour of flocs is represented according to the description by Kranenburg (1994). The main characteristic sizes of flocs (with diameter D_i, mass m_i and density $\rho_{\mathrm{f},i}$) can be expressed via the fractal dimension d_f:

$$m_i = \rho_\mathrm{p}\,\frac{\pi}{6}\,D_\mathrm{p}^3\left(\frac{D_i}{D_\mathrm{p}}\right)^{d_f} \tag{3.5}$$

$$\rho_{\mathrm{f},i} = \rho + (\rho_\mathrm{p} - \rho)\left(\frac{D_\mathrm{p}}{D_i}\right)^{3-d_f} \tag{3.6}$$

where ρ and ρ_p are the density of water and of the primary particles, respectively. Exchanges between classes are allowed through flocculation processes and governed by the kernels for shear aggregation $I_{\gamma,i,j}$ (cf. to Eq. (3.2)) and

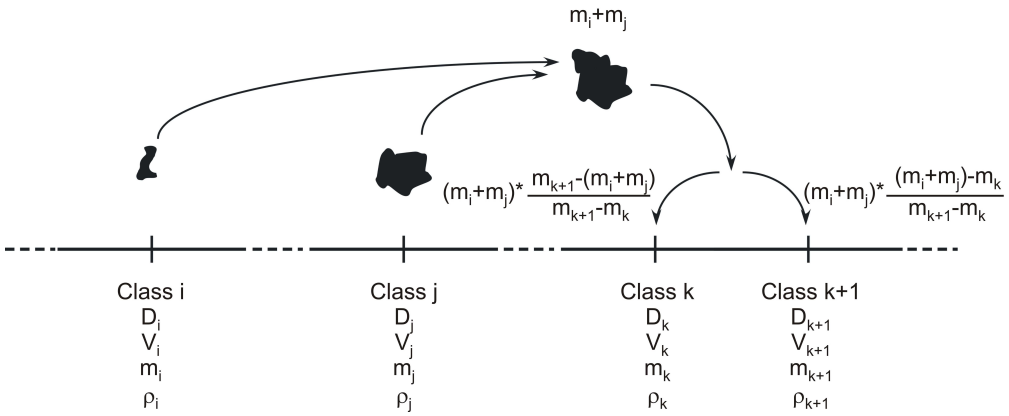

Figure 3.1: Aggregation of flocs of mass m_i and m_j into mass $m_i + m_j$ and subsequent distribution into the nearest size classes by using a mass-weighted interpolation. V_i and ρ_i are the volume and the effective density of a floc in size class i, respectively.

fragmentation $B_{\gamma,i}$:

$$\frac{\mathrm{d}\, n_k}{\mathrm{d}\, t} = \alpha \frac{1}{2} \sum_{i+j \simeq k} n_i\, n_j\, I_{\gamma,i,j} - \alpha \sum_{i=1}^{N} n_i\, n_k\, I_{\gamma,i,k} + \sum_{i \simeq k+1}^{N} F_{\mathrm{D},i,k}\, B_{\gamma,i}\, n_i - B_{\gamma,k}\, n_k \tag{3.7}$$

where n_k is the number of particles in class k (in $\#/\mathrm{m}^3$) and $F_{\mathrm{D},i,k}$ the distribution function of fragmented flocs. Note that $i + j \simeq k$ is written instead of the usually used $i + j = k$ to account for the above described mass-conservative interpolation scheme. In the present study, a binary fragmentation is used, i. e. the fragmentation of a particle of mass m_i results in two particles of equal mass $m_i/2$. The fragmentation kernel, Eq. (3.3), is directly used

$$B_{\gamma,i} = f_\mathrm{b}\, \gamma^{1.5}\, D_i^2 \tag{3.8}$$

where f_b is a constant integrating the cohesiveness of particles. In order to optimize computation time, exchange kernels are calculated once at the initialization with discrete values of γ ranging from 0 to a maximum value reproduced experimentally, i. e. $\gamma_\mathrm{max} = 12\,\mathrm{s}^{-1}$.

Distribution-based model

In order to reduce model complexity, Maerz and Wirtz (2009) used the moment closure approach of Wirtz and Eckhardt (1996) to develop a distribution-based (DB) aggregation model. The general idea is to follow only the first moment of the concentration distribution function and the total concentration. The concentration distribution function C_i is given by the SPM mass per volume and bin width ΔR_i in each size class i. Hence, the total concentration is $C = \sum_i C_i \, \Delta R_i$. The average radius of the concentration distribution $\langle r \rangle$ is represented by

$$\langle r \rangle = \sum_i r_i \, \frac{C_i \, \Delta R_i}{C} \tag{3.9}$$

where r_i is the radius in size class i. The change of $\langle r \rangle$ can therefore be written as

$$\frac{\mathrm{d}\,\langle r \rangle}{\mathrm{d}\,t} = \sum_i r_i \, \frac{\dot{C}_i \, \Delta R_i}{C} - \frac{\dot{C}}{C} \sum_i r_i \, \frac{C_i \, \Delta R_i}{C} \tag{3.10}$$

where $\dot{C}_i$ and $\dot{C}$ are the changes of the concentration in size class i and in total, respectively. Eq. (3.10) can also be written as

$$\frac{\mathrm{d}\,\langle r \rangle}{\mathrm{d}\,t} = \langle r \cdot \hat{\mu} \rangle - \langle r \rangle \cdot \langle \hat{\mu} \rangle \tag{3.11}$$

where $\hat{\mu}$ is the relative growth rate defined as $\hat{\mu}_i = \dot{C}_i / C_i$. Expanding $\hat{\mu}$ in a Taylor-series around $\langle r \rangle$ and using a moment closure leads to (see Wirtz and Eckhardt, 1996)

$$\frac{\mathrm{d}\,\langle r \rangle}{\mathrm{d}\,t} \simeq \delta r^2 \cdot \frac{\mathrm{d}\,\hat{\mu}(\langle r \rangle)}{\mathrm{d}\,r} \, . \tag{3.12}$$

Hence, temporal changes of $\langle r \rangle$ follow a local gradient of $\hat{\mu}$. The rate of change is proportional to the gradient itself and the variance of the aggregate concentration distribution δr^2. This can also be seen, if one writes Eq. (3.10) as

$$\frac{\mathrm{d}\,\langle r \rangle}{\mathrm{d}\,t} = \sum_i r_i \cdot (\hat{\mu}_i - \langle \hat{\mu} \rangle) \, \frac{C_i \, \Delta R_i}{C} \tag{3.13}$$

where each rate (summand) contributing to the change of $\langle r \rangle$ is dependent on the difference between the relative growth rate $\hat{\mu}_i$ in size class r_i and the average relative growth rate $\langle \hat{\mu} \rangle$ multiplied by the fraction of the concentration

corresponding to that size class. So, if the relative growth rate and the size covary, the change of the average radius is high (see also Eq. (3.11)).

The moment approximation does not require specific assumptions on the underlying distribution function, but looses accuracy for non-Gaussian distributions. The latter is also the reason for using $\langle r \rangle$ as state variable because the concentration distribution is closer to a Gaussian distribution than the number distribution of the aggregates.

In the following, we use Eq. (3.12) to develop the aggregation formulation for a continuous distribution function. In a first step, we substitute the mass by the radius in Eq. (3.1). It is important to note that at this step, mass conservation is not fulfilled any more, but will be assured afterwards. The resulting equation can be transformed in order to describe the change of the concentration for each radius by multiplying with the weight of an aggregate $w(r) = w_0 \cdot r^{d_f}$. The weight factor w_0 is written as $w_0 = 2^{d_f}\, \rho_\mathrm{p}\, \pi\, D_\mathrm{p}^{3-d_f}/6$. Division of this transformed equation by the concentration $C(r)$ results in the relative growth rate $\hat{\mu}(r)$. As underlying aggregate number distribution $n(r)$, an exponential approach is used in $\hat{\mu}$,

$$n(r) = N_0 \cdot \exp(-\beta r) \tag{3.14}$$

where the factor β and N_0 denote the slope and the intersection with the ordinate, respectively, for the straight line in a logarithmic representation. The assumption of an exponential number distribution can be justified by measurements for aggregate distributions in tidal areas (Lunau et al., 2006). Now, we use the rectilinear kernel for shear, Eq. (3.2), in $\hat{\mu}$ and solve the integrals in $\hat{\mu}$.

To assure mass conservation, we have to require that the total concentration does not change, resulting in the condition $\langle \hat{\mu} \rangle = 0$. The average of the relative growth rate can be calculated by using a second order closure

$$\langle \hat{\mu} \rangle = \hat{\mu} + y' \cdot \frac{\partial^2 \hat{\mu}}{\partial r^2} = 0 \tag{3.15}$$

as correction with choosing y' in such a way that Eq. (3.15) is fulfilled. The coefficient y' depends on the distribution function and would be given by $y' =$

$0.5\,\delta r^2$ for a Gaussian distribution. Using the integral of the concentration distribution

$$C = \int_0^\infty C(r)\,\mathrm{d}r = \int_0^\infty n(r)\,w(r)\,\mathrm{d}r = \int_0^\infty N_0\,\exp(-\beta r)\,w_0\,r^{d_f}\,\mathrm{d}r \tag{3.16}$$

as well as the resultant relations $\delta r^2 = \langle r\rangle^2/(d_f+1)$, $\beta = (d_f+1)/\langle r\rangle$ together with $\langle\hat{\mu}\rangle$ in Eq. (3.12) leads to

$$\frac{\mathrm{d}\,\langle r\rangle}{\mathrm{d}\,t} = \alpha\,\gamma\,K_\gamma(d_f)\,\frac{C}{w_0}\,\langle r\rangle^{4-d_f} \tag{3.17}$$

where $K_\gamma(d_f)$ is a function of the fractal dimension d_f and describes the correction for the difference between the underlying concentration distribution and a Gaussian distribution. $K_\gamma(d_f)$ is given by

$$K_\gamma(d_f) = 0.65 \cdot \frac{(d_f+1)^{d_f-1}\,(2\,d_f^4 + 3\,d_f^3 - 3\,d_f^2 + 17\,d_f + 57)}{(d_f^2 + d_f - 1)\,\Gamma(d_f+2)} \tag{3.18}$$

where $\Gamma(x)$ is the Gamma function.

For the change of the $\langle r\rangle$ due to fragmentation, the fragmentation kernel (Eq. (3.3)) is used for the mean radius by multiplying it with $2\langle r\rangle$

$$\frac{\mathrm{d}\,\langle r\rangle}{\mathrm{d}\,t} = -8\,f_\mathrm{b}\,\gamma^{1.5}\,\langle r\rangle^3 \tag{3.19}$$

resulting in a similar formulation as proposed in Winterwerp (1998) who considered a characteristic diameter of a particle distribution.

3.1.3 Results

In order to evaluate the performances of DB and SCB modeling approaches, model results are compared with experimental data reproducing the behaviour of a floc population during a tidal cycle. A comparison is made i) in terms of the mean floc diameter weighted by the projected area of a floc and ii) by their distribution. Furthermore, as the vertical flux of sediment is of main interest in higher dimensional models, we calculate an average settling velocity depending on the calculated distribution. Next, the sensitivity of both models

with respect to several key parameters such as the fractal dimension or the initial distribution is examined (see Sec. 3.1.3).

Validation data

For validation of both models an experimental data set is used (Verney et al., 2010). In this experiment, the floc population was investigated under changing hydrodynamic conditions. Turbulent shear was changed stepwise between $\gamma = 0$ and $12\,s^{-1}$ to mimic a tidal cycle. This range of turbulent shear was observed during field measurements above intertidal mudflats (Verney et al., 2006). The device consists in a cylindrical test chamber (13 cm width and 20 cm height) equipped with a 10-speed impeller for controlling turbulent agitation. Turbulent kinetic energy inside the chamber was measured by a Doppler velocimeter revealing a fair shear rate homogeneity that makes the experiment suitable for 0 D model comparisons (Mikes et al., 2004; Verney et al., 2009).

Floc sizes were evaluated in terms of the equivalent circular diameter (ECD) and determined by a postprocessing of images derived from a Sony CCD camera system with a pixel resolution of 8 µm. The latter limits the consistency of measurements for small flocs. For this reason, particles smaller than 50 µm were not taken into account during the analysis. The concentration distribution is calculated on the basis of the ECD and the related mass using fractal theory, Eq. (3.5). As inoculum, SPM collected in the upper part of the Seine estuary, France (freshwater part, muddy sediments with an organic matter content of around 5 %) in winter 2005, was used in a concentration of $93\,mg \cdot L^{-1}$. After filling the test chamber, high turbulence mixing was applied to reach a microfloc population as initial condition. An upstream flow in the middle of the test chamber prevented potential deposition of particles at the bottom during times of shear.

During the first 2 h of constant turbulent shear $\gamma = 1\,s^{-1}$, the mean ECD increases up to ca. 250 µm. During a stepwise increase of shear up to $\gamma = 12\,s^{-1}$, the mean ECD decreases down to ca. 60 µm. After this time, a decrease of the shear rate leads again to an increasing mean ECD that decreases during time spans of no shear due to settling of the particles followed by a second cycle of changing shear rates (see Fig. 3.2).

Model and data comparison

For model intercomparison and validation, the main parameters used in the SCB and the DB model (initial mean floc size, concentration C, density of primary particles ρ_p) were determined from the laboratory experiment. The primary particle size D_p was set to 4 µm in accordance with other cohesive sediment studies (e. g. Winterwerp, 1998) and the fractal dimension to $d_f = 1.9$ according to estimations made during similar laboratory experiments of Verney et al. (2009). Therefore, both models use identical parameter values (cf. Tab. 3.1) except for the break-up factor f_b and the collision efficiency α that are varied independently for both models in order to minimize the error between model results and data. The error is calculated from the least square method on the entire dataset excluding the period, where settling is the dominant process for size distribution changes ($6\,\mathrm{h} < t \leq 7\,\mathrm{h}$) as this process is not taken into account in the model formulation.

Table 3.1: Parameter (P) set for the reference runs. In case of the break-up factor f_b and the collision efficiency α values are given as DB/SCB values.

P	Description	Value	Literature value	Unit
α	Collision efficiency	0.18 / 0.4	0.005-0.8 [a]	–
C	Total SPM concentration	0.093	0.01-6 [b]	$\mathrm{kg\,m^{-3}}$
d_f	Fractal dimension	1.9	1.5 – 2.4 [c]	–
D_p	Primary particle diameter	$4 \cdot 10^{-6}$	$1 - 10{\cdot}10^{-6}$ [d]	m
f_b	Break-up factor	12068/48000	– [e]	$\mathrm{s^{0.5}\,m^{-2}}$
ρ_p	Primary particles density	2600	2300-2800 [f]	$\mathrm{kg\,m^3}$
μ	Dynamic viscosity	$1.02 \cdot 10^{-3}$	$1 - 1.8 \cdot 10^{-3}$	$\mathrm{kg\,m^{-1}\,s^{-1}}$

[a] Kiørboe et al. (1990); Dam and Drapeau (1995) for algae; [b] Guezennec et al. (1999); Manning and Bass (2006); [c] Manning and Dyer (1999); [d,f] Fettweis (2008); [e] no measurements available

Average diameter As can be seen in Fig. 3.2, both models are in good agreement with the data and follow the size dynamics equally well. We emphasize here again that the goodness of the data is limited by the lower resolution of the camera system that could lead to an overestimation of the mean

diameter of the particles. During time spans where aggregation rates dominate fragmentation rates, the mean floc size increases smoothly. Otherwise, when fragmentation dominates, the mean floc size decreases abruptly and reaches rapidly a new equilibrium related to increasing shear. These two different behaviours are well reproduced by both the SCB and the DB model. They correspond to differences in process timescales between aggregation (slow response) and fragmentation (fast response): aggregation is caused by the collision of flocs and only a fraction of these collisions leads to aggregation while fragmentation is only a function of floc size, cohesiveness and shear stress. This leads to a steep negative slope, when fragmentation dominates and a more gentle positive slope, when aggregation dominates.

Comparison of the distributions While the mean floc size reveals the general behavioural trend of the floc population, the analysis of the floc size distribution allows for precisely investigating the changes within the population itself. This examination requires a discretization of the continuous distribution function of the DB model based on the SCB model size class discretization. The interpolation method used in the SCB model for a normalized floc mass distribution C'_i is applied:

$$C'_i = \frac{w_i}{C} \cdot \left(\int_{r_{i-1}}^{r_i} n(r) \frac{w(r) - w_{i-1}}{w_i - w_{i-1}} \,\mathrm{d}r + \int_{r_i}^{r_{i+1}} n(r) \frac{w_{i+1} - w(r)}{w_{i+1} - w_i} \,\mathrm{d}r \right) \quad (3.20)$$

where w_i is the weight of an aggregate of size r_i in the SCB model.

The comparison of the distributions reveals that both models simulate smoother distributions than the ones observed in the laboratory experiment (cf. Fig. 3.3 and 3.4). Slight discrepancies between the two models can be explained by the structure of each model and their underlying assumptions: the SCB model is only controlled by the exchange processes between flocs of each size class while the DB model prescribes the distribution function to represent the floc population. The experimental data suggest that the concentration distribution changes with time and tends to have a peak-like form especially in case of high shear rates. In both models, this behaviour is not properly represented.

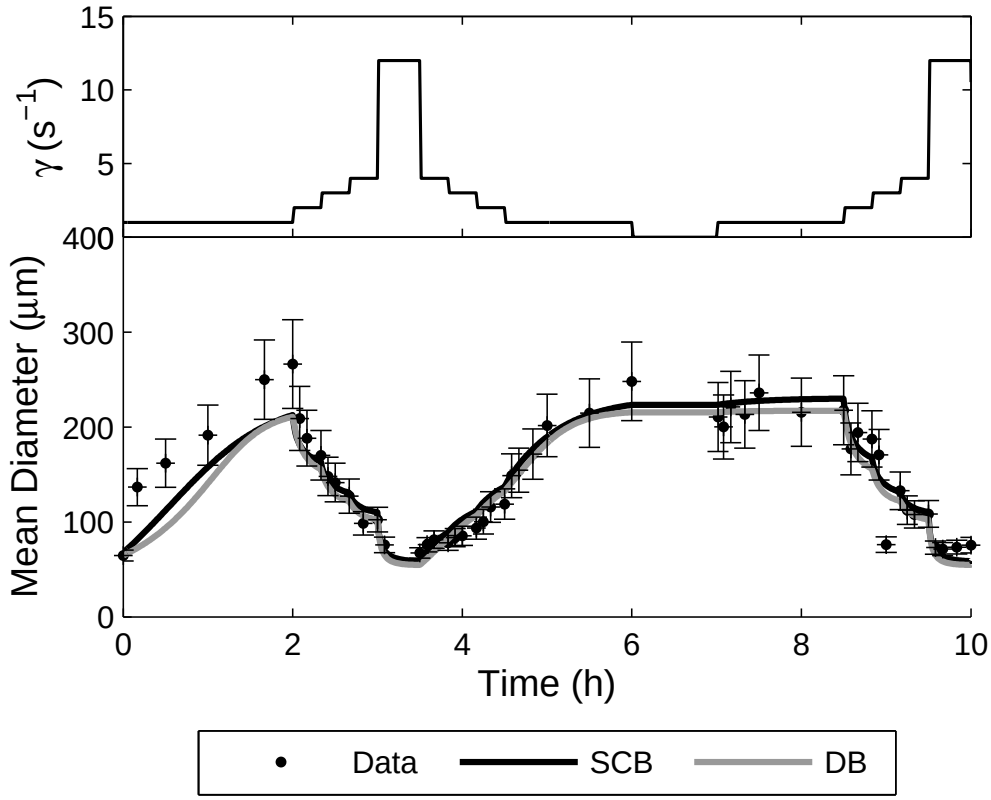

Figure 3.2: Mean floc size variation during a simulated tidal cycle: comparison between laboratory measurements and models results. Note that the mean diameter of the observed flocs might be overestimated due to limitations of the camera system. SCB: size class-based and DB: distribution-based model.

Average settling velocity Different distributions of aggregates have an impact on the vertical fluxes of sediment as macroflocs settle faster than microflocs. This is particularly important for simulating SPM dynamics in spatially explicit models. Therefore, we calculate a theoretical average settling velocity for the experimentally observed particle distribution as well as for both models. The settling velocity v_s of fractal particles with diameter D (e. g. Winterwerp, 1998, without the proposed correction term) is given by

$$v_\mathrm{s}(D) = \frac{1}{18\,\mu}\,(\rho_\mathrm{p} - \rho)\,g\,D_\mathrm{p}^{3-d_f}\,D^{d_f-1} \tag{3.21}$$

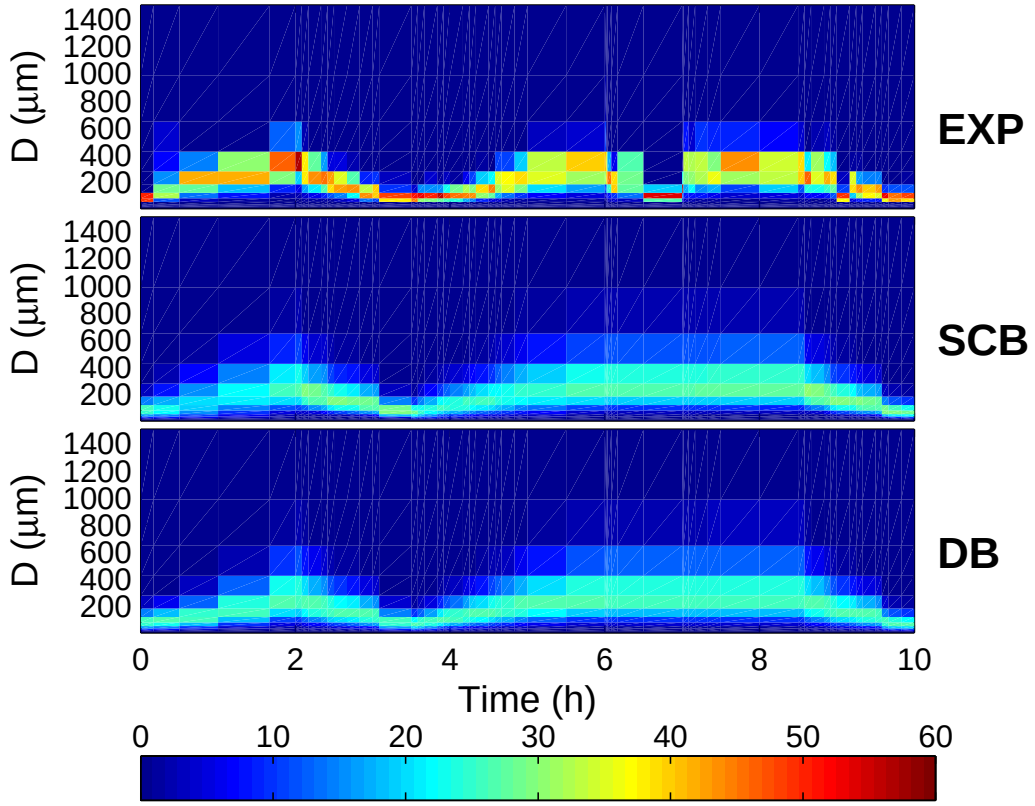

Figure 3.3: Normalized concentration in % of the experimentally derived distribution (EXP), size class-based model (SCB) and distribution-based model (DB). Note that both models fail for the time 6 h $< t \leq$7 h as settling is not taken into account in the model comparison.

where μ is the dynamic viscosity and g is the gravitational acceleration constant. In case of the DB model the average settling velocity can also be computed from the underlying distribution by dividing the total flux (calculated using Eqs. (3.16) and (3.21) by the total concentration resulting in

$$\langle v_s \rangle = \frac{1}{18\,\mu} \left(\rho_\mathrm{p} - \rho\right) g\, D_\mathrm{p}^{3-d_f}\, 2^{d_f-1}\, \langle r \rangle^{d_f-1} \left[\frac{4^{d_f}\,(d_f+1)^{1-d_f}\,\Gamma(d_f+0.5)}{2\,d_f\,\sqrt{\pi}}\right] \quad (3.22)$$

where $\Gamma(x)$ is the Gamma function. Obviously, comparing Eqs. (3.21) and (3.22), a factor, dependent on d_f, appears when calculating the average settling

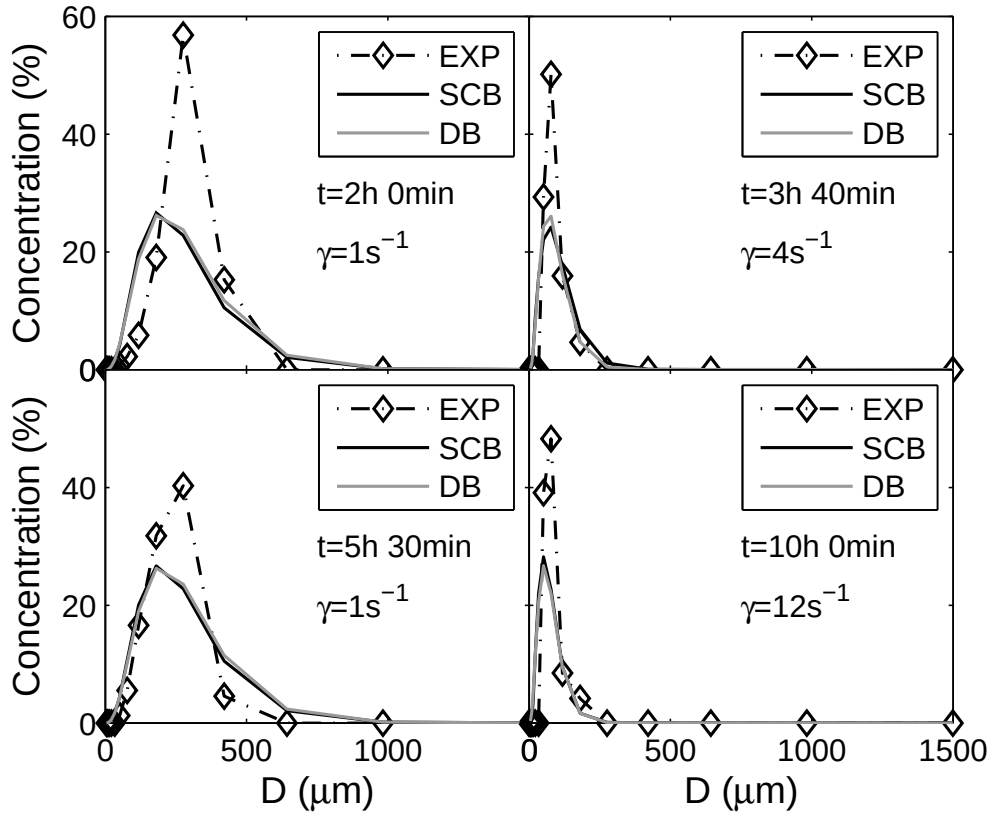

Figure 3.4: Normalized concentration in % of the experimentally derived distribution (EXP), size class-based (SCB) and distribution-based (DB) model for different times (t).

velocity upon the basis of $\langle r \rangle$. This factor is close to 1 for the value of the fractal dimension used in the model comparison. Nevertheless, it is important to emphasize here that the average settling velocity is not necessarily equal to the settling velocity of a particle of size $\langle r \rangle$ especially if particles tend to be compact.

As can be seen in Fig. 3.5 both models are able to represent the mean settling velocity well after some transient time. Note that the mean settling velocity calculated from the observed particle distribution might be overestimated due to limitations of the camera system.

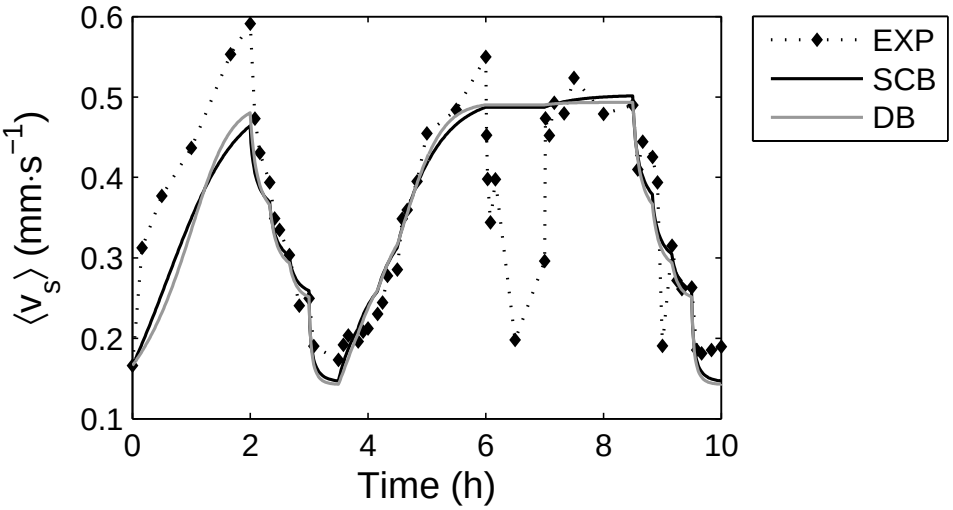

Figure 3.5: Mean settling velocity for experimentally observed particles, size class-based model (SCB) and distribution-based model (DB) calculated by Eqs. (3.21) (data, SCB model) and (3.22) (DB model). Note that both models fail for the time $6\,\mathrm{h} < t \leq 7\,\mathrm{h}$ as the models do not account for changes in the size distribution by settling.

Sensitivity analysis

Some parameters are still inaccessible (like e. g. collision efficiency) or difficult to determine (e. g. fractal dimension) when observing SPM dynamics. It is hence useful to perform a sensitivity study for such parameters in order to estimate the resulting uncertainty in model outcomes. Here, we focus on the fractal dimension d_f, the collision efficiency α and the often unknown or only roughly known initial conditions. Furthermore, since the models differ in their representation of the particle distribution, we study the process of aggregation in more detail.

Initial phase without break-up When looking only at the process of aggregation without using the fragmentation term, the results of both models show a divergence in the average diameter after a short time. This is enhanced by different values of the collision efficiency α used in both models for the reference runs. But there is another effect that also causes the divergence

which is explained in the following. The shape of the distribution function changes in case of the SCB model. This leads to a drastically changed distribution within a short period of time (cf. Fig. 3.6) with an increasing number of large aggregates. As a consequence, the collision frequency increases with time (cf. Eq. (3.2)) resulting in an increasing relative growth rate for larger size classes that enhances the growth rate of the mean diameter compared to the initial distribution. By contrast, in the DB model the growth rate of $\langle r \rangle$ always relies, due to the model structure, on the prescribed exponential number distribution function. As a consequence, the distribution that would evolve from pure aggregation cannot evolve and is always "forced back" to a prescribed distribution. This model structure dependent mechanism acts as a distribution-internal mass redistribution, and thus, as fragmentation. This additional fragmentation, which is only present in the DB model and not in the SCB model, would result in different vertical fluxes due to discrepancies in the concentration distribution. For this reason, a smaller value of the fragmentation factor f_b has to be chosen for the DB model to compensate the model-dependent artificial fragmentation.

Sensitivity to initial conditions For studying the sensitivity on initial conditions, the initial distribution has been changed by shifting the average diameter by $\pm 20\,\mu\mathrm{m}$. Additionally, the initial distribution for the SCB model was calculated from the prescribed distribution function of the DB model. As can be seen in Fig. 3.7 both models lose their dependence on the initial conditions after a short transient time and adapt their distributions to the hydrodynamical conditions after 2 h to 3 h. Hence, both models can be used in modeling situations with unknown initial conditions.

Sensitivity to fractal dimension Since fractal dimension can be measured with various methods (e. g. Billiones et al., 1999; Manning and Dyer, 1999), often resulting in different values (from 1.5 to 2.4, Manning and Dyer, 1999), it is always a parameter of rather high uncertainty. Therefore its influence on model results must be examined. Our results reveal that a variation of d_f of about 5 % leads to a strong under- or overestimation of the average diameter for increasing or decreasing fractal dimension, respectively (cf. Fig. 3.8). The SCB

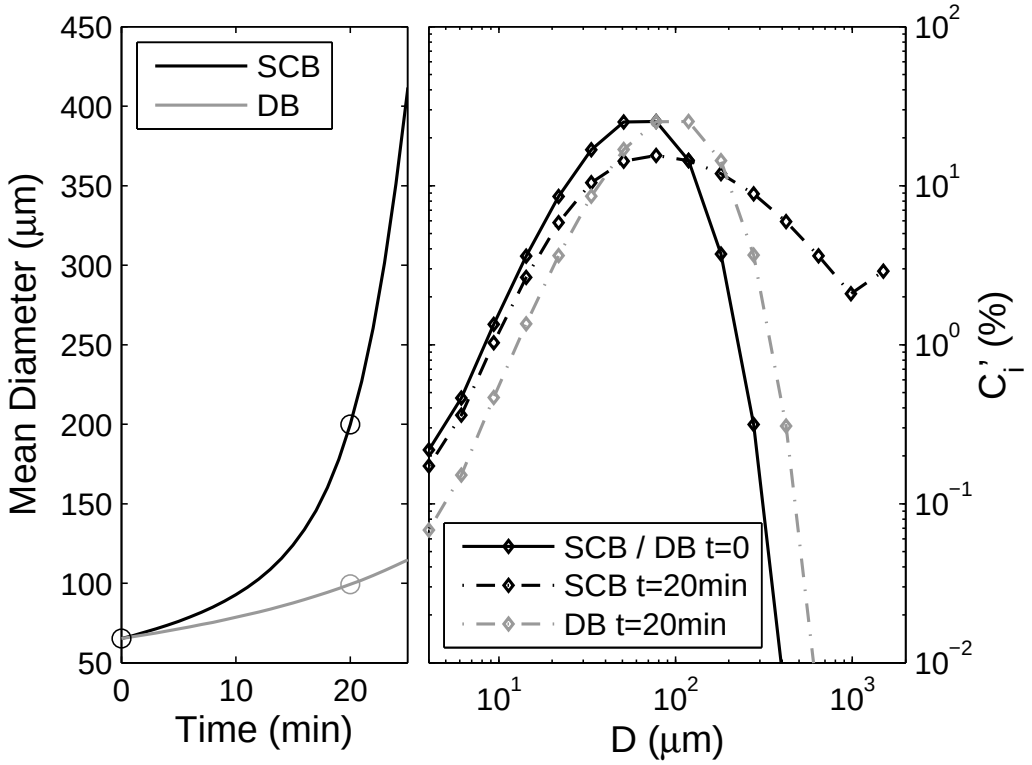

Figure 3.6: Left: Time evolution of the mean floc diameter as simulated by the distribution-based (DB) and the size-class based (SCB) model. Right: Floc size distribution computed by both models at simulation start and after 20 min (indicated by open circles in the left panel). Notice that only the term of aggregation is taken into account with the same initial distribution and the same parameter set used in the comparison with data (see Tab. 3.1).

model is more sensitive to changes in fractal dimension than the DB model. As both aggregation and fragmentation rates are strongly dependent on the fractal dimension (directly and indirectly), it is the most sensitive parameter in both models. Furthermore, as can be seen from Eq. (3.21) and (3.22), fractal dimension strongly influences the vertical flux.

Sensitivity to collision efficiency, break-up factor and shear The collision efficiency and the fragmentation factor are parameters that cannot be measured routinely, yet. These parameters are dependent on various influ-

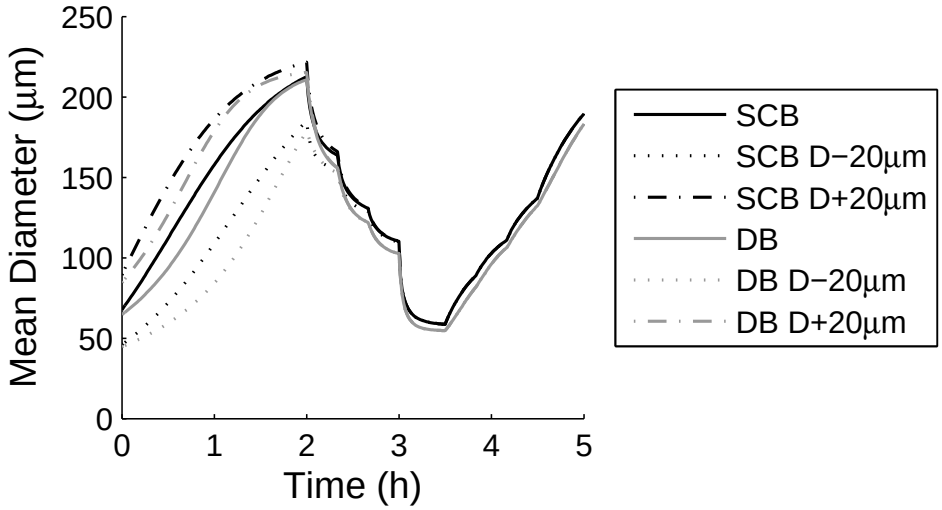

Figure 3.7: Sensitivity of both models to initial conditions. SCB: size class-based model; DB: distribution-based model.

ences like e. g. salinity (Van Leussen, 1994), organic matter content (Chen et al., 2005), involved phytoplankton species (e. g. Kiørboe et al., 1990), extracellular polymeric substances (EPS, e. g. Thornton, 2002; Dam and Drapeau, 1995), maybe the degradation state of aggregates as different settling velocities have been observed for differently degraded particles (Goutx et al., 2007), etc.

Moreover, collision efficiency and the break-up factor are closely related to each other. Furthermore, both processes, aggregation and fragmentation, always occur simultaneously. Together, they force the particle distribution to reach a steady state that is strongly dependent on the present hydrodynamic conditions. Hence, the influence of the collision efficiency and the break-up factor on the model behaviour should be examined together, but also in combination with the turbulent shear. Nevertheless, we first treat the parameters separately and study the influence of the collision efficiency on the model results by varying α by $\pm 5\,\%$. This corresponds to the same range of variation as for the fractal dimension. As can be seen by a comparison of Fig. 3.8 and 3.9, both models are much less sensitive to changes of the collision efficiency than to fractal dimension. While the response of the mean diameter to a changed collision efficiency is linear, perturbations in d_f also lead to nonlinear effects that are even not uniform over time.

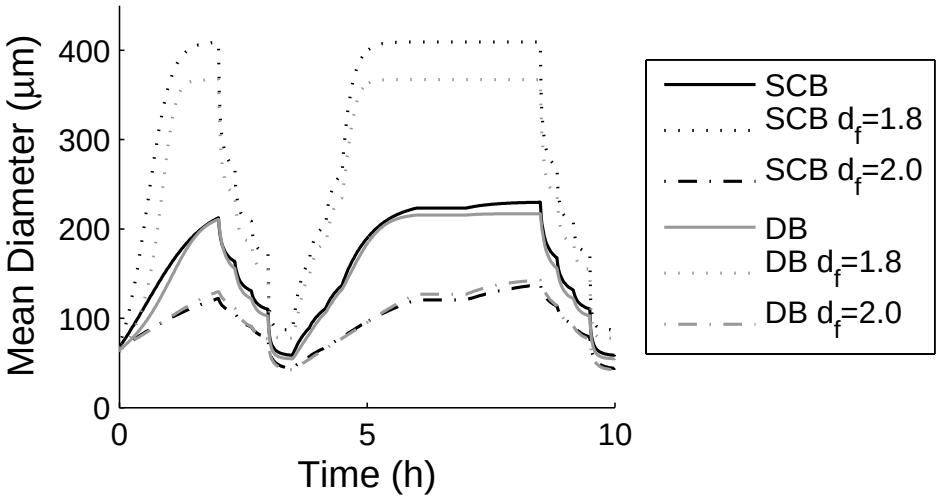

Figure 3.8: Sensitivity of both models to changed fractal dimension compared to the reference runs. SCB: size class-based model; DB: distribution-based model.

When examining both the collision efficiency and the break-up factor together, it is always possible to find a pair of these parameters to reach a defined steady state with both models, e. g. $\langle r \rangle^* = 100\,\mu\text{m}$. This can be exemplarily seen in Fig. 3.10A, that was calculated for the DB model. Obviously, the growth rates for a specific radius $\langle r \rangle$ are different for changed parameter pairs α and f_b. In model runs, this results in different curvatures of the time evolution. For different shear rates, the growth rates for a specific mean radius are also different, shown for the DB model in Fig. 3.10B. Furthermore, the steady state shifts towards smaller radii for higher shear rates and vice versa. This effect is also nonlinear since different exponents are used for the dependence on shear in the aggregation and the fragmentation description. In principle, this behaviour, described for the DB model, can also be found for the SCB model.

3.1.4 Discussion

In this study, two different kinds of flocculation models are compared. Their main difference is the representation of the particle distribution. While the SCB approach explicitly resolves a number of discrete size classes, the DB model uses variable moments of a prescribed distribution function.

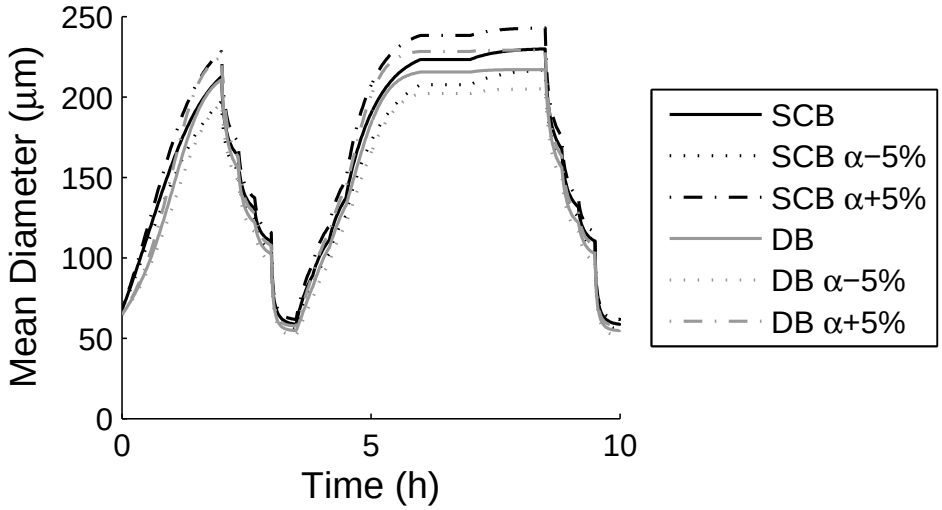

Figure 3.9: Sensitivity of both models to variations in collision efficiency compared to the reference runs. SCB: size class-based model; DB: distribution-based model.

In comparison to SPM size dynamics observed in a laboratory experiment, both models were able to reproduce the dynamics of the average diameter equally well, although both models exhibit a particle distribution smoother than the observed one that can either be caused by the numerical diffusion in the models (for the SCB model, see e. g. Prakash et al., 2003) or by the limited temporal resolution of the measurement probably losing rare occurring large particles. On the other hand, a number of particles smaller than the resolution limit could have occurred during the experiment. Moreover, floc restructuring may have occurred which would lead to changes of the fractal dimension (discussed e. g. by Verney et al., 2010). All the aforementioned reasons might limit the accuracy of the models' representation of the observed distribution (seen in Fig. 3.4) and the goodness of the achieved $\alpha : f_b$ couple. However, the sensitivity study showed a robust model behaviour in its dynamics concerning these two parameters, and hence, it is likely that both models could be useful to represent the floc dynamics disregarding a possible minor change in this parameter couple. Nevertheless, the models could be improved by i) better account for the numerical diffusion (SCB model) or other distributions (DB model, see below), and ii) introducing a variable fractal dimension.

Even in the sensitivity analysis, both models generally show the same behaviour. There are only slight differences concerning the influence of the fractal dimension where the DB model is less sensitive than the SCB model. It turned out that both models are most sensitive to changes of the fractal dimension as it contributes to aggregation and fragmentation in a nonlinear way. Fractal dimension is highly relevant for calculating the settling velocity and, hence, the vertical fluxes. In the presented laboratory experiment, the fractal dimension might be underestimated leading to uncertainties for the model runs. Its value, however, is in general difficult to obtain. Therefore, in order to improve and better validate flocculation models, we suggest to standardize measurements of fractal dimension or to aim for comparability of particles' fractal dimension values and to enhance knowledge related to changes of the fractal dimension. The latter is important to derive a process-based description for the change of the fractal dimension which could be included into – and improve – flocculation models.

Surface properties of flocs (like e. g. the cohesiveness), in the models represented by the collision efficiency α and the break-up factor f_b, have shown to be relevant for the reaction kinetics in terms of i) the reaction time, changing the curvatures in the time evolution and ii) the steady state. Therefore, supposing a qualitatively and quantitatively correct model formulation and known hydrodynamical conditions, it would be possible to access particles' surface properties by inverse modeling, as the strongly related parameter pair α and f_b could only be constrained in a small range. Inverse modeling studies had already been carried out for estimating the collision efficiency of organic aggregates by Kiørboe et al. (1990).

Structural differences in the model formulation and their underlying assumptions can explain the above-mentioned discrepancies to observations and might limit the applications of both models. The SCB model would preferably be used to study the dynamical evolution of the shape of the particle distribution, like e. g. bimodal distributions (e. g. observed by Benson and French, 2007), since the type of distribution is preset in the DB model. Despite this fact, other features of the experimentally observed particle distribution, e. g. their mean settling velocity, can be well calculated by both models. Hence, the application of the DB model is not restricted to an exponential distribu-

tion but can also be used for similar distribution patterns. Intrinsically, the moment closure approach is independent of the functional form of the distribution and only gains accuracy for the Gaussian-like mass distribution assumed here. Therefore, it can also be used for other distribution functions. But this requires the reformulation of the model from first principles which can be a high analytical effort. Lacking flexibility is a deficit of the DB model compared to the SCB model. On the other hand, the DB model significantly reduces computational costs and hence, might be more suitable to be coupled to hydrodynamical models.

In the DB model, an implicit mass redistribution occurs during aggregation in such a way that the approximation of the prescribed distribution is fulfilled any time, as the growth rate for $\langle r \rangle$ is always based on this distribution function. This kind of mass redistribution is also present during fragmentation. By contrast, in the SCB model, the process of aggregation does not include an implicit fragmentation. Additionally, the SCB model faces the problem of numerical diffusion towards larger size classes due to logarithmically distributed size classes. These facts result in a smaller fragmentation factor f_b in the DB model although the collision efficiency had to be chosen smaller than in the SCB model. In general, one should keep in mind that different types of models require usually a different parametrization to describe the same experimental observations. These different parameters account for model-dependent internal realizations of the various processes even in cases where the basic assumptions about these processes are the same.

In comparison to empirical models of e. g. Manning and Dyer (1999, 2007) and Van Leussen (1994), process-based models like SCB and DB models are more flexible to use. Empirical models are more restricted since they are based on observations in a system with specific hydrodynamical, sedimentological and biological conditions. Nevertheless, as emphasized before, the DB model in its present form is also restricted to exponential-like particle number distributions. Therefore, the SCB model is the most flexible model, but with the drawback of high computational costs. Similar to the SCB model, the quadrature of moments method (QMOM; e. g. Prat and Ducoste, 2006) uses several weighting classes, but follows only the moments of the particle density function. This allows for higher flexibility compared to the DB model where the distribution

function is prescribed. However, it is difficult to regenerate the size distribution by using the QMOM approach. Moreover, it has higher computational costs than the DB model.

In contrast to the model of Winterwerp (1998) the DB and the SCB model also provide information about the entire particle distribution. This is useful for calculating the mean settling velocity since it is not necessarily equal to the settling velocity of a particle having the average size (cf. Eq. (3.21) and (3.22)). Furthermore, other features, e. g. turbidity, can be obtained that are relevant in ecosystem models.

An application of the models in spatially explicit SPM transport models or ecosystem models has to face a number of remaining difficulties arising from model assumptions. Especially in case of the DB model, where a redistribution of mass, similar like during aggregation and fragmentation, will occur during transport. The same problem arises in the characteristic diameter based model when coupled to a 1 D vertical model (Winterwerp, 2002). Nevertheless, Kriest and Evans (2000) applied a DB aggregation model for the open ocean in a 1 D vertical model. In turn, due to different settling velocities of particles, numerical diffusion is different for each size class when applying the SCB model in a 1 D vertical model.

3.1.5 Conclusion

The size class-based (SCB) as well as the distribution-based (DB) model are able to represent the change of the average aggregate size, the floc distribution function and the mean settling velocity under different turbulent conditions. These findings indicate that both models have the potential to be included in spatially explicit models.

The fractal dimension is the most sensitive parameter in both models and can strongly influence the vertical flux. Therefore, it is necessary to enhance the knowledge about processes that change the fractal dimension in order to improve SPM transport models.

At the present state, the application of the DB model is limited to exponential-like particle number distributions. Nevertheless, it is computationally very efficient. Furthermore, it can be applied to other distribution functions by

reformulating the terms derived from the moment closure.

The main drawback of the SCB model is its high computational cost. On the other hand, it is more useful to represent temporally highly variable particle distribution patterns like bimodal distributions.

To conclude, the SCB model is useful to study the time evolution of floc distributions, especially under highly variable conditions. The DB model reduces the complexity of flocculation modeling. Hence, by a reduction of state variables, it is especially suitable to be coupled to spatially large scale SPM transport and biogeochemical models.

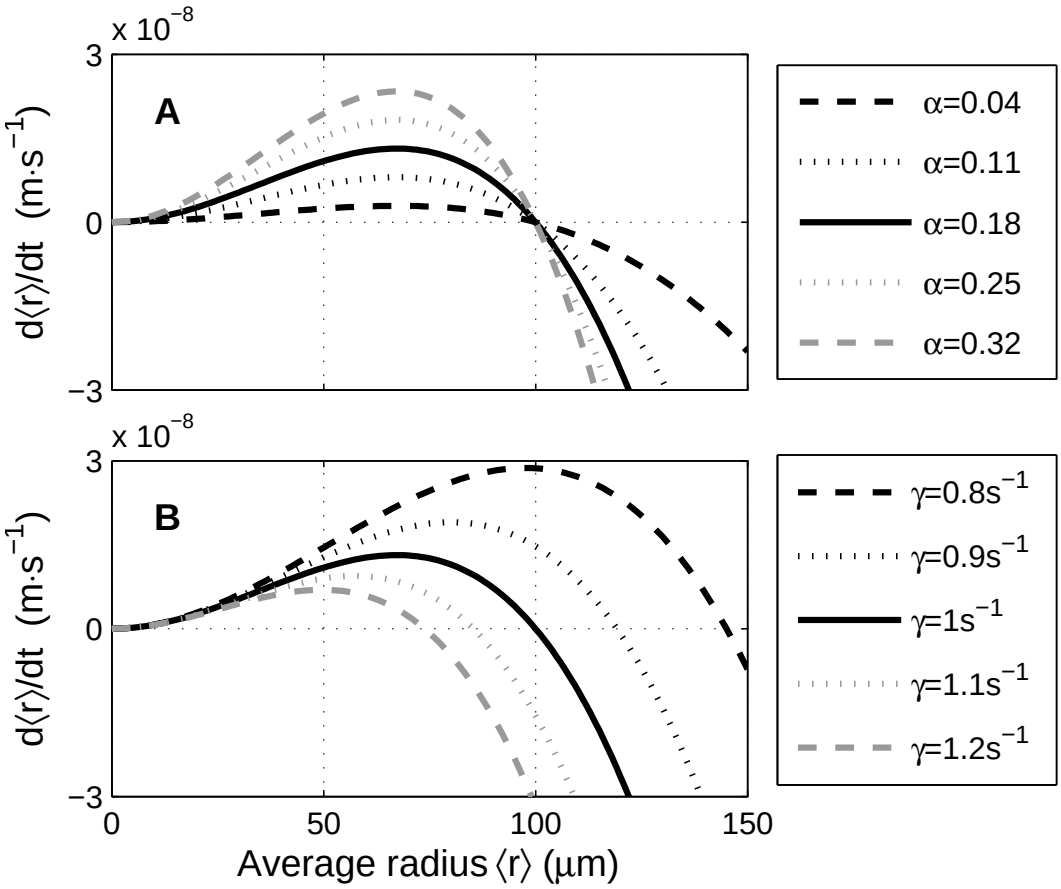

Figure 3.10: Growth rates for the mean radius of the DB model. A) Different α and f_b pairs for the same steady state ($\langle r\rangle^* = 100\,\mu\mathrm{m}$). The correspondent α:f_b values are: $0.04 : 2801\,\mathrm{s}^{1/2}\cdot\mathrm{m}^{-2}$, $0.11 : 7701\,\mathrm{s}^{0.5}\cdot\mathrm{m}^{-2}$, $0.18 : 12602\,\mathrm{s}^{0.5}\cdot\mathrm{m}^{-2}$, $0.25 : 17503\,\mathrm{s}^{0.5}\cdot\mathrm{m}^{-2}$, and $0.32 : 22404\,\mathrm{s}^{0.5}\cdot\mathrm{m}^{-2}$. B) The same α and f_b pair as for the reference run, but using different shear values.

3.2 Resolving physically and biologically driven suspended particulate matter dynamics in a tidal basin with a distribution-based model

Joeran Maerz[5] and Kai Wirtz[6]

Published in Estuarine, Coastal and Shelf Science[7]

Abstract

To understand suspended particulate matter (SPM) dynamics in coastal waters is a key for assessing changes in coastal sediment budgets and biogeochemical fluxes. SPM dynamics are subject to various physical and biological factors and processes such as e. g. tidal currents and aggregation which can be enhanced by extracellular polymeric substances (EPS) that are produced by algae and bacteria. It is still unclear how the different factors and processes interact and together determine SPM dynamics. To unravel the interacting processes and factors, we propose a new distribution-based modeling approach. Based on the derivation of explicit equations for size distribution characteristics of SPM such as the average radius, we derived a model of reduced complexity characterized by low initialization and parametrization effort as well as low computational cost. The proposed 0-D model includes the processes of aggregation and fragmentation due to shear, aggregation due to differential settling, deposition, resuspension and tidal exchange, and describes the evolution of the SPM concentration in the water column linked by the settling velocity to the change of the mass average radius of the aggregate distribution. A systematic parameter variation for critical bottom shear stress of erosion, the size of resuspended aggregates, the fractal dimension, the collision efficiency, and the aggregate strength has been performed and compared to observations in the back-barrier basin of Spiekeroog island in the German Wadden Sea. This analysis confirms the hypothesis that in winter biological influences on SPM dynamics are smaller compared to summer. This is mainly reflected by a significant shift in the various parameters. We hence conclude that biological control mechanisms have a much more quantitative relevance for SPM dynamics than currently represented by state-of-the-art SPM transport models.

[5]Institute for Chemistry and Biology of the Marine Environment (ICBM), University of Oldenburg, Oldenburg, Germany

[6]Institute for Coastal Research, GKSS Research Center, Geesthacht, Germany

[7]We acknowledge the DFG for funding of the Research Group BioGeoChemistry of Tidal Flats (FOR 432)

3.2.1 Introduction

Suspended particulate matter (SPM) plays a crucial role in the complex dynamics of coastal systems. Due to its organic and inorganic composition it is directly linked to the transport of particulate organic matter and provides a habitat for microbial communities which are responsible for a large part of nutrient recycling (Azam and Malfatti, 2007). Furthermore, SPM controls the light climate and, in this way, also affects primary production (Colijn and Cadée, 2003). In addition, its transport properties influence the coastal sediment budget. These properties generally exhibit strong temporal and spatial fluctuations and are closely linked to the variable size distribution of aggregates in shallow turbid marine and estuarine waters (Chen et al., 2005; Lunau et al., 2006; Van der Lee, 2000). Such variability is visible on different time scales reflecting a variety of driving forces and the dependency on internal aggregation and fragmentation processes.

Aggregates are formed by coagulation of detritus and a relatively high proportion of very fine inorganic sediment particles (Postma, 1981). Aggregation seems to be particularly sensitive to the concentration of extracellular polymeric substances (EPS) like transparent exopolymeric particles (TEP) produced by algae and bacteria (Simon et al., 2002; Thornton, 2002). In addition, EPS-induced stickiness affects the erodibility of the sediment (Black et al., 2002; Stal, 2003). Beside this, seasonal changes of aggregate morphology have been reported by Chen et al. (2005) for the Scheldt estuary (the Netherlands), which also might be due to changing EPS production in the course of the year. Size, density and shape of aggregates determine the transport behavior which significantly differs with respect to the primary monomineralic particles.

Observations and subsequent analysis of the SPM dynamics in the semidiurnal, mesotidal back-barrier basin of Spiekeroog Island, German North Sea (see Fig. 3.11), suggest both seasonally and diurnally changing influences of biological factors (Lunau et al., 2006). But it is still unclear, how physical and biological factors interact and how their influences vary. In principle, integrated models are able to unravel the mechanisms driving the complex SPM dynamics. Models resolving the aggregation process have been developed for the open ocean (e. g. Jackson, 1990; Riebesell and Wolf-Gladrow,

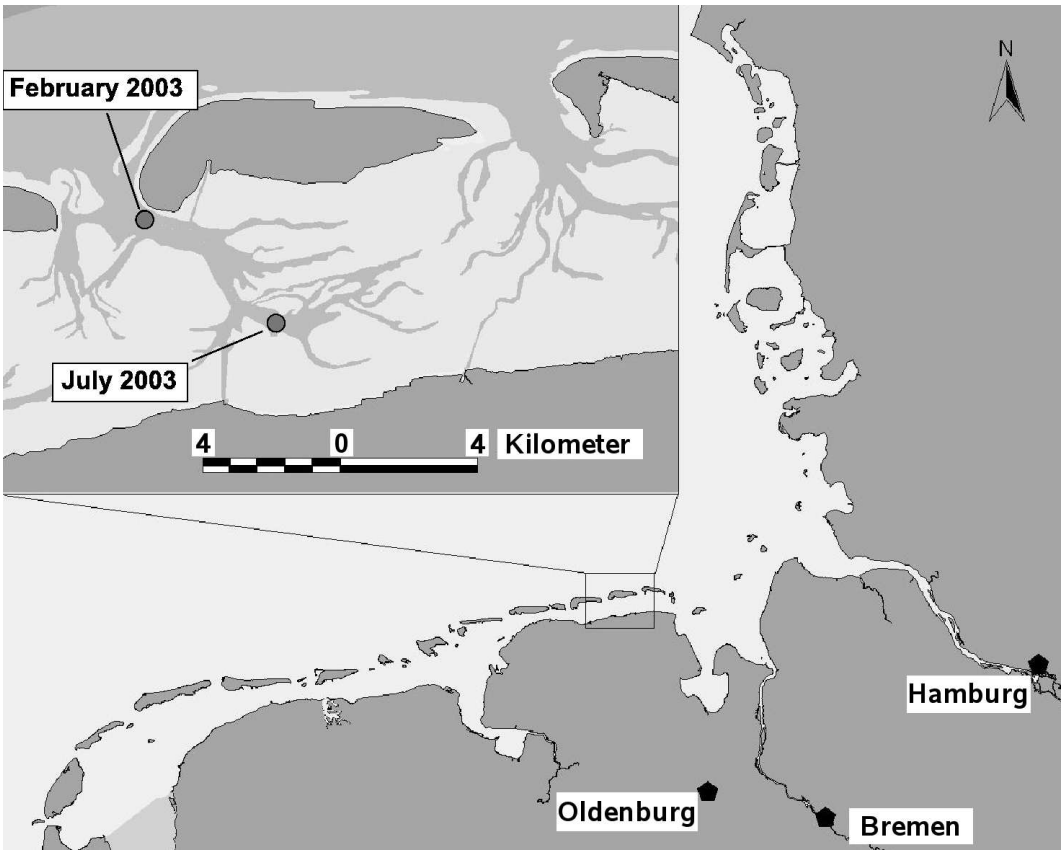

Figure 3.11: Geographic location (53° 45′ N, 7° 45′ W) within the German Bight, intertidal physiography, and anchor positions of two sampling campaigns on 17./18.2.2003 and 22./23.7.2003 conducted by Lunau et al. (2006)

1992; Ruiz, 1997; Stemmann et al., 2004a) but also for near-shore SPM dynamics (McAnally and Mehta, 2002; Winterwerp, 1998; Winterwerp et al., 2006). However, most approaches developed so far, consider large numbers of individual size classes. This model complexity causes high computational costs and a lower potential for validation due to insufficient resolution of existing data sets. Both aspects complicate a coupling of SPM modules with biogeochemical, ecosystem or morphodynamic models.

There have been few attempts to reduce model complexity and related computational costs. A model for the change of a characteristic diameter due to shear-induced aggregation and fragmentation has been developed by Win-

terwerp (1998). A mechanistic and distribution-based approach was proposed by Kriest and Evans (1999). Here, size classes are implicitly described using the aggregate number and mass as state variables. The approach combines a structural description of interactions between different-sized aggregates, while requiring low computational and initialization effort. Its application to near-shore systems, however, can be questioned for a number of reasons. First, Kriest and Evans used a power-law number distribution of aggregates. But as can be seen from the data presented by Lunau et al. (2006) (see also Fig. 3.13) an exponential number distribution is more appropriate. Second, it is difficult to include additional processes in the analytically derived model, e. g. resuspension and shear-induced fragmentation that are relevant in coastal systems.

Therefore, we here propose a new method based on the derivation of explicit equations for the dynamics of distribution characteristics such as the average radius. Such derivation should not depend on (1) the functional form of the size distribution, (2) the number of processes to be resolved by the model, and (3) their (nonlinear) functional representation. We regard such flexibility as essential for developing near-shore SPM models, even though it will most probably exclude an exact or strict analytical derivation. Changes of the average radius as imposed by the distribution-based model are then linked to SPM concentration dynamics through the size dependency of the deposition rate. Although an independence of the functional form of the size distribution is desirable, it is easy to compare model results with observations if an underlying distribution is defined. On this basis, we aim to quantify the relative importance of biological and physical factors determining aggregate dynamics in shallow coastal waters by using a systematic parameter variation for two different seasonal situations. Data for constraining the unvaried parameters used in this study primarily originate from the joint research initiative “Bio-GeoChemistry of tidal flats” with its main monitoring area in the back-barrier basin of Spiekeroog island, German North Sea.

3.2.2 Methods

Model derivation

In the following, a 0-D model is presented where we assume a fully mixed water column with an in- and outflow that represents tidally induced exchange of SPM between the back-barrier basin and the North Sea. In order to describe the often observed variability in settling velocity and therefore in deposition rate (e. g. Manning and Bass, 2006), the change of the SPM concentration is linked to the dynamically derived average radius of the particle mass distribution.

Suspended particulate matter fluxes With respect to SPM concentration changes in the water column, we adopt classical sedimentological approaches. The change of the pelagic SPM concentration C [g $\cdot$ cm^{-3}] is given by the sum of the fluxes (F) due to deposition (dep), resuspension (res) and tidal exchange (tidex), respectively

$$\frac{\mathrm{d}}{\mathrm{d}\,t} C \;=\; F_{\mathrm{res}} - F_{\mathrm{dep}} + F_{\mathrm{tidex}} \quad . \tag{3.23}$$

The varying volume ratio between sources and sinks of the fluxes depending on the time-variable water depth h is included in the individual flux estimates. In the case of erosion/resuspension, we assume an infinite amount of resuspendable material according to Partheniades (1984). SPM is resuspended at a rate M_0, which is an empirical constant, if the bottom shear stress τ is twice the critical value τ_{c}

$$F_{\mathrm{res}} = \frac{M_0}{h}\left(\frac{\tau}{\tau_{\mathrm{c}}} - 1\right) \quad . \tag{3.24}$$

As stated by e. g. Winterwerp (2007), deposition is independent of a critical bottom shear stress. Hence, the deposition rate for a specific concentration $C(r)$ is determined by the water depth and the settling velocity v_{s} that depends on the size of aggregates r

$$F_{\mathrm{dep},r} = \frac{C(r)\, v_{\mathrm{s}}(r)}{h} \quad . \tag{3.25}$$

In order to calculate the settling velocity, the concept of fractal aggregates is used here (Kranenburg, 1994). Hence, the settling velocity is given by

$$v_{\mathrm{s}}(r) = \frac{2^{d_f-1}\,(\rho_{\mathrm{p}} - \rho)\,g\,D_{\mathrm{p}}^{3-d_f}\,r^{d_f-1}}{18\,\mu} \quad , \tag{3.26}$$

where μ is the dynamic viscosity, g the gravitational acceleration constant, ρ the density of water and ρ_{p} the density of the primary particles of diameter D_{p} of which the aggregates with a fractal dimension d_f consists.

The mean settling velocity $\langle v_{\mathrm{s}} \rangle$ is used to calculate the flux for the total concentration C. Assuming an exponential particle-size distribution, it results in a function of the average radius of the particle mass distribution $\langle r \rangle$ (see Sec. 3.2.2, 3.2.2)

$$\langle v_{\mathrm{s}} \rangle = v_{\mathrm{s}}(\langle r \rangle) \cdot \left(\frac{4^{d_f}\,(d_f+1)^{1-d_f}\,\Gamma(d_f + \frac{1}{2})}{2\,d_f\,\sqrt{\pi}} \right) \quad , \tag{3.27}$$

where $\Gamma(x)$ is the Gamma function.

In- and efflux due to tidal exchange between the back-barrier basin and the North Sea is most simply described by a first-order mixing process,

$$F_{\mathrm{tidex}} = E_{\mathrm{w}}\,(C_{\mathrm{o}} - C) \tag{3.28}$$

with E_{w} being a time-dependent exchange rate (see Sec. 3.2.2) and C_{o} the external SPM concentration that passes the tidal inlet.

Reducing complexity in size dynamics Mass fluxes in Eq. (3.23) are coupled with the average radius by the average settling velocity Eq. (3.27). The average radius, in turn, exhibits strong temporal changes induced by shifts in the aggregate size distribution. These shifts are driven by size dependent processes like e. g. deposition, aggregation and fragmentation. Classical aggregation model approaches (e. g. Jackson, 1990; McCave, 1984) divide the distribution into several size classes. In contrast to this approach, we here use the distribution-based approach proposed by Wirtz and Eckhardt (1996) to reduce the complexity of the model.

The basic aim of the distribution-based approach is to derive an explicit evolution equation for statistical properties such as the average radius of the mass concentration distribution $\langle r \rangle$:

$$\langle r \rangle = \sum_i r_i \frac{C_i \, \Delta R_i}{C} \tag{3.29}$$

with $C = \sum_i C_i \, \Delta R_i$. C_i represents a mass concentration of a specific particle size class r_i with a bin width ΔR_i. Further on, the relative growth rate $\hat{\mu}$ can be defined

$$\hat{\mu}(r_i) := \frac{\dot{C}_i}{C_i} \quad , \tag{3.30}$$

where $\dot{C}_i$ denotes the temporal change of the concentration C_i. The $\langle r \rangle$ dynamics can be expressed by statistical means using $\lim_{\Delta R_i \to 0} \hat{\mu}(r_i) = \hat{\mu}(r)$ as

$$\frac{\mathrm{d}}{\mathrm{d}\, t} \langle r \rangle \quad = \quad \langle r \cdot \hat{\mu}(r) \rangle - \langle r \rangle \, \langle \hat{\mu}(r) \rangle \quad . \tag{3.31}$$

One of the main ideas of the approach is to develop the relative growth rate as a Taylor series around $\langle r \rangle$. A higher moment closure, where higher moments $\langle r^m \rangle$ are expressed in terms of $\langle r^{m-1} \rangle$ and $\langle r^{m-2} \rangle$ (Wirtz and Eckhardt, 1996), leads to

$$\frac{\mathrm{d}}{\mathrm{d}\, t} \langle r \rangle \quad = \quad \delta r^2 \cdot \frac{\mathrm{d}}{\mathrm{d}\, r} \hat{\mu}(\langle r \rangle) \quad . \tag{3.32}$$

Hence, temporal changes of $\langle r \rangle$ follow a local gradient of the $\hat{\mu}$. The rate of this adjustment is proportional to the gradient itself and the variance of the aggregate distribution δr^2. This effective variable approximation (EVA) does not require specific assumptions on the underlying distribution function, but looses accuracy for non-Gaussian distributions. The latter is the reason for using $\langle r \rangle$ as state variable because the mass concentration distribution is closer to the Gaussian distribution than the number distribution. Furthermore, the usage of $\langle r \rangle$ in combination with the method described above allows to base its dynamics on a mass conserving formulation.

The overall change of $\langle r \rangle$ [cm] which is coupled to the concentration flux F_{dep} is given by

$$\frac{\mathrm{d}}{\mathrm{d}\,t}\langle r \rangle \;=\; R_{\mathrm{aggv}} + R_{\mathrm{aggv}} - R_{\mathrm{break}} + R_{\mathrm{res}} - R_{\mathrm{dep}} + R_{\mathrm{tidex}} \quad . \tag{3.33}$$

Here, the respective effect of the fluxes F_X (cp. Eqs. (3.23) – (3.25) and (3.28)) on the size dynamics are formulated by using the time derivative of Eq. (3.29) (R_{res}, R_{tidex}) or by using Eq. (3.32) (R_{dep}). Aggregation due to shear (R_{aggv}) and differential settling (R_{aggv}) are processes that internally modify the size distribution without changing the total concentration. Both are formulated using Eq. (3.32). For break-up due to shear (R_{break}) which is also a mass-conserving process, we use a similar approach as Winterwerp (1998).

Endogenous and exogenous control of size dynamics Suspended aggregates are generally formed by coagulation. This process occurs by three mechanisms: Brownian motion, aggregation induced by shear, and by differential settling. Since Brownian motion is only relevant for particles and aggregates smaller than one micrometer (McCave, 1984), it is here neglected. For the formulation of aggregation, we combine the EVA approach with the classical size class-based aggregation approach (see also App. 3.2.6). We here use the curvilinear aggregation kernel in order to take the flow field around the assumed spherical aggregates into account. Using the curvilinear kernel, one obtains for the aggregation due to shear

$$R_{\mathrm{aggv}} = \alpha\,\gamma\,K_{\gamma}(d_f)\,\frac{C}{w_0}\,\langle r \rangle^{4-d_f} \quad , \tag{3.34}$$

where α denotes the collision efficiency ("stickiness"), γ the turbulent shear rate, and $w_0 = 2^{d_f}\rho_{\mathrm{p}}\pi D_{\mathrm{p}}^{3-d_f}/6$ a factor for the radius-weight relationship. The dependence of the specific aggregation function K_{γ} on the fractal dimension d_f is a result of collecting first order moments in the closure approximation (see App. 3.2.6).

In the case of aggregation due to differential settling, the choice of a curvilinear kernel leads to

$$R_{\mathrm{aggv}} = \alpha\, g\, \pi\, K_{\mathrm{v}}(d_f) \cdot (\langle \rho_{\mathrm{f}} \rangle - \rho)\, \frac{C}{w_0\, \mu}\, \langle r \rangle^{5-d_f} \quad , \tag{3.35}$$

where in analogy to K_γ, K_{v} is a nonlinear function of the fractal dimension of the aggregates (see App. 3.2.6). Furthermore, $\langle \rho_{\mathrm{f}} \rangle$ is the mean effective density of SPM aggregates given by

$$\langle \rho_f \rangle = \rho + \frac{2^{d_f}\, (d_f+1)^{3-d_f}\, D_p^{3-d_f}}{8\, \langle r \rangle^{3-d_f}} \cdot \frac{(\rho_{\mathrm{p}} - \rho)\, \Gamma(2d_f - 2)}{\Gamma(d_f + 1)} \quad . \tag{3.36}$$

Since actual data for the break-up rates are not available yet (Stemmann et al., 2004a), we chose a simple break-up term that ensures fragmentation even beside shear-induced aggregation

$$R_{\mathrm{break}} = f_{\mathrm{b}}\, \gamma^b\, \langle r \rangle^q \quad . \tag{3.37}$$

Here, f_{b} is a specific factor for the break-up and b is an exponent for the influence of the shear on the aggregates. By setting $b > 1$, disaggregation gains relevance in highly turbulent regimes, which is in accordance with a number of studies (e. g. Chen et al., 1994; Fugate and Friedrichs, 2003). From Eq. (3.34) it is clear that the balance condition between aggregation due to shear and break-up requires a value of the exponent for the radius q that is greater than $4 - d_f$.

Loss and gain of SPM due to deposition and resuspension also affect the aggregate distribution and, thus, $\langle r \rangle$. Bigger aggregates sink faster than smaller ones (implying equal shape and density). The resulting decline of $\langle r \rangle$ by deposition is determined by Eq. (3.25), (3.26) and (3.32):

$$R_{\mathrm{dep}} = (d_f - 1)\, \delta r^2\, \frac{F_{\mathrm{dep},r}(\langle r \rangle)}{C \cdot \langle r \rangle} \quad . \tag{3.38}$$

The variance of the aggregate concentration distribution is given by $\delta r^2 = \langle r \rangle^2/(d_f + 1)$ (see App. Eq. (3.45) and (3.48)).

Resuspension can be calculated using the time derivative of Eq. (3.29) and leads to a mixing effect by eroded particles of radius r_b:

$$R_{res} = \frac{F_{res}}{C} (r_b - \langle r \rangle) \quad . \tag{3.39}$$

In analogy to Eq. (3.39) the change of $\langle r \rangle$ due to tidal exchange is given by:

$$R_{tidex} = E_w \frac{C_o}{C} (r_o - \langle r \rangle) \quad , \tag{3.40}$$

where r_o is the average radius of the aggregates that are transported into the back-barrier tidal basin of Spiekeroog island.

Physical forcing by tidal currents

As forcings for the model, we use sinusoidal approximations of the model output for the East Frisian Wadden Sea documented by Stanev et al. (2003a), regardless of the ebb-dominated tidal system. The bottom shear stress τ is estimated using the calculated turbulent kinetic energy (TKE) at the bottom: $\tau = \mathrm{TKE} \cdot \rho$. Values range between zero during the turn of the tide to $5\,\mathrm{N \cdot m^{-2}}$ during midtide. The turbulent shear can be estimated from the relation $\gamma = (\epsilon/\nu)^{1/2}$, where ϵ is the energy dissipation rate computed by the model of Stanev et al. (2003a) and ν is the kinematic viscosity. Values for the turbulent shear range between zero and $3\,\mathrm{s^{-1}}$ in the upper water column. During one tidal cycle with a period of 12 h and 25 minutes, the bottom shear stress and the turbulent shear reach their maximum two times during midtide. In the area of the sampling sites, the tidal channels, mean water depth reaches in average a maximum of about 9.5 m at high tide and a minimum of 6.5 m at low tide.

The exchange rate E_w is mainly controlled by tidal currents. It is set to zero for the ebb tide assuming that the aggregate distribution in the back-barrier basin regularly reaches a homogeneous state. This implies that only aggregates transported by incoming water have a different average radius. For the flood tide we assume a sinusoidal characteristic with a maximum value of $1/44700\,\mathrm{s^{-1}}$ between the turn of the tides.

Model validation

Stirred tank system Time series revealing the dynamics of aggregation and fragmentation under different turbulence intensities were obtained from a study with a polystyrene particle/$Al(OH)_3$/water system in a stirred tank documented by Flesch et al. (1999). Mass distribution averages were digitized from the original publication. The fractal dimension of aggregates was set to $d_f = 2.3$ in accordance with the value estimated by Flesch et al.. Only R_{break} and $R_{\text{agg}\gamma}$ were used during the integration of $\langle r \rangle$ in this first model test. Their capability to describe the transient size dynamics were checked after calibrating the shear rate exponent $b = 1.45$, the radius exponent $q = 2.3$ as well as the specific coefficient for break-up and shear-induced aggregation ($f_{\text{b}} = 4 \cdot 10^{-4}\,\mu\text{m}^{-1.3}\text{s}^{-0.45}$ and $\alpha \cdot K_\gamma \cdot C/w_0 = 1.2 \cdot 10^{-5}\,\mu\text{m}^{-0.7}\text{s}^{-1}$).

Back-barrier basin Spiekeroog island Lunau et al. (2006) carried out observations on the aggregate dynamics in the back-barrier basin of Spiekeroog island (see Fig. 3.11), using a sampling device for microaggregates in turbid aquatic systems (Lunau et al., 2004). Samples were taken in February and July 2003, in both cases during two tidal cycles just below the water surface at two different locations. General hydrodynamic and meteorological conditions during the campaigns were comparable. SPM concentration was determined as dry weight (DW). In parallel, images from a digital camera-laser system were analyzed by Lunau et al. (2006) to estimate the aggregate number frequency distribution, which yields the equivalent circular radius (ECR), a useful measure to compare differently shaped aggregates. A mass-weighted average radius can not be directly determined from image analysis. Therefore, assuming an exponential aggregate number distribution, we developed the relation

$$\frac{\langle r \rangle}{d_f + 1} + r_{\text{min}} = \frac{\int_{r_{\text{min}}}^{\infty} r \cdot n(r)\,\text{d}r}{\int_{r_{\text{min}}}^{\infty} n(r)\,\text{d}r} \tag{3.41}$$

to compare the mass average radius $\langle r \rangle$ and the average ECR (given by the right-hand side), where $r_{\text{min}} = 7.5\,\mu\text{m}$ is the detection limit of the used camera system.

Winter and summer parametrization

In order to find seasonal parameter shifts that may originate from biological influences, a subset of the model parameters was varied systematically against each other. In particular, the collision efficiency α, the aggregate strength f_b, the fractal dimension d_f, the critical bottom shear stress for resuspension τ_c, and the average radius of resuspended aggregates r_b were varied. In order to estimate the deviation between the simulation and the experimental data, we defined a cost function

$$\mathrm{err} \quad = \quad \frac{1}{M} \sum_{j}^{M} \left(\frac{\frac{1}{2} \left| \delta x_j - \delta y_j \right|}{\delta y_j} + \frac{1}{N} \sum_{i}^{N} f_{i,j} \right) \quad , \tag{3.42}$$

where $f_{i,j} = (|\langle y_j \rangle - x_{i,j}| - \delta y_j)/\delta y_j$ if $|\langle y_j \rangle - x_{i,j}| - \delta y_j > 0$ else $f_{i,j} = 0$. Here, j in an index for the $M = 2$ target variables (C and $\langle r \rangle$, the latter used in combination with Eq. (3.41)) and δy_j and δx_j the standard deviation of the data and the simulation, respectively. N denotes the number of simulation results after the transient phase. Hence, the cost function essentially calculates deviations in time mean and time standard deviation between the simulation and the data. The systematic parameter variation was done in three steps. Firstly, we started with the same parameter range for both situations. After that, the resultant parameter sets were sorted by the value of the cost function. A mean value and a standard deviation were then calculated for each parameter for the best 100 simulations. Secondly, the parameter range was limited for each situation by only using the mean value plus/minus the standard deviation. This step was repeated to obtain the best parameter set for the winter and the summer situation, again producing mean and standard deviation values.

The remaining parameters were fixed as follows. The density of water is $\rho = 1\,\mathrm{g \cdot cm^{-3}}$ and the dynamic viscosity was set to $\mu = 0.018\,\mathrm{g \cdot cm^{-1} \cdot s^{-1}}$ and $\mu = 0.01\,\mathrm{g \cdot cm^{-1} \cdot s^{-1}}$ for winter (February) and summer (July), respectively. In analogy to Winterwerp (1998), the power for shear and for the average radius in the break-up formulation were set to $b = 1.5$ and $q = 3$, respectively and the density of primary particles $\rho_\mathrm{p} = 2.6\,\mathrm{g \cdot cm^{-3}}$. For the erosion rate, we use $M_0 = 3.7 \cdot 10^{-7}\,\mathrm{g \cdot cm^{-2} \cdot s^{-1}}$ following Stanev et al. (2007), who used that value in a SPM transport model of the Spiekeroog back-barrier basin. The

external concentration of SPM that passes the tidal inlet was constrained to an interval similar to the range of values in the back-barrier by using available data (Lunau, pers. communication). We therefore chose a value of $C_o = 3 \cdot 10^{-5}\,\mathrm{g \cdot cm^{-3}}$ for both cases. First simulations revealed a small influence of the external average radius on the model results. We therefore fixed this unknown parameter to $r_o = 0.0015\,\mathrm{cm}$. The best fitting values of the variable and the *a priori* fixed parameters are listed in Tab. 3.3. A list of state, auxiliary and forcing variables can be found in Tab. 3.2.

Model analysis

The explicit form of the equations for the changes of $\langle r \rangle$ allows a direct assessment of the underlying processes. In order to estimate the relative importance of a process R_i (e. g. resuspension) for the change of $\langle r \rangle$ at time t, we define the relative contribution index RCI_i^t:

$$RCI_i^t = \frac{R_i^t}{\sum_i |R_i^t|} \quad . \tag{3.43}$$

For a sensitivity study, the winter and the summer parametrization are used as reference runs. After varying the value of d_f by $\pm 5\,\%$ and the other varied parameters by $\pm 50\,\%$, their effect on the average settling velocity $\langle v_s \rangle$ was assessed.

3.2.3 Results

A part of the model, in particular the change of the average radius by aggregation and break-up due to shear, Eq. (3.34) and (3.37), was tested i) versus experimental results in a stirred tank system of Flesch et al. (1999) (see Fig. 3.12) and ii) in a model comparison with a size class-based model (Maerz et al., 2010, cf. also to Sec. 3.1), both being compared to laboratory experiments. In both cases, the model was very well able to follow the evolution of the aggregate size.

Table 3.2: State variables (*), auxiliary and forcing variables (f)

Variable	Description	Unit
C	total pelagic SPM concentration (*)	$\mathrm{g \cdot cm^{-3}}$
δr^2	aggregate size variance based on SPM mass distribution	$\mathrm{cm^2}$
E_w	water exchange rate (f)	$\mathrm{s^{-1}}$
γ	shear rate (f)	$\mathrm{s^{-1}}$
K_γ	factor for aggregation due to shear	–
K_v	factor for aggregation due to differential settling	–
$\langle r \rangle$	average radius based on the SPM mass distribution(*)	cm
$\langle \rho_\mathrm{f} \rangle$	average SPM density	$\mathrm{g \cdot cm^{-3}}$
τ	bottom shear stress (f)	$\mathrm{N \cdot m^{-2}}$
v_s	aggregate settling velocity	$\mathrm{cm \cdot s^{-1}}$
w_0	factor for radius-weight relation	$\mathrm{g \cdot cm^{-d_f}}$
h	water depth (f)	cm

Table 3.3: List of model parameters with values for the winter (Feb.) and the summer (July) situation (varied in parameter variation: (*))

	Description	Feb.	July	Unit
α	collision efficiency(*)	0.0166	0.0059	–
q	break-up exponent for the radius	3		–
C_o	external SPM concentration	$3 \cdot 10^{-5}$		$\mathrm{g \cdot cm^{-3}}$
d_f	fractal dimension(*)	2.24	2.03	–
M_0	resuspension rate	$3.7 \cdot 10^{-7}$		$\mathrm{g \cdot cm^{-2} \cdot s^{-1}}$
f_b	specific break-up factor(*)	2.76	1.15	$\mathrm{s^{b-1} \cdot cm^{1-q}}$
g	gravitational acceleration	981		$\mathrm{cm \cdot s^{-2}}$
b	break-up exponent for the shear	1.5		–
μ	dynamic viscosity	0.018	0.01	$\mathrm{g \cdot cm^{-1} \cdot s^{-1}}$
ρ	density of water	1.0		$\mathrm{g \cdot cm^{-3}}$
r_b	mean radius of resuspended aggregates(*)	0.0108	0.034	cm
r_o	mean radius of incoming aggregates	0.015		cm
ρ_p	density of primary particles	2.6		$\mathrm{g \cdot cm^{-3}}$
τ_c	critical bottom shear stress(*)	0.29	0.36	$\mathrm{N \cdot m^{-2}}$

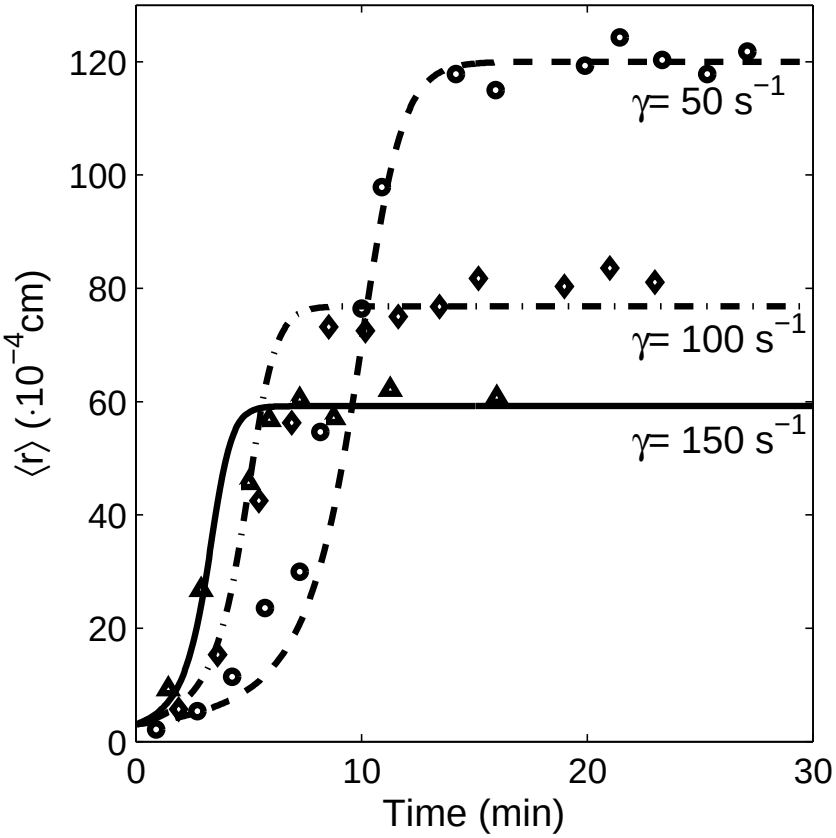

Figure 3.12: Observed and simulated average radius $\langle r \rangle$ changing over time in a stirred tank system. Data from experiments for a range of different turbulent shear rates originate from Flesch et al. (1999).

Aggregate number frequency distribution

In Fig. 3.13, aggregate number densities as measured by Lunau et al. (2006) are shown for samplings in February and July 2003, in both cases for three different tidal phases. High variability in the abundance of aggregates is evident both during single tidal cycles as well as between seasons. Nevertheless, the aggregate number frequency distribution always follows an exponential law. For this reason, we used an exponential number distribution as prescribed by Eq. (3.44) in the model. The fitted exponential functions, however, have the tendency to overestimate aggregate numbers for larger size classes.

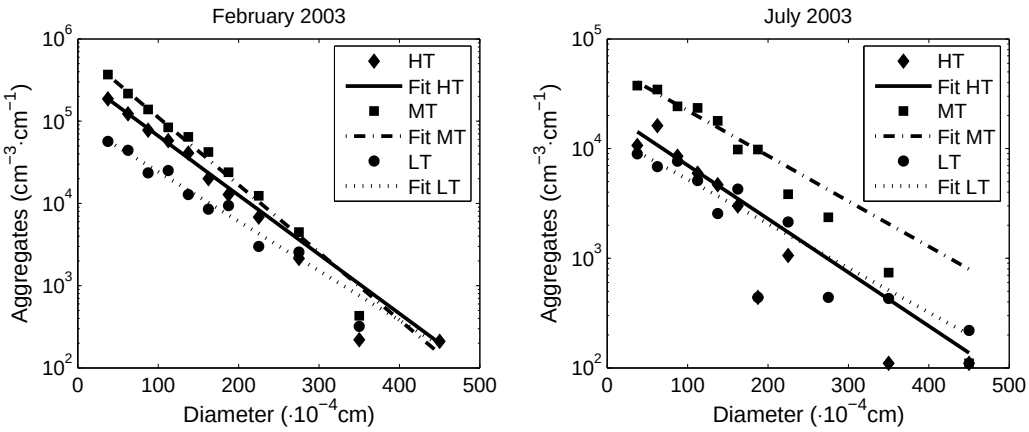

Figure 3.13: Aggregate number frequency distribution (per cubic volume and size class bin width) in different tidal situations in February 2003 (winter) and July 2003 (summer) (Lunau et al., 2006) and datafits to better illustrate the exponential decrease of aggregate numbers. HT: high tide; LT: low tide; MT: mean tide

Winter situation

In winter (February) the observed average ECR ranges between 22 µm and 36 µm with a superimposed noisy tidal signal (see Fig. 3.14a). At the turn of the tide or the next sampling thereafter (e. g. about 1 h later), the average ECR is initially small but with few exceptions increases afterwards. The model run with the best fitting parameter set (see Tab. 3.3) minimizes the cost function to err=0.128. This value takes both the temporal averages and the standard deviations of ECR and SPM into account. For the regularly oscillating SPM concentration, this translates to small individual deviations. In contrast, irregular fluctuations in ECR are not precisely redrawn despite a satisfying match between the statistical properties of simulated and measured values (Fig. 3.14a). From one turn of the tide to another, the simulated $\langle r \rangle$ decreases to a minimum during the highest shear rates and increases again afterwards. The amplitude of the $\langle r \rangle$ variation is slightly smaller during low tide than during high tide. This originates from the changing water level as aggregates need less settling time during low tide compared to high tide. This can be seen in Fig. 3.14b where, in addition, the contribution of the different processes to the change of the average radius is shown. A typical succession

can be seen in each semi-tidal period. During the turn of the tides, aggregation due to differential settling and deposition are the main processes in the system. Shortly after the turn of the tide, break-up and aggregation due to shear becomes relevant. With up to 60 %, break-up is the main process during the time of high shear rates and both aggregation processes cannot balance it during that time. Furthermore, the resuspended aggregates influence the size dynamics of the aggregates up to 25 %. With decreasing shear rates, aggregation due to differential settling and deposition become more relevant again and dominate the system during the turn of the tide. Given by the model conditions, tidal exchange is only relevant during the flood phase and contributes less than 8 % to the change of the average radius during that time. Overall, the zero-dimensional model shows less short-term fluctuations than the observed average ECR.

Measured values of the SPM concentrations in February vary between $18\,\mathrm{mg(DW)\cdot L^{-1}}$ and $68\,\mathrm{mg(DW)\cdot L^{-1}}$ (Fig. 3.15). They show clear tidal cycles. The minimum values are reached during the turn of the tides, whereas maximum SPM concentrations are observed at times of high current velocities. This pattern is robustly described by the model. A dilution effect due to the changing water level leads to lower SPM concentrations at low tide than at high tide.

Summer compared to winter situation

The systematic parameter variation resulted in a different parameter set for the winter and the summer situation. For the summer situation, the error for the best parameter set given in Tab. 3.3 is again small (err = 0.128). We found the following mean and standard deviation values for the winter situation: $\langle\alpha\rangle = 0.0161 \pm 8.65\cdot10^{-4}$, $\langle d_f\rangle = 2.2353 \pm 0.0089$, $\langle f_\mathrm{b}\rangle = 2.55 \pm 0.3313\,\mathrm{s^{0.5}\cdot cm^{-2}}$, $\langle r_\mathrm{b}\rangle = 0.0099 \pm 0.0015\,\mathrm{cm}$ and $\langle\tau_\mathrm{c}\rangle = 0.2947 \pm 0.0089\,\mathrm{N\cdot m^{-2}}$. Whereas for the summer situation, the parameter variation leads to $\langle\alpha\rangle = 0.0059 \pm 3.84\cdot10^{-4}$, $\langle d_f\rangle = 2.0283 \pm 0.0094$, $\langle f_\mathrm{b}\rangle = 1.232 \pm 0.087\,\mathrm{s^{0.5}\cdot cm^{-2}}$, $\langle r_\mathrm{b}\rangle = 0.0369 \pm 0.0023\,\mathrm{cm}$ and $\langle\tau_\mathrm{c}\rangle = 0.3653 \pm 0.0136\,\mathrm{N\cdot m^{-2}}$. Hence, all parameters differ significantly, and an increase in τ_c, r_b and a decrease in α, f_b and d_f were computationally found compared to the winter situation.

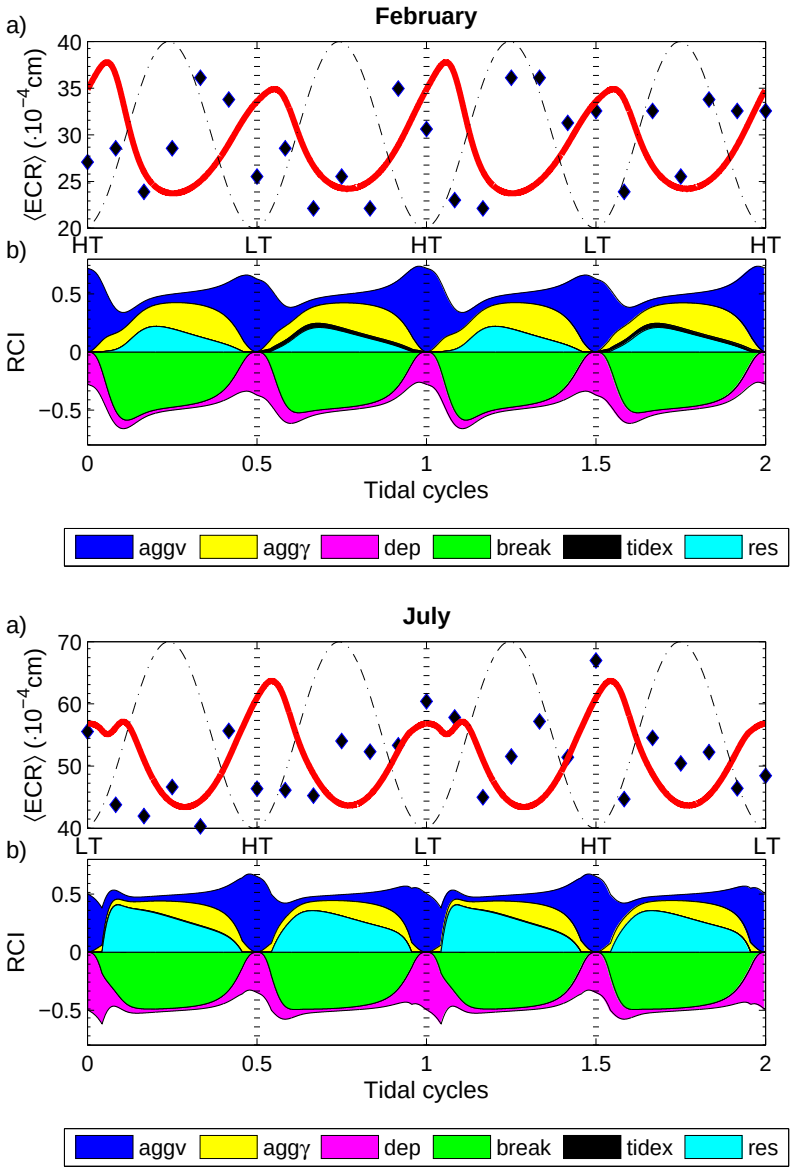

Figure 3.14: a) Observed average ECR in February 2003 (winter) and July (summer) during two tides in the back-barrier basin of Spiekeroog island (diamonds) compared to the simulation (continuous line). The solid-dashed line shows the scaled oscillation in γ and τ (see Sec. 3.2.2 for minimum and maximum values). b) Relative contribution index (RCI) for the driving processes R_i ($i = \text{aggv}, \text{agg}\gamma, \text{break}, \text{res}, \text{dep}, \text{tidex}$) of the simulated $\langle r \rangle$ dynamics. (HT: high tide LT: low tide)

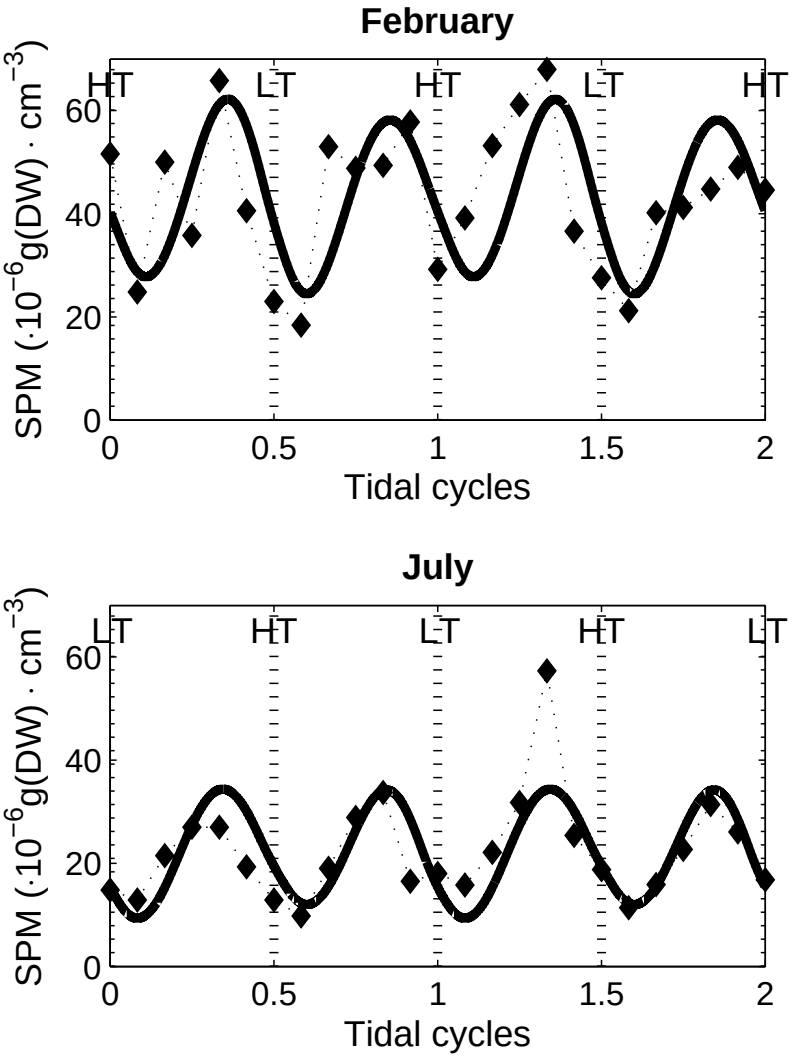

Figure 3.15: Observed (diamonds) and simulated (line) suspended matter concentrations in the back-barrier basin of Spiekeroog island during two tides in February 2003 (winter; upper panel) and July 2003 (summer; lower panel). (HT: high tide; LT: low tide; DW: Dry weigth)

In the summer situation, measured SPM concentrations range from 10 mg (DW)·L^{-1} to 57 mg(DW)·L^{-1} and are significantly lower than in winter. Only the shapes of their dynamics remain roughly the same and are again well described by the simulated SPM concentrations (see Fig. 3.15).

The observed average ECR is higher in summer than in winter, but shows a more pronounced short-term variability (see Fig. 3.14a). The general trends of the simulations are the same, apart from a small dip shortly after low tide in summer. Those differences are triggered by the relation between the simulated $\langle r \rangle$ and r_b during the onset of resuspension. This relation is also responsible for the seasonally different contributions of resuspension on the size dynamics of the $\langle r \rangle$ which is about 40 % in summer compared to 25 % in winter. During low tide, the contribution of deposition to the change of $\langle r \rangle$ is also slightly enhanced during summer relative to winter.

Sensitivity analysis

A sensitivity analysis was performed for both the winter and the summer situation using as target size the mean settling velocity of SPM (Eq. (3.27)) which is a key property in sediment transport modeling. We varied the stickiness α, the break-up factor f_b, the radius of resuspended aggregates r_b, the critical bottom shear stress τ_c for ±50 %, and the fractal dimension d_f for ±5 %.

Apart from the fractal dimension, the model is relatively sensitive to the stickiness in both situations compared to f_b, τ_c and r_b. In the case of variations of the latter four parameters, the general periodic dynamics turns out to be robust (see Fig. 3.16).

The model is most sensitive to the fractal dimension, which can also change the general behavior of the model. This is due to the interaction between the processes of deposition, resuspension and aggregation due to differential settling. Especially the ratio between aggregation due to different settling and deposition rates determines whether the average size of aggregates increases or decreases during the turn of the tides. During times of high shear rates, the eroded aggregates also have a strong impact, as can be seen from the relative contribution of erosion on the size dynamics presented in the previous section. Depending on the size of the eroded aggregates, resuspension can decrease

or increase the size of the aggregates in the water column. This complex interplay of the processes leads to tidally and seasonally different dynamics of the average radius and therefore of the settling velocity. Furthermore, the strong dependency of the main processes like aggregation and deposition on the seasonally variable fractal dimension leads to their huge impact on that interplay. Hence, the model also shows different seasonal sensitivities to the parameters.

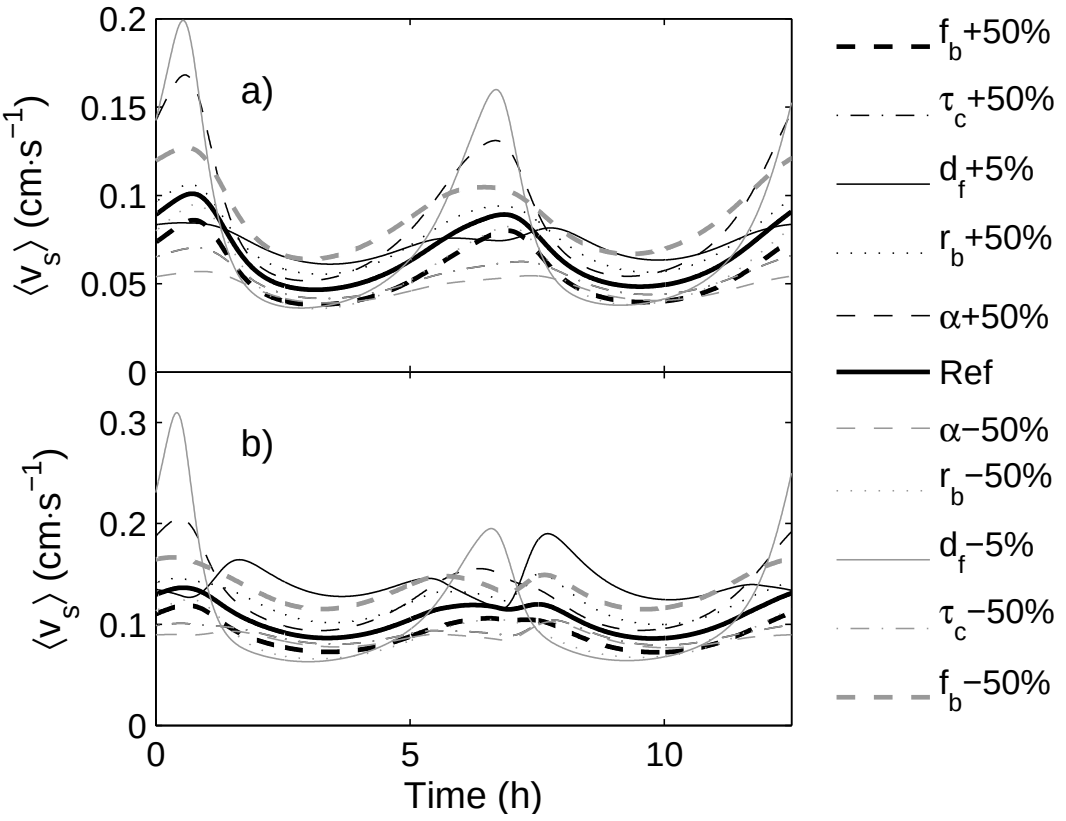

Figure 3.16: Mean settling velocity of the modified runs compared to the reference run a) February and b) July. Note that d_f is varied by $\pm 5\,\%$, all other parameters by $\pm 50\,\%$.

3.2.4 Discussion

A basic assumption of our analysis was the exponential form of the aggregate number distribution. As can be seen from Fig. 3.13, this assumption is realistic for tidal basins of the Wadden Sea. This is in contrast to other regions such as estuaries or the open ocean from where bimodal (Chen et al., 2005) or power law and log-normal (e. g. McCave, 1984) distributions have been reported.

It is obvious that biological processes such as primary production show a strong seasonal variability. For instance, measurements by Lunau et al. (2006), reveal e. g. low chlorophyll *a* (Chl *a*) concentrations in February (ca. 1 µg Chl $a \cdot L^{-1}$), whereas in summer the concentrations were about six times higher. This ratio can be even more pronounced on shorter time scales, e. g. when comparing Chl *a* of incoming North Sea water in winter with a spring bloom situation (e. g. see data in Wirtz and Wiltshire, 2005). Algae are important producers of extracellular polymeric substances (EPS; Passow et al., 2001) that can form transparent exopolymeric particles (TEP; Thornton, 2002), and hence, a positive relationship between Chl *a* and TEP can be found (e. g. Claquin et al., 2008). Furthermore, bacteria are also known to produce EPS ubiquitously (Decho, 1990), however, their role for the generation, preservation and destruction of TEP is still unclear (Passow et al., 2001). TEP can increase the stickiness of SPM (Thornton, 2002; Simon et al., 2002; Passow, 2002c). Reviews of literature data (Myklestad, 2000) or inverse modeling studies (Schartau et al., 2007) reveal a rather intricate relationship between Chl *a* concentration and stickiness. Generally, two modes of TEP production are found. The first is due to passive leakage of low molecular weight organic carbon during phytoplankton blooms. The second, and more prominent, mode occurs under nutrient-limited conditions when it is decoupled from algal growth, being characterized by active transport, in particular of polysaccharides, through the cell membrane. As a result, significantly raised stickiness due to exopolymers can be assumed not only during algal blooms but also in the periods following the spring and summer blooms. The systematic model calibration study did surprisingly not indicate increased values of stickiness in summer. Nevertheless, although the calibrated value of stickiness is very low in both seasonal situations, it is within the range reported in the literature.

Kiørboe et al. (1990) found values between $\alpha = 5 \cdot 10^{-3}$ and $\alpha = 10^{-1}$ for different algae species whereas Dam and Drapeau (1995) found values of $\alpha < 0.1$ and up to $\alpha = 0.8$.

On the other hand, the incorporation of TEP into aggregates could lead to looser and organic rich aggregates with embedded sediment particles like those reported by Ayukai and Wolanski (1997), and hence, to smaller aggregate densities compared to pure mineralic aggregates. In the model simulation, the change in morphology and density by e. g. the incorporation of TEP into aggregates would be represented by a smaller fractal dimension. We indeed find a lower fractal dimension in summer than in winter. The study of Chen et al. (2005) in the Scheldt estuary, which is similar to the Spiekeroog back-barrier basin, also emphasize the importance of biological factors for the SPM dynamics. They found larger and looser aggregates in summer than in winter, which is in good agreement with our findings, and identified biological activity and concentration of organic matter as key factors for the morphology of aggregates.

Both, the role of EPS in the collision efficiency and its influence on the fractal structure of an aggregate can lead in different ways to changes in aggregation rates. We found a decrease in stickiness and fractal dimension in summer. Particularly in the case of aggregation due to shear, a reduced collision efficiency might be compensated by an increase of the collision frequency due to a lower fractal dimension. Thus, the shear aggregation rate can be nearly the same in both seasons. The deposition rate, in turn, might be strongly affected by the influence of EPS on the aggregate structure (De La Rocha and Passow, 2007; Ploug et al., 2002). This probable effect of EPS should be addressed in further studies.

The parameter variation also revealed a higher critical bottom shear stress value and a larger average radius of resuspended aggregates in summer than in winter. This is an indication for the influence of biological processes on the SPM dynamics in that benthic algae can stabilize the sediment (Stal, 2003; Black et al., 2002). For the adjacent back-barrier tidal basin of Langeoog island, Lanuru (2004) indeed found that the critical bottom shear stress correlated positively with the Chl *a* concentration of phytobenthos.

In summary, the differences of the calibrated values in the parameter sets support major findings of Chen et al. (2005) and Lunau et al. (2006). They pointed out that aggregate dynamics in different tidal systems are mainly controlled by physical processes in winter, whereas in summer biological processes gain high relevance. Similar seasonal differences are also found in deeper tidal systems such as the Chesapeake Bay (Fugate and Friedrichs, 2003). The control mechanisms identified in this study may thus be relevant to a broader geographic spectrum of sites. As the present study was restricted to only two different seasonal situations, further studies such as that of Lumborg and Pejrup (e. g. 2005), but with a better representation of biological influences, are needed to assess biological effects in the long term.

Model properties

The strong influence of aggregation due to differential settling with respect to aggregation due to shear was somewhat unexpected considering the findings of e. g. Lick et al. (1993). However, Lick et al. initially used particles of same size. Hence, they might have underestimated the aggregate growth rates compared to a natural aggregate distribution where the aggregate settling velocities differ substantially. The latter leads to an increased aggregation rate compared to a narrow distribution in the experiment. Nevertheless, it is still uncertain how precise the model predicts the relative contributions. This should hence be the subject of further investigations.

The main difficulty arises from the zero-dimensionality of our model. Upward and downward migration of aggregates is strongly determined by vertical as well as lateral transport processes. Our assumption of well-mixed tidal waters leaving the back-barrier basin turns out to be rather weak, given the larger short-term model-data misfits, connected with a larger variability inherent in the measurements. Different water bodies still carry individual sediment characteristics during their passage through the main tidal inlet (cp. Fig. 3.11). A spatially explicit representation of the water column could enhance our understanding of and quantitative estimates for the feedback between aggregation and sinking. In order to obtain a first estimate of the effect due to vertical transport, we currently include the model in a 1-D turbulence model.

Already in its zero-dimensional form, our modeling approach is able to link the high variability in near-shore SPM dynamics to the succession of driving factors. This has been made possible by two novel elements, i. e. (1) by reducing the complexity inherent in e. g. aggregate-aggregate interactions and a number of biologically mediated physical processes to few model equations, and (2) by introducing an index (RCI) to quantify the relative contribution of those processes in shaping the SPM distribution. Both, simplicity and analytical structure enhance the transparency of the approach, in particular compared to former size class-based aggregation models (Jackson, 1990; Riebesell and Wolf-Gladrow, 1992; Stemmann et al., 2004a; McAnally and Mehta, 2002). Remarkably, the model equation for the aggregation due to shear is in its form ($\propto r^{4-d_f}$) similar to the aggregation and fragmentation model for a characteristic diameter proposed by Winterwerp (1998). However, on the basis of the underlying size distribution of our model, one can generate further variables, e. g. light climate, relevant in ecosystem models.

With respect to the distribution-based model introduced by Kriest and Evans (2000), the moment expansion proposed here introduces a small error by employing a higher moment closure. Instead of seeking analytical solutions, it uses lengthy but mostly straightforward calculations to derive approximate solutions which, however, are still linked to the underlying, semi-mechanistic assumptions such as kernel functions. This approach has the benefit of being compatible with an arbitrary number of processes. With moderate analytical effort one can include or exclude individual interactions and their effects on the mean characteristics of the aggregate distribution. Furthermore, the model can be developed for different aggregate number distributions than the exponential form used in this study, and which may not be valid in a broader context or in different regions like the shelf. We believe that the resulting flexibility during a model developing phase supports a more efficient selection and description of processes with consequences for a later coupling of SPM models to hydrodynamic as well as ecosystem models. The availability of the moment approximation to systematically adapt both distribution and kernel functions as introduced in App. 3.2.6, improves models for the dynamics of a characteristic diameter (e. g. Winterwerp et al., 2006). These models require a higher number of parameters which have to be evaluated separately for individual case studies.

In comparison to size class-based models, initialization as well as computational effort are substantially reduced by using a minimal number of state variables. On the other hand, the quantitative error following from the moment expansion as well as from the underlying assumption of a fixed functional form of the aggregate number distribution can be regarded as small relative to the still existing uncertainties in the process description of e. g. sinking, aggregation or break-up. The quantitative error, in addition, does not affect the analytical form of the resulting equation.

3.2.5 Conclusion

We propose a new distribution-based model that is tested for its capability to investigate the relevance of physical and biological processes and parameters on aggregate dynamics of SPM in turbid shallow waters. By a systematic parameter variation for a winter and a summer situation, we were able to identify seasonal shifts in major parameters of the SPM dynamics. The tidal signal with its strong currents is the main forcing factor for aggregate dynamics. The study confirmed the hypothesis that in winter biological impacts on the aggregate size dynamics are lower or negligible compared to summer when biological factors influence e. g. the fractal dimension of aggregates and the critical bottom shear stress more intensively. In particular, EPS excretion by algae and bacteria has a remarkable effect on the aggregate dynamics regarding both the size dynamics as well as the total SPM concentration. As a consequence, one should pay more attention to biological control mechanisms in SPM transport models, especially if periods of high primary production as well as microbial activity or nutrient-depleted conditions are simulated.

As the distribution-based model resolves a nearly complete set of processes, subsequent applications may address biologically affected processes like aggregation and deposition as well as resuspension and may link these processes to coastal morphodynamics, SPM budgets or biogeochemical cycles. Due to its simplicity in terms of state variable number, the model has low computational costs and parametrization effort, but has relevant and clearly defined interfaces. Therefore, a coupling to other models can be expected to be reasonable. Regarding models for SPM transport, the average settling velocity would be the

relevant output variable. For ecosystem models, additional relevant variables could be generated, e. g. light climate or aggregate surface to volume ratios relevant for bacterial degradation. The present study has already demonstrated the usefulness of an integrated description of biological, biogeochemical and sedimentary processes, particularly in view of the potential to study mutual feed-backs. However, the identification of major shifts between the summer and the winter parametrization also strongly indicates that, besides average size, further SPM characteristics have to be subjected to an analogous treatment. We recommend that future models explicitly acknowledge the seasonal time evolution of the fractal dimension of aggregates. This property is only rarely addressed by field studies so far. By highlighting such data gaps, this model study helps in designing future research in the intricate field of coupled physical-biogeochemical systems at the land-ocean interface.

3.2.6 Appendix: Aggregation

Similar to the approach of Kriest and Evans (1999), we split the concentration distribution into the aggregate number distribution $n(r)$ and the aggregate weight $w(r)$. Following the data presented by Lunau et al. (2006) an exponential number distribution is assumed where β is the slope of the distribution

$$n(r) = N_0 \, \exp(-\beta r) \quad . \tag{3.44}$$

N_0 denotes the number of infinitesimal small aggregates which depends on $\langle r \rangle$ and the concentration C

$$C = \int_0^\infty N_0 \, \exp(-\beta r) \, w_0 \, r^{d_f} \, \mathrm{d}r \quad . \tag{3.45}$$

The weight is simply given by $w(r) = w_0 \, r^{d_f}$ where d_f is the fractal dimension and $w_0 = 2^{d_f} \, \rho_\mathrm{p} \, \pi \, D_\mathrm{p}^{3-d_f}/6$ is a specific model constant reflecting the composition of coagulated particles. Using the Gamma function together with the rule $\Gamma(x+1) = x \cdot \Gamma(x)$ the integral form of $\langle r \rangle$:

$$\langle r \rangle = C^{-1} \int_0^\infty n(r) \, w_0 \, r^{d_f+1} \, \mathrm{d}r \tag{3.46}$$

becomes a simple relationship between the slope β of the number distribution, $\langle r \rangle$ and the fractal dimension of aggregates:

$$\beta \cdot \langle r \rangle = d_f + 1 \quad . \tag{3.47}$$

Similarly, we find for the variance:

$$\delta r^2 = \frac{\langle r \rangle^2}{d_f + 1} \quad . \tag{3.48}$$

Since the resulting concentration distribution is a unimodal function of the radius, the basic requirement for the accuracy of the EVA methodology is fulfilled.

The equation for aggregation proposed by Jackson (1990) can be brought into an integral form that allows analytical integration if we suppose that the radius and not mass is conserved. Mass conservation, however, will be later assured by a subsequent re-formulation. In the size-conserving version, the net gain due to coagulation for aggregates of radius r reads:

$$\begin{aligned} \frac{\mathrm{d}\, n(r)}{\mathrm{d}\, t} &= \frac{1}{2}\,\alpha \int_0^r n(r')\, n(r-r') \cdot I(r', r-r')\, \mathrm{d}r' \\ &\quad - \alpha\, n(r) \int_0^{r_\infty} n(r') \cdot I(r, r')\, \mathrm{d}r' \quad . \end{aligned} \tag{3.49}$$

In the first term of the right-hand side, n aggregates of size r' and $r - r'$ collide with a collision frequency given by the aggregation kernel $I(r', r - r')$. They stick together with the collision efficiency α. The second term quantifies the loss of aggregates of radius r due to aggregation. For the aggregation kernel we use the curvilinear version - in the case of shear-induced aggregation: $I_\gamma(r, r') = 10\,\gamma\,(r + r')^2\, r$ and for differential settling: $I_v(r, r') = \frac{1}{2}\,\pi\, r^2\, |v_\mathrm{s}(r') - v_\mathrm{s}(r)|$.

The relative concentration change of aggregates with a specific radius ($\hat{\mu}(r)$) is the product of $\mathrm{d}\, n(r)/\mathrm{d}\, t$ and the weight of aggregates $w(r)$ divided by the concentration $C(r)$. For aggregation due to shear ($\hat{\mu}_{\mathrm{agg}\gamma}$), insertion of

Eq. (3.47) and with $r_\infty \to \infty$ and $\beta > 0$ one yields:

$$\hat{\mu}_{\mathrm{agg}\gamma}(r) = \frac{5\,\alpha\,N_0\gamma}{2\,\beta^3}\left(\beta^3\,r^4 - 4\,\beta^2\,r^3 - 8\,\beta r^2 - 8\,r\right) \quad . \tag{3.50}$$

Averaged over the entire distribution, the relative change due to aggregation has to vanish as aggregation does not change the total concentration. This distribution average, in turn, can be approximated by a 2nd or 4th order closure in order to ensure the mass conservation (here shown for the 2nd order closure):

$$\langle\hat{\mu}_{\mathrm{agg}\gamma}(r)\rangle = \hat{\mu}_{\mathrm{agg}\gamma}(\langle r\rangle) + y_\gamma\,\frac{\partial^2\,\hat{\mu}_{\mathrm{agg}\gamma}(\langle r\rangle)}{\partial\,r^2} = 0 \quad , \tag{3.51}$$

where the factor y_γ depends on the type of the underlying distribution and, in the case of a Gaussian function, equals $\delta r^2/2$ (Wirtz and Eckhardt, 1996). Since Eq. (3.51) is linear in y_γ, it generates together with Eq. (3.47) a formulation of y_γ as a polynomial of d_f. Based on the principal equation (3.32) supplemented by Eq. (3.51) and Eq. (3.45), the formulation for aggregation due to shear then reads

$$\begin{aligned} R_{\mathrm{agg}\gamma} &= \delta r^2 \cdot \frac{\mathrm{d}}{\mathrm{d}\,r}\left(\hat{\mu}_{\mathrm{agg}\gamma}(\langle r\rangle) + y\,\frac{\partial^2\,\hat{\mu}_{\mathrm{agg}\gamma}}{\partial\,r^2}(\langle r\rangle)\right) \\ &= \alpha\,\gamma\,K_\gamma(d_f)\,\frac{C}{w_0}\,\langle r\rangle^{4-d_f} \end{aligned} \tag{3.52}$$

with

$$K_\gamma(d_f) = \frac{5\,(d_f+1)^{d_f-2}}{(3\,d_f^2-7)\,\Gamma(d_f+2)} \cdot \sum_{i=0}^{5} a_i\,d_f^i \quad , \tag{3.53}$$

where $a_0 = 112$, $a_1 = 155$, $a_2 = 48$, $a_3 = -14$, $a_4 = 0$, $a_5 = 3$. Winterwerp (1998) derived the same size exponent $4 - d_f$ for the aggregation rate due to shear for a characteristic diameter.

In the case of aggregation due to differential settling, we use the same calculation scheme with a 4th order closure and differentiate between the cases $r > r'$ and $r \leq r'$ in the step of integration. As it is impossible to do the integration step in a general way with the settling velocity given by Eq. (3.26),

we analytically incorrectly use the Stokes settling velocity for particles with a density independant of r during the integration. After the complete calculation scheme as described above, we then use the mass-weighted average aggregate density

$$\langle \rho_{\mathrm{f}} \rangle = \rho + \frac{2^{d_f}\,(d_f+1)^{3-d_f}\,D_p^{3-d_f}}{8\,\langle r \rangle^{3-d_f}} \cdot \frac{(\rho_{\mathrm{p}} - \rho)\,\Gamma(2\,d_f - 2)}{\Gamma(d_f+1)} \tag{3.54}$$

as the density of the aggregates. This might lead to small deviations for $d_f < 3$, but is totally valid for $d_f = 3$. This procedure leads to a general equation, dependent on d_f, for the change of the average radius due to differential settling

$$R_{\mathrm{aggv}} = \alpha\, g\, \pi K_{\mathrm{v}}(d_f) \cdot (\langle \rho_{\mathrm{f}} \rangle - \rho)\, \frac{C}{w_0\, \mu}\, \langle r \rangle^{5-d_f} \quad , \tag{3.55}$$

where the function $K_{\mathrm{v}}(d_f)$ is:

$$\begin{aligned} K_{\mathrm{v}}(d_f) \;=\; & \frac{(d_f+1)^{d_f-2}}{216\,\Gamma(d_f+2)} \Bigg(\sum_{i=0}^{4} b_i\, d_f^i + \exp(-d_f - 1) \sum_{i=0}^{7} c_i\, d_f^i \\ & \qquad + \exp(-2\,d_f - 2) \sum_{i=0}^{4} d_i\, d_f^i \Bigg) \\ & \cdot \Bigg(-45\,d_f + 51 + \exp(-d_f - 1) \cdot \sum_{i=0}^{3} e_i\, d_f^i \Bigg)^{-1} \quad , \end{aligned} \tag{3.56}$$

where: $b_0 = -24615$, $b_1 = -12465$, $b_2 = 6174$ $b_3 = 675$, $b_4 = -405$, $c_0 = -34236$, $c_1 = -137496$, $c_2 = -74376$, $c_3 = 40164$, $c_4 = 10020$, $c_5 = -3216$, $c_6 = -96$, $c_7 = 36$, $d_0 = -21504$, $d_1 = -75776$, $d_2 = -25600$, $d_3 = 7168$, $d_4 = 3072$, $e_0 = 96$, $e_1 = 144$, $e_2 = -128$, $e_3 = 16$.

Chapter 4

Potential applications of the novel flocculation model

The distribution-based flocculation model, introduced in Sec. 2.4, 3.1 and 3.2, is originally intended also to be coupled to spatially explicit sediment transport models. In this section, its capability for such coupling is demonstrated while a validation of the in the following described resulting 1D vertical model with data has yet to be done. However, a comparison with a size class-based model is carried out in a first approach. Such a spatially explicit SCB model has been successfully used by Xu et al. (2008) in comparison with experimental laboratory data. The SCB model can thus be regarded as a plausible reference for SPM concentration and size dynamics in a tidally forced water column. Hence, a comparison of the DB model with the SCB model results can give first insights into its capability for the representation of SPM dynamics in a water column. Further on, a possible application to simulate fluxes of substances to or from particles is shown. This could be a relevant aspect in the perspective of coupling SPM dynamics with microbial processes where the organisms can either be particle-associated or free-living, and hence linked to fluxes of organic compounds like e. g. amino acids to or from particles. In this context, the microbial ad- or disadvantage of being associated to particles has been investigated under tidally changing conditions.

Thus, this section should be regarded as part of an anticipated, extended outlook directing to possible future model applications and research directions.

4.1 The distribution-based model in a 1D vertical water column

In the following the hydrodynamic model is shortly introduced to which the DB model is applied in order to simulate SPM concentration and size dynamics in a spatially explicit context.

4.1.1 Vertical transport processes in the 1DV SiAM model developed at IFREMER

The 1D vertical turbulence model *SiAM (Simulation d'Advection Multivariable)* has been developed by Le Hir et al. (2001) at the IFREMER[1] to study physical and biogeochemical processes in coastal waters related to sediment transport processes. In this model, the primitive hydrodynamic equations are solved in σ-coordinates for a 1D water column under the assumption i) of hydrostatic pressure, ii) that no horizontal gradients are present except the pressure that is given as forcing of the model, and iii) that non-linear terms in the momentum equation are negligible. In the present study, even vertical velocities are neglected which would arise from changes of the water level. Thus, the equations of motions read for a momentum conservation in the horizontal plane

$$\frac{\partial u}{\partial t} = -g\frac{\partial \zeta}{\partial x} - \frac{1}{\rho}\frac{\partial p_{\mathrm{atm}}}{\partial x} + \frac{1}{h^2}\frac{\partial}{\partial \sigma}\left(N_{\mathrm{v}}\frac{\partial u}{\partial \sigma}\right) + fv \quad , \tag{4.1}$$

$$\frac{\partial v}{\partial t} = -g\frac{\partial \zeta}{\partial y} - \frac{1}{\rho}\frac{\partial p_{\mathrm{atm}}}{\partial y} + \frac{1}{h^2}\frac{\partial}{\partial \sigma}\left(N_{\mathrm{v}}\frac{\partial v}{\partial \sigma}\right) - fu \quad . \tag{4.2}$$

In these equations, u and v represents the velocities in the horizontal plane in x- and y-direction, respectively. g is the gravitation constant, and ζ is the sea level elevation. ρ is the density of water and p_{atm} is the atmospheric pressure. The water height is given by h and σ represents the dimensionless σ coordinates. f is the coriolis parameter. The vertical eddy viscosity is given by

[1] IFREMER, Hydrodynamics and Sediment Dynamics laboratory (DYNECO/PHYSED), BP70, 29280 Plouzané, France

N_v which is derived according to the eddy viscosity concept using the mixing length theory of Munk and Anderson (1948).

4.1.2 Representation of the SPM transport in the SiAM model

Following the equations of motion in σ-coordinates as described above, the general form of the diffusive-advective equation for the SPM concentration C_i in a specific size class i can be written as

$$\frac{\partial C_i}{\partial t} - \frac{1}{h}\frac{\partial \left(v_\mathrm{s}(r_i)\, C_i\right)}{\partial \sigma} = \frac{1}{h^2}\frac{\partial}{\partial \sigma}\left(A_\mathrm{v}\frac{\partial C_i}{\partial \sigma}\right) + F_i \quad , \tag{4.3}$$

where $v_\mathrm{s}(r_i)$ is the settling velocity of particles with radius r_i and A_v is the eddy diffusivity, the latter calculated from the equations of motion. Sources and sinks, noted by the flux term F_i, can be the resuspension and the deposition of particles, respectively, which will be explained afterwards. In the SCB model the concentration is subdivided into distinct SPM classes C_i, and hence, aggregation and fragmentation as described in Sec. 3.1 also constitute sources and sinks for each particular size class i. It is obvious that the total concentration is given by $C = \sum_i C_i$, and, in analogy to the DB model, with $C_i = C_i' \Delta R_i$ where ΔR_i is the bin-width of the size class and C_i' is the frequency distribution in that bin. Therefore, it is $\lim_{\Delta R_i \to 0} C_i \to C(r)$.

4.1.3 The spatially explicit distribution-based SPM model

In contrast to the SCB model, the total concentration C is transported in the DB model. Therefore, C_i becomes C in Eq. (4.3), the flux term becomes a flux for total concentration F, and the mean mass-weighted settling velocity $\langle v_\mathrm{s} \rangle$, derived in Eq. (2.67), has to be used instead of the settling velocity $v_\mathrm{s}(r_i)$

$$\frac{\partial C}{\partial t} - \frac{1}{h}\frac{\partial \left(\langle v_\mathrm{s} \rangle\, C\right)}{\partial \sigma} = \frac{1}{h^2}\frac{\partial}{\partial \sigma}\left(A_\mathrm{v}\frac{\partial C}{\partial \sigma}\right) + F \quad . \tag{4.4}$$

A more intricate way to transport $\langle r \rangle$ in the water column has to be used than for the C as it is a characteristic of the SPM concentration. In principle, the $\langle r \rangle$ has to be transported with a weighting by the concentration. But to account for the underlying distribution, especially in the settling term, a more intricate derivation is applied.

In order to derive an analytical equation for the transport of the $\langle r \rangle$, the assumption of

$$0 < \quad C \quad < \infty \quad , \text{ and} \tag{4.5}$$

$$0 < \quad \langle r \rangle \quad < \infty \tag{4.6}$$

is used to solve the integral version for the change of the average radius

$$\frac{\mathrm{d}}{\mathrm{d}\,t}\langle r \rangle = \frac{1}{C} \int_0^\infty r\,\dot{C}(r)\,\mathrm{d}r - \frac{\dot{C}}{C}\,\langle r \rangle \quad . \tag{4.7}$$

These assumptions are needed to be able to allow the interchange between the integral and the differentiation, thus:

$$\int_0^\infty \frac{\partial}{\partial\, x}\, C(r)\,\mathrm{d}r \;=\; \frac{\partial}{\partial\, x} \int_0^\infty C(r)\,\mathrm{d}r \quad , \tag{4.8}$$

where x represents any variable in this case. While especially the prerequisites of $C > 0$ and $\langle r \rangle > 0$ (which indeed can be violated in reality as the concentration and thus the average radius can become zero) seems to be restrictive, it turns out that these assumptions do not harm the possible use for numerical schemes. Even for $C \to 0$ and $\langle r \rangle \to 0$ the resultant numerical scheme is stable and physically realistic. The derivation for the specific numerical scheme for the implementation into the SiAM model can be found in App. A.5.

In the following, a derivation for the change of $\langle r \rangle$ by the specific processes is carried out.

4.1.4 Sinking

Under the assumptions implied above, the change of the concentration due to settling (for a specific size and the total concentration, respectively)

$$\left.\frac{\partial C(r)}{\partial t}\right|_{v_\mathrm{s}} = \frac{1}{h}\frac{\partial\left(v_\mathrm{s}(r)\,C(r)\right)}{\partial\sigma} \quad , \qquad \left.\frac{\partial C}{\partial t}\right|_{v_\mathrm{s}} = \frac{1}{h}\frac{\partial\left(\langle v_\mathrm{s}\rangle\,C\right)}{\partial\sigma} \tag{4.9}$$

can be introduced in Eq. (4.7) yielding the change of the $\langle r\rangle$ for the process of settling. Exemplarily, the analytical way will be shown here for the derivation

$$\begin{aligned}\left.\frac{\mathrm{d}}{\mathrm{d}\,t}\langle r\rangle\right|_{v_\mathrm{s}} &= \frac{1}{C}\int_0^\infty r\,\frac{1}{h}\frac{\partial\left(C(r)\,v_\mathrm{s}(r)\right)}{\partial\sigma}\,\mathrm{d}r - \frac{1}{C}\,\langle r\rangle\,\frac{1}{h}\frac{\partial\left(C\,\langle v_\mathrm{s}\rangle\right)}{\partial\sigma} \\ &= \frac{1}{C\,h}\frac{\partial}{\partial\sigma}\int_0^\infty r\,C(r)\,v_\mathrm{s}(r)\,\mathrm{d}r - \frac{\langle r\rangle}{C\,h}\frac{\partial\left(C\,\langle v_\mathrm{s}\rangle\right)}{\partial\sigma} \quad .\end{aligned}$$

The settling velocity is given by

$$v_\mathrm{s}(r) = \underbrace{\frac{2^{d_f-1}}{18\,\mu}\left(\rho_\mathrm{p}-\rho\right)g\,D_\mathrm{p}^{3-d_f}}_{K}\;r^{d_f-1} \quad , \tag{4.10}$$

and the concentration dependent on the radius is

$$C(r) = n(r)\,w(r) \;=\; N_0\,\exp(-\beta\,r)\,w_0\,r^{d_f} \quad , \tag{4.11}$$

thus

$$\begin{aligned}\left.\frac{\mathrm{d}}{\mathrm{d}\,t}\,\langle r\rangle\right|_{v_\mathrm{s}} &= \frac{1}{C\,h}\frac{\partial}{\partial\sigma}\int_0^\infty r\,N_0\,\exp(-\beta\,r)\,w_0\,r^{d_f}\,K\,r^{d_f-1}\,\mathrm{d}r - \frac{\langle r\rangle}{C\,h}\frac{\partial\left(C\,\langle v_\mathrm{s}\rangle\right)}{\partial\sigma} \\ &= \frac{1}{C\,h}\frac{\partial}{\partial\sigma}\left(\beta^{-1-2\,d_f}\,K\,N_0\,w_0\,\Gamma(1+2\,d_f)\right) - \frac{\langle r\rangle}{C\,h}\frac{\partial\left(C\,\langle v_\mathrm{s}\rangle\right)}{\partial\sigma} \quad .\end{aligned}$$

By using the known relations

$$\beta = \frac{d_f+1}{\langle r\rangle} \quad , \quad N_0 = \frac{C\,(d_f+1)^{d_f+1}}{w_0\,\langle r\rangle^{d_f+1}\,\Gamma(d_f+1)} \quad , \tag{4.12}$$

one yields

$$\left.\frac{\mathrm{d}}{\mathrm{d}\,t}\langle r\rangle\right|_{v_\mathrm{s}} = \frac{K\,\Gamma(1+2\,d_f)\,(d_f+1)^{d_f+1}}{\Gamma(d_f+1)}\,\frac{1}{C\,h}\,\frac{\partial}{\partial\,\sigma}\left(\left(\frac{d_f+1}{\langle r\rangle}\right)^{-1-2\,d_f}\cdot\frac{C}{\langle r\rangle^{d_f+1}}\right) - \frac{\langle r\rangle}{C\,h}\,\frac{\partial\,(C\,\langle v_\mathrm{s}\rangle)}{\partial\,\sigma} \quad .$$

As final result for the change of the average radius due to settling, one yields

$$\boxed{\left.\frac{\mathrm{d}}{\mathrm{d}\,t}\langle r\rangle\right|_{v_\mathrm{s}} = K'\,\frac{1}{C\,h}\,\frac{\partial}{\partial\,\sigma}\left(\langle r\rangle^{d_f}\cdot C\right) - \frac{\langle r\rangle}{C\,h}\,\frac{\partial}{\partial\,\sigma}\left(C\,\langle v_\mathrm{s}\rangle\right) \quad , \qquad (4.13)}$$

where K' is given by

$$K' = \frac{2^{d_f-1}}{18\,\mu}\,(\rho_\mathrm{p}-\rho)\,g\,D_\mathrm{p}^{3-d_f}\,\frac{\Gamma(2\,d_f+1)}{(d_f+1)^{d_f}\,\Gamma(d_f+1)} \quad , \qquad (4.14)$$

and partly accounts for the distributional effects on the change of the $\langle r\rangle$.

4.1.5 Turbulent diffusion

Similarily to sinking, the change of the $\langle r\rangle$ can be derived for turbulent diffusion using the change of the concentration (for a specific size and the total concentration, respectively)

$$\left.\frac{\partial\,C(r)}{\partial\,t}\right|_{A_\mathrm{v}} = \frac{1}{h^2}\,\frac{\partial}{\partial\,\sigma}\left(A_\mathrm{v}\,\frac{\partial\,C(r)}{\partial\,\sigma}\right) \quad , \qquad \left.\frac{\partial\,C}{\partial\,t}\right|_{A_\mathrm{v}} = \frac{1}{h^2}\,\frac{\partial}{\partial\,\sigma}\left(A_\mathrm{v}\,\frac{\partial\,C}{\partial\,\sigma}\right) \quad . \qquad (4.15)$$

Introducing Eq. (4.15) in Eq. (4.7), one yields for the change of the $\langle r\rangle$ due to turbulent diffusion

$$\boxed{\left.\frac{\mathrm{d}}{\mathrm{d}\,t}\langle r\rangle\right|_{A_\mathrm{v}} = \frac{1}{C\,h^2}\,\frac{\partial}{\partial\,\sigma}\left(A_\mathrm{v}\,\frac{\partial}{\partial\,\sigma}(C\,\langle r\rangle)\right) - \frac{\langle r\rangle}{C\,h^2}\,\frac{\partial}{\partial\,\sigma}\left(A_\mathrm{v}\,\frac{\partial}{\partial\,\sigma}C\right) \quad . \qquad (4.16)}$$

Thus, the respective partial differential equation to Eq. (4.4) for the change of the average radius is given by

$$\frac{\partial}{\partial t}\langle r\rangle \;-\; \left(K'\,\frac{1}{C\,h}\,\frac{\partial}{\partial\,\sigma}\left(\langle r\rangle^{d_f}\cdot C\right) - \frac{\langle r\rangle}{C\,h}\,\frac{\partial}{\partial\,\sigma}\left(C\,\langle v_\mathrm{s}\rangle\right)\right) = \frac{1}{C\,h^2}\,\frac{\partial}{\partial\,\sigma}\left(A_\mathrm{v}\,\frac{\partial}{\partial\,\sigma}(C\,\langle r\rangle)\right) - \frac{\langle r\rangle}{C\,h^2}\,\frac{\partial}{\partial\,\sigma}\left(A_\mathrm{v}\,\frac{\partial}{\partial\,\sigma}C\right) + R \quad (4.17)$$

where R represents changes of the $\langle r\rangle$ by aggregation, fragmentation, resuspension/erosion and deposition, the two latter explained below. Moreover, R could also represent changes of the $\langle r\rangle$ by bio-geochemical processes like e. g. the decomposition of particles by bacteria in future applications of the model. Exemplarily for advective transport processes in case of a further application to 3D hydrodynamic models, the vertical transport of the $\langle r\rangle$ is shown in App. A.5.5.

4.1.6 Erosion / Resuspension

The change of the concentration due to resuspension/erosion is given by

$$\frac{\mathrm{d}}{\mathrm{d}\,t}\,C\Big|_{e,z=0} = \frac{M_0}{h}\left(\frac{\tau}{\tau_\mathrm{c,e}} - 1\right) \quad \text{if}: \tau > \tau_\mathrm{c,e} \qquad (4.18)$$

according to Partheniades (1984). The critical bottom shear stress for erosion is here calculated by $\tau_\mathrm{c,e} = a_\mathrm{e}\,C_\mathrm{sed}^{b_\mathrm{e}}$, where C_sed represents the SPM concentration in the sediment, a_e and b_e are empirical constants. The subscript $z = 0$ represents the lowest water volume (or box in the numerical discretization, respectively). The $\langle r\rangle$ can also change due to eroded/resuspended particles. The change of the $\langle r\rangle$ thus reads for resuspension

$$\frac{\mathrm{d}}{\mathrm{d}\,t}\,\langle r\rangle\Big|_{e,z=0} = \frac{M_0}{C_{z=0}\,h}\left(\frac{\tau}{\tau_\mathrm{c,e}} - 1\right)\left(r_\mathrm{b} - \langle r\rangle_{z=0}\right)\;, \qquad (4.19)$$

where r_b is, in accordance to the model description in Sec. 2.5.1, the average radius of eroded flocs.

4.1.7 Deposition

In contradiction to the model in Sec. 3.2 the SiAM model uses in its original form a deposition in dependence on a critical bottom shear stress. Therefore, the change of concentration in the lowest water volume (described by the subscript $z = 0$) is given by

$$\left.\frac{\mathrm{d}}{\mathrm{d}\,t}\,C\right|_{d,z=0} = -\max\left(0, 1 - \frac{\tau}{\tau_{\mathrm{c,v}} + \epsilon_{\mathrm{v}}}\right) \frac{\tau_{\mathrm{c,v}}}{\tau_{\mathrm{c,v}} + \epsilon_{\mathrm{v}}} \frac{1}{h}\, v_{\mathrm{s}}\, C \quad , \tag{4.20}$$

where $\tau_{\mathrm{c,v}}$ is the critical shear stress for deposition and ϵ_{v} is a constant. This representation has been originally used in the SiAM model, but it has recently been discussed by Winterwerp (2007) that deposition is independent of any critical bottom shear stress. For this reason, the parameters has been chosen in such a way that the expression becomes (see Tab. 4.1)

$$\left.\frac{\mathrm{d}}{\mathrm{d}\,t}\,C\right|_{d,z=0} \approx -\frac{1}{h}\, v_{\mathrm{s}}\, C \quad . \tag{4.21}$$

Applying the moment closure approach to the deposition like described in Sec. 2.5, the change of the $\langle r \rangle$ is given by

$$\left.\frac{\mathrm{d}}{\mathrm{d}\,t}\,\langle r \rangle\right|_{d,z=0} = -\frac{d_f - 1}{d_f + 1}\, F' \max\left(0, 1 - \frac{\tau}{\tau_{\mathrm{c,v}} + \epsilon_{\mathrm{v}}}\right) \frac{\tau_{\mathrm{c,v}}}{\tau_{\mathrm{c,v}} + \epsilon_{\mathrm{v}}} \frac{1}{h}\, \langle r \rangle^{d_f} \quad , \tag{4.22}$$

where

$$F' = \frac{2^{d_f - 1}}{18\,\mu}\, (\rho_{\mathrm{p}} - \rho)\, g\, D_{\mathrm{p}}^{3 - d_f} \quad . \tag{4.23}$$

In the following, the above derived equations for the change of the $\langle r \rangle$ (together with aggregation and fragmentation due to shear) are used in combination with Eq. (4.4) in the SiAM model to simulate the SPM dynamics in a 1D vertical water column under changing hydrodynamic conditions. Explicitly, the rectilinear kernel for shear-induced aggregation has been used (in both, the SCB and the DB model). The results are compared to the size class-based model described in Sec. 3.1, where in this application several size classes

are transported according to Eq. (4.3) instead of transporting the total SPM concentration and the mean radius of particles like in the DB model.

4.1.8 Comparison of the SCB and the DB model in a water column

In Fig. 4.1 and 4.2 the model runs for the SCB and the DB model can be seen in a 1D vertical water column. The hydrodynamic model has been parametrized to account for tidal (M2-tide) and lunar variations of the flow velocity due to changing pressure gradients resulting in changing shear conditions. The SCB model run is parametrized in accordance with the parameter set resulting from the model comparison in Sec. 3.1. Due to different model structures (partly discussed in Sec. 3.1), it has been necessary to carry out a parameter variation to identify a parameter set for the DB model that leads to the best result compared to the SCB model. Therefore, the cost function

$$\begin{aligned} \mathrm{err} \quad = \quad & \frac{\sum_{t=1}^{n_t}\sum_{k=1}^{n_z}(C_{\mathrm{SCB}}(t,k)-C_{\mathrm{DB}}(t,k))^2}{n_t\cdot n_k\cdot(C_{\mathrm{SCB,max}}-C_{\mathrm{SCB,min}})} \\ & + \frac{\sum_{t=1}^{n_t}\sum_{k=1}^{n_z}(\langle D_{\mathrm{SCB}}(t,k)\rangle-\langle D_{\mathrm{DB}}(t,k)\rangle)^2}{n_t\cdot n_k\cdot(\langle D_{\mathrm{SCB,max}}\rangle-\langle D_{\mathrm{SCB,min}}\rangle)} \end{aligned} \tag{4.24}$$

was used. $C_{\mathrm{SCB}}(t,k)$ and $C_{\mathrm{DB}}(t,k)$ are the respective total SPM concentrations at each time t at water level k of n_t total time steps and n_z boxes representing the water column. $C_{\mathrm{SCB,max}}$ and $C_{\mathrm{SCB,min}}$ are the maximum and minimum SPM concentrations occuring in the SCB model during the reference model run. Similarily, $\langle D_{\mathrm{SCB}}(t,k)\rangle$ and $\langle D_{\mathrm{DB}}(t,k)\rangle$ are the mean diameters of aggregates in the water column at each time step and $\langle D_{\mathrm{SCB,max}}\rangle$ and $\langle D_{\mathrm{SCB,min}}\rangle$ are the maximum and minimum average diameters resulted from the SCB reference run. In order to find the best parameter set for the DB model that can represent the SCB models' results, a parameter variation for the two parameters α and f_{b} has been performed for the DB model.

Both, the SCB and the DB model show similar results for the total SPM mass in the water column as visible in the second panel in Fig. 4.1 and 4.2. They both show typical resuspension-deposition cycles induced by flood and ebb currents as observed in many tidally affected areas (see e. g. Jago et al.,

Table 4.1: Parameter values for the comparison between the SCB and the DB model and its sensitivity study (with variations of the parameters by ±10 %) in a 1D vertical application to the SiAM model (no value means no variation). The parameter values of the SCB model are choosen according to Sec. 3.1.

Run	α [−]	f_b $\left[\frac{\mathrm{s}^{0.5}}{\mathrm{m}^2}\right]$	d_f [−]	r_b [m]	M_0 $\left[\frac{\mathrm{kg}}{\mathrm{m}^2}\right]$	a_e $\left[\frac{\mathrm{N\,m}^{3b_\mathrm{e}}}{\mathrm{m}^2\,\mathrm{kg}^{b_\mathrm{e}}}\right]$	b_e [−]	$\tau_\mathrm{c,v}$ $\left[\frac{\mathrm{N}}{\mathrm{m}^2}\right]$	ϵ_v $\left[\frac{\mathrm{N}}{\mathrm{m}^2}\right]$
Ref SCB	0.35	100600	1.9	$2 \cdot 10^{-5}$ *	0.0004	0.002	0.7	100	10^{-7}
Ref DB	0.1	12000	1.9	$2 \cdot 10^{-5}$	0.0004	0.002	0.7	100	10^{-7}
α_-	0.09								
α_+	0.11								
$f_{\mathrm{B}-}$		10800							
$f_{\mathrm{B}-}$		13200							
d_{f-}			1.71						
d_{f+}			2.09						
$r_{\mathrm{b}-}$				$18 \cdot 10^{-6}$					
$r_{\mathrm{b}+}$				$22 \cdot 10^{-6}$					

* Note that the eroded aggregates of mean radius $20 \cdot 10^{-6}$ m are distributed according to an exponential number distribution.

2006; Bartholomä et al., 2009). However, the DB model shows a higher variability of the total SPM mass on a tidal time scale and thus higher vertical fluxes with respect to the SCB model. The upper limit of total SPM mass in the water column is due to a finite resuspendable amount of SPM in the system as predefined in the SiAM model for the here shown test case. Although the DB model shows a higher variability of the SPM mass on a tidal time scale, it shows less variability than the SCB model on a lunar timescale: During high shear periods of a lunar cycle (days 0 – 4 and 9 – 12 in Fig. 4.1 and Fig. 4.2, respectively – around spring tide) more sediment stays suspended in the water column during the turn of the tides than in the DB model. By contrast, after the 5 $^{\mathrm{th}}$ day, the SCB model shifts towards less SPM mass in the water column than the DB model and hence shows a higher variability on a lunar time scale.

Comparing the SPM concentration pattern by using the ratio between the results of the SCB and the DB model, it becomes obvious that during high shear periods of a lunar cycle (days 0 – 4 in Fig. 4.1 and 9 – 12 in Fig. 4.1 and Fig. 4.2, respectively) the SCB model shows higher SPM concentrations in the bottom layers during the ebb- and flood current-induced high shear rates. Moreover, during these high shear periods on the lunar scale, the SCB model shows higher SPM concentrations in the upper water column during the turn of the tides.

During low shear periods of the lunar cycle (around neap tide, here days 5 – 9), more SPM stays in the water column in the DB than in the SCB model, while the total mass is comparable low in both models with respect to high shear periods.

The size dynamics of the SPM in terms of the mean diameter of the aggregates shows a more complicated behavior. Due to the different reaction times of aggregation and fragmentation, an asymmetry appears in the mean diameter around the high shear rates induced by ebb or flood currents. During the onset of shear, erosion dominates over deposition enhancing the SPM concentration in the water column while aggregation is not fast enough to increase the floc size significantly. Fragmentation is too strong. Especially in the bottom region, fragmentation overcomes aggregation during high shear rates leading to relatively small aggregates. During the time when shear decreases towards the turn of the tide, aggregation can overcome fragmentation and enhance the aggregate size significantly. However, due to different model structures, the two models differ in their response to changing hydrodynamic conditions. The SCB model can react faster due to a more variable size distribution as discussed in Sec. 3.1. This leads to a faster onset of aggregation and thus to some shift of the time with maximum floc size on a tidal cycle in the DB model. This shift in the timing of the DB models' maximum floc size compared to the SCB model results in such relatively high size ratios between the SCB and the DB model that can be seen in Fig. 4.1 and 4.2 in the lowest panel.

Nevertheless, the size dynamics of both models is qualitatively the same despite the time shift that appears in the DB model compared to the SCB model. Further studies extended by a validation of the models with observa-

tions are however needed to enhance the knowledge about the applicability of both models under other conditions than here preassumed by the parametrization of the SiAM model and the initial sediment concentrations.

4.1.9 Sensitivity of the DB model in a water column

In order to get first insights into the DB model behavior with changing parameters, a short sensitivity study is carried out with parameter sets defined according to Tab. 4.1 where the parameters are varied by ±10 %. The resulting SPM concentration and size dynamics are shown in Figs. 4.3 – 4.10 by calculating the ratios between the DB reference run (DB_{ref}) and the sensitivity run (DB) with the respective changed parameter.

Changing the collision efficiency by $-10\,\%$ with respect to the reference run, the distribution of SPM in the water column changes (see Fig. 4.3). Higher amounts of SPM are transported in the upper water column due to the general trend to smaller aggregates (or at least of equal size compared to the reference run) that lead to smaller sinking velocities and hence a decreased vertical transport to the bottom. An enhanced SPM concentration in the upper water column is the result. In the bottom region, however, the SPM concentration decreases during high shear rates during ebb or flood tide. Especially in lunar periods of low shear rates (around neap tide), the total SPM concentration in the water column increases with decreasing stickiness as the flocs keep longer in suspension and undergo less vertical transport through the water column to the bottom due to decreased sinking velocities.

An increased stickiness has the opposite effect, leading to less SPM concentrations in the upper water column and during lunar periods of high shear rates to higher SPM concentrations in the bottom region. Generally, the increased stickiness tend to lead to larger particles leading to increased vertical fluxes and thus, especially during periods of low shear rates, to less SPM in the water column (see Fig. 4.4 during days 4 – 10).

The change of the break-up factor f_b by $-10\,\%$ has a very similar effect as an increase of the stickiness by $+10\,\%$ (see Fig. 4.5 and 4.4, respectively). It leads to less fragmentation and thus to larger aggregates that in turn can

sink faster. This leads to higher SPM concentrations of the reference run in the upper water column than the sensitivity run especially during the turn of the tides and during lunar periods of low shear rates. However, the SPM concentration increases in the sensitivity run in the bottom layers during high shear rates through the days 0 – 4 and 10 – 12.

By contrast, the increase in f_b by 10 % compared to the reference run changes the SPM concentration and size dynamics very similar as a decrease in stickiness by 10 % (see Fig. 4.6 and 4.3, respectively).

A change of the fractal dimension of the aggregates by $-10\,\%$ leads to significant changes in the SPM concentration and size dynamics (see Fig. 4.7). Especially during the turn of the tides, the SPM concentration is much smaller when the fractal dimension is lower. This is due to an highly increased aggregation as the change of the $\langle r \rangle$ due to shear-induced aggregation is proportional to $\langle r \rangle \propto \langle r \rangle^{4-d_f}$. The increase of aggregation due to a decreased fractal dimension compared to the reference run leads to much larger aggregates as can be seen by the ratio in the lower panel of Fig. 4.7. During the turn of the tides shear rates are close to or equal to zero that decreases the relative contribution of aggregation and fragmentation to the change of the average size and thus the average diameter decreases towards values of the reference run due to a higher vertical flux of much larger aggregates that lead to higher SPM concentrations of the reference run in these times. However, even during the turn of the tides, the diameter is larger as not only aggregation was higher before, but also the floc sinking velocity for same sizes is different due to the changed fractal dimension leading to slower sinking velocities due to a decreased d_f.

An increase of d_f by $+10\,\%$ leads to higher sinking velocities and thus to higher SPM concentrations in the reference run than in the sensitivity run (see Fig. 4.8). As aggregation due to shear decreases with increasing d_f, aggregates cannot grow that large anymore leading to absolutely slower sinking velocities although an increase in d_f increases also the sinking velocity (– but only for particles of same size!). This is especially the case during the turn of the tides leading to higher SPM concentrations in the upper water column compared to the reference run.

A change of size of the eroded aggregates by the order of $\pm 10\,\%$ has the smallest influence on the concentration and size dynamics of SPM compared with the other sensitivity runs (compare Fig. 4.9 and 4.10 to Figs. 4.3 – 4.8). A decrease of r_{b} by $-10\,\%$ leads to a slightly decreased mean size of aggregates in the water column, especially during the lunar period of low shear rates (days 4 – 9). This influences the SPM concentration slightly leading to higher SPM concentrations during that time due to a slightly decreased vertical flux as the sinking velocity is affected negatively.

By contrast, when increasing the mean average size of eroded aggregates by $+10\,\%$, the dynamics of SPM concentration changes in a way that it tend to be slightly decreased when compared to the reference run. This is due to a slightly increased mean size of aggregates especially during lunar periods of low shear rates.

Summarizing the sensitivity analysis, a change of the fractal dimension leads (comparable to the 0D study Sec. 3.1) to the highest variability of the size and concentration dynamics. For a discussion of the DB model application in a 1D vertical framework see Sec. 4.3.1 and Chap. 5.

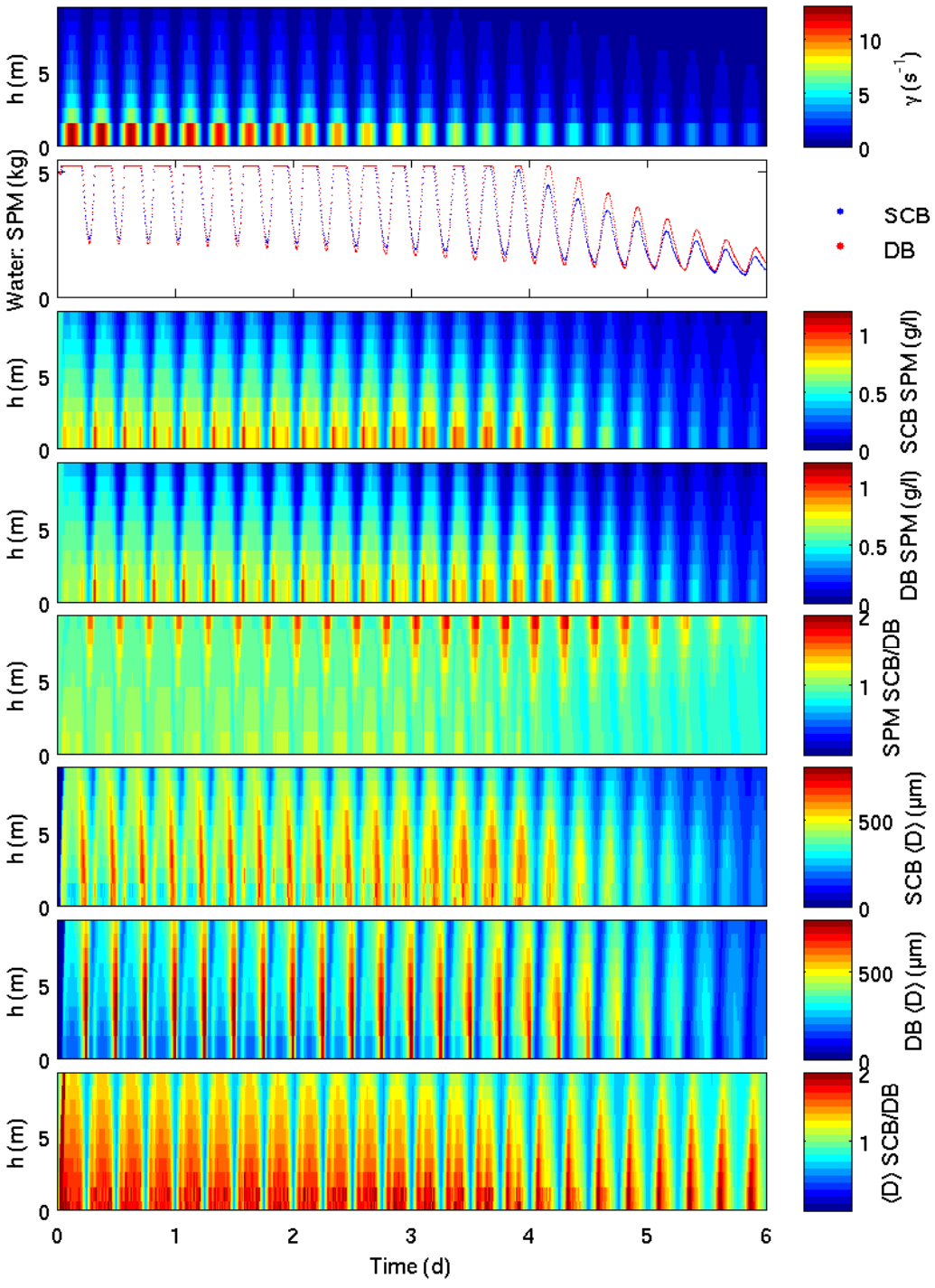

Figure 4.1: Reference run: Shear rate, sediment budget in the water column, SPM concentration of the SCB an the DB model, their ratio, the mean diameter of the SCB and DB model and their ratio.

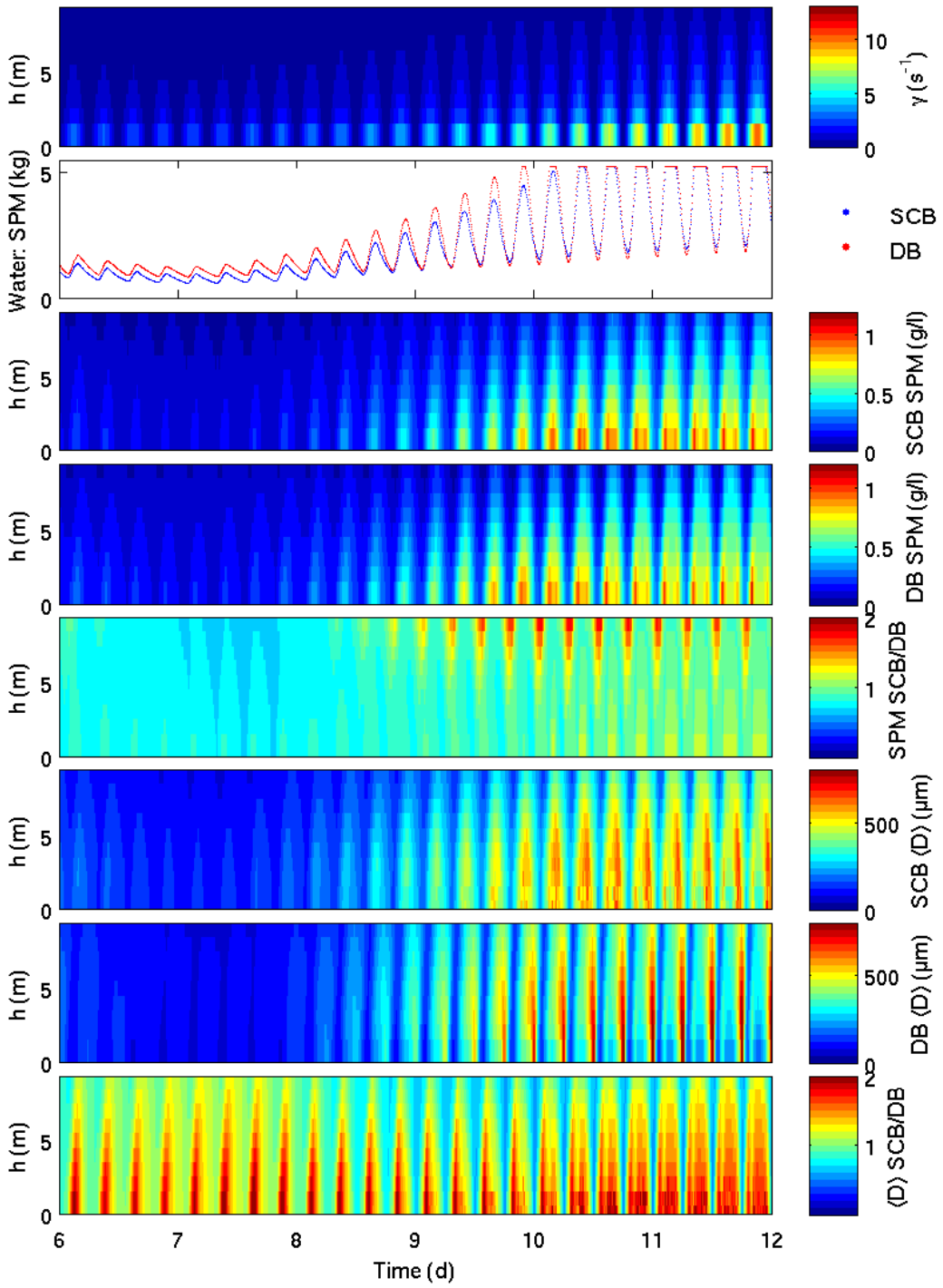

Figure 4.2: Reference run: Shear rate, sediment budget in the water column, SPM concentration of the SCB an the DB model, their ratio, the mean diameter of the SCB and DB model and their ratio.

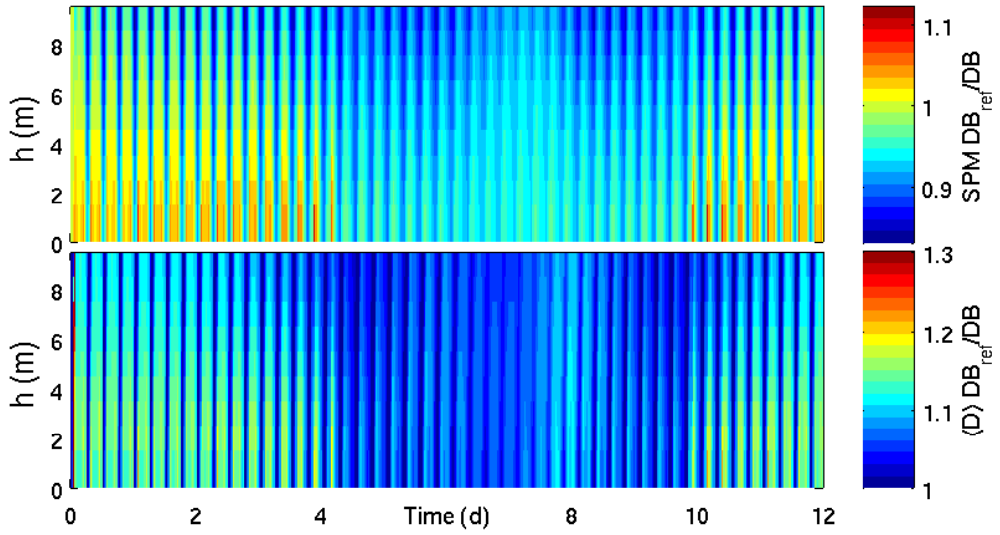

Figure 4.3: Ratios for SPM concentration and mean floc size of the DB model between the reference run and the sensitivity run with $\alpha - 10\,\%$.

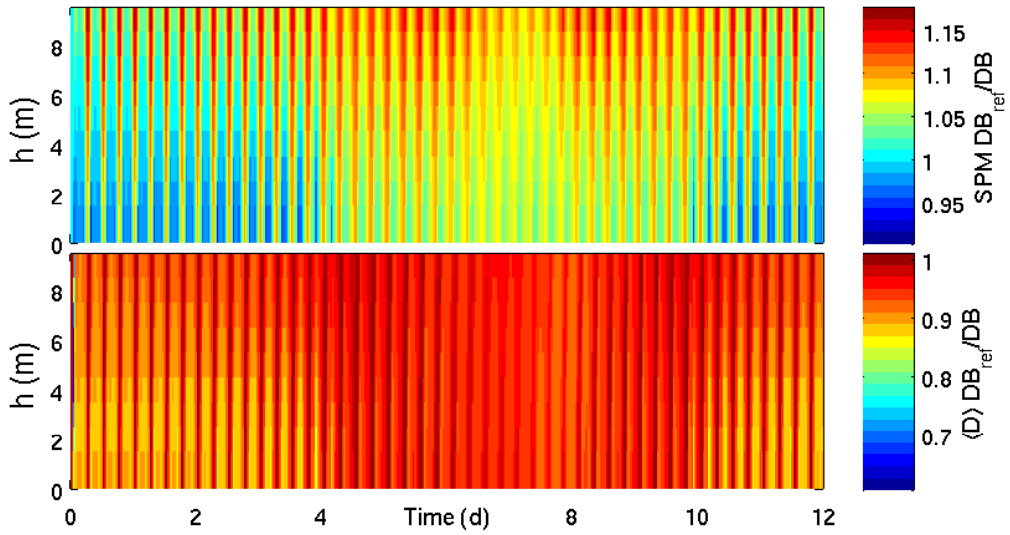

Figure 4.4: Ratios for SPM concentration and mean floc size of the DB model between the reference run and the sensitivity run with $\alpha + 10\,\%$.

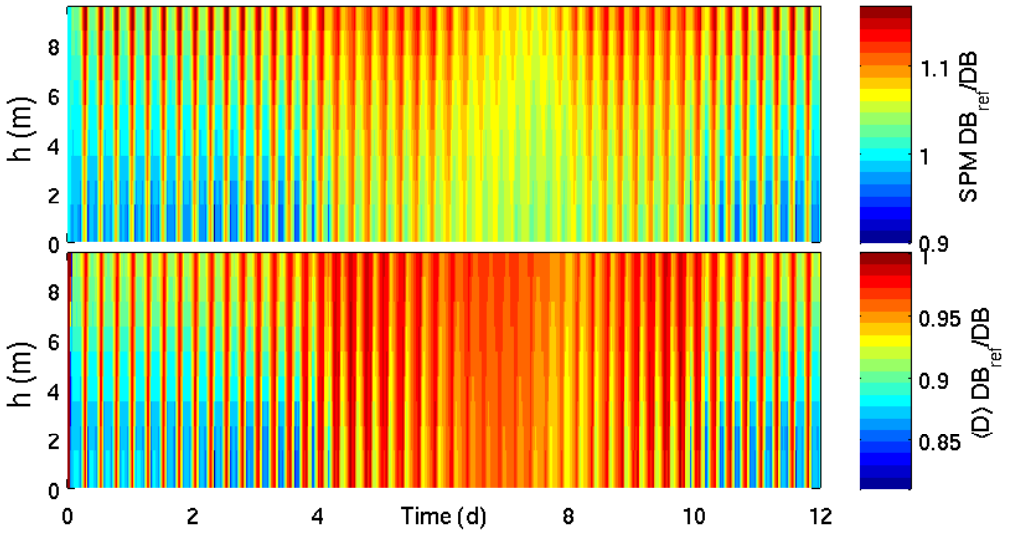

Figure 4.5: Ratios for SPM concentration and mean floc size of the DB model between the reference run and the sensitivity run with $f_\mathrm{b} - 10\,\%$.

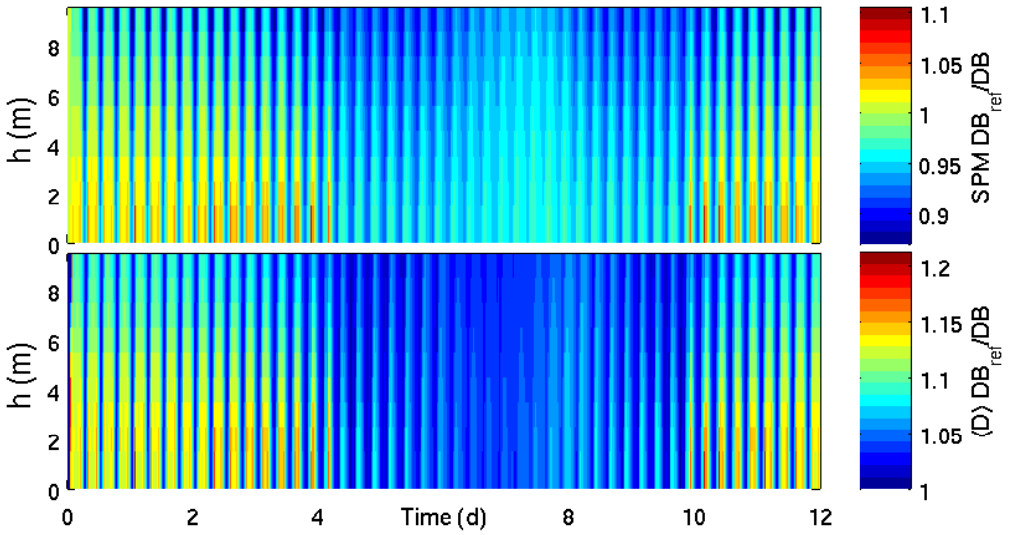

Figure 4.6: Ratios for SPM concentration and mean floc size of the DB model between the reference run and the sensitivity run with $f_\mathrm{b} + 10\,\%$.

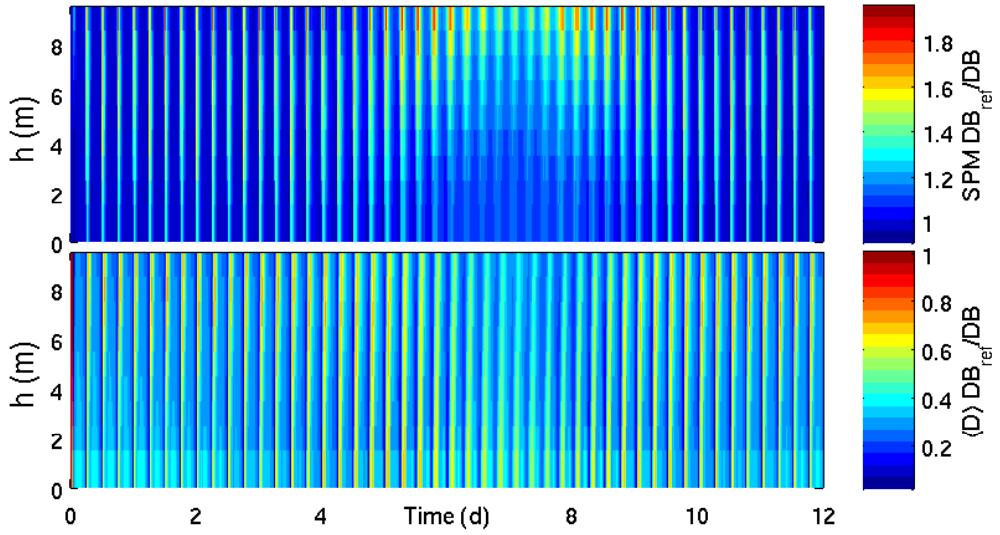

Figure 4.7: Ratios for SPM concentration and mean floc size of the DB model between the reference run and the sensitivity run with $d_f - 10\,\%$.

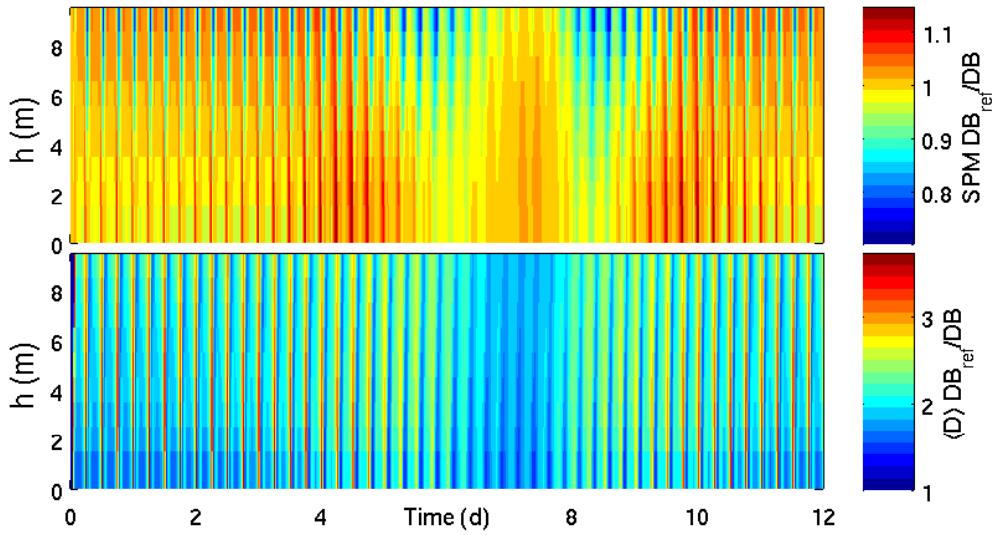

Figure 4.8: Ratios for SPM concentration and mean floc size of the DB model between the reference run and the sensitivity run with $d_f + 10\,\%$.

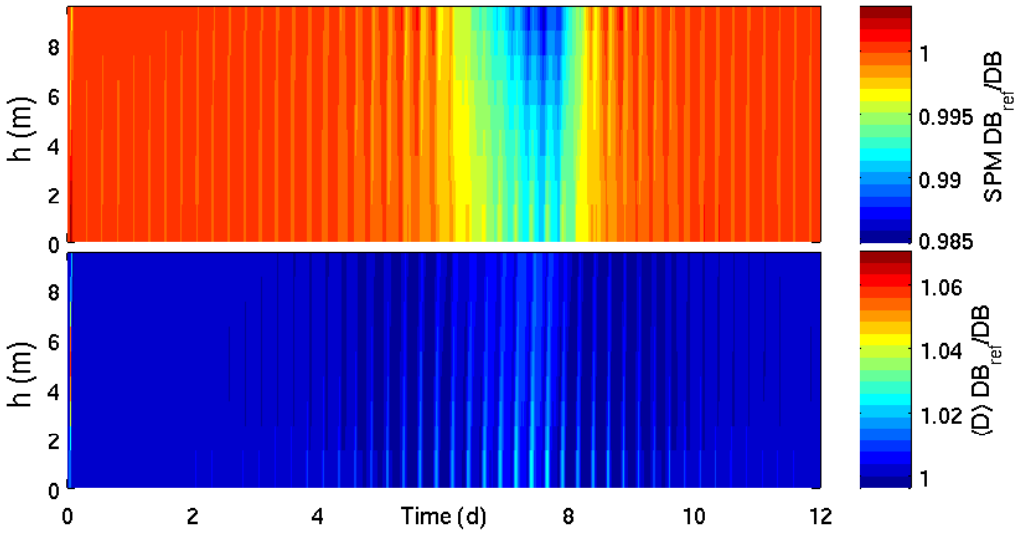

Figure 4.9: Ratios for SPM concentration and mean floc size of the DB model between the reference run and the sensitivity run with $r_b - 10\,\%$.

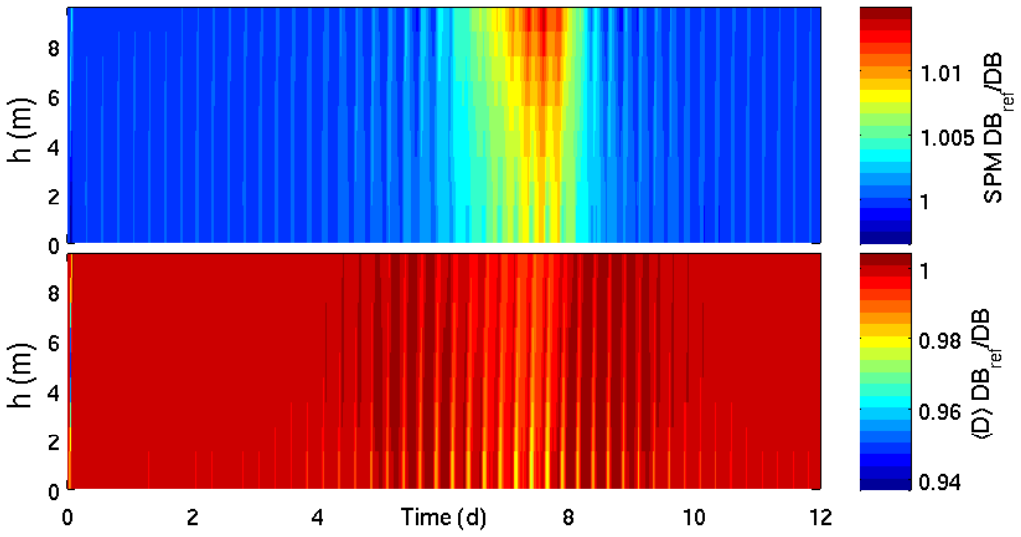

Figure 4.10: Ratios for SPM concentration and mean floc size of the DB model between the reference run and the sensitivity run with $r_b + 10\,\%$.

4.2 Fluxes to and from particles – a link to microbial processes

Originally, the distribution-based model is intended to fill a gap between sediment transport models and ecosystem modeling approaches. By following the distribution of particles and not only the mean size, several applications for biological systems are assumable. Among them, the distribution could be used to calculate the shadowing of phytoplankton due to particle-originated turbidity, the transport of POM in cohesive sediment-organic material agglomerates serving microbes as a food source, and others.

As reported by Ploug et al. (1999) POM rich aggregates serve as important food source leading to 2000-fold higher microbial densities on aggregates than in the surrounding water (observed on marine snow from surface waters of Southern California Bight). Furthermore, bacterial production is 5- to 10-fold higher, when aggregates are kept in suspension during incubation experiments compared to static conditions, where aggregates are allowed to settle (Ploug and Grossart, 2000). For the backbarrier basin of Spiekeroog island, Lemke et al. (2009) found some evidence for a temporal, but also spatially differing particle association of bacteria – the latter horizontal, but also vertical. A study in the same area by Stevens et al. (2005) even reported clusters of microbial communities – a freely suspended, an oxic sediment surface-associated, and a particle-associated community (that had some overlaps).

A chemotactic response of bacteria to aggregates and settlement is well known (e. g. Fenchel, 2002; Azam and Malfatti, 2007). It is in discussion that bacteria cannot only take advantage of particles as a food source (e. g. Ploug et al., 1999; Fenchel, 2002), but also to overcome diffusive limitations or at least increase diffusive fluxes due to a higher settling velocity of aggregates compared to a single cell (Ritzau, 1996). In order to enlighten the role of aggregates for bacteria in such a dynamic system, like e. g. the backbarrier basin of Spiekeroog island, the influence of turbulence on the diffusive flux towards or from particles will be examined in the following as an example for a possible application of the DB model.

First, the role of aggregates in the generation of DOM variability on a tidal time scale as e. g. observed by Grossart et al. (2004a) for amino acids (AA;

in the tidal basin of Spiekeroog island) will be examined. Second, the mean *potential* advantage or disadvantage of a cell of a particle-associated bacteria population/community compared to a single cell in the ambient water *only* due to an increase of flux towards aggregates owing to turbulence and the particles' sinking is investigated.

4.2.1 Mass transfer from or towards a spherical particle

Mass transfer towards a spherical body (like a particle or a cell) under fluid shear is given by (e. g. Batchelor, 1980)[2]

$$J = 4\,\pi\,r\,D\;(C_\infty - C_\mathrm{p})\;Sh \quad , \tag{4.25}$$

where D (from now on re-defined) is the substance specific molecular diffusion coefficient (e. g. for amino-acids, Ritzau (1996): D=$0.87 \cdot 10^{-6}\,\mathrm{cm}^2 \cdot \mathrm{s}^{-1}$), C_∞ is the background concentration of the substance and C_p the concentration on the particle. The increase of diffusive flux due to the influence of advective flow is represented by the dimensionless Sherwood number Sh. The Sherwood number can be estimated on basis of the dimensionless Péclet number $Pé$ (Karp-Boss et al., 1996)[3]

$$Pé \;=\; \frac{r^2\,\gamma}{D} \tag{4.26}$$

that is dependent on the radius of the sphere r (the characteristic length), the turbulent shear $\gamma = (\epsilon/\nu)^{1/2}$ with ϵ being the turbulent kinetic energy dissipation rate and ν the kinematic viscosity, and the molecular diffusion coefficient D. The Péclet number gives an indication about the effectiveness of advective compared to diffusive transport through the fluid (Karp-Boss et al., 1996). See Fig. 4.11 for Péclet numbers of typical particles in coastal waters.

[2]Instead of the Sherwood number Sh, Batchelor (1980) used the nomenclature of the Nusselt number, which is the heat transfer analogue to the mass transfer related Sherwood number.

[3]There is also another definition for the Péclet number: $Pé = (U\,r)/D$, where U is the characteristic velocity (swimming or sinking velocity), compare with Karp-Boss et al. (1996).

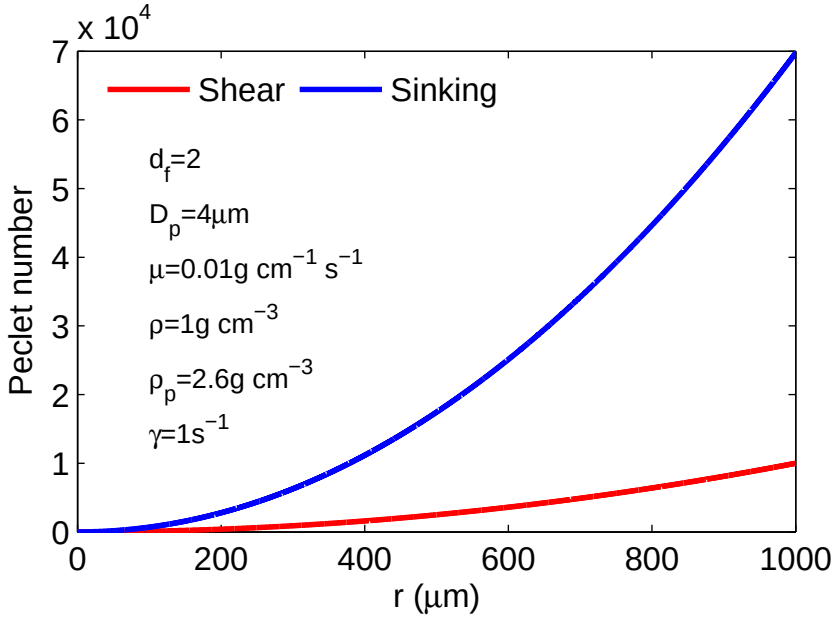

Figure 4.11: The Péclet number for turbulent shear is estimated using Eq. (4.26) and the Péclet number for sinking is estimated using the definition $Pé = (U\,r)/D$ (see e. g. Karp-Boss et al., 1996), where the characteristic velocity U is here the sinking velocity of a particle calculated by using Eq. (2.52).

Characterization of the hydrodynamic regime

The calculation of the Sherwood number for a spherical body is dependent on the hydrodynamic regime. Following Karp-Boss et al. (1996), who give a broad overview of various Sherwood numbers and their usage under different hydrodynamic regimes, it can be characterized by mainly four dimensionless measures: The already introduced Péclet number, the Reynolds number Re, the Kolmogorov length scale η, and the Batchelor length scale η_b.

The Reynolds number

$$Re = \frac{r\,U}{\nu} \tag{4.27}$$

determines whether inertial or viscous forces dominate on the characteristic length scale r for a given fluid velocity U (e. g. a particle of radius r and its sinking velocity $U = v_\mathrm{s}$). For $Re > 1$ the inertial forces dominate over viscous forces. The latter dominate when $Re < 1$ and the Stokes regime is present

where a symmetry of flow lines around a particle occurs. With increasing Re, this symmetry disappears (e. g. Tritton, 2005). For Reynolds numbers of typical particles in coastal waters see Fig. 4.12.

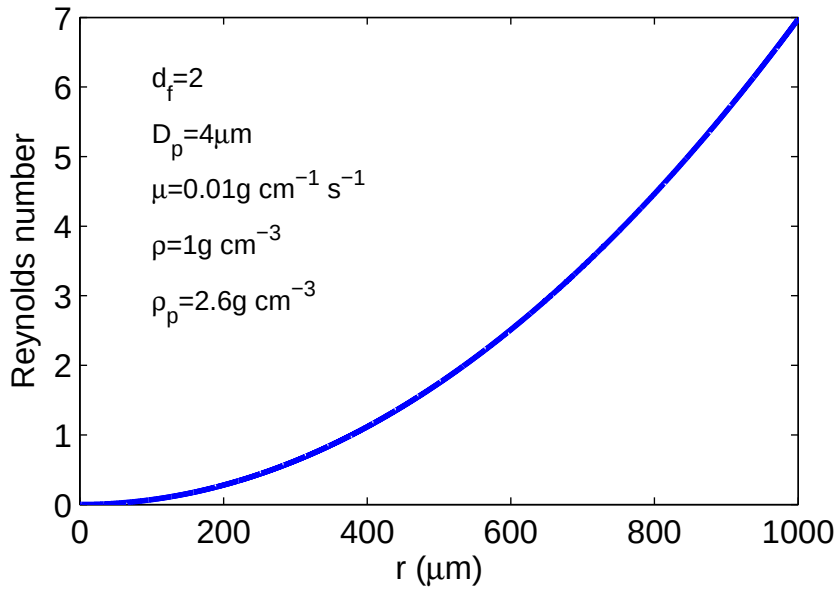

Figure 4.12: Reynolds number (Eq. (4.27)) based on the settling velocity for fractal particles (refer to Eq. (2.52)) with the given parameter values.

The Péclet and the Reynolds number are related to each other by the Schmidt number Sc

$$Sc = \frac{Pé}{Re} = \frac{\nu}{D} \tag{4.28}$$

that is the relation between viscous momentum transport and the diffusive molecular transport. Typically, the Schmidt number is of order 1000 in water, as the diffusion coefficient for momentum is greater than for molecules (of order $10^{-2}\,\mathrm{cm^2\,s^{-1}}$ and $10^{-5}\,\mathrm{cm^2\,s^{-1}}$, respectively; Karp-Boss et al., 1996). The reason is that mass transfer requires displacement of molecules, while momentum can be transfered via the successive collision of molecules without as much net displacement (Karp-Boss et al., 1996).

The Kolmogorov length scale

$$\eta = \left(\frac{\nu^3}{\epsilon}\right)^{\frac{1}{4}} \tag{4.29}$$

gives the size of the smallest eddy in turbulent flow. Above the Kolmogorov scale, the flow is turbulent and thus irregular and inertial forces dominate (Karp-Boss et al., 1996). Below the Kolmororov length scale, viscous forces dominate leading to laminar shear and a statistical state of fluctuations being considered as homogeneous, isotropic and practically steady (Monin and Yaglom, 1975). However, recent studies have shown sub-Kolmogorov scale velocity fluctuations (e. g. Schuhmacher, 2007) that could explain enhanced bacterial activity under turbulent shear conditions in laboratory experiments (e. g. Hondzo and Wüest, 2009).

The length scale defined by Batchelor (1952)

$$\eta_\mathrm{b} = \left(\frac{\nu\, D^2}{\epsilon}\right)^{\frac{1}{4}} \tag{4.30}$$

gives the smallest fluctuation size of a passive advected scalar like e. g. nutrients. As can be seen from the Schmidt number, the Batchelor length scale is much smaller than the Kolmogorov length scale. Below the Batchelor length scale, molecular diffusion dominates transport and is faster than variations of the flow as the characteristic time scale of diffusion

$$\tau_\mathrm{D} = \frac{L_\mathrm{c}^2}{D} \tag{4.31}$$

becomes $(\nu/\epsilon)^{1/2}$ for the characteristic length $L_\mathrm{c} = \eta_\mathrm{b}$. This also implies that the flow can be approximated as steady shear below η_b (Karp-Boss et al., 1996).

In coastal waters like the German Wadden sea, kinetic energy dissipation rates of $\epsilon = 0.1 - 2 \cdot 10^{-4}\,\mathrm{m^2\,s^{-3}}$ are calculated on basis of a 3D hydrodynamic model (Stanev et al., 2003b). As a result, the Kolmogorov length scale is in the range of $\eta = 250 - 600\,\mu\mathrm{m}$ (for $\nu = 10^{-6}\,\mathrm{m^2\,s^{-1}}$) and the Batchelor length scale (with D=$10^{-5}\,\mathrm{cm^2\,s^{-1}}$) $\eta_\mathrm{b} = 8 - 18\,\mu\mathrm{m}$, respectively. Therefore, aggregates in coastal waters are usually of sizes below the Kolmogorov scale while having particle Reynolds numbers of order $Re \approx 1$.

Relevant Sherwood numbers for specific hydrodynamic regimes

Many authors have calculated and used Sherwood numbers under various assumptions for different hydrodynamic regimes (Batchelor, 1980; Logan and Hunt, 1987; Kiørboe et al., 2001, see Karp-Boss et al. (1996) for an overview). In Fig. 4.2, the most often used Sherwood numbers used for calculations on particles in shear flow are given.

Sherwood numbers for the same Péclet regime are heterogeneous (see Fig. 4.13). The Sherwood number for shear (used by Logan and Hunt, 1987, see Tab. 4.2)

$$Sh = 1 + 0.55\, Pé^{\frac{1}{3}} \tag{4.32}$$

is applied here for a particle experiencing shear. It was used in the study of Logan and Hunt (1987) to determine intra-floc uptake capabilities of particle-attached microbes. It is therefore used in both studies (particle's DOM flux, and uptake capability of particle-associted bacteria) for a particle experiencing shear. In comparison to other Sherwood numbers for the same hydrodynamic regime, the used Sherwood number for shear is of the same order, but slightly larger than Sherwood numbers used in other publications (see Tab. 4.2, and Fig. 4.13).

According to Karp-Boss et al. (1996) and Batchelor (1980), a superposition of the contribution of (turbulent) shear and sinking to the diffusive flux towards or from a particle can be used to calculate the Sherwood number for a particle in the Stokes regime. Similar to the Sherwood number for turbulence effects, some different representations for the Sherwood number for sinking particles have been reported by e. g. Batchelor (1980) and Kiørboe et al. (2001). A visual comparison can be found in Fig. 4.14. The following Sherwood number has been chosen to represent the contribution of sinking to the flux towards or from a particle

$$Sh = \left(1 + 0.48 \left(\frac{r\, v_\mathrm{s}}{D}\right)^{\frac{2}{3}}\right)^{\frac{1}{2}} \quad , \tag{4.33}$$

again following the study of Logan and Hunt (1987). As most of the particles are in the Stokes regime, the two Sherwood numbers contribute linearly to each other. Thus, a superposition can be carried out to estimate the total effect of sinking and shear to the flux of substances to or from a particle. However,

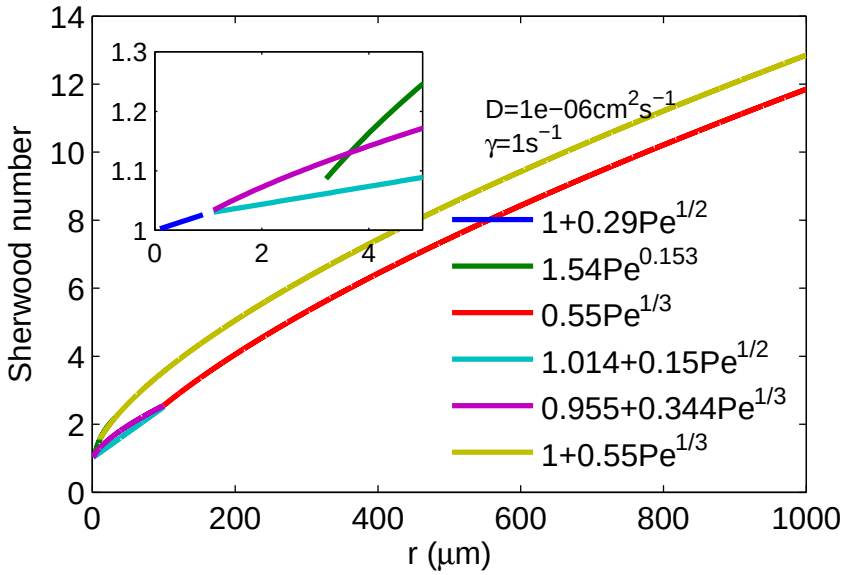

Figure 4.13: Sherwood numbers for shear listed in Tab. 4.2. The figure inlet shows the detail for very small particles.

few of the aggregates can exceed particle Reynolds number of $Re \approx 1$ (see Fig. 4.12) and thus the estimates can be regarded as conservative as the flux likely increases with higher Reynolds numbers.

4.2.2 Variabilities in the hydrodynamic regime and resulting SPM dynamics as an explanation for intertidal variability of DOM

As bacterial extracellular enzyme activity is taking place on aggregates (e. g. Ziervogel and Arnosti, 2008), dissolved substances are produced on particles. Using the preliminary results of the DB model, the total flux from the particles into the water column can be calculated for variable hydrodynamic conditions

$$J_{\mathrm{T}} = \int_0^\infty n(r)\, J(r)\, \mathrm{d}r \quad , \tag{4.34}$$

where $n(r)$ is the particle distribution at each time step and layer and $J(r)$ the flux to or from a particle of radius r calculated from Eq. (4.25) in combination with the above-introduced Sherwood number either for shear (J_{T} becomes

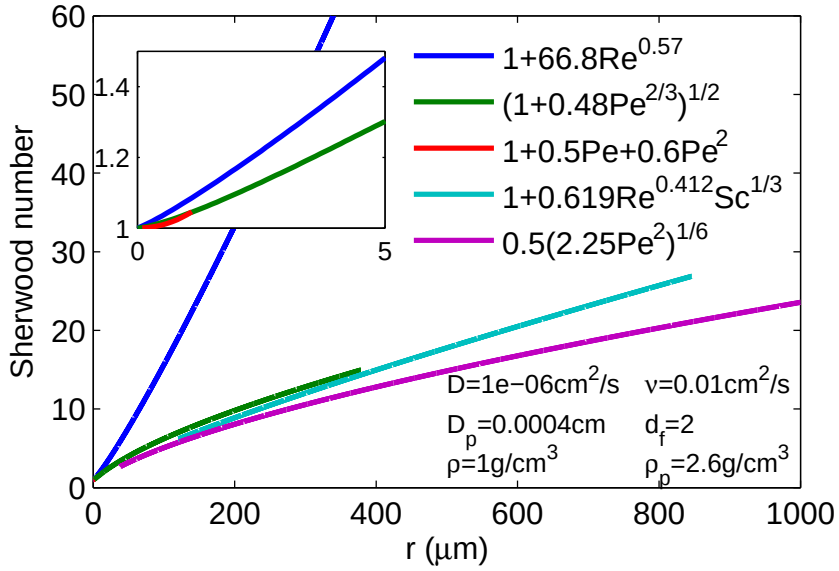

Figure 4.14: Sherwood numbers as listed in Tab. 4.2 for sinking particles. The figure inlet shows the detail for very small particles. Note that for some Sherwood numbers, limitations were not given in the respective, citet literature (see Tab. 4.2).

$J_{\mathrm{T},\gamma}$) or for sinking (J_{T} becomes $J_{\mathrm{T,v}}$). Thus, the fluxes read

$$J_{\mathrm{T,v}} = 4\,\pi\,D\,(C_\infty - C_\mathrm{p})\,N_0 \int_0^\infty r\,\exp(-\beta r)\left(1 + 0.48\left(\frac{v_\mathrm{s}\,r}{D}\right)^{\frac{2}{3}}\right)^{\frac{1}{2}}\mathrm{d}r \quad (4.35)$$

$$J_{\mathrm{T},\gamma} = 4\,\pi\,D\,(C_\infty - C_\mathrm{p})\,N_0 \int_0^\infty r\,\exp(-\beta r)\left(1 + 0.55\,P\acute{e}^{\frac{1}{3}}\right)\mathrm{d}r$$

$$= 4\,\pi\,D\,(C_\infty - C_\mathrm{p})\,N_0\left(\frac{\langle r\rangle^2}{(d_f+1)^2} + 0.8275\left(\frac{\gamma}{D}\right)^{\frac{1}{3}}\left(\frac{\langle r\rangle}{d_f+1}\right)^{\frac{8}{3}}\right) \quad (4.36)$$

The resulting pattern for the flux induced by particle sinking, shear and the processes' superposition can be seen in Figs. 4.15 – 4.20 for two different molecular diffusivities ($D = 1\cdot10^{-5}\,\mathrm{cm^2\,s^{-1}}$ and $D = 1\cdot10^{-7}\,\mathrm{cm^2\,s^{-1}}$). The latter represent the molecular diffusivities of small molecules like amino acids and large macromolecules, respectively (Logan and Hunt, 1987).

Assuming a constant difference between the background C_∞ and concentration of a substance on the aggregates C_p (with a higher concentration on

the aggregates), it becomes clear from Figs. 4.15 – 4.20 that it is very likely that a high variability of fluxes of solutes from the particles towards the water column exists on a tidal timescale. Depending on the molecular diffusion coefficient, the potential release rate ($J_T/(C_\infty - C_p)$) varies strongly. Especially under high shear rates, the release of solutes could be significantly enhanced. The turbulence can therefore contribute to the change of solutes in the ambient water in a two-fold way: By increase of particle concentration (due to erosion) and size (due to aggregation) and by helping to increase solute transport from the particles surface. The release of substances in aggregates can be contributed to the enzymatic activity of microbes on the aggregates.

In the here used reference run of the DB model to calculate potential release rates, the potential flux would be a little bit more enhanced due to shear than due to the sinking of the particles. Moreover, the potential release rate not only varies on a tidal time scale, but also on a lunar time scale due to changing SPM concentrations and sizes as result of generally reduced shear rates during neap tide.

The relative contributions of shear and sinking of particles to the total advectively enhanced flux from particles into the ambient water would not be distinguishable in *in situ* measurements. Both add – within the applicability of the underlying theory – linearly to the total change of solutes due to an advectively enhanced flux from the particles. However, a possible validation method could be to investigate the change of substances with different molecular diffusivities, as their concentration in the ambient water should change differently with respect to the here applied theory. The higher the molecular diffusivity (related to small molecules), the higher the change in the ambient water should be (cmp. Figs. 4.15 – 4.17 with Figs. 4.18 – 4.20) neglecting the uptake of the substance by microorganisms in the water column in this simplified picture.

For the discussion of the results see Sec. 4.3.2 and Chap. 5.

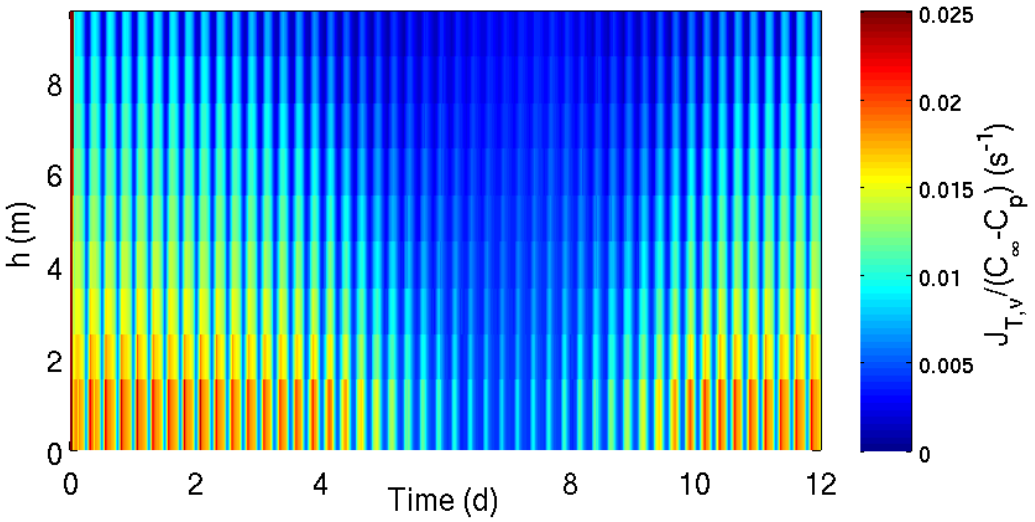

Figure 4.15: Estimated fluxes for a molecular diffusion coefficient of the substance of $D = 1 \cdot 10^{-5}\,\mathrm{cm}^2\,\mathrm{s}^{-1}$ for sinking particles.

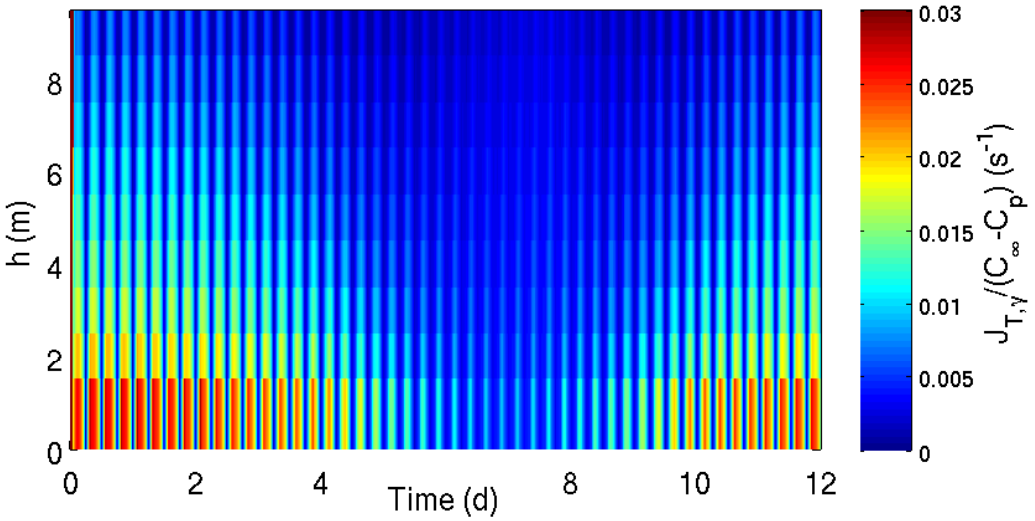

Figure 4.16: Estimated fluxes for a molecular diffusion coefficient of the substance of $D = 1 \cdot 10^{-5}\,\mathrm{cm}^2\,\mathrm{s}^{-1}$ for particles experiencing shear.

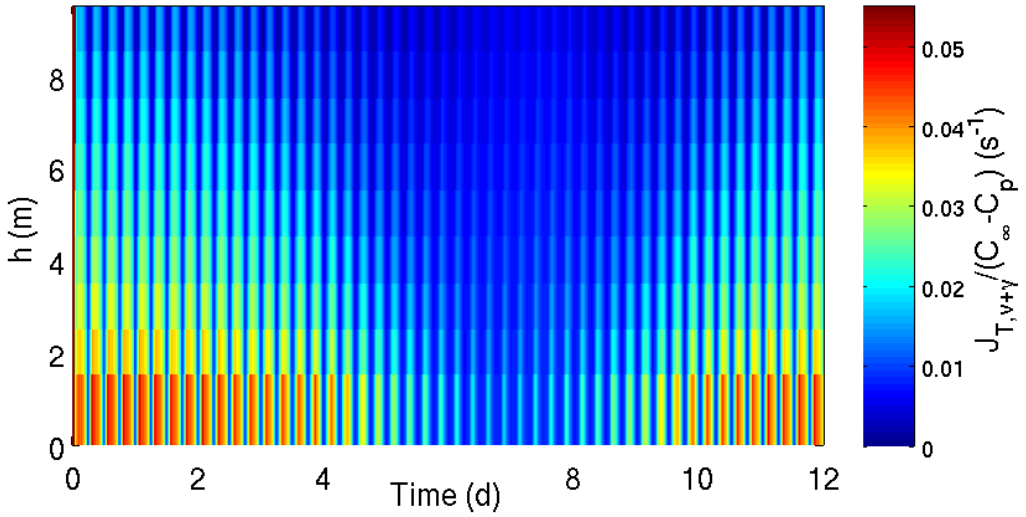

Figure 4.17: Estimated fluxes for a molecular diffusion coefficient of the substance of $D = 1{\cdot}10^{-5}\,\mathrm{cm^2\,s^{-1}}$ for particles experiencing shear and sinking.

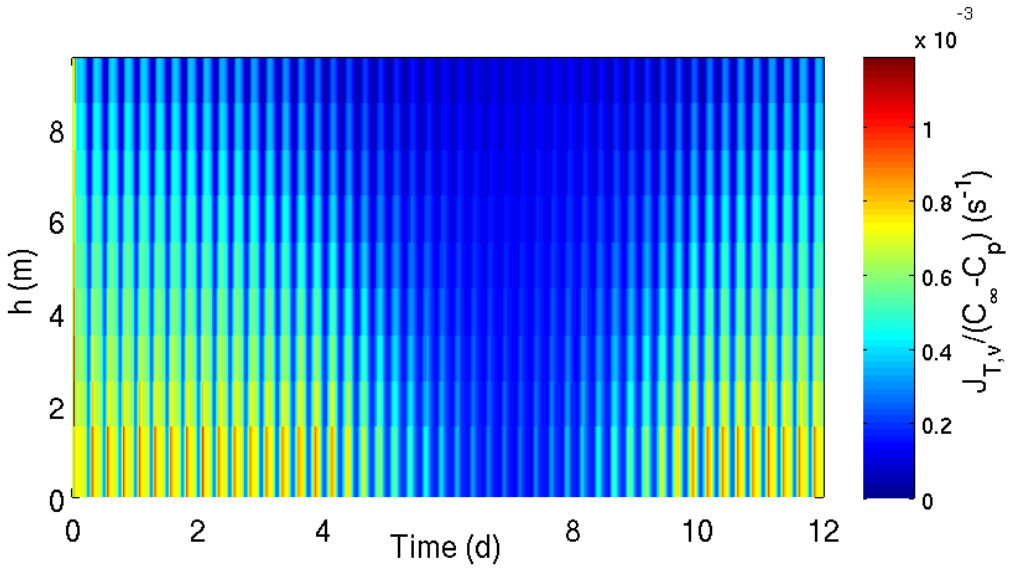

Figure 4.18: Estimated fluxes for a molecular diffusion coefficient of the substance of $D = 1 \cdot 10^{-7}\,\mathrm{cm^2\,s^{-1}}$ for sinking particles.

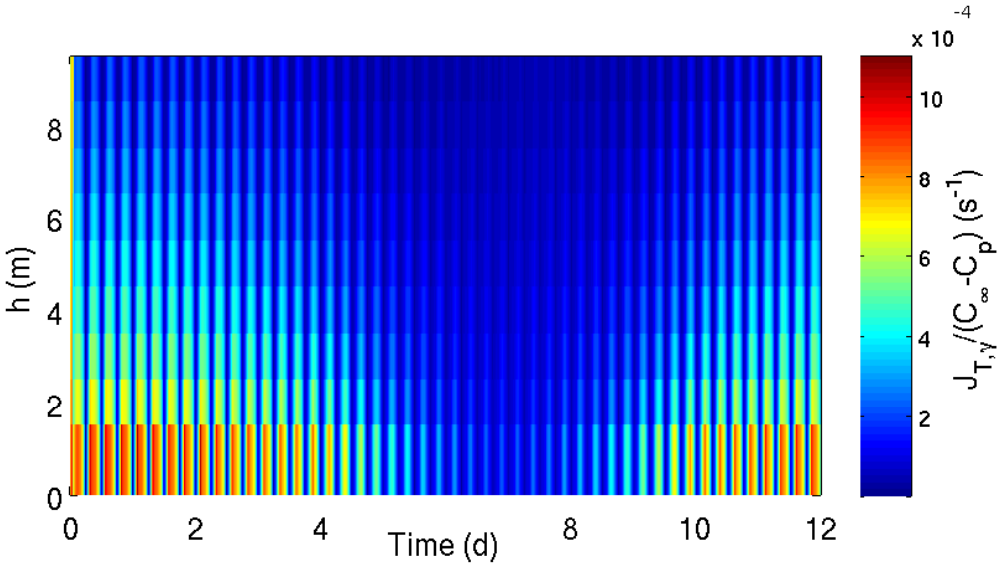

Figure 4.19: Estimated fluxes for a molecular diffusion coefficient of the substance of $D = 1 \cdot 10^{-7}\,\mathrm{cm^2\,s^{-1}}$ for particles experiencing shear.

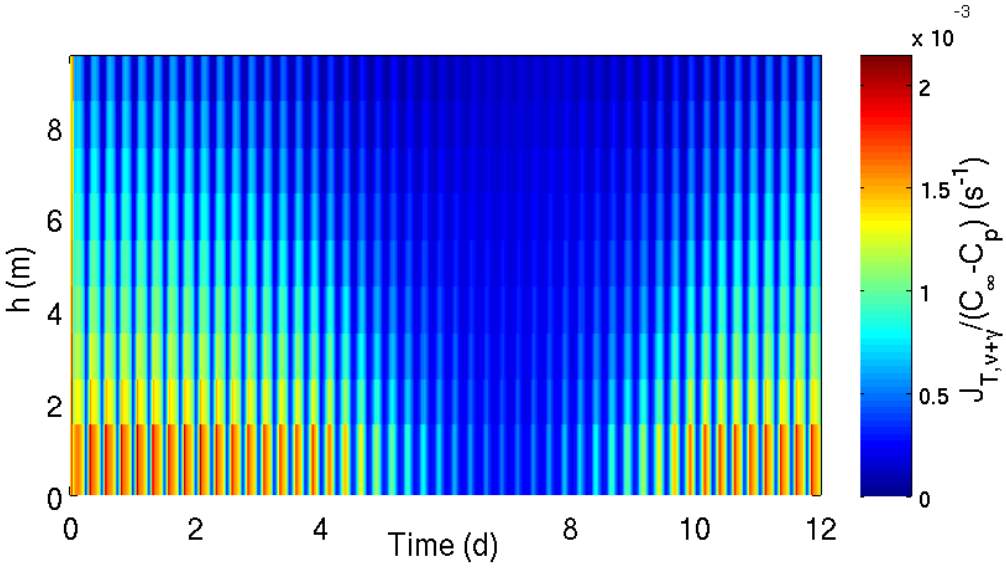

Figure 4.20: Estimated fluxes for a molecular diffusion coefficient of the substance of $D = 1{\cdot}10^{-7}\,\mathrm{cm^2\,s^{-1}}$ for particles experiencing shear and sinking.

Table 4.2: Sherwood numbers Sh for shear (based on $Pé = r^2\,\gamma/D$) and sinking (based on $Pé = r\,v_s/D$, $Re = v_s\,r/\nu$ and $Sc = Pé/Re = \nu/D$) and references

Sh for turbulent shear	Péclet regime	Reynold regime	Reference
$1 + 0.29\,Pé^{\frac{1}{2}}$	$Pé < 0.01$	$Re << 1$	Karp-Boss et al. (1996)[1]
$1.54\,Pé^{0.153}$	$0.1 < Pé < 10$	$Re << 1$	Logan and Hunt (1987)[2]
$0.55\,Pé^{\frac{1}{3}}$	$1 << Pé$	$Re < 1$	Batchelor (1980); Karp-Boss et al. (1996)
$1 + 0.55\,Pé^{\frac{1}{3}}$	$10 < Pé$		Logan and Hunt (1987)
$1.014 + 0.15\,Pé^{\frac{1}{2}}$	$0.01 < Pé < 100$	$Re << 1$	Karp-Boss et al. (1996)[3]
$0.955 + 0.344\,Pé^{\frac{1}{3}}$	$0.01 < Pé < 100$	$Re << 1$	Karp-Boss et al. (1996)[4]

Sh for sinking	Péclet regime	Reynold regime	Reference
$1 + 0.619\,Re^{0.412}\,Sc^{\frac{1}{3}}$	$30 < Pé < 50.000$	$0.1 < Re < 20$	Kiørboe et al. (2001)
$(1 + 0.48\,Pé^{\frac{2}{3}})^{\frac{1}{2}}$	$Pé < 10^4$	$Re << 1$	Sherwood et al. (1975); Logan and Hunt (1988)
$1 + 45 \cdot 2^{0.57} \cdot\ Re^{0.57}$			Logan and Alldredge (1989)[5]
$1 + 0.5\,Pe + 0.6\,Pe^2$	$Pé < 10^4$		Munk and Riley (1952); Logan and Dettmer (1990)
$a \cdot (2.25\,Pé^2)^{\frac{1}{6}}$	$100 < Pé$		e. g. Levich (1962); Batchelor (1980)
			Karp-Boss et al. (1996); $0.495 \leq a \leq 0.545$

[1] recalculated by Karp-Boss et al. (1996) for turbulent shear from Frankel and Acrivos (1968), who orignally derived $1 + 0.26\,Pé^{\frac{1}{2}}$ for a Peclet number in laminar shear; [2–4] formulations gained by interpolation; [3] lower limit; [4] upper limit; [5] note that the factor $2^{0.57}$ originates from the originally used $Re = (v_s\,d)/\nu$, where d is here the floc diameter.

4.2.3 Mean effect of turbulence and sinking of aggregates on bacterial substrate uptake capability

A distribution of aggregates occur in reality on which a bacterial population can settle. As shown by Logan and Hunt (1987), the (dis-) advantage of a particle-associated bacterium due to fluid flow compared to a single suspended cell experiencing shear is a function of aggregate size. This picture, however, neglects the presence of POM on the aggregates and the resulting microbial benefit. Nevertheless, it is questionable, whether a particle-attached microbial population takes, in sum, advantage or disadvantage simply from intra-floc and floc-surface flow induced by sinking of and shearing around the aggregates. It is therefore necessary to take the whole aggregate distribution into account. Moreover, the settlement of microbes on aggregates has, in principle, to be considered. They could either be homogeneously distributed throughout the whole volume of the aggregate, or – as they can actively sense and chemotactically follow particles – could settle mainly on the particle surface. However, especially in such highly dynamic systems like turbid coastal environments flocculation processes redistribute SPM mass and thus attached bacteria. This probably leads preferentially to a homogeneous distribution throughout the whole aggregate at least during strong flocculation.

In the following, the effect of turbulence and the settling of aggregates on fluxes and their relevance for particle-associated bacteria will be investigated under changing hydrodynamic conditions, *neglecting any benefits from enzymatic POM decomposition and its uptake on the aggregates by bacteria.*

Intra-floc flow rates

Conceptually, the calculations are based on and follow the publication of Logan and Hunt (1987) and Adler (1981), but are extended and adapted with respect to the DB model.

Intra-floc flow due to sinking of aggregates According to Adler (1981) the average intra-aggregate flow rate $u_{\mathrm{f,v}}$ due to sinking of a permeable (spherical) aggregate of radius r with sinking velocity v_{s} (calculated according to Eq. (2.52) for consistency with the previous section, but underestimating the

sinking velocity slightly resulting in a conservative estimate) can be calculated by

$$u_{\mathrm{f,v}} = v_{\mathrm{s}} \frac{r_f^*(\xi_1)^2}{r^2} \qquad (4.37)$$

on basis of the drainage radius $r_f^*(\xi_1)$ given by Adler (1981, Eq. (4))

$$r_f^*(\xi_1) = r \cdot \left(1 - \frac{T}{\xi_1} - \frac{S}{\xi_1^3}\right)^{\frac{1}{2}} \quad . \qquad (4.38)$$

It is dependent on the dimensionless value $\xi_1 = r/\lambda^{\frac{1}{2}}$ where λ is the permeability of the aggregate. The functions S and T are given by (Adler, 1981)

$$l = 2\,\xi_1^2 + 3 - 3\,\frac{\tanh\,\xi_1}{\xi_1} \quad , \qquad (4.39)$$

$$S = -\frac{1}{l}\left(\xi_1^5 + 6\,\xi_1^3 - \frac{\tanh\,\xi_1}{\xi_1}\left(3\,\xi_1^5 + 6\,\xi_1^3\right)\right) \quad , \qquad (4.40)$$

$$T = \frac{1}{l} \cdot 3\,\xi_1^3 \left(1 - \frac{\tanh\,\xi_1}{\xi_1}\right) \quad . \qquad (4.41)$$

According to the Davis correlation, the permeability λ of an aggregate can be deduced from its porosity ϕ (Logan and Hunt, 1987) and the primary particle radius r_{p}

$$\lambda = \frac{r_{\mathrm{p}}^2}{16\,(1-\phi)^{\frac{3}{2}}\,(1 + 56\,(1-\phi)^3)} \quad . \qquad (4.42)$$

Originally, this empirical relationship is based on a fibrous medium, but Luna et al. (2004) used it successfully for a biofilm model, where r_{p} was the average radius of bacterial cells (r_{p} will be the radius of a primary particle in the following).

Following Li and Logan (2001), the permeability of aggregates can be calculated based on the fractal dimension of aggregates. As discussed by Li and Logan (2001), the usage of the primary particle size in the relationship between the fractal dimension of the aggregates and their respective permeability leads

to an underestimation of the permeability. Li and Logan (2001) proposed a relationship based on the size of principal clusters in order to account for resulting higher porosity. Nevertheless, a relationship to the primary particle size is used here leading to a conservative estimate for intra-floc velocities (see also Sec. 4.3.2) due to lower permeability, but being consistent with the DB model approach used in Sec. 4.1.3 for the coupling to the 1D vertical model SiAM. Following Logan and Hunt (1987, Eq. (5)), the porosity is related to the excess floc density $\Delta\rho = \rho_\mathrm{f} - \rho$ by

$$\frac{\Delta\rho}{\rho} = \frac{\rho_\mathrm{p} - \rho}{\rho}\,(1-\phi) \quad . \tag{4.43}$$

Using Eq. (2.6) it follows directly that

$$\boxed{1-\phi = \left(\frac{r_\mathrm{p}}{r}\right)^{3-d_f} \qquad \text{for}: r \geq r_\mathrm{p} \quad ,} \tag{4.44}$$

and thus, the porosity can be expressed dependent on the fractal dimension. Using $r_\mathrm{p} = D_\mathrm{p}/2$ together with Eq. (4.44) in Eq. (4.42), one obtains the permeability of an aggregate (see Fig. 4.21). The average intra-aggregate flow rate becomes therefore a function $u_\mathrm{f,v} \rightarrow u_\mathrm{f,v}(r, d_f, D_\mathrm{p}, \rho, \rho_\mathrm{p}, \mu)$ when one calculates the settling velocity according to Eq. (2.52). The intra-floc velocity in dependence on the fractal dimension and the radius of the aggregate can be seen in Fig. 4.22 where a maximum intra-floc flow velocity occurs for a fractal dimension of $d_f \approx 1.6$. Interestingly, this value is close to measured fractal dimensions of diatom marine snow (where $d_f = 1.52 \pm 0.19$ as reported by Logan and Alldredge, 1989).

Intra-floc flow due to shear around aggregates In the hydrodynamic regime of sub-Kolmogorov scale, an aggregate experiences laminar shear G that can assumed to be (Logan and Hunt, 1987)

$$G \approx \gamma = \left(\frac{\epsilon}{\nu}\right)^{\frac{1}{2}} \quad . \tag{4.45}$$

For such a hydrodynamic regime, the average intra-floc flow velocity is given by (Adler, 1981)

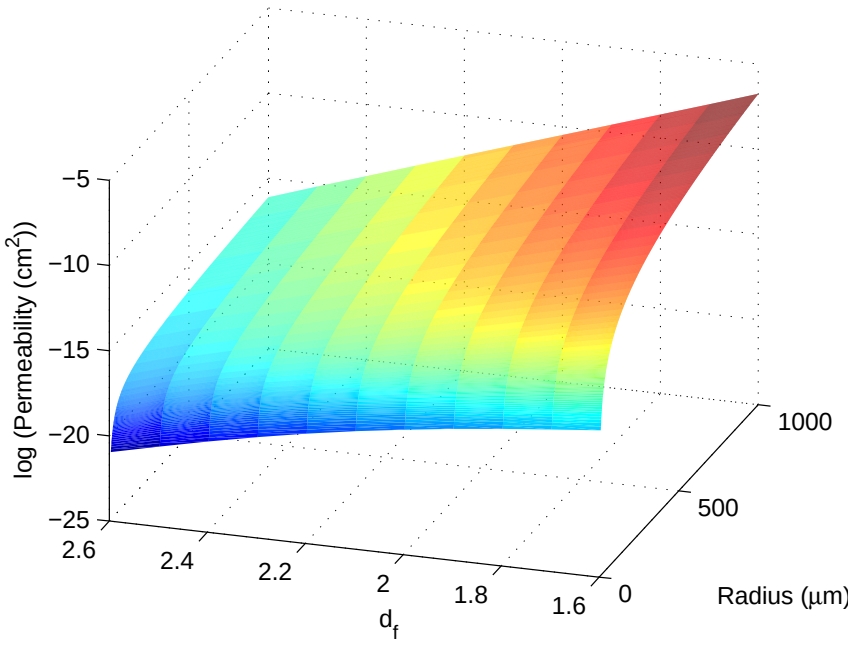

Figure 4.21: Floc permeability as calculated from Eq. (4.44) and (4.42) using $r_\mathrm{p} = 2\,\mu\mathrm{m}$.

$$u_{\mathrm{f},\gamma} = \frac{2}{3\,\pi} E_0^{\frac{1}{2}}(\xi_1)\,\gamma\,r \quad , \tag{4.46}$$

where E_0 is a function of the dimensionless variable ξ whose values are shown in Fig. 4.23 as tabulated in Adler (1981) fitted with a much simplier function used in this work (see Fig. 4.23). For $\xi_1 \leq\sim 10.8$, intra-aggregate flow is possible and for $\xi_1 >\sim 10.8$, only diffusive transport occurs. Again, as described above, permeability is calculated using the porosity-fractal dimension relationship found in Eq. (4.44) together with Eq. (4.42). The ξ_1 values for specific fractal dimensions and aggregate sizes can be seen in Fig. 4.24 together with the critical value $\xi_{1,c}$ that gives the value of ξ_1 up to which a drainage occurs. Above, no intra-floc velocity due to shear takes place. In the following, a description of the uptake capability by particle-associated bacteria is derived in dependence on the intra-aggregate flow velocity.

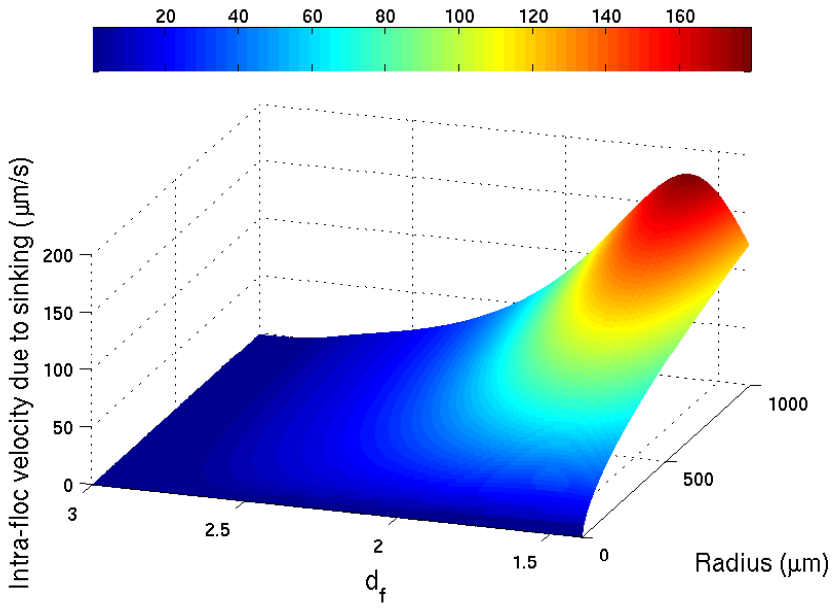

Figure 4.22: Intra-floc velocity due to sinking of an aggregate (Eq. (4.37)) with $D_\mathrm{p} = 4\,\mu\mathrm{m}$, $\rho_\mathrm{p} = 2.6\,\mathrm{g\,cm^{-3}}$, $\rho = 1\,\mathrm{g\,cm^{-3}}$, $\mu = 0.01\,\mathrm{g\,cm^{-1}\,s^{-1}}$ and $g = 981\,\mathrm{cm\,s^{-2}}$ used to calculate the sinking velocity according to Eq. (2.52).

Uptake of substrate by a single cell in a sheared fluid and under laminar flow

As already introduced in Sec. 4.2.1, the mass transfer to a spherical particle is given by (e. g. Batchelor, 1980)

$$J = 4\,\pi\,r\,D\,(C_\infty - C_\mathrm{p})\,Sh \quad . \tag{4.47}$$

Applying this concept to a microbial cell of radius r_c under the assumption (following Logan and Hunt, 1987) that the concentration of a substrate at the cell surface is zero due to instantaneous uptake, one yields

$$J_\mathrm{c} = 4\,\pi\,r_\mathrm{c}\,E_\mathrm{B}\,D\,C_\infty\,Sh \quad , \tag{4.48}$$

where E_B is the cell surface fraction that contains transport enzymes for any substrate in question. E_B has been found to be of order $0.0035 - 0.025$ for

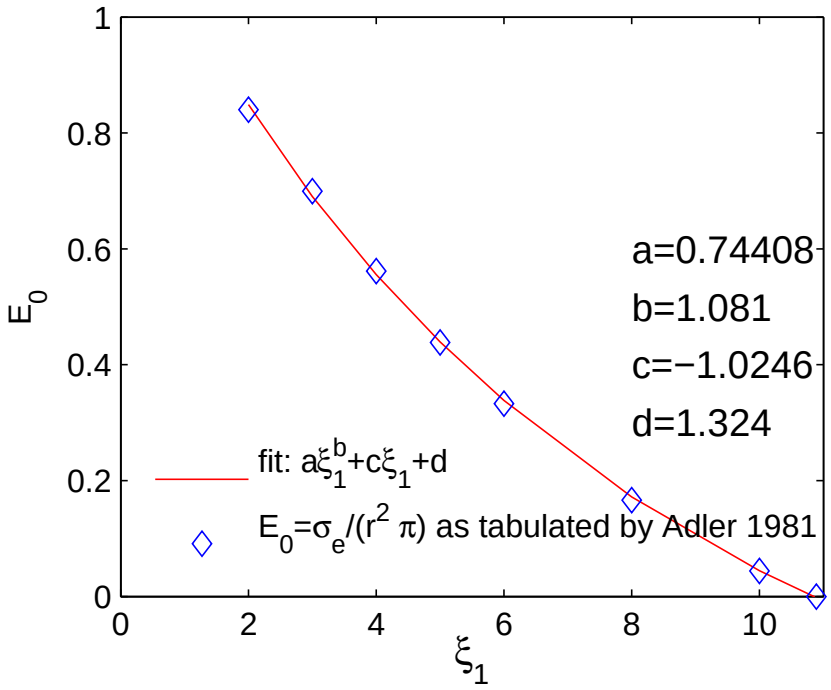

Figure 4.23: E_0 as tabulated in Adler (1981) and the fitting function used for the calculations. Note that tabulated E_0 values from Adler (1981) were only taken into account for $\xi_1 \geq 2$ for the fitting function as this is the relevant range of occuring values (see also Fig. 4.24).

different substrates (Canelli and Fuhs, 1976; Logan, 1986; Logan and Hunt, 1987). In analogy to Logan and Hunt (1987), $E_\mathrm{B} = 0.0035$ will be used in the following. Using first-order uptake kinetics, the change of concentration can be calculated according to

$$\frac{\mathrm{d}}{\mathrm{d}\,t} C_\infty = -\mu_\mathrm{up}\, C_\infty \quad , \tag{4.49}$$

where the uptake rate μ_up can be expressed as

$$\mu_\mathrm{up} = \frac{J_\mathrm{c}}{C_\infty} N_\mathrm{c} \tag{4.50}$$

with N_c being the number of cells attached to the particles per unit volume. Assuming microbial cells (either attached, or in the ambient water) with an

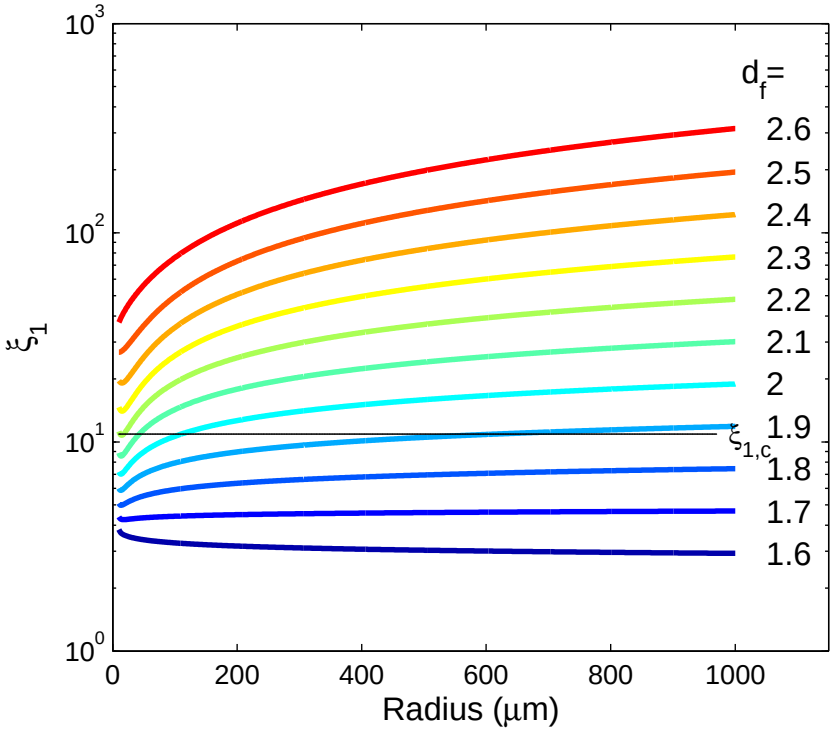

Figure 4.24: The dimensionless value $\xi_1 = r/\sqrt{\lambda}$ for various fractal dimensions and radii for $D_\mathrm{p} = 4\,\mu\mathrm{m}$. Note the critical value $\xi_{1,c}$ for intra-floc flow due to laminar shear. Note moreover that ξ_1 is larger than two in the plotted region even for $d_f = 1.6$ so that the simplified relation for E_0, found in Fig. 4.23, holds. $d_f = 1.6$ is a small value compared to fractal dimension measured in coastal waters (in coastal waters: $d_f \approx 2$, e. g. Dyer and Manning, 1999; Kranenburg, 1994).

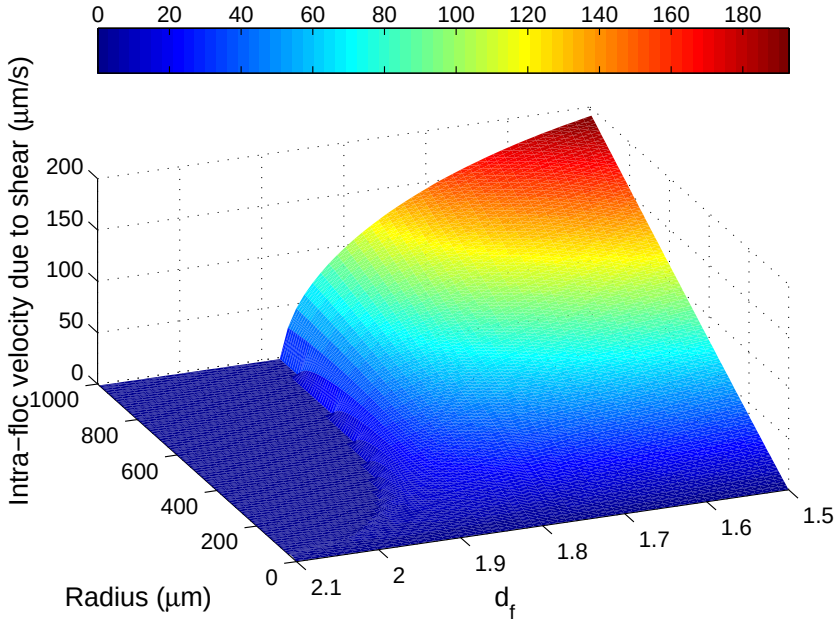

Figure 4.25: Intra-floc velocity due to shear (here $\gamma = 1$) calculated using Eq. (4.46) with $D_\mathrm{p} = 4\,\mu\mathrm{m}$.

average radius of $r_c = 1\,\mu m$, the respective Sherwood number for a cell in suspension experiencing shear is (Logan and Hunt, 1987, see also Tab. 4.2)

$$Sh_\gamma = 1.54\, Pé_\gamma^{0.153} \quad , \qquad (4.51)$$

where the Péclet number can be calculated as $Pé_\gamma = r_c\,\gamma/D$. As a consequence of particle-attachment of cells, they can experience a laminar flow in the floc as described above. The Sherwood number for a cell attached to a particle is therefore given by

$$Sh_u = (1 + 0.48\, Pé_u^{\frac{2}{3}})^{\frac{1}{2}} \qquad (4.52)$$

that can also be applied for a sinking particle. The Péclet number is here given by $Pé_u = r_c\, u_f/D$ (Logan and Hunt, 1987) where u_f can be the intra-floc flow velocity induced either by shear or by sinking of the particle ($u_{f,\gamma}$ (Eq. (4.46)) and $u_{f,v}$ (Eq. (4.37)), respectively) in this case.

Following Logan and Hunt (1987) the here used Sherwood number for the particle experiencing shear is given by

$$Sh_{p,\gamma} = 1 + 0.55\, Pé_\gamma^{\frac{1}{3}} \quad . \qquad (4.53)$$

Relative uptake capability of particle-attached bacteria

As many microbial cells settle on aggregates, their influence on the available substrate concentration has to be considered in order to estimate an average uptake compared to a free suspended cell. A relative uptake factor χ is the quotient between the uptake cabability of a cell settled on an aggregate (experiencing laminar intra-floc fluid flow) and a cell that experiences fluid shear. It is given by (Logan and Hunt, 1987)

$$\chi_a = \frac{Sh_u}{Sh_\gamma} \cdot \frac{1 - \exp(-\Phi_a)}{\Phi_a} \quad , \qquad (4.54)$$

where Φ_a is the advective Thiele modulus

$$\Phi_a = \frac{2\,r\,\mu_{up}}{u_f} \quad . \qquad (4.55)$$

Here, u_f is the average intra-floc flow velocity either calculated by Eq. (4.37) for a sinking aggregate or by Eq. (4.46) for a floc experiencing laminar shear. The quotient $(1 - \exp(-\Phi_a))/\Phi_a$ is an advective effectiveness factor. It is the relation between *i)* the uptake in a floc (resulting in a gradient inside the aggregate) and *ii)* the first order uptake kinetics for a cell experiencing the bulk substrate concentration. This relation can be calculated on basis of a steady state solution of an advection-reaction equation

$$u\,\nabla\,C_\infty = -\mu_{up}\,C_\infty \qquad (4.56)$$

by assuming a cubed aggregate having a volume of $8\,r^3$ and gives the effectiveness of advection *versus* the uptake (see also Logan and Hunt, 1988). Relation Eq. (4.54) holds for an advective transport to cells that is larger than diffusive transport (Logan and Hunt, 1987). The relative uptake capability for diffusive transport to a cell in an aggregate versus a cell in the ambient water experiencing shear can be calculated by (Logan and Hunt, 1987)

$$\chi_d = \frac{Sh_p}{3\,\Phi_d^2\,Sh_\gamma}\,\frac{3\,\Phi_d\,\cosh\,3\,\Phi_d - \sinh\,3\,\Phi_d}{3\Phi_d\,\cosh 3\,\Phi_d + (Sh_p - 1)\,\sinh\,3\,\Phi_d} \qquad (4.57)$$

where Sh_p is the Sherwood number for an aggregate either for shear (Eq. (4.53)) or for sinking (Eq. (4.52), using $P\acute{e}_u = r\,v_s(r)/D$). The diffusive Thiele modulus Φ_d is given by

$$\Phi_d = \frac{1}{3}\,r \cdot \left(\frac{\mu_{up,d}}{D}\right)^{\frac{1}{2}} \qquad (4.58)$$

where the rate parameter $\mu_{up,d}$ can be estimated analogously to Eq. (4.50) by setting $Sh = 1$

$$\mu_{up,d} = 4\,\pi\,r_c\,E_B\,D\,N_c \quad . \qquad (4.59)$$

How to derive an estimate for the number of cells on an aggregate will be discussed below, when this approach will be coupled to the DB model in a 1D vertical water column. This is done in order to get an insight whether a particle-attached living microbial population or community can benefit from transport within the particles under changing hydrodynamic conditions and thus also changing size distributions of aggregates.

Calculating the relative uptake capability based on the DB model and SiAM

By using the fractal relationship to calculate permeability deduced from the porosity of an aggregate, it is possible to apply the model for intra-floc flow and the uptake of substrates to the DB model. In measurements, bacterial cell counts are most often a bulk value – subdivided in particle-associated microbes and cells in the ambient water. Cell counts in dependence on the floc size are rare. Kiørboe (2003) reported a nearly constant number of particle-associated bacteria independent of aggregate size due to predator prey interactions. A constant number of microbial cells is, however, at least questionable for small flocs. Thus, a volume-weighted approach is used here. According to the approach of the DB model, the total volume of aggregates V_t is given by (using additionally Eq. (2.45))

$$V_\mathrm{t} = \int_0^\infty n(r)\, V(r)\mathrm{d}r \quad , \tag{4.60}$$

$$= \frac{8\,\pi\,(d_f+1)^{d_f-3}\,C\,\langle r\rangle^{3-d_f}}{w_0\,\Gamma(d_f+1)} \tag{4.61}$$

where the volume of an aggregate of radius r is given by $V(r) = \frac{4}{3}\,\pi\,r^3$. Thus, the number of microbial cells per aggregate $N_\mathrm{c}(r)$ of radius r can be assumed to be

$$N_\mathrm{c}(r) = \frac{V(r)}{V_\mathrm{t}}\,N_\mathrm{t} \quad , \tag{4.62}$$

with N_t being the total particle-associated bacterial cell number per volume. Under the assumption that the bacterial number is proportional to the SPM concentration, the cell number on an aggregate can be expressed via a factor leading to

$$N_{\mathrm{c}}(r) = \frac{V(r)}{V_{\mathrm{t}}}\, C\, B \quad , \qquad (4.63)$$

where $B = 10^9 \# \,/\, 50\,\mathrm{mg\,L^{-1}}$ (an estimate based on observations by Lemke et al., 2009, in the backbarrier tidal basin of Spiekeroog island) gives the number of bacterial cells associated to a specific amount of SPM.

The mean relative potential uptake capability for a cell of a particle-attached population or community under changing hydrodynamic conditions and thus changing particle distribution conditions can be calculated at each vertical layer at each time step according to

$$\langle \chi(\mathbf{x}, t) \rangle = \frac{\int_{r_{\mathrm{p}}}^{\infty} n(r, \mathbf{x}, t)\, \chi(r)\, \mathrm{d}r}{\int_{r_{\mathrm{p}}}^{\infty} n(r, \mathbf{x}, t)\, \mathrm{d}r} \quad . \qquad (4.64)$$

For some aggregate sizes, diffusive transport is faster than advective transport. For these aggregates, diffusive transport and thus the relative uptake for diffusion according to Eq. (4.57) is assumed during the integration:

$$\chi(r) = \begin{cases} \chi_{\mathrm{d}}(r) & \text{if}: \chi_{\mathrm{d}}(r) > \chi_{\mathrm{a}}(r) \\ \chi_{\mathrm{a}}(r) & \text{if}: \chi_{\mathrm{d}}(r) \leq \chi_{\mathrm{a}}(r) \end{cases} \quad . \qquad (4.65)$$

In the case of faster advective transport, either sinking-induced or shear-induced intra-floc flow (according to Eq. (4.37) or Eq. (4.46), respectively) is accounted for in the relative uptake capability (Eq. (4.54)) used in Eq. (4.64). The mean relative potential uptake capability is therefore based on a combination of diffusive and advective transport in aggregates. Thus, the mean relative uptake capability (Eq. (4.64)) is either calculated for diffusion and sinking-induced intra-floc flow (and thus becomes $\langle \chi_{\mathrm{v}} \rangle$) or for diffusion and shear-induced intra-floc flow ($\langle \chi \rangle$ becomes $\langle \chi_{\gamma} \rangle$).

Although assuming the particle-associated microbial community as proportional to the total SPM concentration, $\langle \chi \rangle$ can change with time due to a changing particle distribution undergoing flocculation and other processes. In order to investigate such tidal and lunar changes of $\langle \chi \rangle$ in a 1D water column, the mean relative uptake factor is calculated on basis of the DB model coupled to the SiAM model using the reference run as parametrized in Sec. 4.1.3.

4.2.4 Mean potential uptake capability under changing hydrodynamic conditions in a 1D water column

For the parameterization of the relative uptake model see Tab. 4.3. The relative uptake capabilities have been calculated on basis of the DB reference run in SiAM (cmp. Sec. 4.1.8).

Table 4.3: Parameter values for the calculations of the relative potential uptake capability.

Parameter	Description	Value
E_{B}	Cell surface fraction with transport enzymes	0.0035
D_{p}	Primary particle diameter	4 µm
D	Molecular diffusion coefficient for substances	10^{-5} / $10^{-7}\,\mathrm{cm^2\,s^{-1}}$
r_{c}	Cell radius	1 µm
d_f	Fractal dimension of aggregates	1.9
ρ_{p}	Primary particle density	$2.6\,\mathrm{g\,cm^{-3}}$
ρ	Fluid density	$1.0\,\mathrm{g\,cm^{-3}}$
B	Bacteria per SPM mass factor	$2 \cdot 10^8$ #/ (mg/L)

The temporally and spatially changing mean relative uptake capabilities of a cell of particle-attached bacteria population/community can be seen in Figs. 4.26 – 4.29 while a tidal mean of the relative uptake capability can be found in Fig. 4.30. Molecular diffusivity values can vary for different soluted substances. Therefore, two different cases are examined as the upper and the lower boundary of a typical range of molecular diffusivities for solutes ($D = 10^{-5}\,\mathrm{cm^2\,s^{-1}}$ and $D = 10^{-7}\,\mathrm{cm^2\,s^{-1}}$, respectively; Logan and Hunt, 1987).

Mean potential uptake capability due to sinking of particles

The spatially changing mean relative uptake capability for substances of molecular diffusivity of $D = 10^{-5}\,\mathrm{cm^2\,s^{-1}}$ due to the sinking of aggregates varies only slightly between 0.99 and 1.04 (see Fig. 4.26). However, especially in the

bottom layer during high shear rates, the mean relative uptake capability is reduced and bacteria cannot benefit from the sinking of flocs. Also during neap tide conditions (days 6 – 8), the mean relative uptake capability is reduced. By contrast, particle-attached bacteria can benefit from sinking during slack water times, when shear is reduced, but sinking of aggregates is still ongoing.

Similarily to the case of $D = 10^{-5}\,\mathrm{cm^2\,s^{-1}}$, bacteria benefit from being particle-attached during times and in spatial regions (– mainly the upper water column –) of low shear rates when the molecular diffusivity is lower of order $D = 10^{-7}\,\mathrm{cm^2\,s^{-1}}$ (Fig. 4.27). In contrast to the case of molecular diffusivity of $D = 10^{-5}\,\mathrm{cm^2\,s^{-1}}$, bacteria can potentially increase their uptake up to 1.6 compared to a cell experiencing shear in the ambient water.

Mean potential uptake capability due to shear around particles

As the shear-induced intra-floc velocities are limited or can even be zero (see Fig. 4.25 for a fractal dimension of $d_f = 1.9$), particle-attached bacteria can only benefit slightly from shear-induced intra-floc velocities in regions (in the bottom layer) and times of high shear rates when the molecular diffusion coefficient is $D = 10^{-5}\,\mathrm{cm^2\,s^{-1}}$ (see Fig. 4.28). The lowest mean relative uptake capabilities occur during the neap tide when shear rates are comparable low.

For a molecular diffusion coefficient of $D = 10^{-7}\,\mathrm{cm^2\,s^{-1}}$, the picture changes. Particle-attached bacteria can benefit most of the time from shear-induced intra-floc velocities, neglecting the turn of the tides and the time around neap tide (see Fig. 4.29), when particle-attached bacteria are more diffusion-limited than a cell in the ambient water.

Tidal mean potential uptake capability

It is obvious from the results described above that the mean relative uptake capability changes spatially and temporally. Assuming that all particles are homogeneously transported through the whole water column during a tidal cycle (and thus collecting the same information of the shear regime which is a rough assumption, especially during slack water), a tidal mean relative uptake capability can be calculated. A further assumption is that the microbial population is constant on the aggregates (and bacteria do not chemotactically sense, settle on and leave aggregates).

The results are shown in Fig. 4.30. In most cases, a microbial population attached to particles can at least slightly benefit from the hydrodynamic effect of higher advectively-induced transport to the cells on a tidal time scale. Only in the case a particles with $D = 10^{-5}\,\mathrm{cm^2\,s^{-1}}$, the tidal mean relative uptake capability can drop below one around neap tide. The highest benefit for a particle-associated microbial population on a tidal time scale is due to the sinking of particles at $D = 10^{-7}\,\mathrm{cm^2\,s^{-1}}$.

However, note that the results are based on a model run, while a validation of both the DB model in a 1D water column and the thereon based calculations of the mean relative uptake capability are still to be done. For further discussion of the results see Sec. 4.3.2 and Chap. 5.

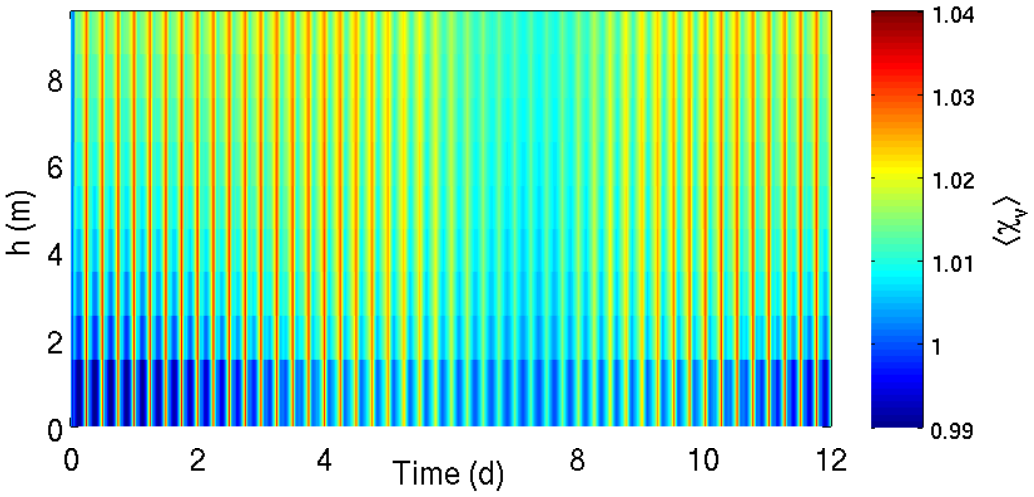

Figure 4.26: $\langle \chi_\mathrm{v} \rangle$ for a molecular diffusion coefficient $D = 1 \cdot 10^{-5}\,\mathrm{cm^2\,s^{-1}}$. Calculation based on the reference run of the DB model in Sec. 4.1.8.

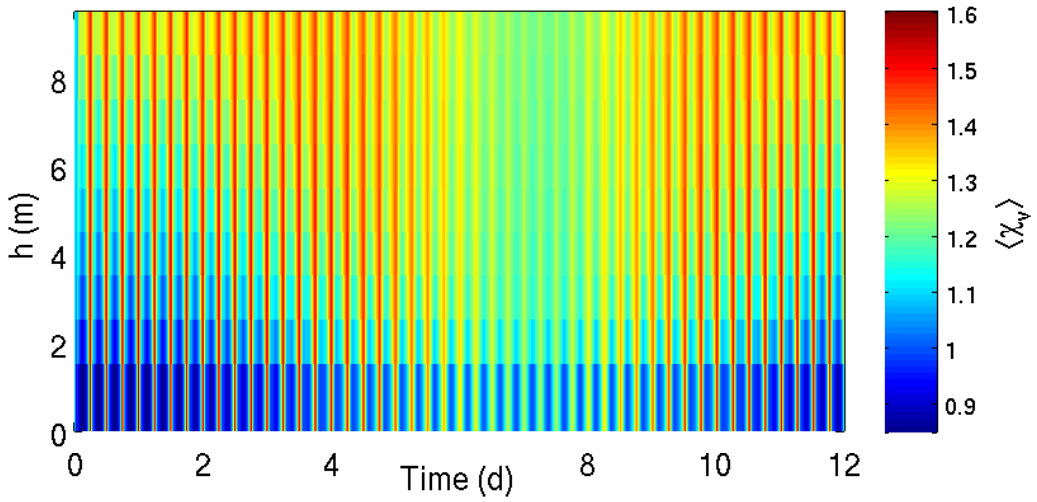

Figure 4.27: $\langle \chi_v \rangle$ for a molecular diffusion coefficient $D = 1 \cdot 10^{-7}\,\mathrm{cm^2\,s^{-1}}$. Calculation based on the reference run of the DB model in Sec. 4.1.8.

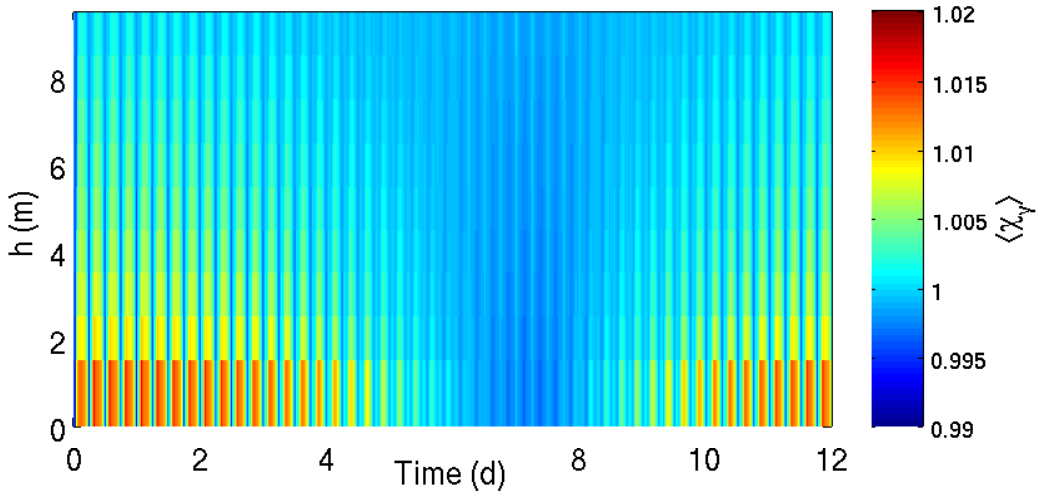

Figure 4.28: $\langle \chi_\gamma \rangle$ for a molecular diffusion coefficient $D = 1 \cdot 10^{-5}\,\mathrm{cm^2\,s^{-1}}$. Calculation based on the reference run of the DB model in Sec. 4.1.8.

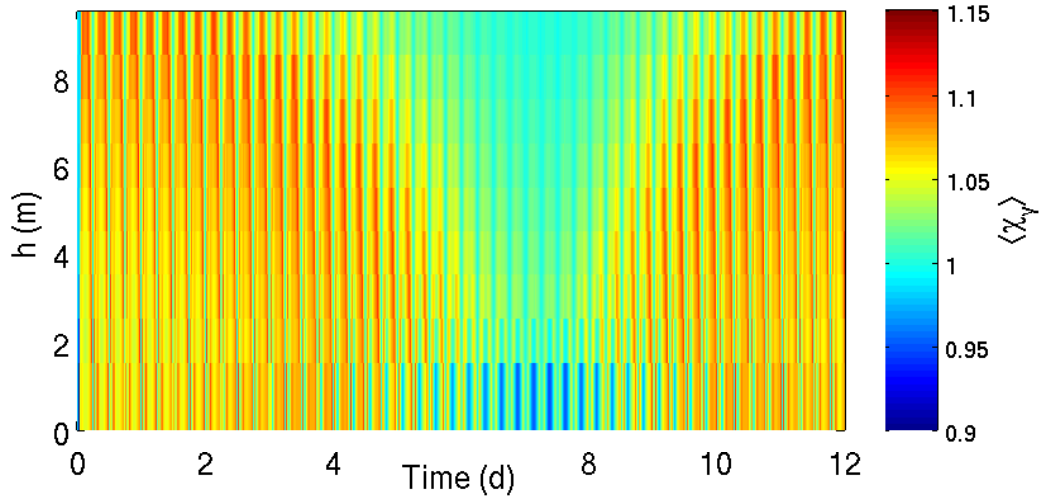

Figure 4.29: $\langle \chi_\gamma \rangle$ for sheared particles and a molecular diffusion coefficient $D = 1 \cdot 10^{-7}\,\mathrm{cm^2\,s^{-1}}$. Calculation based on the reference run of the DB model in Sec. 4.1.8.

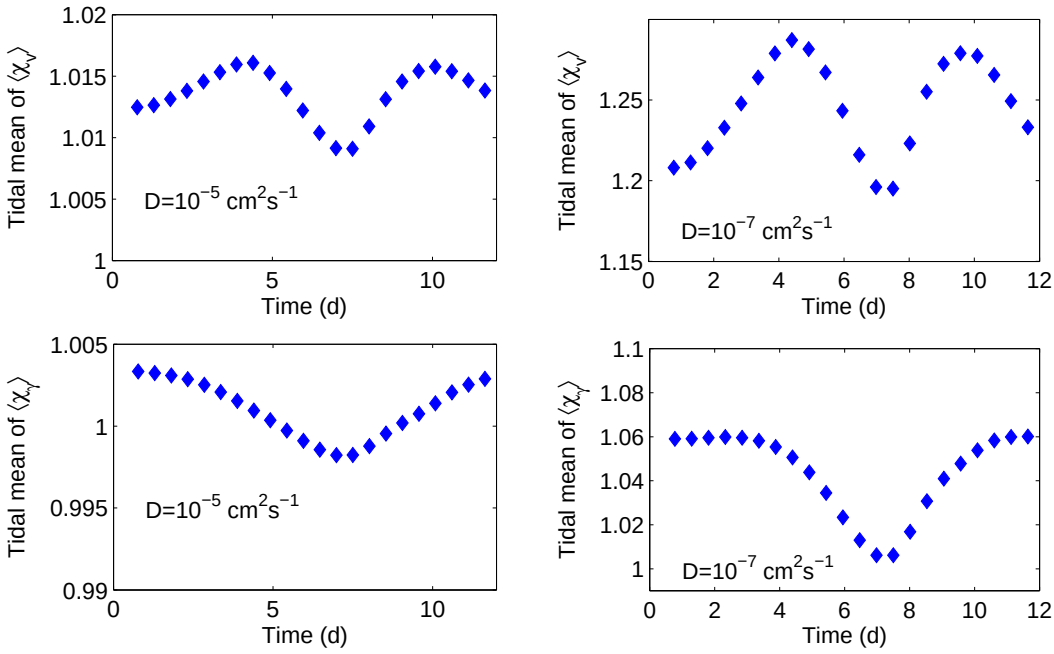

Figure 4.30: Tidal mean $\langle \chi_\mathrm{v} \rangle$ and $\langle \chi_\gamma \rangle$ for molecular diffusion coefficients of $D = 1 \cdot 10^{-5}\,\mathrm{cm^2\,s^{-1}}$ and $D = 1 \cdot 10^{-7}\,\mathrm{cm^2\,s^{-1}}$. Calculation based on the reference run of the DB model in Sec. 4.1.8.

4.3 Discussion of the potential applications

The implementation of the DB model into a 1D vertical hydrodynamic model (Sec. 4.1), the calculation of a potential, tidally variable DOM flux into the water column due to advectively increased fluxes from the aggregates (Sec. 4.2.2) and the calculations for the mean relative uptake capability of particle-attached bacteria (Sec. 4.2.3) have been examined in the perspective of a future application of the DB model in a coupling of SPM transport and ecosystem models. Although a validation of the DB model in a 1D vertical water column and the resulting estimates based on these simulations have still to be done, the applications and their qualitative results will be discussed in the following.

4.3.1 SiAM coupling and the comparison to the SCB model

Both models, the SCB and the DB model, show reasonable results under lunarly varying hydrodynamic conditions. They reproduce a typical tidal cycle of SPM – with increasing bottom shear stress increasing erosion, subsequent flocculation and deposition. Such a behavior is observable in many coastal and estuarine regions that are subject to tidal forcing (see e. g. Jago et al., 2006; Bartholomä et al., 2009). These first qualitative promising results give rise to the expectation that both models are favorable candidates for the simulation of SPM concentration and size dynamics. But owing to structural differences, the application of the models to answer specific questions might be a subject for discussion. A comprehensive discussion has been already carried out in Sec. 3.1 (part 3.1.4) for the 0D case. Especially the higher variablity of the aggregate distribution that can potentially be reproduced by the SCB model was a point of discussion. Structural differences have again lead to different parameter values of α and f_{b} in the 1D comparison. An internal mass redistribution occurs during the sinking of flocs due to the fixed form of the underlying distribution. This is similar to the already in Sec. 3.1 discussed mass redistribution during flocculation processes. As these mass redistributions combine in a simulated 1D water column, the ideal parameter pair (α and f_{b}) for a fit to the SCB model results has changed again. A more general discussion con-

cerning structural elements of the DB model, additionally to Sec. 3.1, can be found in Chap. 5. Nevertheless, it should be stressed again at this point that the DB model is computationally much more effective than the SCB model, as this has also implications for the calculation and accessibility of further observables such as e. g. the DOM fluxes investigated in Sec. 4.2.2. For example, depending on the used Sherwood numbers, a simple relationship between the mean size of aggregates, the SPM concentration and the respective flux into the water column can, in principle, be received.

The hydrodynamic model SiAM was used as the forcing for the SPM concentration and size dynamics in the contecxt of this study. It was successfully used in studies by Le Hir et al. (2001) and thus can be regarded as appropriate for examinations of the qualitative behavior of the SCB and the DB model. As the priority of Chap. 4 was an anticipation of future research and application directions of the DB model, only a short sensitivity study was carried out for the DB model to get first insights into its behavior under changing environmental conditions that can lead to changes of parameters. In direct comparison with the SCB model it became obvious that even though the SPM size and concentration dynamics show comparable results, the DB model had a slightly different reaction to changing hydrodynamic conditions. The SCB model reacted faster to changing shear and turbulent diffusion rates, while the DB model showed a lag compared to the SCB model. Whether this lag and also the slightly higher total SPM mass variability in the water column on a tidal, but less variability on the lunar time scale (compared to the SCB model) matters significantly when comparing the models with observations, is an open question. Moreover, it is questionable whether this behaviour is obligatory or can change under different conditions and parametrizations.

The sensitivity study has shown that the DB model in its current development is most sensitive on the fractal dimension of the aggregates. However, numerical studies by Verney et al. (2010) in a 0D framework have shown that this high sensitivity strongly depends on the used fragmentation term. Thus, a closer adoptation of the model for fragmentation of Winterwerp (1998) for the change of a characteristic diameter of aggregates could reduce the here found high sensitivity on d_f. Nevertheless, even in the present state, the behavior of the model on parameter changes are qualitatively reasonable.

The discrepancies between the DB and the SCB model are likely to result from the structural differences of both models already discussed in Sec. 3.1. Additionally to the redistribution of mass by fragmentation and aggregation processes, the sinking term also contributes to such redistribution of mass in the present state. However, a calculation of the error that is made by taking into account the preassumed underlying exponential number distribution in the development of the sinking term (Sec. 4.1.4) is not easily accessible. Even a numerical intercomparison with a SCB model is difficult due to a sinking velocity depending numerical diffusion in spatially explicit models. To enlighten the factor of internal redistribution of mass induced by the sinking term, only a validation with observation could help to *i)* see its effects and *ii)* maybe improve the process description by correction factors.

To summarize, it has been shown that the DB model can at least qualitatively reproduce typical SPM concentration and size dynamics. It shows the typical erosion and increase of SPM in the water column with increasing shear rates. Depending on the chosen parameters, flocculation processes force the aggregates' size distribution towards larger or smaller aggregates leading to asymmetries of the resulting tidal size dynamics due to different time scales of aggregation and fragmentation. The high amount of SPM in the water column during high shear rates is reduced after the shear peak owing to aggregation and thus enhanced vertical fluxes. Stressing the computational effectivity of the model, it is most likely a favorable candidate for the coupling also to 3D hydrodynamic sediment transport models. The DB model is especially useful for future research activities where a possible studying focus is the interaction between (micro-) biogeochemical processes and cohesive sediment transport.

4.3.2 DOM fluxes and mean relative potential uptake capabilities

The DB model was originally intended to help to close the gap between cohesive sediment transport and ecosystem models. It is therefore convenient to anticipate future applications of the DB model by testing and developing possible interfaces to (micro-) biological processes.

Based on the reference run of the DB model coupled to the hydrodynamic SiAM model, potential release rates of solutes from aggregates into the water column have been investigated in Sec. 4.2. As natural aggregates are a favorable substrate for many microbes, their enzymatic activity on the particles (e. g. Ziervogel and Arnosti, 2008) leads to the successive decomposition of aggregates as e. g. observed by Goutx et al. (2007). A release of organic matter and nutrients into the interstitial water of the aggregates is the consequence. As not all enzymatically decomposed OM can be taken up directly by particle-associated bacteria (Azam and Long, 2001), aggregates are known to enhance the DOM concentration in their vicinity favouring microbial growth also in the ambient water (Kiørboe and Jackson, 2001). This DOM release accounts for a significant proportion of water column bacterial production (up to 50 %, Azam and Malfatti, 2007). Both, the sinking and the shear that particles experience, can contribute to an increase of advectively-enhanced flux from or to particles into the water column. Due to a highly variable hydrodynamic regime in coastal waters, the flux of DOM from particles into the water column is likely to vary on a tidal, and as shown, even on a lunar time scale. Another factor than the increase of flux due to shear around and sinking of the aggregates is their break-up itself, where a high amount of interstitial water enriched in DOM is released (Goldthwait et al., 2005). Moreover, diffusive release from the sediment is also a source of DOM. The changing SPM concentration due to deposition and resuspension during tidal cycles itself also contributes to a variability of suspended POM that can potentially be mobilized and released as DOM into the water column. A tidally changing flux from particles into the water column thus can be a co-mechanism that helps to explain intertidal concentration changes of solutes in the water column as observed by e. g. Grossart et al. (2004b). They observed a highly variable dissolved combined amino acid (DCAA)[4] concentration on a tidal time scale. During November, the DCAA concentration showed a clear tidal cyclicity, while in May the dynamics might be more affected by biological processes that lead to a more variable signal. However, a direct comparison with observations has still to be done. Moreover,

[4]DCAA: dissolved combined amino acids are di-, oligo-, or polymers of amino acids in solution; DFAA: dissolved free amino acids are monomers of amino acids in solution; PCAA: particulate combined amino acids are amino acids of any size bound to larger particles

only few measurements on interstitial DOM concentrations in aggregates are availaibe. Alldredge (2000) has found highly enhanced DOM concentrations in marine snow compared to the surrounding water (enrichment factor of 16 – 78 times). These particles were of mainly organic origin. In such areas like the backbarrier basin of Spiekeroog island, tidally changing water bodies can carry particles of different origin with high sediment loads. The high sediment component in coastal aggregates (up to 95 % of dry weight, Joerdel et al., 2004) is likely to reduce DOM concentrations within flocs compared to open ocean aggregates that can consist to more than 80 % of organic material (Herndl, 1988). This would also reduce the DOM flux from particles into the ambient water as it is strongly dependent on the concentration gradient. However, a high seasonal variability in primary production and thus floc composition can lead to highly variable fluxes from the particles and thus complicates the picture additionally. Despite the problems of fast microbial uptake of nutrients also in the particles' surrounding water, the different fluxes of substances due to their differences in molecular diffusivity could help to gain further experimental insights into the role of aggregates in the release of DOM, but also trace metals into the water column.

As aggregates in coastal waters are in the intermediate hydrodynamic regime between the Stokes regime (for small particles) and a regime, where inertial forces start to play a role (for particles having a Reynolds number of $Re \approx 1$ and higher), the calculations for the fluxes can be regarded as conservative estimates. Moreover, it is likely that intra-floc flow as introduced in the investigation on the mean relative uptake capability of bacterial cells attached to particles in Sec. 4.2.3 favors fluxes of solutes from the particles into the ambient water column (that needs further investigations). The flux of solutes into the ambient water column might also have an effect on the settlement of bacteria on the particles. Changing fluxes from the particles with changing hydrodynamic conditions might be relevant for finding strategies when bacteria try to chemotactically sense and actively settle on aggregates. Moreover, as also extracellular enzymes can be transported away, particle-associated bacteria may physiologically react to changing hydrodynamic conditions as the effectiveness of ectoenzyme production related to the possible uptake may

change. Fluxes of solutes of different molecular diffusivities leading to imbalances in availability may also have an influence on the ectoenzymatic activity of particle-associated bacteria. For example, Sala et al. (2001) have shown changing ectoenzymatic activities of bacteria due to imbalances of nitrate and phosphate in enrichment experiments.

The calculations for the relative potential uptake capability have followed widely the approach of Logan and Hunt (1987). However, a more variable and flexible to use relationship between the fractal dimension and the porosity has been introduced. This allows for the calculation of intra-floc velocities also under different conditions than assumed in the original publication of Logan and Hunt (1987). For consistency with the DB model, some assumptions have been made that lead to a more conservative estimate of the intra-floc flow velocities. Among them, in the calculation of the floc sinking velocities, the permeability has not been taken into account. This would lead to a slight increase of sinking velocity and thus to an enhanced flow through the aggregate. Moreover, the porosity has been related to the size of the primary particle composing the aggregates. As discussed by Li and Logan (2001), such a relationship underestimates the porosity and hence also leads to a conservative estimate of the intra-floc velocity. However, gel-like particles like TEP can clogg up pores (as already discussed by De La Rocha and Passow, 2007) leading to less fluxes than assumed by such calculations on basis of a cluster size (cmp. to Li and Logan, 2001). Thus, being conservative in the formulation of the model, its results give an estimate of the lower limit of the influence of an advectively-enhanced uptake capability on particle-associated bacteria. However, changing fractal dimension and primary particle size are relevant factors influencing the mean relative potential uptake capability of bacteria on aggregates – the intra-floc velocity increases with larger primary particles, but decreases with higher fractal dimension.

Microbes that are attached to particles do benefit from the increased substrate availability (Azam and Long, 2001), especially in the open ocean, where aggregates are composed of organic-rich material like phytoplankton cells, and detritus like e. g. faecal pellets. By contrast, in coastal areas, aggregates are dominated by inorganic particles and in higher latitudes, a seasonal variability

of freshness of the particles' composing organic material occurs due to pronounced annual primary productivity cycles. Microbes attached to particles cannot only benefit from organic substances composing the aggregates, but under some circumstances as shown in Sec. 4.2.4 also owing to the here investigated hydrodynamic and diffusive processes that can enhance the substance availability especially for larger molecules with lower molecular diffusivities. As already discussed before, the DOM flux from particles into the water column might have an effect on the settlement of bacteria on aggregates. As both, the DOM flux into the water column and the relative potential uptake capability changes on a tidal time scale, the interaction of these factors might lead to an intricate way how bacteria react to these highly variable changing environmental conditions - either by active settlement or by detachment from particles. The deposition and thus a likely decrease in bacterial activity (Ploug and Grossart, 2000) may also contribute to the intricate way how bacteria react to the hydrodynamicly very dynamic environment in tidally affected coastal areas. Being deposited, bacteria may on the other hand benefit from uptake of soluable fractions of EPS releases by microphytobenthos.

As the composition and structure of aggregates change on a seasonal time scale (see also Sec. 3.2 and Chen et al., 2005), the significance for bacteria of on the one hand composition and on the other hand higher relative uptake capabilities might shift throughout the season in regions like the Wadden Sea. In summer, when biological processes play a high role in SPM dynamics (cmp. with Sec. 3.2) the composition may be the major factor from which particle-associated bacteria can benefit. The latter can explain higher cellular particle-attached bacterial production rates observed in spring and early summer by Sintes et al. (2010). During the winter season, when organic compounds like particulate combined amino acids (PCAA) have a more refractary origin (Grossart et al., 2004b), the uptake capability for nutrients might be a relevant factor for particle-attached bacteria. Such changing environmental conditions may also play a role in community structure changes of aggregate-associated bacteria (as observed by Rink et al., 2007) that needs further investigations.

Summarizing the discussion, the DB flocculation model in 1D is able to reproduce the typical tidal and lunar SPM concentration and size dynamics at

least qualitatively well, while a validation with observations has yet to be done. The intertidal and interlunar variability can have a significant effect on the DOM release from particles into the water column and furthermore might lead to changing favorable conditions for free-living and particle-associated bacteria. The DB flocculation model is a good candidate to bridge the gap between cohesive sediment transport and ecosystem models. It provides effective and clear interfaces for the dynamic coupling of biogeochmical processes to cohesive sediment or, more general, flocculation dynamics while being computationally effective.

Chapter 5

Discussion & Conclusions

Within this thesis, a novel model for aggregation - fragmentation processes has been proposed. In contrast to many other models (e. g. McCave, 1984; Jackson, 1990; Riebesell and Wolf-Gladrow, 1992; Dam and Drapeau, 1995; Logan et al., 1995; Ruiz, 1997; Stemmann et al., 2004a; Verney et al., 2010), it is based on the dynamics of the total cohesive SPM fraction and its related average size of the constituent aggregates. Moreover, an underlying exponential number distribution has been considered according to observations of Lunau et al. (2006) in the backbarrier basin of Spiekeroog island as well as the fractal properties of aggregates that has been proposed by e. g. Kranenburg (1994). Especially the novelty of a strongly decoupled treatment of the average size of aggregates, their related distribution and the total concentration of cohesive sediment enables the model to be easily coupled to other – biological, chemical and/or physical – processes, accompanied by minor computational costs than by size class-based models. The core of the flocculation model describes the change of the average radius $\langle r \rangle$ by aggregation due to *i)* differential settling and *ii)* shear, and moreover, by fragmentation due to shear.

In Sec. 3.1, the distribution-based model has been compared to a "classical" size class-based flocculation model, and both have been validated with experimentally derived data. The here proposed distribution-based model shows a good agreement with the size class-based model predictions, but also with the experimental observations. However, small discrepancies occured that were discussed in Sec. 3.1 and will be revisited in the following.

The flocculation model has been coupled to further sediment transport-related processes, namely resuspension, deposition and transport (Sec. 3.2). Still in 0D and applied to the backbarrier basin of Spiekeroog island, the model was used to identify seasonal changes of sediment transport-related properties that might be influenced by biological processes.

As the transport of sediment is a spatial process, it is evident that such a flocculation model, as proposed in Sec. 2.4, has to be applied to hydrodynamic models in order to describe the fate of cohesive sediments in 2D or 3D. A first step into such a direction has been achieved by coupling the DB flocculation model to the 1D vertical model SiAM (Chap. 4). It is compared to a SCB model run. The reference run has been further used to estimate advectively-enhanced potential DOM release rates from particles into the water column and to examine the relative potential uptake capability of aggregate-associated bacteria compared to cells in the ambient water experiencing shear.

In Sec. 3.1, 3.2 and Sec. 4.3, the DB model has been already discussed concerning its structural differences (compared to a SCB model) and its potential applications. However, a comprehensive discussion and a conclusion will be given in the following part that is organized into three major sections:

- First, physical and biological aspects and influences are discussed,
- second, the model and its underlying assumptions will undergo a critical review,
- third, a short conclusion is given.

5.1 Physical and biological implications

An overview of several biological processes that can influence aggregate formation and dynamics has already been given in Chap. 1. The coupled 0D distribution-based flocculation model has been used to identify seasonal changes of SPM dynamics-related properties, reflected by shifts in the model parameters (Sec. 3.2). Within this section, relevant biological processes will be therefore discussed concerning their capability to affect cohesive sediment transport processes that might explain the identified shifts in model parameters.

However, other factors, namely the two different sampling stations and the aggregates' dependency on the spatial hydrodynamic regime, which is not explicitly taken into account in Sec. 3.2, could also be an explanation for the identified model parameter shifts. Although Lemke et al. (2009) observed a tendency for differences between the inlet and the inner tidal basin of the Spikeroog backbarrier basin for various parameters like SPM concentration on a daily time scale, their study revealed that the seasonal variability of most parameters is higher than the spatial variability on a tidal time scale. Thus, it is very likely that the parameter shifts found in Sec. 3.2 are mainly due to seasonally changed environmental conditions and not due to spatial heterogeneity.

Most likely, biological processes influence cohesive sediment transport-related properties. For example, Chen et al. (2005) have reported seasonally changing morphologies of aggregates in the Scheldt estuary and related their observations to the influence of POM. Moreover, Chang et al. (2006b) reported observations of less turbid seawater when large flocs are formed – commonly observed in summer – and more turbid waters when flocs are small – commonly observed in winter. This is in contradiction to the theoretically expected behavior, as the SPM concentration is lower in summer than in winter leading to less collisions in summer und thus, theoretically, to smaller aggregates. Assuming the weather conditions have been similar during the observations of Chang et al. (2006b) – and hence the hydrodynamic regime, aggregate properties must have changed to explain the occurence of larger flocs in summer.

Obviously, seasonal patterns of the primary productivity exist in the North Sea and, particularly, in the backbarrier basin of Spiekeroog island. Chlorophyll *a* (Chl *a*) concentrations between $1\,\mu g\,Chl\,a\,L^{-1}$ and $6\,\mu g\,Chl\,a\,L^{-1}$ (in winter and in summer, respectively) have been reported by Lunau et al. (2006) and Lemke et al. (2009). It is well known that algae produce EPS (e. g. Decho, 1990, 2000) of which a subfraction, TEP, can be generated (Thornton, 2002). These TEP are discussed to be a major factor in the sedimentation of matter as it forms precursors for aggregation and is discussed to enhance the collision efficiency (Passow et al., 2001; Passow, 2002c). Claquin et al. (2008) found a

linear relationship between the production of TEP (in xanthan equivalents[1]) and Chl *a* for eight pelagic microalgae species. It is therefore likely that a seasonal pattern of EPS and TEP due to their coupling to primary productivity can be assumed for the backbarrier basin of Spiekeroog island with higher EPS/TEP concentrations in summer than in winter.

Black et al. (2002) stated that phytobenthos with its production of EPS tend to generally stabilize the sediment surface against erosion. The model results in Sec. 3.2 are consistent with this statement as a higher critical shear stress for erosion/resuspension was found in summer than in winter. These model results are also supported by Chang et al. (2006a) who found a generally increasing mud fraction in the surface sediments of the backbarrier of Spiekeroog island (in four transects off shore from the landward margin) during the summer months, while they reported a depletion of this fraction in winter time (apart from one station, where this behavior was inverse). They relate their findings to the aggregation of cohesive sediments in the water column and their subsequent faster deposition in summer than in winter. A faster deposition is not only due to larger aggregates, but also due to a smaller viscosity of water in summer. Further on, Chang et al. (2006a) argued that the winter is more energetic than the summer month promoting the erosion of sediment and disaggregation of flocs. However, it is likely that biological activity in form of benthic primary productivity can also be accounted for the increase of erosion resistence in the summer time. Chang et al. (2006b) postulate that without aggregates, the mixed flats observed in the study area of the backbarrier basin of Spiekeroog island would not be able to develop. It is clear that this would have several implications not only for sediment budgets, but also for the settlement of higher organisms like e. g. worms and bivalves.

An increasing sediment stabilization in summer due to the *glueing* of sediment particles by EPS might to account for the erosion of larger, *carpet-like* particles which would explain the increasing radius of eroded aggregates found in the model for the summer situation. However, this finding might be ptentially artifical as the high shear rates in the bottom boundary layers should

[1]For the measurement of TEP concentration in xanthan equivalents see Passow and Alldredge (1995).

be strong enough to fragment such sediment-EPS matrix particles. According to Burchard (2002), the kinetic energy dissipation rate ϵ above the sediment surface in height z can be calculated from the friction velocity u_*, the von Kármán constant κ (=0.4) and the bed roughness z_0 under the assumption of a logarithmic velocity profile by

$$\epsilon = \frac{u_*^3}{\kappa\,(z + z_0)} \quad . \tag{5.1}$$

As the bottom shear stress is calculated by

$$\tau = u_*^2\,\rho \quad , \tag{5.2}$$

the shear rate above the bottom can be calculated according to

$$\gamma = \left(\frac{\epsilon}{\nu}\right)^{\frac{1}{2}} = \left(\frac{\left(\sqrt{\frac{\tau}{\rho}}\right)^3}{\kappa\,(z + z_0)} \cdot \frac{1}{\nu}\right)^{\frac{1}{2}} \quad . \tag{5.3}$$

Calculating the shear rate for typical values ($\tau = 0.5\,\mathrm{Nm}$, $\rho = 1000\,\mathrm{kg\,m^{-3}}$, $z_0 = 0.0001\,\mathrm{m}$, $\nu = 1 \cdot 10^{-6}\,\mathrm{m^2\,s^{-1}}$, $\kappa = 0.4$), where erosion occurs, the shear rate is $529\,\mathrm{s^{-1}}$ directly at the surface, and $16.7\,\mathrm{s^{-1}}$ at 0.1 m above the bed.

On the other hand, if a single eddy erodes and transports such a particle from the sediment surface to higher water layers (ca. 10 cm above bed), the surrounding shear rate is strongly decreasing which may help to prevent the particle from fragmentation. Nevertheless, experimental observations are needed to verify these considerations. In the case that erosion with subsequent fragmentation of particles is the dominant process, the found increased radius of eroded aggregates would have to be assigned to an additional boundary condition of the model.

As already brouched above, EPS cannot only stabilize the sediment, but can act as a precursor for aggregation and increase the stickiness of particles. On the other hand, especially in coastal waters, TEP can be regarded as a source of different primary particles than as pure cohesive sediment. TEP consist mainly of carbon compounds like acidic sugars and encage a high amount of

water and have thus an excess density close to zero or even a negative excess density of $-0.16\,\mathrm{g\,cm^{-3}}$ to $-0.3\,\mathrm{g\,cm^{-3}}$ (Azetsu-Scott and Passow, 2004). A consequence of the low density of TEP is the decrease of the floc mass-to-size ratio with an increasing volumetric amount of TEP ("primary" particles[2]) in aggregates. The relationship between size and density of aggregates is represented in the model by the fractal concept and thus, an increasing amount of TEP in flocs would lead to a decreasing fractal dimension. The latter has indeed been found with the model in the summer compared to the winter situation. This is also in agreement with the looser flocs in summer reported by Chen et al. (2005) for the Scheldt estuary, where the sediment particles are loosely bound together by an organic matrix. Such an embedding of sediment particles in a gel matrix has also been reported by Ayukai and Wolanski (1997) for the Fly River Plume, Papua New Guinea. Unfortunetely, TEP are a possible candidate to escape traditional measures of SPM dry-weight, as TEP can be partially sucked through classical glas fibre filters. Furthermore, TEP constitute *in situ* an amount of particles by volume, which cannot be represented by traditional dry-weight SPM and carbon content measuring. Thus their importance in aggregate formation could be underestimated, especially in sediment load-dominated coastal environments, for which studies concerning the flocs' composition are still rare.

In contradiction to the postulated increase in stickiness by TEP, a decreased collision efficiency, and additionally, a decreased break-up factor f_b have been found for the summer compared to the winter situation. One possible explanation for the found decrease of stickiness might be a potentially increased bacterial activity on aggregates. Such an effect of bacteria on particle stickiness has been reported by Kiørboe and Hansen (1993) for some algae cultures. Lemke et al. (2009) have shown a significantly increased bacterial biomass production (a sum of both, bacteria attached to particles and in the ambient water) during summer (July) compared to winter (January). They also reported a higher number of bacteria per volume attached to particles during July than in January, while the total SPM concentration has decreased.

[2]The quotation marks should account for the fact that TEP are aggregated polymers which can, in principle, be broken up into smaller molecules and thus do not constitute a unfragmentable particle like a sediment primary particle.

Thus, it is likely that the bacterial activity per aggregate has been increased. This might explain a reduced stickiness due to the faster turnover of reactive chemicals by bacteria. Admittedly, a decrease of α accompanied by a decrease of f_{b}, where the latter relates to an increasing aggregate stability, is in contradiction or at least counterintuitive. Either the stickiness is not necessarily positively related to the floc stability or, more likely, model uncertainties that are discussed in Sec. 5.2 can be accounted for this counterintuitive finding. However, more experimental research is needed to answer the effect of bacterial activity on parameters like stickiness, but also on fractal dimension due to degradational loss of POM.

The decrease in stickiness can be compensated by a decreased fractal dimension. The decrease of the fractal dimension leads to an increase of the exponent for aggregation due to shear on which the changing rate $\langle \dot{r} \rangle \propto \langle r \rangle^{4-d_f}$ depends, and thus, the rate must not necessarily decrease. On the other hand, the aggregation due to differential settling is always $\langle \dot{r} \rangle \propto \langle r \rangle^2$ when using the fractal relationship for the floc density introduced in Sec. 2.4 (see Eq. (2.62)), and thus in the power of $\langle r \rangle$ independent of the fractal dimension. The relative contribution of aggregation due to differential settling to total aggregation descreases compared to shear-induced aggregation with a decrease of fractal dimension. In this context, already Kiørboe et al. (1990) pointed towards the uncertainty of the "packing" of aggregates for the estimation of α. Thus, an examination of the influence of the fractal dimension on the stickiness is worth to do in laboratory experiments. Such studies should be accompanied by a better comparability and reproducibility of fractal dimension measures. Studies are also needed to unravel processes influencing the fractal dimension (or synonymously the floc density) of aggregates beyond homogeneous particle compositions like used in Serra and Casamitjana (1998). Such studies are needed as the fractal dimension of marine aggregates can range dependent on the type of primary particles and the different mechanisms of coagulation (Logan and Kilps, 1995). An understanding of processes influencing the floc density is critical to better model and predict SPM transport and fate.

Similar to aggregation, the process of break-up is also influenced by the fractal dimension and the stickiness of TEP particles. However, fragmentation is rarely addressed in experimental studies, although recent theoretical work by

e. g. Zahnow et al. (2009) gives reasonable supposition that fragmentation is the major process determining the shape of the aggregate distribution at least in chaotic advection. Especially in turbid, turbulence-driven coastal waters, break-up may play a significant role as also indicated by its strong relative contribution to the evolution of the mean size (Sec. 3.2). Stressing the relevance of biological processes again, the change of aggregate morphology (and thus fractal dimension) due to e. g. release of TEP by algae might be a relevant factor for the resistence of flocs against shear stress. Thus, the relevance of primary particle source and e. g. microbial degradation as observed by e. g. Goutx et al. (2007) on aggregate break-up needs further investigations.

In Chap. 4 the distribution-based flocculation model has been coupled with a 1D vertical hydrodynamic model and thereafter used for further applications. A comprehensive discussion was achieved in Sec. 4.3. Only a brief summarizing discussion is therefore carried out in the following.

It turned out that the DB model in 1D reproduces the SPM dynamics very similar as the compared SCB model. Both models show a good qualitative agreement with typical tidally affected coastal SPM dynamics as observed e. g. by Jago et al. (2006) and Bartholomä et al. (2009). The tidally and lunarly changing size dynamics due to flocculation processes influenced the SPM dynamics and *vice versa*. A tidal asymmetry of SPM concentration and size appears due to different time scales of aggregation and fragmentation, where the latter is faster. While fragmentation leads to smaller flocs during the increasing shear phase, large flocs can form after the shear peak. This increases the vertical flux in this period. On the other hand, the resuspended amount of SPM also controls the maximum sizes of flocs. During lunar periods of high shear rates, high collision probabilities are present due to higher SPM loads in the water column. This results in larger aggregates than during lunar low-shear periods. The intricate coupling between hydrodynamic conditions, size dynamics, and biological processes as assessed in Sec. 3.2 that interact with the physical driven processes, can be regarded as the major source of uncertainty when modelling SPM dynamics.

The possible role of SPM dynamics for DOM fluxes into the water column has been analyzed qualitatively. It is well known that particle-associated bac-

teria degrade POM on aggregates (e. g. Kiørboe and Jackson, 2001; Ziervogel and Arnosti, 2008). This leads to an excess DOM release into the interstitial pore water of aggregates (Azam and Long, 2001). They are therefore a source of DOM that can favour microbial growth in the aggregates' vicinity (Kiørboe and Jackson, 2001; Azam and Malfatti, 2007). However, high loads of suspended sediments, highly variable hydrodynamic conditions and primary production can affect this picture in coastal waters. Therefore, the possible influence of tidal and lunar variability of hydrodynamic conditions on SPM dynamics and the subsequent potential release of DOM has been investigated. It turned out that the overall potential release rates of DOM from aggregates into the ambient water varies on a tidal, but also a lunar time scale. Generally, high shear rates tend to foster DOM release from aggregates. This is due to *i)* stronger erosion and thus higher SPM concentrations, and *ii)* subsequent potentially larger growing aggregates in the water column. Additionally, and not yet included in the model, fragmentation and the subsequent release of DOM enriched interstitial water (Goldthwait et al., 2005) during such periods is a potential factor for DOM variability. A release of DOM due to resuspension is also likely to occur. The calculated potential release rates are even spatially distributed as the main part of SPM concentration stays accumulated close to bottom. This might be in contradiction to findings of Lemke et al. (2009) who found a vertically homogeneous DOC distribution in the backbarrier basin of Spiekeroog island throughout the whole year. However, vertical mixing processes might be an explanation for such a homogeneous distribution of DOM/DOC in the water column. They are not subject to vertical fluxes as SPM that has been found to show indeed higher concentrations close to the bottom in the same study, at least in some periods of the year. The tidal variability of potential DOM release rates enhanced by an advective component to diffusive fluxes from particles might be a co-factor that can help to explain intertidal variability of DOM concentrations. Such intertidal variability of dissolved combined amino acids (DCAA) was e. g. observed by Grossart et al. (2004a) in a tidal flat ecosystem.

It has been already shown by Logan and Hunt (1987, 1988) that microbes attached to particles may also take advantage from better substrate availability due to intra-aggregate fluid flow that enhances diffusive fluxes. However,

this has been shown for very fragile flocs, and moreover, not under variable environmental conditions. An extension of the basic concept of Logan and Hunt (1987) for microbial uptake capability within flocs has therefore been introduced. A more flexible description of the permeability of flocs via a relationship to their fractal dimension made it possible to investigate the mean relative uptake capability under tidally and lunarly changing hydrodynamic conditions. The model was tested within the framework of the distribution-based flocculation model in the 1D vertical water column that has been already discussed above. As a conservative result, it turned out that the mean relative uptake capability was not significantly or only slighly enhanced by fluid shear. This is in contradiction to Logan and Hunt (1987), but can be explained by a higher fractal dimension and thus lower permeability of the flocs compared to their study. However, as already discussed in Sec. 4.3, this might be underestimated as the permeability has been calculated to be related to primary particle cluster sizes (Li and Logan, 2001). Nevertheless, as De La Rocha and Passow (2007) argued that gel-like particles can clogg-up pores, it might be questionable which description is more appropiate.

The mean relative uptake capability due to particle sinking was certainly enhanced for low ($D = 1 \cdot 10^{-7}\,\mathrm{cm^2\,s^{-1}}$), while only slightly for high molecular diffusivities ($D = 1 \cdot 10^{-5}\,\mathrm{cm^2\,s^{-1}}$) that corresponds to large polymers and monomers, respectively (Logan and Hunt, 1987). Integrated over a complete tidal cycle, the tidal mean relative uptake capability of particle-associated bacteria was mainly around one and thus equal to a free living cell in the ambient water. However, a significantly higher mean relative uptake capability has been found due to sinking and a molecular diffusivity of $D = 1 \cdot 10^{-7}\,\mathrm{cm^2\,s^{-1}}$. A slight variability throughout a lunar cycle can be stated, and be explained by a changing SPM size dynamics within the lunar cycle. This makes additionally clear that the findings are also very sensitive not only to the fractal dimension (as can be infered from Fig. 4.22 and 4.25 on page 156 and 159, respectively), but also to the SPM size dynamics. To hypothesize, such effects like higher substrate availability due to an increase of diffusive flux by an advective component might be relevant to partly explain such nearly constant bacterial activity on aggregates throughout the whole year as found by Sintes et al. (2010) in coastal waters off the Dutch coast. As already brouched

above, another explanation for high microbial activity on flocs is the aggregates' POM component that can be hydrolized and subsequently utilized by particle-attached bacteria (e. g. Azam and Long, 2001).

5.2 Model properties

The distribution-based flocculation (DB) model presented in this thesis has been compared to a size class-based model (SCB) in Sec. 3.1 (Maerz et al., 2010). It shows very similar results compared to the SCB model apart from the optimized parameter set of the stickiness α and the break-up factor f_b that were determined to best-fit the experimentally derived laboratory data. The difference in α and f_b between the two optimized parameter sets may be caused by the two models' intrinsic structure which will be examined and discussed in the following.

SCB models (e. g. in Jackson, 1990; Verney et al., 2010) usually solve the integro-differential Smoluchowski equation by introducing a – sometimes high – number of size classes. The latter interact via an aggregation kernel that describes the collision frequency of particles estimated for a specific process (like aggregation due to shear, differential settling or Brownian motion). A numerical diffusion between the size classes is the consequence, and is strongly dependent on the used number of size classes – the finer the resolution, the less the numerical diffusion (see e. g. Prakash et al., 2003, for the integration scheme used in the model comparison in Sec. 3.1).

In contrast to the SCB model, the integrals are solved analytically in the presented DB model leading to a simple ordinary differential equation. The analytical solution of the integrals is realized using some few approximations: First, a specific aggregate number distribution (in this thesis an exponential one in accordance with observations of Lunau et al., 2006) has been implied. Second, the mass conservation is violated during the process of integration, but ensured afterwards by a moment closure. The latter is not elegant and tackels the problem in a roundabout way – as it is not possible to treat it directly, but leads to an expression for the change of $\langle r \rangle$. Moreover, the results of Winterwerp (1998) support the here proposed model, as the author originally

came up with a very similar equation for shear-induced aggregation for a characteristic diameter. In addition, these elaborations capture the information of an underlying particle distribution which can be an important extension in the context of the coupling to bio-geochemical models (see Chap. 6).

Nevertheless, the approximations due to the violation of the mass conservation during the step of integration and the moment closure (which ensures the mass conservation again) lead to some inaccuracy that need to be discussed. First, as can be seen in App. A.3 it matters how to translate the mass-conserving Smoluchowski equation into an equation that is solvable, but not mass concerving anymore. Second, the order of closure is a factor of uncertainty that has to be considered (again see App. A.3). As can be found in App. A.3, different formulations can be achived for the K_γ function, dependening on the translation and the order of closure. Two versions show asymptotic behavior for fractal dimensions of the lower limit in observable aggregates which is a physically unrealistic result. They should not be used in future applications. The K_γ functions derived by a second order closure for the rectilinear case converge with the upper limit of fractal dimension, while the curvilinear- and fourth order-derived K_γ functions do not converge. The higher values of K_γ for fractal dimensions in the naturally observable range (1.6–2.4 Manning and Dyer, 1999) in the case of the fourth order closures compared to second order closures are most likely due to the inclusion of higher moments into the closure, representing more information of the distribution. The majority of curvilinear-derived K_γ functions are greater than the respective rectilinear functions – leading to higher rates of changes for the $\langle r \rangle$ than in the rectilinear case. When comparing the rectilinear and the curvilinear kernel for shear (refer to Eq. (2.31) and 2.32), this counterintuitive result becomes clear. By deviding the curvilinear through the rectilinear kernel for shear, it becomes evident that there exists a constraint in which the curvilinear is smaller than the rectilinear kernel for shear. The constraint $(10\,r)/(1.3\,(r + r')) < 1$ has to be, in average, fulfilled during the integration step of the derivation for the change of the $\langle r \rangle$. As the number of aggregates are decreasing with the radius of flocs respective to the underlying distribution, this can hardly be fulfilled, and hence, the curvilinear K_γ function is mainly larger than the rectilinear one.

Apart from this, however, is is remarkable that the discrepancies only occur in the moment collecting function K_γ while the dependency of the change of $\langle r \rangle$ on $\langle r \rangle$ is strictly given by a specific power law (in the case of shear-induced aggregation: $\dot{\langle r \rangle} \propto \langle r \rangle^{4-d_f}$, which is also in agreement with Winterwerp, 1998). Besides, already Thomas et al. (1999) indicated that e. g. the parameter stickiness can account for uncertainties in the kernel formulations of aggregation models, and thus, it can be used in the here proposed DB model to compensate uncertainties of the model derivation. It is clear that not only aggregation does depend on the fractal dimension, but also fragmentation does. Thus, the f_b value also accounts for such uncertainties in the power dependence of $\langle r \rangle$ in the process of break-up. This can be one explanation for the discrepancies between the DB and the SCB models' optimized parameter sets in the comparison in Sec. 3.1, respectively. Moreover, the strong sensitivity of the models to the fractal dimension shown in Sec. 3.1 might be less than reported. Verney et al. (2010) showed that the incorporation of the fractal dimension into the fragmentation term leads to a decreased sensitivity to it. Thus, it is important to choose the fragmentation term carefully (Verney et al., 2010) and it should be accounted for in future applications.

However, the fixed functional form of the underlying number distribution might be another source of differences. Ideally, the shape of a particle distribution should be variable, so that even bi- or other modal distribution shapes can be modeled. In SCB models, it can be realized technically more easily compared to the DB model where this is not the case in the current stage of development and might be done by high analytical effort. However, although the form of the underlying distribution is given, it can vary in its funcionally predefined limits, which is exemplarily shown in Sec. 3.1.

Another more general constraint is given by the used methodology of the moment closure approach presented by Wirtz and Eckhardt (1996). It is based on the assumption of a Gaussian (-like) distribution and becomes inaccurate the more the underlying distribution deviates from a Gaussian distribution. Thus, extremely skewed or even bi- or more-modal distributions could only be handled with the restriction of lower accuracy. The here presented model is

based on a concentration distribution $C(r)$ which has the form:

$$C(r) \;=\; N_0 \,\exp(-\beta\, r)\, w_0\, r^{d_f} \qquad \text{with}: \;\; \beta,\, d_f,\, N_0,\, w_0 > 0 \tag{5.4}$$

and is skewed positive relative to a Gaussian distribution

$$s(x) \;=\; \frac{E((x-E(x))^3)}{\mathrm{Var}(x)^{\frac{3}{2}}} \tag{5.5}$$

$$\;=\; \frac{\frac{\int_0^\infty (r-\langle r\rangle)^3\, n(r)\, w(r)\mathrm{d}r}{\int_0^\infty n(r)\, w(r)\,\mathrm{d}r}}{\left(\frac{\langle r\rangle^2}{d_f+1}\right)^{\frac{3}{2}}} \tag{5.6}$$

$$\;=\; \frac{2}{\sqrt{d_f+1}} \quad , \tag{5.7}$$

but is uni-modal. Thus, it should not be too limiting for the application of the moment closure approach.

It is evident that the choice of the underlying distribution depends on the application of the model. More concrete, it determines the functional form of the differential equation, and thus, e. g. whether – like in the current version of the DB model – $\langle r\rangle$ can, in principle, grow infinitely (because an underlying distribution is always presumed). Furthermore, the shape of the distribution determines collision frequencies (depending on the kernel) and thus – together with the collision efficiency – the growth rate of the average size. Hence, a skewness of the particle distribution towards large particles would lead e. g. to higher collision frequencies and therewith to faster particle growth than a distribution skewed towards smaller aggregates. Further on, it becomes clear from this argumentation that small discrepancies between evolving modeled distributions would lead to changes in the growth rates. Moreover, during the aggregation and fragmentation process, the distribution is always 'forced back' to its original functional form. This introduces mass redistributions within the aggregate distribution schematically visualized in Fig. 5.1 for the aggregation process. Such internal mass redistribution can also occur during transport of $\langle r\rangle$ in spatially explicit models. Note, however, that a redistribution also exists in SCB models due to the occurence of numerical diffusion owing to the numerical scheme used to solve the Smoluchowski equation. Moreover, different

numerical diffusion for size dependent transport processes like sinking is also present in SCB models. The aforementioned rationale are again an intrinsic

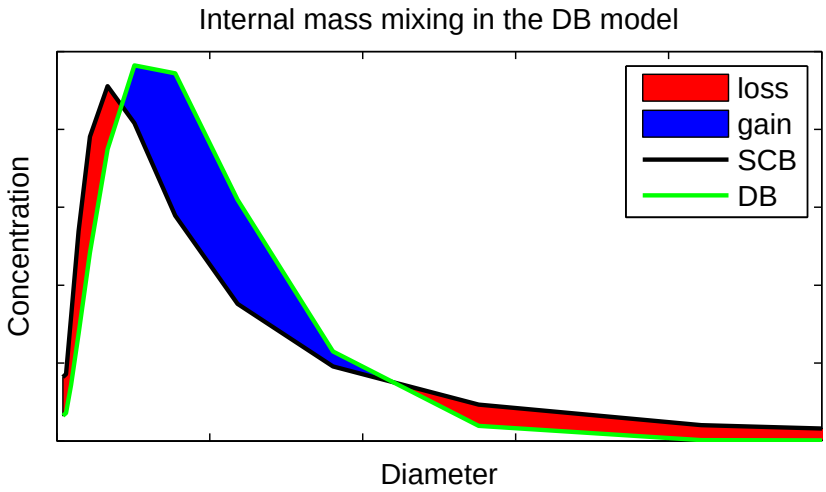

Figure 5.1: Schematical visualization of the internal mass redistribution effect in the distribution-based (DB) compared to the size class-based (SCB) model. Loss and gain means losses and gains due to internal mass redistribution compared to the SCB model. In the latter, such redistribution cannot occur due to a more variable shape of the distribution.

structural element that may explain the discrepancies between the two derived optimized parameter sets of the DB and the SCB model in Sec. 3.1 and 4.1. Supplementary, the dependence of the growth rate on the distribution is a factor which likely is needed to be considered when developing statistical models for flocculation processes like e. g. in Manning and Dyer (1999), especially when a broader application than for a specific system is intended.

Keeping this fact in mind, different viewpoints can be taken when choosing the underlying distribution – either from the initial state – or from the steady state distribution in a specific system. Both (and, most likely, others in the stages in between) might not have the same shape. Therefore, the growth rates can differ significantly and one has to decide which is the relevant phase that should be examined. The observations of Lunau et al. (2006) give rise to the assumption that the various driving processes (flocculation, transport, deposition and erosion processes) seem to drive the distribution mostly to one

specific form – the observed exponential number distribution. Hence, the derived aggregation equations can be assumed to represent the "driving force" towards larger particles in a system close to or in a dynamic equilibrium or, at least, that the processes interact with each other in a similar manner independent of the tidal phase. However, observations of Winter et al. (2007b) and Badewien et al. (2009) suggest a more variable distribution form in German coastal waters. It is still in question, how and why specific distributions are shaped. Recent work of Zahnow et al. (2009), however, indicate a domination of the distribution by the fragmentation process, at least in chaotic flow. Such a dominance would be in good agreement with the model results found in Sec. 3.2 where the process of break-up has the highest relative contribution during high shear rates compared to other processes. The resuspension of SPM as a source of potentially aggregable material may cause a deviation from typically in the open ocean found power law distributions (pers. communication with G.A. Jackson). Remarkably, Hill (1998) summarized controls on floc size in the oceans and found disagreements between the proposed theoretical relationships between fragmentation and the turbulent energy dissipation rate ϵ and experimental results. Based on theoretical studies by Adler (1979) and on field studies by Hill et al. (1998), he suggested a limitation of floc size mainly due to the stress that aggregates experience owing to sinking. Hill (1998) argued that this might be the case as long as ϵ falls below a critcal value that seems to be apparently high compared to typical oceanic conditions.

In Sec. 3.1 it has been shown that the DB model for flocculation processes due to shear is applicable to describe the average size and, prone to discrepancies, also the distribution. In Sec. 3.2, the flocculation model has been adapted and extended to examine biological influences on aggregate and sediment properties in the backbarrier basin of Spiekeroog island. Within the extension of the model, especially the change of the $\langle r \rangle$ by aggregation due to differential settling had to be developed. While the rectilinear and curvilinear aggregation kernels for differential settling are known and used in SCB models, a differential equation for the change of the average size by this process has not been established before (to the authors knowledge). In addition to the above dicussed assumption and approximation, a further one has been used

to come up with a general equation for the change of $\langle r \rangle$ by aggregation due to differential settling. The direct integration with a kernel for differential settling depending on the fractal dimension of the aggregates was not possible. Therefore, an analytically incorrect way has been chosen to nevertheless derive a general equation for aggregation due to differential settling applicable to any realistically occuring fractal dimension. First, a solution has been derived by using the classical Stokes equation for the settling velocity, using the parameter of floc density instead of using a size dependent density (as dependent on fractal theory). Second, the mean floc density has been calculated which was then introduced in the derived equation. A comprehensive direct comparison of the finally derived differential equation for the change of $\langle r \rangle$ by differential settling with a SCB model is outstanding. Nevertheless, notice that for $\lim_{d_f \to 3}$, the relation becomes completely valid within the limits of the discussed assumptions for shear-induced aggregation.

The order of closure and the mass-conservation violating step before integration have an impact on the derived d_f-dependent functions K_γ and K_v (see App. A.3 and A.4, refer also the discussion for shear-induced aggregation above for K_γ). By using α to compensate such uncertainties in the model derivation, this might lead to an introduction of a new parameter in the way that α becomes $\alpha \cdot \alpha'$. α' would be a correction factor to ensure the correct relative contribution of the two processes (aggregation due to shear and differential settling) to each other. Such discrepancies between the orders of the moment closures might also have influenced the unexpected high relative contribution of aggregation due to differential settling to the change of the $\langle r \rangle$ in Sec. 3.2. However, as already argued in Sec. 3.2, experimental results obtained by Lick et al. (1993) can be discussed, as especially aggregation due to differential settling strongly depends on a distribution of particles with different settling velocities. Thus, it is most likely that the growth rates observed by Lick et al. (1993) based on laboratory experiments underpredict the growth rates due to differential settling in natural waters. They initially used homogeneous-sized particles which results in very small collision frequencies (see also App. A.2 for a visual impression of the collision frequency, given by the aggregation kernels). Future experimental and numerical studies with particle-based algorithms with naturally observed distributions might help to further enlighten this question.

In Chap. 4 the distribution-based flocculation model has been included into the 1D vertical SiAM hydrodynamic model. The discussion on the SiAM model itself is out of the scope of this thesis, but it was used successfully in earlier applications (Le Hir et al., 2001). The distribution-based model shows good agreement with results of the SCB model, but still needs a validation with experimental or field data. It has been already discussed in Sec. 4.3.1. By implementing also the aggregation due to differential settling and testing against an also extended SCB model, the model could be improved and directed towards more realistic scenarios.

Differences between the two model approaches (the DB and the SCB model) that can be accounted for the discrepancies between the parameter sets of α and f_b have been earlier discussed in this section .

Although the DB model is already computationally efficent, further simplification could be assumed. Small deviations between $\langle v_\mathrm{s} \rangle$ and $v_\mathrm{s}(\langle r \rangle)$ can be found for the most relevant range of fractal dimensions in coastal waters (where $d_f \approx 2$, Dyer and Manning, 1999, refer also to Eq. (2.67) and Fig. 2.5 on page 54 and 55, respectively, where it is shown that for $d_f = 2$ the $\langle v_\mathrm{s} \rangle = v_\mathrm{s}(\langle r \rangle)$, as the appearing factor for $\langle v_\mathrm{s} \rangle$ equals one). Therefore, the lengthy calculation for the mean sinking velocity could be reduced by loosing generality which might be acceptable in many study applications.

In its present form, the results of the DB model in 1D have been used to get a qualitative impression, how SPM dynamics can influence DOM fluxes into the water column. Due to the model's underlying distribution, a simple functional dependency on the mean radius of the particles can be found (refer to Eq. (4.36) on page 146). This is at least true for the DOM flux dependence on the shear rate, while for the settling dependence, a numerical integration has been carried out to keep consistence with the applied functional form for the mean relative uptake capabilities. In a SCB model, such a derivation of DOM fluxes would be much more computationally expensive as each size class would have to be calculated seperately. In the perspective of a coupling with ecosystem models, this would be disadvantegeous. However, as can be seen in Fig. 4.13, the used Sherwood number for shear has an offset compared to the other Sherwood numbers for shear. In this qualitative study it has been used

in consistency with a study of Logan and Hunt (1987), also to calculate the mean relative uptake capabilities according to their approach. Such an offset might be critical for quantitative DOM flux calculations. Another uncertainty originates from the applicability of the Sherwood numbers. They are all developed for a certain Péclet and Reynolds number regime (refer to Tab. 4.2 on page 151) and coastal particles can reach (and sometimes exceed) the upper limit of applicability. However, a comparison between recent numerical simulations by Kiørboe et al. (2001) and the in this study used Sherwood number for sinking (see Fig. 4.14 on page 146) suggests that the upper limits of applicability might be underestimated or at least very conservative for analytically derived formulations. Nonetheless, it is a question of future research to derive formulations for Sherwood numbers also under circumstances, where inertia starts to play a role (when particle $Re \geq 1$).

In order to study the relative uptake capability of particle-associated bacteria in coastal waters qualitatively, the approach of Logan and Hunt (1987) has been extended via a relationship between the fractal dimension of aggregates and their porosity and permeability. It has been shown, however, by Li and Logan (2001) that the used relationship results in a conservative estimate, as the size of intra-floc pores are likely to be correlated with cluster sizes of primary particles. The advantage of microbes might therefore be underestimated. However, De La Rocha and Passow (2007) stated that gel-like particles like TEP can clogg-up pore spaces. It is therefore questionable, which formulation for the permeability should be used. Another rather intricate assumption is the association of bacteria with particles. It is here assumed that the number of microbes attached to the particles correlates with their volume. When comparing this assumption with measurements of Kiørboe (2003), it turned out to be rather weak. In his measurements, the bacterial cell counts on aggregates were independent of the particle size. Such distribution is however questionable at least for small aggregates. Further experimental studies are therefore needed to enlighten this question.

5.3 Conclusion

Within this thesis, a novel distribution-based (DB) model for aggregation – fragmentation processes has been proposed. In contrast to many other models, it is based on the dynamics of the total cohesive SPM fraction and its related average size of the constituent aggregates. Moreover, an underlying size distribution has been considered as well as the fractal properties of aggregates. Although the underlying structual assumptions of the model may limit its general applicability as discussed in the previous section, it has been successfully used in a variety of studies as summarized and concluded in the following.

The novel distribution-based model for shear-induced aggregation and fragmentation has been compared to a traditional size class-based (SCB) model, and both to experimentally derived laboratory data. The models were well able to simulate the observed evolution of the mean aggregate size. While both models have shown remarkably similiar evolution of the particle size distribution, they were prone to differences compared to the experimentally observed distribution. Resulting from the model comparison, the DB model is well suited to capture the general size dynamics of SPM while being computationally effective.

The DB model for flocculation has been further applied to the backbarrier basin of Spiekeroog island by coupling it to other processes like aggregation due to differential settling, erosion, deposition and tidal exchange processes. Still in 0D, the model has been successfully used to support the hypothesis of biologically influenced cohesive sediment transport processes in this area. This was especially possible due to its computational efficiency that allowed for an extensive parameter variation. The model was successfully used to simulate a typical winter and summer situation to gain insights into seasonal parameter shifts that reflect biological influences on SPM transport. In particular, it revealed a decreased stickiness and break-up factor in summer, of which the first was counterintuitive, while the latter can be explained by a stabilization of flocs by fresh organic components produced by primary producers. Moreover, a reduced fractal dimension of aggregates in summer compared to winter was found that can be related to exudation of EPS by phytoplankton and -benthos

during spring and summer months leading to looser bound flocs. Phytobenthos is likely to account for the stabilization of the sediment that was reflected by an increased critical bottom shear stress resistence and a larger size of eroded aggregates in summer time. This application of the model revealed the usefulness of an integrated description of SPM dynamics to study mutual feedbacks of biogeochemical and sedimentary processes.

As cohesive sediment transport is a spatial process, first steps were achieved to couple the flocculation model to a 1D vertical hydrodynamic model. A novelty here is the consideration of the distribution in the transport of particles in order to better predict vertical fluxes in future applications of the model. A comparsion with a SCB model that served as a correspondence and validation cornerstone has been carried out. An intricate coupling between the tidally and lunarly changing hydrodynamic forcing, the evolution of the spatial concentration and size distribution has been found. First, during high shear periods, much sediment is resuspended into the water column and a strong aggregation sets in after the shear rate peaked during the turn of the tides. This leads to high deposition fluxes. During lunarly low shear periods, the amount of suspended sediment decreased significantly and thus the mean size of aggregates did due to lower collision probabilities. Therefore, even in the present state of development, the DB model was well able to qualitatively reproduce typically observed spatially and temporally variable SPM concentration and size dynamics in tidally forced coastal waters.

Based on these promising results, the influence of turbulent shear and SPM concentration and size dynamics on the DOM flux from or towards particles has been investigated. While being qualitative in its validity, the potential DOM release rates from aggregates into the water column suggests a potentially significant role of aggregates in the DOM variability on a tidal time scale. This is especially likely when reconsidering the importance of marine snow in the open ocean for microbes in its vicinity as calculated by Kiørboe and Jackson (2001).

Going further beyond purely physical applications of the DB model, mean relative uptake capabilities of aggregate-associated bacteria has been revisited under changing hydrodynamical conditions. Based on an extension of the

principal concept of Logan and Hunt (1987), an intra-tidally, -lunarly and spatially variable mean relative uptake capability on aggregates has been found to occur likely throughout a lunar cycle. However, as can be infered from the relations for intra-floc flow velocities, the quantitative effect strongly depends on the moelcular diffusivity of the substance in question, the fractal dimension, and the mean size of aggregates. Depending on these factors, being associated to aggregates can be either advantageous or disadvantageous for a microbial population in terms of substrate fluxes to the attached cells. This is only the case when neglecting obvious advantages for bacteria due to available POM on the particles.

The last two qualitative studies based on the DB model went far beyond pure sediment transport processes. Obviously, they show the great potential for applications of the novel distribution-based flocculation model in the investiation of coupled physical-biogeochemical systems on the edge between SPM transport and ecological functioning. This is in particular possible due to the inclusion of an underlying aggregate size distribution that is often helpful to regenerate additional relevant variables needed in ecosystem models, such as light climate, POM and DOM fluxes and others. Moreover, especially the novelty of a strongly decoupled treatment of the average size of aggregates, their related distribution and the total concentration of cohesive sediment enables the model to be easily coupled to other – biological, chemical and/or physical – processes, accompanied by minor computational costs than by size class-based models.

Chapter 6

Outlook & Future research perspectives

Recent modeling work of Krivtsov et al. (2008) has included the effects of SPM transport on a complex ecosystem model. The SPM dynamics were used as forcing for the ERSEM model. Infered from findings in Sec. 3.2 and feedback loops reviewed in Sec. 1.2.4, however, it is likely that biological processes have, at least on a seasonal time scale, an influence on SPM dynamics. It is therefore necessary to step forward in the dynamic coupling of sediment transport and biogeochemical models to get a better understanding of the intricate way in which biogeochemical interact with physical processes.

As concluded in the previous chapter, the here presented novel distribution-based flocculation model could be a proper tool to bridge the gap between sediment transport and ecosystem models. The DB models' process-based description of flocculation processes in combination with a computationally effective formulation gives a favorable starting point for various further appli-actions.

A first consequent step is its coupling to 3D sediment transport models in order to better represent cohesive sediment dynamics also in spatially heterogeneous environments. Going beyond sediment dynamics, the turbidity and thus chading of algae could be derived based on the particle distribution to represent the variable light climate in coupled sediment transport and primary production models. For example, Tian et al. (2009) have shown that

SPM dynamics are a potential control factor for the onset of a spring bloom in the German Bight. Such examples show the necessity to aim for variable, process-based descriptions of the light climate depending on SPM dynamics.

Another application could be the investigation of the coupling between POM transport, its remineralization, DOM generation and the microbial interaction with and reaction on changing hydrodynamical and biological conditions. Sintes et al. (2010) found a seasonality in DOM concentrations off the Dutch coast, but a relatively stable activity of particle-associated bacteria while the total number of bacteria (free-living and particle-associated) also showed a high variability partly associated with Chl *a* concentrations. Investigating the role of particle-associated bacteria in hydrodynamically high dynamic areas might help to better understand fluxes of nutrients on different time scales.

ADCP are widely used to gain insights into velocity profiles, but also sediment dynamics. However, the differentiation between the signal for turbulence and cohesive flocs is especially critical under high turbulent conditions like during extreme events. The flocculation model could be a proper tool to extrapolate the floc evolution during extreme events in order to result in better algorithms for the analyses of ADCP data. This might enable researchers to distinguish between signals from on the one hand turbulence and on the other hand sediment particles.

Ample evidence exists that bi- and more-modal particle distributions occur in coastal and estuarine systems. A derivation of a distribution-based model for such more-modal distributions would be therefore helpful for the representation of this phenomenon in models for corresponding areas.

Further model extensions can be assumed. Parameters like the fractal dimension (or alternatively the floc density) are weakly constrained by experimental observations. However, many studies have shown that different processes result in different fractal dimensions. This also depends on the particle composition. When thinking about sediment transport and ecosystem coupling, an integration of *i)* primary particles of different origin and *ii)* a variable fractal dimension into SPM flocculation models is therefore worth to aspire. Accepting this, it is necessary to gain for a better understanding

of influences of EPS/TEP production by microbes and algae on flocculation processes.

Understanding the intricate interaction between biological and physical processes that determine the morphology, packing, composition of aggregates, and their affinity for microbes, but also trace chemicals is still a research task with many pitfalls. For example, most of the recent flocculation models apply fractal theory to describe the floc structure. However, little is known about repacking processes, the influence of component properties on them and thus the changing structure of aggregates. Moreover, only few is known about the role of aggregate-associated microorganisms on this issue. They are mainly acknowledged to degrade on aggregates and use them as a micro-habitat. But, as discussed by Azam and Malfatti (2007), the structuring activity of microoranisms onto their environment is still an open field of research. Their role in aggregation processes, the interaction with turbulence-induced features of their environment like microscale patchiness of nutrients should further be addressed in future experimental and modelling studies. *In situ* 3D visualization of particles in combination with staining techniques for microorganisms and organic components under changing hydrodynamical conditions might be considered to enlighten hydrodynamic-microbial-POM/sediment interactions.

Appendix A

Supplementary material

A.1 Change of the average size due to erosion and deposition in 0D

A.1.1 Deposition

The deposition flux has been formulated in Sec. 2.5.1 as

$$F_{\mathrm{dep}} = \dot{C} = \frac{C\,\langle v_{\mathrm{s}}\rangle}{h} \quad . \tag{A.1}$$

For a concentration C_i in a specific size class i, this reads

$$F_{\mathrm{dep,i}} = \dot{C}_i = \frac{C_i\, v_{\mathrm{s}}(r_i)}{h} \quad . \tag{A.2}$$

By introducing these formulation in Eq. (2.12)

$$\frac{\mathrm{d}}{\mathrm{d}\,t}\langle r\rangle = \sum_i r_i \frac{\dot{C}_i\,\Delta R_i}{C} - \frac{\dot{C}}{C}\sum_i r_i \frac{C_i\,\Delta R_i}{C} \quad , \tag{A.3}$$

gives

$$\begin{aligned}\frac{\mathrm{d}}{\mathrm{d}\,t}\langle r\rangle &= \sum_i r_i \frac{\frac{C_i\, v_{\mathrm{s}}(r_i)}{h}\,\Delta R_i}{C} - \frac{\frac{C\,\langle v_{\mathrm{s}}\rangle}{h}}{C}\sum_i r_i \frac{C_i\,\Delta R_i}{C} \\ &= \frac{1}{h\,C}\sum_i r_i\, C_i\, v_{\mathrm{s}}(r_i)\,\Delta R_i - \frac{\langle v_{\mathrm{s}}\rangle\,\langle r\rangle}{h} \quad .\end{aligned} \tag{A.4}$$

By using the same assumptions as in Sec. 4.1.3, this term can be expressed as

$$\frac{\mathrm{d}}{\mathrm{d}\,t}\langle r\rangle = \frac{1}{h\,C}\int_0^\infty r\,C(r)\,v_{\mathrm{s}}(r)\,\mathrm{d}r - \frac{\langle v_{\mathrm{s}}\rangle\,\langle r\rangle}{h} \quad . \tag{A.5}$$

By using $C(r) = n(r)\,w(r)$ according to Eq. (2.25), and Eq. (2.67) for $\langle v_{\mathrm{s}}\rangle$, it results in

$$\boxed{\left.\frac{\mathrm{d}}{\mathrm{d}\,t}\langle r\rangle\right|_{\mathrm{dep}} = \frac{F\,\langle r\rangle^{d_f}}{h}\,\frac{2^{2\,d_f-1}\,\Gamma(d_f+1)}{d_f\,\sqrt{\pi}}\cdot\frac{d_f-1}{(d_f+1)^{d_f}}} \tag{A.6}$$

with $F = 2^{d_f-1}\,(\rho_{\mathrm{p}}-\rho)\,g\,D_{\mathrm{p}}^{3-d_f}\,/\,(18\,\mu)$.

A.1.2 Erosion / Resuspension

Equivalent to the formulation for deposition, the general relation of Eq. (2.12) can be used to derive a functional dependency for the change of the average radius due to erosion / resuspension. Resuspension as formulated by Partheniades (1984, see also Sec. 2.5.2)

$$F_{\mathrm{res}} = \dot{C} = \frac{M_0}{h}\left(\frac{\tau}{\tau_{\mathrm{c}}} - 1\right) \quad , \tag{A.7}$$

can be re-written in the form

$$F_{\mathrm{res,i}} = \dot{C}_i = \frac{M_{0,i}}{h}\left(\frac{\tau}{\tau_{\mathrm{c}}} - 1\right) \quad , \tag{A.8}$$

under the assumption that the critical bottom shear stress is the same for each cohesive sediment size class. Therefore, the change of the average radius can be written as

$$\begin{aligned} \frac{\mathrm{d}}{\mathrm{d}\,t}\langle r\rangle &= \sum_i r_i \frac{\frac{M_{0,i}}{h}\left(\frac{\tau}{\tau_{\mathrm{c}}} - 1\right)\Delta R_i}{C} - \frac{\frac{M_0}{h}\left(\frac{\tau}{\tau_{\mathrm{c}}} - 1\right)}{C}\langle r\rangle \\ &= \frac{1}{C\,h}\left(\frac{\tau}{\tau_{\mathrm{c}}} - 1\right)\sum_i r_i\, M_{0,i}\,\Delta R_i - \frac{M_0}{C\,h}\left(\frac{\tau}{\tau_{\mathrm{c}}} - 1\right)\langle r\rangle \quad . \end{aligned} \tag{A.9}$$

By introducing the relationship

$$r_{\mathrm{b}} = \frac{1}{M_0}\sum r_i\, M_{0,i}\,\Delta R_i \tag{A.10}$$

for the average radius of resuspended particles, one can write

$$\begin{aligned} \frac{\mathrm{d}}{\mathrm{d}\,t}\langle r\rangle &= \frac{1}{C\,h}\left(\frac{\tau}{\tau_{\mathrm{c}}} - 1\right)\frac{M_0}{M_0}\sum_i r_i\, M_{0,i}\,\Delta R_i - \frac{M_0}{C\,h}\left(\frac{\tau}{\tau_{\mathrm{c}}} - 1\right)\langle r\rangle \\ &= \frac{M_0}{C\,h}\left(\frac{\tau}{\tau_{\mathrm{c}}} - 1\right) r_{\mathrm{b}} - \frac{M_0}{C\,h}\left(\frac{\tau}{\tau_{\mathrm{c}}} - 1\right)\langle r\rangle \quad . \end{aligned} \tag{A.11}$$

Thus, the change of the average radius is given by

$$\boxed{\left.\frac{\mathrm{d}}{\mathrm{d}\,t}\langle r\rangle\right|_{\mathrm{res}} = \frac{M_0}{C\,h}\left(\frac{\tau}{\tau_{\mathrm{c}}} - 1\right)\left(r_{\mathrm{b}} - \langle r\rangle\right) \quad .} \tag{A.12}$$

A.2 Rectilinear aggregation kernels for shear and differential settling

For the rectilinear kernel for aggregation due to differential settling

$$I_v(r, r') \;=\; \pi\,(r + r')^2\,|v_\mathrm{s}(r) - v_\mathrm{s}(r')| \quad , \tag{A.13}$$

(where the fractal scaling for the density of flocs is used), see Fig. A.1.

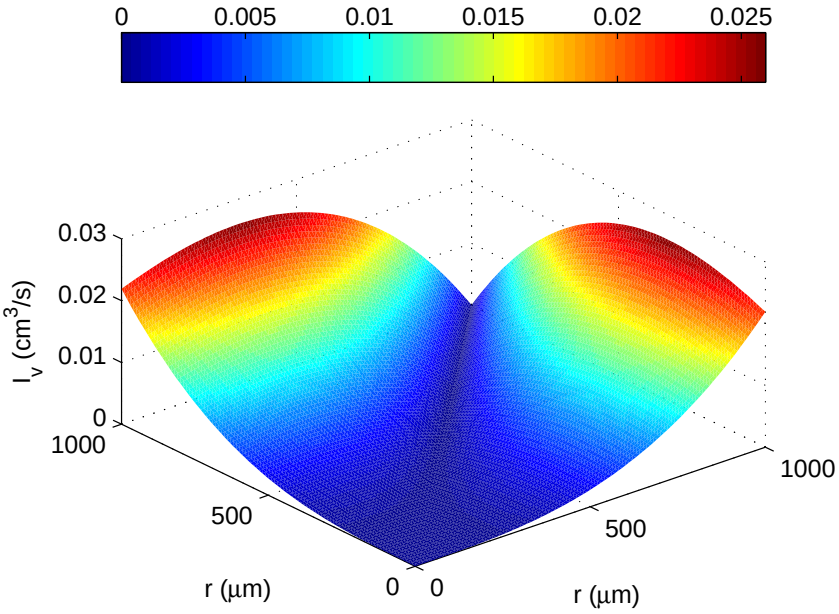

Figure A.1: The rectilinear kernel for aggregation due to differential settling $\rho_\mathrm{p} = 2.6\,\mathrm{g\,cm^{-3}}$, $\rho = 1.0\,\mathrm{g\,cm^{-3}}$, $\mu = 0.01\,\mathrm{g\,cm^{-1}\,s^{-1}}$ $D_\mathrm{p} = 4\,\mu\mathrm{m}$, $d_f = 2$.

For the rectilinear kernel for aggregation due to shear

$$I_\gamma(r, r') \;=\; 1.3\,\gamma\,(r + r')^3 \tag{A.14}$$

see Fig. A.2.

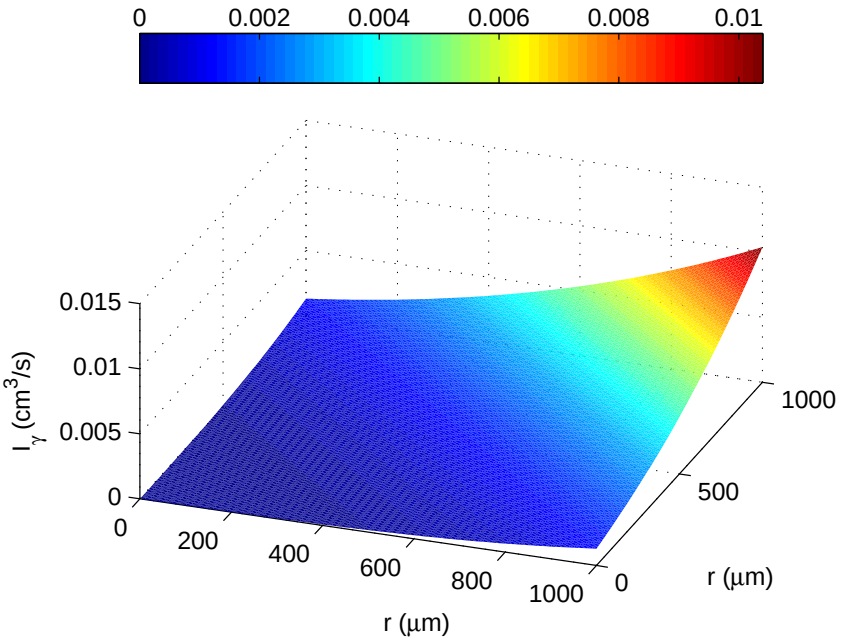

Figure A.2: The rectilinear kernel for aggregation due to shear $\gamma = 1$.

A.3 Aggregation due to shear: the K_γ function

In principle, the Smoluchowski equation

$$\begin{aligned}\frac{\mathrm{d}}{\mathrm{d}\,t}\,n(m) &= \frac{1}{2}\,\alpha \int_0^m n(m')\,n(m-m')\,I(d(m'),d(m-m'))\,\mathrm{d}m' \\ &\quad - \alpha\,n(m) \int_0^{m_\infty} n(m')\,I(d(m),d(m'))\,\mathrm{d}m' \end{aligned} \tag{A.15}$$

is identically to

$$\begin{aligned}\frac{\mathrm{d}}{\mathrm{d}\,t}\,n(m) &= \alpha \int_0^{\frac{m}{2}} n(m')\,n(m-m')\,I(d(m'),d(m-m'))\,\mathrm{d}m' \\ &\quad - \alpha\,n(m) \int_0^{m_\infty} n(m')\,I(d(m),d(m'))\,\mathrm{d}m' \quad . \end{aligned} \tag{A.16}$$

However, the elaborations used in Sec. 2.4 to derive an analytical model for aggregation cause a non-equality of the resulting equations for the change of the average radius.

The transition from m to r to derive the relative growth rate $\hat{\mu}(r)$ in Eq. (2.22) violates the equality. In detail,

$$\begin{aligned}&\overbrace{\frac{\alpha}{2\,n(r)} \int_0^r n(r')\,n(r-r')\,I(r',r-r')\,\mathrm{d}r' - \alpha \int_0^{r_\infty} n(r')\,I(r,r')\,\mathrm{d}r'}^{\text{v2}} \\ \neq\ &\underbrace{\frac{\alpha}{n(r)} \int_0^{\frac{r}{2}} n(r')\,n(r-r')\,I(r',r-r')\,\mathrm{d}r' - \alpha \int_0^{r_\infty} n(r')\,I(r,r')\,\mathrm{d}r'}_{\text{v1}} \quad . \end{aligned} \tag{A.17}$$

In the following the left hand side of the non-equality sign is called version 1 (v1) and the right hand side is called version 2 (v2). The resulting equations for the change of the average radius (derived by analogy with Sec. 2.4) will be compared in the following. More precisely, the resulting K_γ functions will be closer examinated.

Further on, a higher oder closure, here in particular a fourth order closure (cmp. Eq. (2.38)) can be used to derive a formulation for aggregation.

$$\begin{aligned}\langle\hat{\mu}(\langle r\rangle)\rangle &= \hat{\mu}(\langle r\rangle) + \frac{1}{2}\,\delta r^2\,\frac{\partial^2}{\partial\, r^2}\,\hat{\mu}(\langle r\rangle) \\ &\quad + \frac{1}{6}\,\delta r^3\,\frac{\partial^3}{\partial\, r^3}\,\hat{\mu}(\langle r\rangle) + \underbrace{y'\,\delta r^4}_{y_\gamma}\,\frac{\partial^4}{\partial\, r^4}\,\hat{\mu}(\langle r\rangle) \;=\; 0 \quad , \end{aligned} \tag{A.18}$$

where $\delta r^3 = 2\langle r\rangle^3/(d_f+1)^2$ and δr^4 are the third and fourth moments of the distribution, respectively.

The change of the average radius can be calculated by applying the different versions of $\hat{\mu}(r)$ – v1 and v2, the rectilinear or curvilinear kernel for aggregation due to shear, and the second or fourth order moment closure. Nevertheless, the general form for aggregation due to shear (Eq. (2.46))

$$\left.\frac{\mathrm{d}}{\mathrm{d}\,t}\,\langle r\rangle\right|_{\mathrm{agg}\gamma} \;=\; \alpha\,\gamma\,K_\gamma(d_f)\,\frac{C}{w_0}\,\langle r\rangle^{4-d_f} \tag{A.19}$$

always maintains, but the function $K_\gamma(d_f)$ changes. For the $K_\gamma(d_f)$ functions in dependence on their origin see Tab. A.1 and for a better comparison Fig. A.3–A.5.

In the case of the rectilinear approach in combination with v2, the K_γ function shows an asymptotic behavior around $d_f = 1.5$, which is not realistic as it would mean an infinitive increase in size due to aggregation. Beside this, it is obvious that the fourth order closure approaches lead to higher changing rates of the average radius than the second order closures for the respective kernels. A higher moment closure reflects more information, in particular of the skewness of the distribution, and thus larger aggregates gain more importance in the aggregation process leading to higher changing rates of the $\langle r\rangle$, and explaining the difference between the orders of closure.

The derived $K_\gamma(d_f)$ functions can be approximated for simplification. Such approximation are shown in Fig. A.6 and A.7.

Table A.1: The different $K_\gamma(d_f)$ functions in dependence on the order of closure, the used kernel for shear-induced aggregation and the initial approach of derivation. Note that $d' = d_f + 1$.

RECTILINEAR KERNEL

2nd order closure		4th order closure	
v1	v2	v1	v2
$\frac{10\,d'^{d'}\,(2\,d'^3+3\,d'^2-3\,d'-2)}{d'^4\,\Gamma(d')}$	$\frac{0.65\,d'^{d_f-1}\,(2\,d_f^4+3\,d_f^3-3\,d_f^2+17\,d_f+57)}{(d_f^2+d_f-1)\,\Gamma(d_f+2)}$	$\frac{d'^{d'}}{\Gamma(d')}\left(\frac{2.6}{d'}+\frac{4.8}{d'^2}-\frac{3.8}{d'^3}-\frac{6}{d'^4}\right)$	$\frac{1.95\,d'^{d'}\,(5\,d_f^3+28\,d_f^2+45\,d_f+18)}{d'^4\Gamma(d')}$

CURVILINEAR KERNEL

2nd order closure		4th order closure	
v1	v2	v1	v2
$\frac{20\,d'^{d'}}{d'^4\,\Gamma(d')}\left(\sum_{i=0}^{3} a_i\,d'^i+\frac{\sum_{i=2}^{6} b_i\,d'^i}{-8\,d'-12\,d'^2+12\,d'^3}\right)$	$\frac{5\,d'^{d_f-2}\,(\sum_{i=0}^{5} c_i\,d_f^i)}{(3\,d_f^2-7)\,\Gamma(d_f+2)}$	$\frac{10\,d'^{d'}\,(2\,d'^3+3\,d'^2-3\,d'-2)}{d'^4\,\Gamma(d')}$	$\frac{10\,d'^{d'}\,(14\,d_f^3+75\,d_f^2+115\,d_f+48)}{3\,d'^4\,\Gamma(d')}$

$a_0 = -1$, $a_1 = -2$, $a_2 = -1.5$, $a_3 = 1$
$b_2 = -12$, $b_3 = 12$, $b_4 = 18$, $b_5 = 15$, $b_6 = -6$
$c_0 = 112$, $c_1 = 155$, $c_2 = 48$, $c_3 = -14$, $c_4 = 0$, $c_5 = 3$

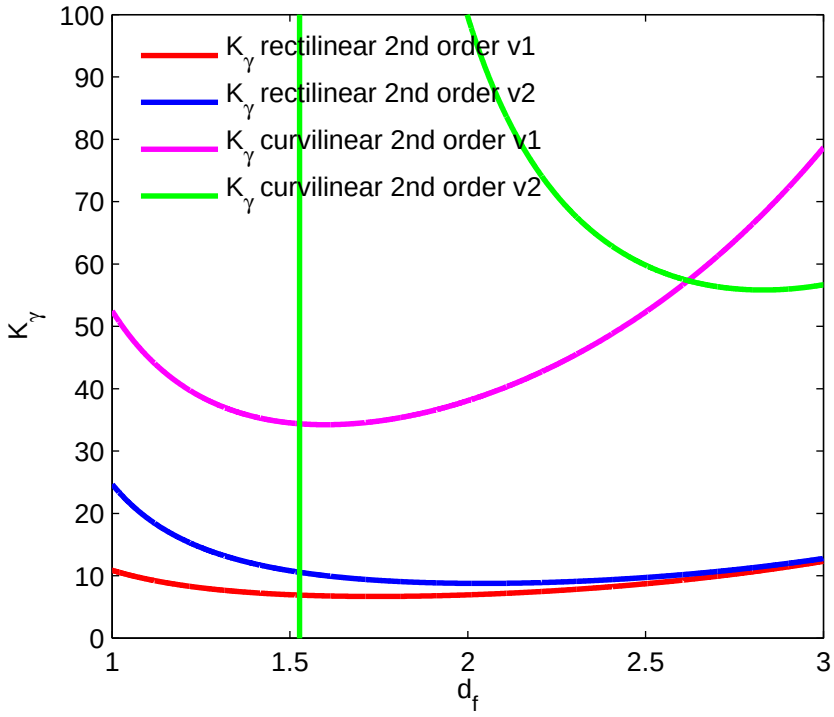

Figure A.3: A comparison of the K_γ functions for *i)* the rectilinear and the curvilinear kernel, and *ii)* for the two different possibilities to start the model derivation violating the mass conservation in the first step of integration.

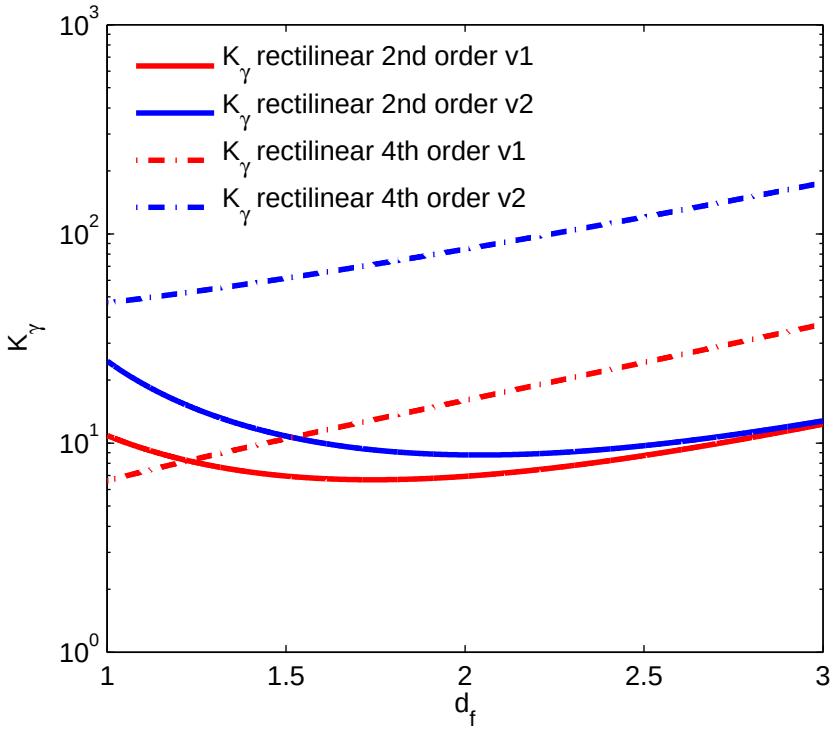

Figure A.4: A comparison of the K_γ funtions of *i)* the rectilinear kernel under different orders of closures, and *ii)* the different versions.

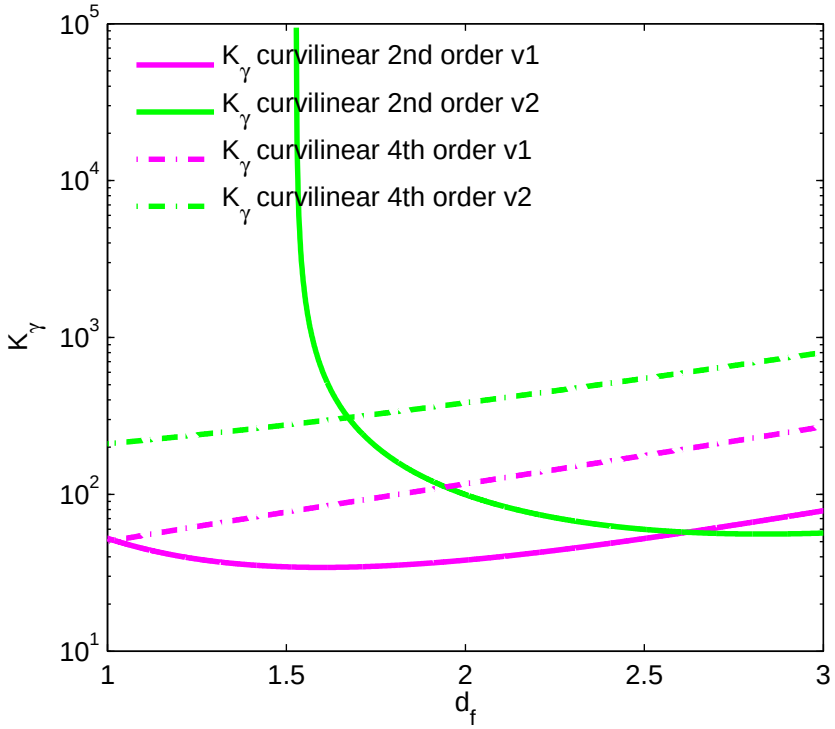

Figure A.5: A comparison of the K_γ funtions of *i)* the curvilinear kernel under different orders of closures, and *ii)* the different versions.

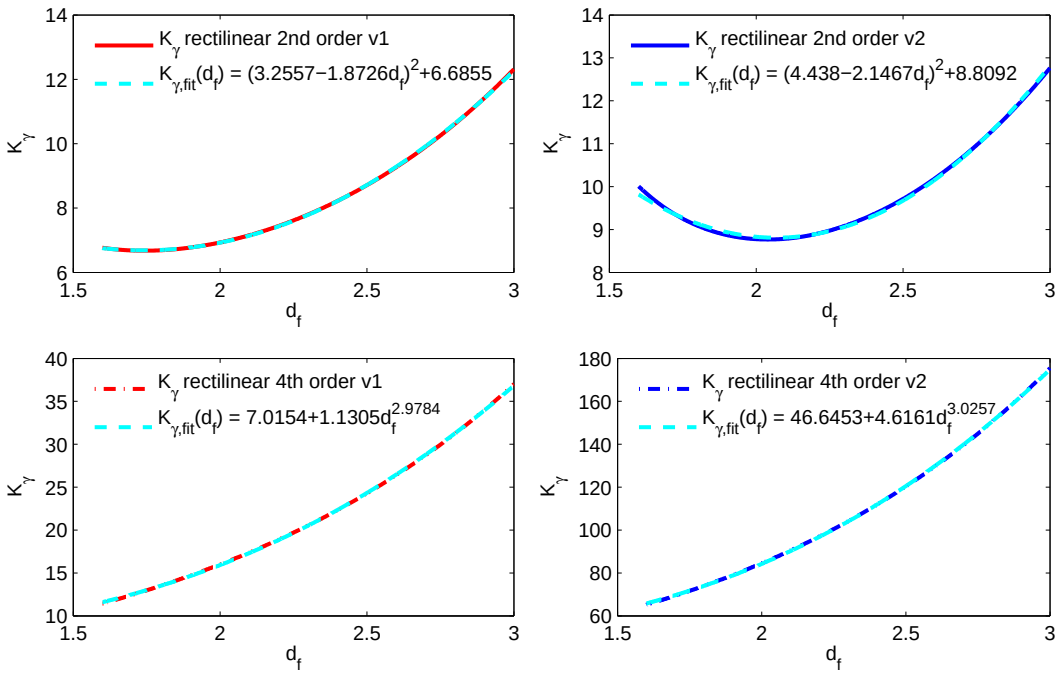

Figure A.6: The different K_γ functions for rectilinear aggregation due to shear and their possible approximation.

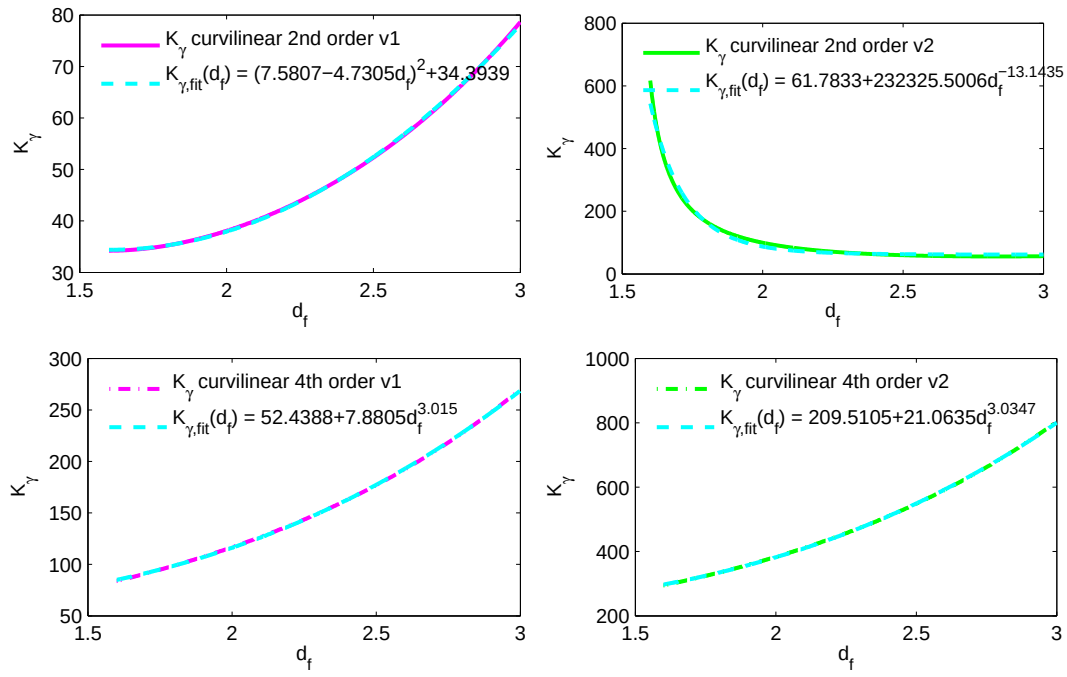

Figure A.7: The different K_γ functions for curvilinear aggregation due to shear and their possible approximation.

A.4 Aggregation due to differential settling: the K_v function

In analogy with aggregation due to shear, two different versions for the aggregation due to differential settling can be calculated. As it is not possible to calculate the change of the $\langle r \rangle$ on basis of a 2nd order closure (as the relative growth rate at the $\langle r \rangle$ would be negative leading to a negative change of the $\langle r \rangle$, which is in dis-agreement with the process of aggregation), only the $K_\mathrm{v}(d_f)$ functions derived on basis of the 4th order closure are summarized in Tab. A.2 and shown in Fig. A.8.

An asymptotic behavior appears for the K_v function by using v2 (see Sec. A.3) for the derivation. Again, this is not realistic as an infinitive growth of the $\langle r \rangle$ would be the result.

Table A.2: The different $K_\mathrm{v}(d_f)$ functions in dependence on the initial approach of derivation. Note that $d' = d_f + 1$

CURVILINEAR KERNEL **4th order closure**	
v1	$\frac{2\,d'^{d'}}{9\,\Gamma(d')}\left(\frac{\exp(-2\,d')\sum_{i=0}^{4} a_i\,d'^i+\exp(-d')\sum_{i=0}^{7} b_i\,d'^i+(-90\,d'^4-90\,d'^3+342\,d'^2-324\,d'-108)}{12\,d'^4\,(\exp(-d')\,(2\,d'^3-22\,d'^2+56\,d'-24)-15\,d'+12}\right)$
v2	$\frac{(d_f+1)^{d_f-2}}{216\,\Gamma(d_f+2)}\left(\frac{\sum_{i=0}^{4} c_i\,d_f^i+\exp(-d_f-1)\sum_{i=0}^{7} e_i\,d_f^i+\exp(-2\,d_f-2)\sum_{i=0}^{4} f_i\,d_f^i}{-45\,d_f+51+\exp(-d_f-1)\,(96+144\,d_f-128\,d_f^2+16\,d_f^3)}\right)$

$a_0 = 768$, $a_1 = 480$, $a_2 = 896$, $a_3 = -160$, $a_4 = 96$
$b_0 = -168$, $b_1 = 1488$, $b_2 = 2412$, $b_3 = 672$, $b_4 = 750$, $b_5 = -237$, $b_6 = -9$, $b_7 = 3$
$c_0 = -24615$, $c_1 = -12465$, $c_2 = 6174$, $c_3 = 675$, $c_4 = -405$
$e_0 = -34236$, $e_1 = -137496$, $e_2 = -74376$, $e_3 = 40164$, $e_4 = 10020$, $e_5 = -3216$, $e_6 = -96$, $e_7 = 36$
$f_0 = -21504$, $f_1 = -75776$, $f_2 = -25600$, $f_3 = 7168$, $f_4 = 3072$

In all the cases of aggregation due to differential settling the change of the $\langle r \rangle$ has been calculated by treating the density of the aggregates as shown in Sec. 2.4. Remarkably, for v1, it is also possible to derive e. g. for $d_f = 2$ an

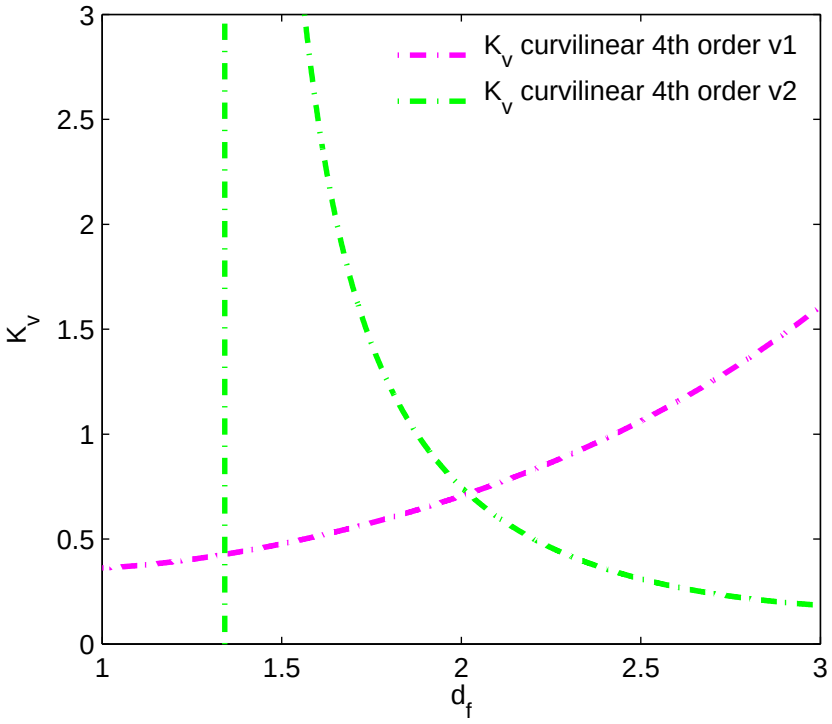

Figure A.8: A comparison of the K_v funtions of the curvilinear kernel for aggregation due to differential settling for the different versions.

analytically correct form by introducing the settling velocity for fractal aggregates (Eq. (2.52)) into the curvilinear kernel for aggregation due to differential settling (by the loss of generality for the change of the $\langle r \rangle$ for different fractal dimensions)

$$\frac{\mathrm{d}}{\mathrm{d}\,t}\langle r\rangle = 0.55\,\alpha\,\frac{C}{\mu\,w_0}\,\pi\,(\rho_\mathrm{p}-\rho)\,g\,D_\mathrm{p}\,\langle r\rangle^2 \quad \text{(only valid for } \mathrm{d_f}=2\text{)} \quad . \tag{A.20}$$

It appears that the deviation from the incorrectly derived general form of the change of the $\langle r \rangle$ by aggregation due to differential settling

$$\frac{\mathrm{d}}{\mathrm{d}\,t}\langle r\rangle = \alpha\,K_\mathrm{v}(d_f)\,\frac{C}{\mu\,w_0}\,\pi\,(\langle\rho_\mathrm{f}\rangle-\rho)\,g\,\langle r\rangle^{5-d_f} \tag{A.21}$$

is insignificant (see Fig. A.9) and vanishes for $d_f = 3$, which is obvious from

the mean floc density

$$\langle \rho_\mathrm{f} \rangle = \frac{\frac{1}{8}\,(d_f+1)^{3-d_f}\,D_\mathrm{p}^{3-d_f}\,2^{d_f}\,\Gamma(2\,d_f-2)\,(\rho_\mathrm{p}-\rho)}{\langle r \rangle^{3-d_f}\,\Gamma(d_f+1)} + \rho \quad . \tag{A.22}$$

It becomes ρ_p in the case of $d_f = 3$ and thus the settling velocity of fractal aggregates reduces to the Stokes settling velocity of particles with density ρ_p.

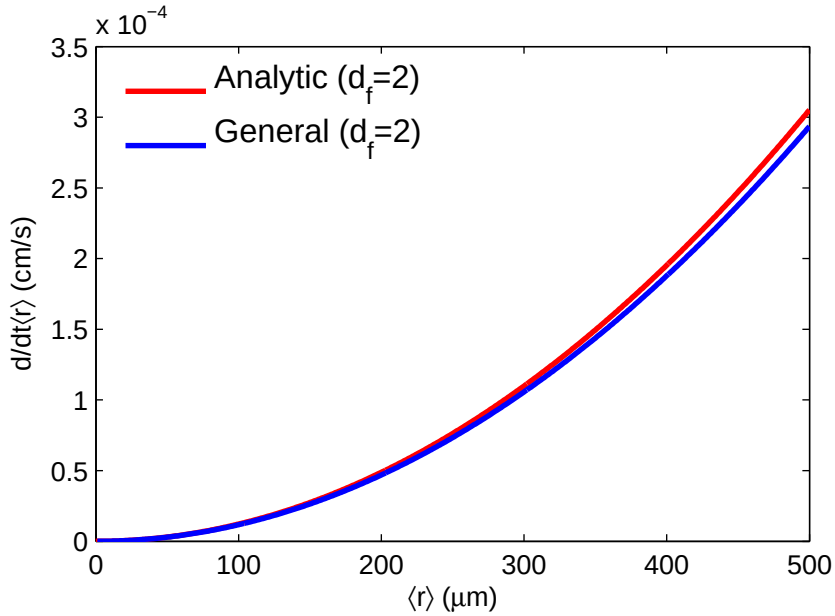

Figure A.9: A comparison of the analytically correct derived change (Eq. (A.20)) of the $\langle r \rangle$ due to differential settling and the general form (Eq. (A.21)), both based on v1, the curvilinear kernel and a 4th order closure, for $d_f = 2$. The (typical) parameter values are: $D_\mathrm{p} = 4\,\mu\mathrm{m}$, $\alpha = 0.05$, $g = 9.81\,\mathrm{m\,s^{-2}}$, $\rho = 1\,\mathrm{g\,cm^{-3}}$, $\rho_\mathrm{p} = 2.6\,\mathrm{g\,cm^{-3}}$, $C = 50\,\mathrm{mg\,L^{-1}}$ and $\mu = 0.0102\,\mathrm{cm^2\,s^{-1}}$

The derived $K_\mathrm{v}(d_f)$ functions can be approximated for simplification. Such approximation are shown in Fig. A.10.

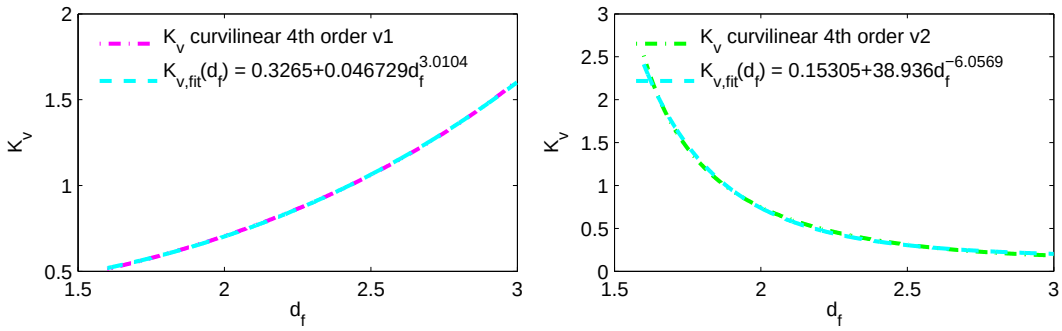

Figure A.10: The different K_γ functions for curvilinear aggregation due to differential sinking and their possible approximation.

A.5 Numerical implementation of the DB model in the SiAM model

The grid structure for the SiAM 1DV is given in Fig. A.11.

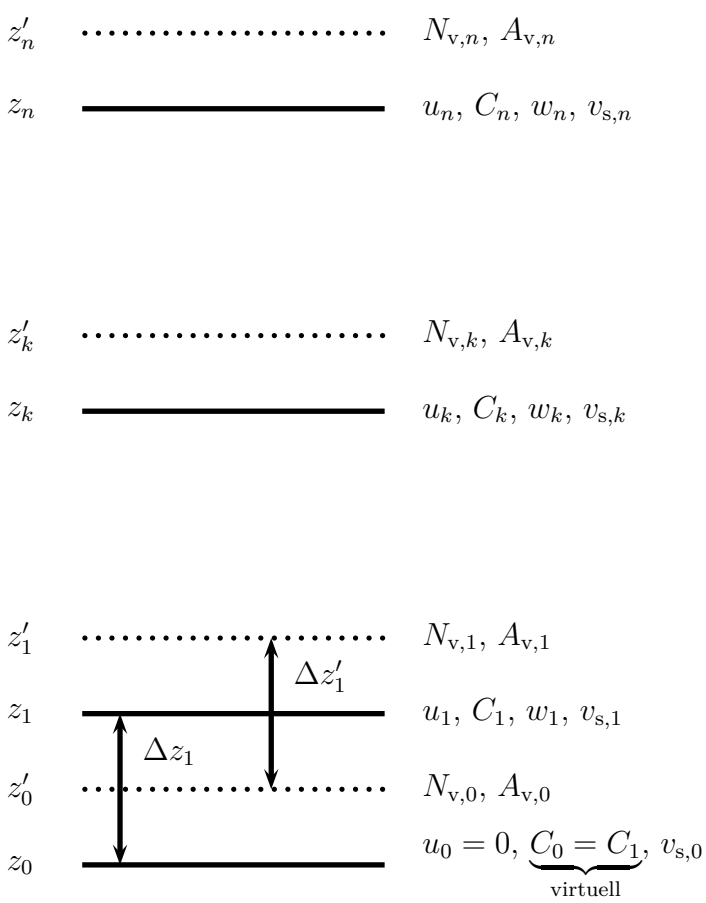

Figure A.11: Grid in the SiAM 1D vertical model.

In order to derive the equations for the transport of the $\langle r \rangle$, one starts from the general definition of the average radius of a concentration distribution

$$\langle r \rangle = \sum_i r_i \frac{C'_i \, \Delta R_i}{C} \quad . \tag{A.23}$$

The time derivative for the $\langle r \rangle$ can easily be accessed

$$\frac{\mathrm{d}}{\mathrm{d}\,t}\langle r\rangle \;=\; \frac{1}{C}\sum_i r_i\,\dot{C}_i'\,\Delta R_i - \frac{\dot{C}}{C}\,\langle r\rangle \quad , \tag{A.24}$$

where $\dot{C}_i$ and $\dot{C}$ are the time derivatives of the concentration in a size class of bin width ΔR_i and of the total concentration, respectively. For these time derivatives, the processes written in Eq. (4.3), page 121, can be inserted. All the following derivations for the numerical schemes to treat the transport of the $\langle r \rangle$ are dependent on the schemes that are used for the concentration. Therefore, the following is rather for the understanding of their derivation.

A.5.1 Turbulent diffusion

For the turbulent diffusion, this reads

$$\left.\frac{\mathrm{d}}{\mathrm{d}\,t}\langle r\rangle\right|_{\mathrm{D}} \;=\; \frac{1}{C}\sum_i r_i \frac{1}{h^2}\,\partial_\sigma\left(A_\mathrm{v}\,\partial_\sigma C_i\right)\,\Delta R_i - \frac{\frac{1}{h^2}\,\partial_\sigma\left(A_\mathrm{v}\,\partial_\sigma C\right)}{C}\langle r\rangle \quad . \tag{A.25}$$

To solve this equation numerically, we moved from the analytical to the numerical scheme of the turbulent diffusion

$$\left.\frac{\Delta C_k}{\Delta t}\right|_{\mathrm{D}} \;=\; \frac{1}{h^2\,\Delta z_k'}\left(A_{\mathrm{v},k}\,\frac{C_{k+1}^t - C_k^t}{\Delta z_{k+1}} - A_{\mathrm{v},k-1}\,\frac{C_k^t - C_{k-1}^t}{\Delta z_k}\right) \quad , \tag{A.26}$$

where Δt is the time step, Δz_k and $\Delta z_k'$ are the vertical resolution for the layers of cell k, the one for the distance between the points for the C_k^t coordinates and the other for the points, where the $A_{\mathrm{v},k}$ are solved, respectively.

Insertion of Eq. (A.26) in Eq. (A.25) yields after some long, but straightforward calculations for the term of turbulent diffusion

$$\begin{aligned}\left.\frac{\Delta\langle r\rangle_k}{\Delta t}\right|_{\mathrm{D}} \;=\; \frac{1}{h^2\,C_k^t\,\Delta z_k'}\Bigg(&A_{\mathrm{v},k}\,\frac{C_{k+1}^t}{\Delta z_{k+1}}\left(\langle r\rangle_{k+1}^t - \langle r\rangle_k^t\right)\\ &+ A_{\mathrm{v},k-1}\,\frac{C_{k-1}^t}{\Delta z_k}\left(\langle r\rangle_{k-1}^t - \langle r\rangle_k^t\right)\Bigg)\end{aligned} \tag{A.27}$$

A.5.2 Sinking

Again we start with Eq. (A.24) and introduce the change of the concentration

$$\left.\frac{\mathrm{d}}{\mathrm{d}\,t}\langle r\rangle\right|_{\mathrm{v_s}} = \frac{1}{C}\sum_i r_i\,\frac{1}{h}\,\partial_\sigma\left(v_{\mathrm{s},i}\,C_i'\right)\,\Delta R_i - \frac{\frac{1}{h}\,\partial_\sigma\left(\langle v_\mathrm{s}\rangle\,C\right)}{C}\,\langle r\rangle \quad , \tag{A.28}$$

where $v_{\mathrm{s},i}$ is the settling velocity of a particle of radius r_i which is given by Eq. (2.52), page 49. By using the numerical scheme for the transport of the concentration

$$\left.\frac{\Delta C_k}{\Delta t}\right|_{\mathrm{v_s}} = \frac{v_{\mathrm{s},k}}{h\,\Delta z_k'}\left(\theta\,C_{k+1}^t + (1-\theta)\,C_k^t\right) - \frac{v_{\mathrm{s},k-1}}{h\,\Delta z_k'}\left(\theta\,C_k^t + (1-\theta)\,C_{k-1}^t\right) \quad , \tag{A.29}$$

where θ is a weighting factor for the settling term, and inserting it into Eq. (A.28) one can easily solve the second part of the right hand side of Eq. (A.28). It is more difficult to yield a solution for the first part of the right hand side, as the distribution of the concentration is needed to solve the sum. For this reason, and to account for the distributional contribution to the change of the $\langle r\rangle$, we use the underlying assumption of the aggregation model that the concentration distribution follows the form

$$C(r) = N_0\,\exp(-\beta\,r)\,w_0\,r^{d_f} \quad , \tag{A.30}$$

where N_0 is the value, where the number distribution crosses the y-axis, and $\beta = (d_f+1)/\langle r\rangle$ is the slope of the number distribution that can easily be calculated from the concentration distribution. To proceed with the formulation of the settling term, one can express N_0 after integration of Eq. (A.30), which results in the total concentration C, as

$$N_0 = \frac{C\,(d_f+1)^{d_f+1}}{w_0\,\langle r\rangle^{d_f+1}\,\Gamma(d_f+1)} \quad . \tag{A.31}$$

Now, one can use the relations of Eq. (A.30) and (A.31) in the first part of the right hand side of Eq. (A.28) after insertion of Eq. (A.29) and moving from the sum to an integral description. After some intricate steps of calculation, one

yields for the change of the $\langle r \rangle$

$$\begin{aligned}\left.\frac{\Delta\langle r\rangle_k}{\Delta t}\right|_{\mathrm{vs}} &= \frac{1}{h\,C_k^t\,\Delta z_k'}\,\frac{4^{d_f}\,F'\,\Gamma(d_f+\frac{1}{2})}{\sqrt{\pi}\,(d_f+1)^{d_f}}\cdot\Big(\theta\,C_{k+1}^t\,\left(\langle r\rangle_{k+1}^t\right)^{d_f} \\ &\quad + (1-2\,\theta)\,C_k^t\,\left(\langle r\rangle_k^t\right)^{d_f} - (1-\theta)\,C_{k-1}^t\,\left(\langle r\rangle_{k-1}^t\right)^{d_f}\Big) \\ &\quad - \frac{\langle v_{\mathrm{s}}\rangle_k^t\,\langle r\rangle_k^t}{h\,C_k^t\,\Delta z_k'}\left(\theta\,C_{k+1}^t + (1-\theta)\,C_k^t\right) \\ &\quad + \frac{\langle v_{\mathrm{s}}\rangle_{k-1}^t\,\langle r\rangle_k^t}{h\,C_k^t\,\Delta z_k'}\left(\theta\,C_k^t + (1-\theta)\,C_{k-1}^t\right) \quad , \end{aligned} \tag{A.32}$$

where

$$F' = \frac{2^{d_f-1}}{18\,\mu}\,(\rho_{\mathrm{p}}-\rho)\,g\,D_{\mathrm{p}}^{3-d_f} \quad . \tag{A.33}$$

A.5.3 Erosion / Resuspension

Following the same way of formulation as the tubulent diffusion and settling term, the change of the $\langle r \rangle$ reads for the erosion / resuspension

$$\left.\frac{\Delta\langle r\rangle_1}{\Delta t}\right|_{\mathrm{res}} = \frac{M_0}{h\,C_1^t\,\Delta z_1'}\left(\frac{\tau}{\tau_{\mathrm{c,e}}}-1\right)\left(r_{\mathrm{b}}-\langle r\rangle_1^t\right) \quad , \tag{A.34}$$

where r_{b} is the mean radius of the eroded aggregates.

A.5.4 Deposition

For the deposition, the gradient dynamic approach of Wirtz and Eckhardt (1996) is used. The deposition flux for the C is given by

$$F_{\mathrm{dep},i} = -\max\left(0, 1-\frac{\tau}{\tau_{\mathrm{c,v}}+\epsilon_{\mathrm{v}}}\right)\frac{\tau_{\mathrm{c,v}}}{\tau_{\mathrm{c,v}}+\epsilon_{\mathrm{v}}}\,\frac{1}{h\,\Delta z_1'}\,v_{\mathrm{s}}(r_i)\,C_i \tag{A.35}$$

in the SiAM model. One can devide it by the C_i to yield the relative growth rate $\hat{\mu}$, which can be used in the general approach of Wirtz and Eckhardt (1996)

$$\frac{\mathrm{d}}{\mathrm{d}\,t}\langle r\rangle = \delta r^2\,\frac{\mathrm{d}}{\mathrm{d}\,r}\,\hat{\mu}(\langle r\rangle) \tag{A.36}$$

to yield with $\delta r^2 = \langle r \rangle^2/(d_f+1)$ the change of the $\langle r \rangle$ due to deposition

$$\left.\frac{\Delta\langle r\rangle_1}{\Delta t}\right|_{\mathrm{dep}} = -\frac{d_f-1}{d_f+1}\,\max\left(0, 1-\frac{\tau}{\tau_{\mathrm{c,v}}+\epsilon_{\mathrm{v}}}\right)\,\frac{\tau_{\mathrm{c,v}}}{\tau_{\mathrm{c,v}}+\epsilon_{\mathrm{v}}}\,\frac{1}{h\,\Delta z_1'}\,\left(\langle r\rangle_1^t\right)^{d_f}\quad . \tag{A.37}$$

A.5.5 Representation of vertical transport for the change of the average radius

Following the approach introduced in Chap. 4, the respective change of the $\langle r \rangle$ due to the vertical transport of the concentration

$$\left.\frac{\mathrm{d}\,C}{\mathrm{d}\,t}\right|_w = \frac{w}{h}\,\frac{\partial\,C}{\partial\,\sigma}\quad , \tag{A.38}$$

where w is the vertical velocity component, can be given by

$$\left.\frac{\mathrm{d}}{\mathrm{d}\,t}\,\langle r\rangle\right|_w = \frac{1}{C}\,\int_0^\infty r\,\frac{w}{h}\,\frac{\partial\,C(r)}{\partial\,\sigma}\,\mathrm{d}r - \frac{w\,\langle r\rangle}{C\,h}\frac{\partial\,C}{\partial\,\sigma} \tag{A.39}$$

resulting in

$$\boxed{\left.\frac{\mathrm{d}}{\mathrm{d}\,t}\,\langle r\rangle\right|_w = \frac{w}{C\,h}\,\frac{\partial}{\partial\,\sigma}\,(C\,\langle r\rangle) - w\,\frac{\langle r\rangle}{C\,h}\,\frac{\partial}{\partial\,\sigma}\,C\quad .} \tag{A.40}$$

Bibliography

Ackleh, A. S., Hallam, T. G., Muller-Landau, H. C., 1995. Estimation of sticking and contact efficiencies in aggregation of phytoplankton: The 1993 SIGMA tank experiment. Deep Sea Research Part II 42 (1), 185 – 201.

Adler, P. M., 1979. A study of disaggregation effects in sedimentation. AlChE Journal 25 (3), 487 – 493.

Adler, P. M., 1981. Streamlines in and around porous particles. Journal of Colloid and Interface Science 81 (2), 531 – 535.

Agrawal, Y. C., Pottsmith, H. C., 2000. Instruments for particle size and settling velocity observations in sediment transport. Marine Geology 168, 89 – 114.

Alldredge, A. L., 2000. Interstitial dissolved organic carbon (doc) concentrations within sinking marine aggregates and their potential contribution to carbon flux. Limnology and Oceanography 45 (6), 1245 – 1253.

Alldredge, A. L., Gotschalk, C. C., 1988. In situ settling behavior of marine snow. Limnology and Oceanography 33 (3), 339 – 351.

Alldredge, A. L., Granata, T. C., Gotschalk, C. C., Dickey, T. D., 1990. The physical strength of marine snow and its implications for particle disaggregation in the ocean. Limnology and Oceanography 35 (7), 1415 – 1428.

Alldredge, A. L., Passow, U., Logan, B. E., 1993. The abundance and significance of a class of large, transparent organic particles in the ocean. Deep Sea Research Part I 40, 1131 – 1140.

Armstrong, R. A., Lee, C., Hedges, J. I., Honjo, S., Wakeham, S. G., 2002. A new, mechanistic model for organic carbon fluxes in the ocean based on the quantitative association of POC with ballast minerals. Deep Sea Research Part II 49, 219 – 236.

Ayala, O., Rosa, B., Wang, L.-P., 2008a. Effects of turbulence on the geometric collision rate of sedimenting droplets. Part 2. Theory and parameterization. New Journal of Physics 10.

Ayala, O., Rosa, B., Wang, L.-P., Grabowski, W. W., 2008b. Effects of turbulence on the geometric collision rate of sedimenting droplets. Part 1. Results from direct numerical simulation. New Journal of Physics 10.

Ayukai, T., Wolanski, E., 1997. Importance of biologically mediated removal of fine sediments from the Fly River plume, Papua New Guinea. Estuarine, Coastal and Shelf Science 44, 629 – 639.

Azam, F., Long, R. A., 2001. Sea snow microcosms. Nature 414, 495 – 498.

Azam, F., Malfatti, F., 2007. Microbial structuring of marine ecosystems. Nature 5, 782 – 791.

Azam, F., Smith, D. C., 1991. Particle analysis in Oceanography. Springer Verlag, Berlin, pp. 213 – 235.

Azetsu-Scott, K., Niven, S. E. H., 2005. The role of transparent exopolymer particles (TEP) in the transport of ^{234}Th in coastal water during a spring bloom. Continental Shelf Research 25, 1133 – 1141.

Azetsu-Scott, K., Passow, U., 2004. Ascending marine particles: significance of transparent exopolymer particles (TEP) in the upper ocean. Limnology and Oceanography 49, 741 – 748.

Badewien, T. H., Zimmer, E., Bartholomä, A., Reuter, R., 2009. Towards continuous long-term measurements of suspended particulate matter (SPM) in turbid coastal waters. Ocean Dynamics 59 (2), 227 – 238.

Bartholomä, A., 1999. Umweltatlas Wattenmeer - Bd. 2 Wattenmeer zwischen Elb- und Emsmündung. Nationalparkverwaltung Niedersächsisches Wattenmeer; Umweltbundesamt, Stuttgart (Hohenheim) Eugen Ulmer Verlag, Ch. Zur historischen und künftigen Entwicklung der Morphologie des Ostfriesischen Wattenmeers, pp. 18 – 19.

Bartholomä, A., Kubicki, A., Badewien, T. H., Flemming, B. W., 2009. Suspended sediment transport in the German Wadden Sea – seasonal variations and extreme events. Ocean Dynamics 59 (2), 213 – 225.

Batchelor, G., 1952. Small-scale variation of convected quantities like temperature in turbulent fluid. Journal of Fluid Mechanics 5, 113 – 133.

Batchelor, G., 1980. Mass transfer from small particles suspended in turbulent fluid. Journal of Fluid Mechanics 98 (3), 609 – 623.

Benson, T., French, J. R., 2007. InSiPID: A new low-cost instrument for in situ particle size measurements in estuarine and coastal waters. Journal of Sea Research 58 (3), 167 – 188.

Bergstedt, M. S., Hondzo, M. M., Cotner, J. B., 2004. Effects of small scale fluid motion on bacterial growth and respiration. Freshwater Biology 49, 28 – 40.

Bhaskar, P. V., Bhosle, N. B., 2005. Microbial extracellular polymeric substances in marine biogeochemical processes. Current Science 88 (1), 45 – 53.

Biddanda, B. A., 1985. Microbial synthesis of macroparticulate matter. Marine Ecology Progress Series 20, 241 – 251.

Billiones, R. G., Tackx, M. L., Daro, M. H., 1999. The geometric features, shape factors and fractal dimensions of suspended particulate matter in the Scheldt estuary (Belgium). Estuarine, Coastal and Shelf Science 48, 293 – 305.

Black, K. S., Tolhurst, T. J., Paterson, D. M., Hagerthy, S. E., 2002. Working with natural cohesive sediments. Journal of Hydraulic Engineering 128 (1), 2 – 8.

Boyd, P. W., Stevens, C. L., 2002. Modelling particle transformations and the downward organic carbon flux in the NE Atlantic Ocean. Progress in Oceanography 52, 1 – 29.

Buessler, K. O., 1998. The decoupling of production and particulate export in the surface ocean. Global Geochemical Cycles 12 (2), 297 – 310.

Bungartz, H., Wanner, S., 2004. Significance of particle interaction to the modelling of cohesive sediment transport in rivers. Hydrological Processes 18, 1685 – 1702.

Burchard, H., 2002. Applied Turbulence Modelling in Marine Waters. Springer.

Burchard, H., Bolding, K., Villarreal, M. R., 2004. Three-dimensional modelling of estuarine turbidity maxima in a tidal estuary. Ocean Dynamics 54, 250 – 265.

Burd, A., Jackson, G. A., 1997. Predicting particle coagulation and sedimentation rates for a pulsed input. Journal of Geophysical Research 102 (C5), 10545 – 10561.

Burd, A. B., Hansell, D. A., Steinberg, D. K., Anderson, T. R., Arístegui, J., Baltar, F., Beaupré, S. R., Buesseler, K. O., DeHairs, F., Jackson, G. A., Kadko, D. C., Koppelmann, R., Lampitt, R. S., Nagata, T., Reinthaler, T., Robinson, C., Robinson, B. H., Tamburini, C., Tanaka, T., 2010. Assessing the apparent imbalance between geochemical and biochemical indicators of meso- and bathypelagic biological activity: What the @$#! is wrong with present calculations of carbon budgets? Deep-Sea Research II 57, 1557 – 1571.

Canelli, E., Fuhs, G. W., 1976. Effect of the sinking rate of two diatoms (*Thalassiosira* sp.) on uptake from low concentrations of phoshate. Journal of Phycology 12, 93 – 99.

Chang, T. S., Bartholomä, A., Flemming, B., 2006a. Seasonal dynamics of fine-grained sediments in a back-barrier tidal basin of the German Wadden Sea (southern North Sea). Journal of Coastal Research 22 (2), 328 – 338.

Chang, T. S., Joerdel, O., Flemming, B., Bartholomä, A., 2006b. The role of particle aggregation/disaggregation in muddy sediment dynamics and seasonal sediment turnover in a back-barrier tidal basin, East Frisian Wadden Sea, southern North Sea. Marine Geology 235, 49 – 61.

Chen, M. S., Wartel, S., Temmerman, S., 2005. Seasonal variation of floc characteristics on tidal flats, the Scheldt estuary. Hydrobiologia 540, 181 – 195.

Chen, S., Eisma, D., 1995. Fractal geometry of *in situ* flocs in the estuarine and coastal environments. Netherlands Journal of Sea Research 32 (2), 173 – 182.

Chen, S., Eisma, D., Kalf, J., 1994. *In situ* size distribution of suspended matter during the tidal cycle in the Elbe Estuary. Netherlands Journal of Sea Research 32, 37 – 48.

Chin, W., Orellana, M. V., Verdugo, P., 1998. Spontaneous assembly of marine dissolved organic matter into polymer gels. Nature 391, 568 – 572.

Claquin, P., Probert, I., Lefebvre, S., Veron, B., 2008. Effects of temperature on photosynthetic parameters and TEP production in eight species of marine microalgae. Aquatic Microbial Ecology 51, 1 – 11.

Colijn, J., Cadée, G. C., 2003. Is light or nitrogen limiting phytoplankton growth in the Wadden Sea? Journal Sea Research 49, 83 – 93.

Dam, H., Drapeau, D., 1995. Coagulation efficiency, organic-matter glues and the dynamics of particles during a phytoplankton bloom in a mesocosm study. Deep Sea Research Part II 42 (1), 111 – 123.

Davoudi, J., Schumacher, J., 2006. Stretching of polymers around the Kolmogorov scale in a turbulent shear flow. Physics of Fluids 18, 10.1063/1.2168187.

de Boer, G. J., Merckelbach, L., Winterwerp, J., 2007. A parameterised consolidation model for cohesive sediments. Estuarine and Coastal Fine Sediment Dynamics, 243 – 262.

de Brouwer, J. F. C., Stal, L. J., 2001. Short-term dynamics in microphytobenthos distribution and associated extracellular carbohydrates in surface sediments of an intertidal mudflat. Marine Ecology Progress Series 218, 33 – 44.

de Jonge, V. N., 2000. Importance of temporal and spatial scales in applying biological and physical process knowledge in coastal management, and example for the Ems estuary. Continental Shelf Research 20, 1655 – 1686.

De La Rocha, C. L., Passow, U., 2007. Factors influencing the sinking of POC and the efficiency of the biological pump. Deep Sea Research Part II 54, 639 – 658.

Decho, A. W., 1990. Microbial exopolymer secretions in oceanic environments: Their role(s) in food web and marine processes. Oceanography and Marine Biology Annual Review 28, 73 – 153.

Decho, A. W., 2000. Microbial biofilms in intertidal systems: an overview. Continental Shelf Research 20, 1257 – 1273.

Dellwig, O., Beck, M., Lemke, A., Lunau, M., Kolditz, K., Schnetger, B., Brumsack, H.-J., 2007. Non-conservative behaviour of molybdenum in coastal waters: Coupling geochemical, biological, and sedimentological processes. Geochimica et Cosmochimica Acta 71, 2745 – 2761.

Deuser, W. G., Brewer, P. G., Jickells, T. D., Commeau, R. F., 1983. Biological control of the removal of abiotic particles from the surface ocean. Science 219, 388 – 391.

Dilling, L., Alldredge, A. A., 2000. Fragmentation of marine snow by swimming macrozooplankton: A new process impacting carbon cycling in the sea. Deep Sea Research Part I 47, 1227 – 1245.

Dyer, K., Manning, A., 1999. Observation of size, settling velocity and effective density of flocs, and their fractal dimensions. Journal of Sea Research 41, 87 – 95.

Eisma, D., Bernard, P., Cadée, G. C., Ittekot, V., Kalf, J., Laane, R., Martin, J. M., Mook, W. G., van Put, A., Schuhmacher, T., 1991a. Suspended-matter particle size in some west-european estuaries; Part II: A review on floc-formation and break-up. Netherlands Journal of Sea Research 28 (3), 215 – 220.

Eisma, D., Bernard, P., Cadée, G. C., Ittekot, V., Laane, R., Martin, J. M., Mook, W. G., Van Put, A., Schuhmacher, T., 1991b. Suspended-matter particle size in some west-european estuaries; Part I: Particle-size distribution. Netherlands Journal of Sea Research 28 (3), 193 – 214.

Fasham, M. J. R., Ducklow, H. W., McKelvie, S. M., 1990. A nitrogen-based model of plankton dynamics in the oceanic mixed layer. Journal of Marine Research 34, 591 – 639.

Fenchel, T., 2002. Microbial behavior in a heterogeneous world. Science 296, 1068 – 1071.

Fettweis, M., 2008. Uncertainty of excess density and settling velocity of mud flocs derived from in situ measurements. Estuarine, Coastal and Shelf Science 78 (2), 426 – 436.

Field, C. B., Behrenfeld, K. J., Randerson, J. T., Falkowski, P., 1998. Primary production of the biosphere: integrating terrestrial and oceanic components. Science 281, 237 – 240.

Flesch, J. C., Spicer, P. T., Pratsinis, S., 1999. Laminar and turbulent shear-induced flocculation of fractal aggregates. AlChE 45 (5), 1114 – 1124.

Flory, E. N., Hill, P. S., Milligan, T. G., Grant, J., 2004. The relationship between floc area and backscatter during a spring phytoplankton bloom. Deep Sea Research Part I 51, 213 – 223.

Frankel, A. N., Acrivos, A., 1968. Heat and mass transfer from small spheres and cylinders freely suspended in shear flow. Physics of Fluids 11, 1913 – 1918.

Friedlander, S., 1957. Mass and heat transfer to single spheres and cylinders at low Reynolds numbers. American Institute of Chemical Engineers Journal 3, 43 – 48.

Fugate, D. C., Friedrichs, C. T., 2002. Determining concentration and fall velocity of estuarine particle populations using ADV, OBS and LISST. Continental Shelf Research 22, 1867 – 1886.

Fugate, D. C., Friedrichs, C. T., 2003. Controls on suspended aggregate size in partially mixed estuaries. Estuarine, Coastal Shelf Science 58, 389 – 404.

Fukuda, H., Koike, I., 2004. Microbial stimulation of the aggregation process between submicron-sized particles and suspended particles in coastal waters. Aquatic Microbial Ecology 37, 63 – 73.

Gemein, N., Stanev, E., Brink-Spalinck, G., Wolff, J., Reuter, R., 2006. Patterns of suspended matter in the East Frisian Wadden Sea: comparison of numerical simulations with MERIS observations. EARSeL eProceedings 5, 180 – 198.

Goldthwait, S. A., Carlson, C. A., Henderson, G. K., Alldredge, A. L., 2005. Effects of physical fragmentation on remineralization of marine snow. Marine Ecology Progress Series 305, 59 – 65.

Goutx, M., Wakeham, S., Lee, C., Duflos, M., Guigue, C., Liu, Z., Moriceau, B., Sempere, R., Tedetti, M., Xue, J., 2007. Composition and degradation of marine particles with different settling velocities in the Northwestern Mediterranean sea. Limnology and Oceanography 39 (4), 1645 – 1664.

Graham, W. M., MacIntyre, S., Alldredge, A. L., 2000. Diel variations of marine snow concentration in surface waters and implications for particle flux in the sea. Deep Sea Research Part I 47, 367 – 395.

Griffith, P., Shiah, F.-K., Gloersen, K., Ducklow, H. W., Fletcher, M., 1994. Activity and distribution of attached bacteria in Chesapeake Bay. Marine Ecology Progress Series 108, 1 – 10.

Grossart, H.-P., Brinkhoff, T., Martens, T., Duerselen, C., 2004a. Tidal dynamics of dissolved and particulate matter and bacteria in a tidal flat ecosystem in spring and fall. Limnology and Oceanography 49 (6), 2212 – 2222.

Grossart, H.-P., Kiørboe, T., Tang, K., Ploug, H., 2004b. Bacterial colonization of particles: Growth and interactions. Applied Environmental Microbiology 69 (6), 3500 – 3509.

Guezennec, L., Lafite, R., Dupont, J.-P., Meyer, R., Boust, D., 1999. Hydrodynamics of suspended particulate matter in the tidal freshwater zone of a macrotidal estuary. Estuaries 22 (3), 717 – 727.

Guo, L., Hung, C.-C., Santschi, P. H., Walsh, I. D., 2002. ^{234}Th scavenging and its relationship to acid polysaccharide abundance in the Gulf of Mexico. Marine Chemistry 78, 103 – 119.

Ha, H., Maa, J. P.-Y., 2009. Evaluation of two conflicting paradigms for cohesive sediment deposition. Marine Geology 265, 120 – 129.

Haidvogel, D. B., Beckmann, A., 1999. Numerical Ocean Circulation Modeling. Vol. 2 of Series Environmental Science and Management. Imperial College Press, 319p.

Hamm, C. E., 2002. Interactive aggregation and sedimentation of diatoms and clay-sized lithogenic material. Limnology and Oceanography 47 (6), 1790 – 1795.

Hansen, J. L. S., Kiørboe, T., Alldredge, A. L., 1996. Marine snow derived from abandoned larvacean houses: sinking rates, particle content and mechanisms of aggregate formation. Marine Ecology Progress Series 141, 205 – 215.

Haslett, S. K., 2000. Coastal systems. Routledge, London, New York.

Hedges, J. I., 1992. Global biogeochemical cycles: progress and problems. Marine Chemistry 39, 67 – 93.

Hedges, J. I., Baldrock, J. A., Gélinas, Y., Lee, C., Peterson, M., Wakeham, S. G., 2001. Evidence for non-selective preservation of organic matter in sinking marine particles. Nature 409, 801 – 804.

Herndl, G., 1988. Ecology of amorphous aggregations (marine snow) in the Northern Adriatic Sea: II. microbial density and activity in marine snow and its implication to overall pelagic processes. Marine Ecology Progress Series 48, 265 – 275.

Herndl, G. J., Peduzzi, P., 1988. Ecology of amorphous aggregations (marine snow) in the Northern Adriatic Sea: I. general considerations. Marine Ecology 9, 79 – 90.

Hill, P. S., 1992. Reconciling aggregation theory with observed vertical fluxes following phytoplankton blooms. Journal of Geophysical Research 97 (2), 2295 – 2308.

Hill, P. S., 1998. Controls on floc size in the sea. Oceanography 11 (2), 13 – 18.

Hill, P. S., Nowell, A. R. M., Jumars, P. A., 1992. Encounter rate by turbulent shear of particles similar in diameter to the Kolmogorov scale. Journal of Marine Research 50, 643 – 668.

Hill, P. S., Syvitski, J. P., Cowan, E. A., Powell, R. D., 1998. In situ observations of floc settling velocities in Glacier Bay, Alaska. Marine Geology 145, 85 – 94.

Hoagland, K. D., Rosowski, J. R., Gretz, M. R., Roemer, S. C., 1993. Diatom extracellular polymeric substances: function, fine structure, chemistry, and physiology. Journal of Phycology 29, 537 – 566.

Hondzo, M., Wüest, A., 2009. Do microscopic organisms feel turbulent flows? Environmental Science and Technology 43, 764 – 768.

Humphries, S., 2009. Filter feeders and plankton increase particle encounter rates through flow regime. Proceedings of the National Academy of Science 106 (19), 7882 – 7887.

Hunt, J. R., 1986. Particle aggregate breakup by fluid shear. In: Mehta, A. J. (Ed.), Estuarine Cohesive Sediment Dynamics. Lecture Notes on Coastal and Estuarine Studies 14.

Jackson, G. A., 1989. Simulation of bacterial attraction and adhesion to falling particles in an aquatic environment. Limnology and Oceanography 34 (3), 514 – 530.

Jackson, G. A., 1990. A model of the formation of marine algal flocs by physical coagulation processes. Deep Sea Research Part A 37 (8), 1197 – 1211.

Jackson, G. A., 1995a. Comparing observed changes in particle size spectra with those predicted using coagulation theory. Deep Sea Research Part II 1, 159 – 184.

Jackson, G. A., 1995b. TEP and coagulation during a mesocosm experiment. Deep Sea Research Part II 42 (1), 215 – 222.

Jackson, G. A., 2001. Effect of coagulation on a model planktonic food web. Deep Sea Research Part I 48, 95 – 123.

Jackson, G. A., Lochmann, S. E., 1993. Environmental Particles. Vol. 2 of Environmental Analytical and Physical Chemistry Series. Lewis Publishers, Boca Raton, Florida, Ch. Modeling coagulation in marine ecosystems, pp. 387 – 414.

Jago, C. F., Jones, S. E., Sykes, P., Rippeth, T., 2006. Temporal variation of suspended particulate matter and turbulence in a high energy, tide-stirred, coastal sea: Relative contributions of resuspension and disaggregation. Continental Shelf Research 26, 2019 – 2028.

Jiang, Q., Logan, B. E., 1991. Fractal dimensions of aggregates determined from steady-state size distributions. Environmental Science and Technology 25, 2031 – 2038.

Joerdel, O., Flemming, B. W., Bartholomä, A., 2004. Flocculation, floc breakup and grain-size composition of suspended sediments in tidal waters of the southern North Sea. In: International Workshop HWK Delmenhorst - From Particle Size to Sediment Dynamics.

Jones, S. E., Jago, C. F., Bale, A. J., Chapman, D., Howland, R. J. M., Jackson, J., 1998. Aggregation and resuspension of suspended particulate

matter at a seasonally stratified site in the southern North Sea: physical and biological controls. Continental Shelf Research 18, 1283 – 1309.

Kahl, L. A., Vardi, A., Schofield, O., 2008. Effects of phytoplankton physiology on export flux. Marine Ecology Progress Series 354, 3 – 19.

Karp-Boss, L., Boss, E., Jumars, P. A., 1996. Nutrient fluxes to planktonic osmotrophs in the presence of fluid motion. Oceanography and Marine Biology: an Annual Review 34, 71 – 107.

Kepkay, P., 1994. Particle aggregation and the biological reactivity of colloids. Marine Ecology Progress Series 109, 293 – 304.

Kilps, J. R., Logan, B. E., Alldredge, A. L., 1994. Fractal dimensions of marine snow determined from image analysis of *in situ* photographs. Deep Sea Research Part I 41 (8), 1159 – 1169.

Kiørboe, T., 2003. Marine snow microbial communities: scaling of abundances with aggregate size. Aquatic Microbial Ecology 33, 67 – 75.

Kiørboe, T., Anderson, K., Dam, H., 1990. Coagulation efficiency and aggregate formation in marine phytoplankton. Marine Biology 107, 235 – 245.

Kiørboe, T., Hansen, J. L., 1993. Phytoplankton aggregate formation: observations of patterns and mechanisms of cell sticking and the significance of exopolymeric material. Journal of Plankton Research 15 (9), 993 – 1018.

Kiørboe, T., Jackson, G. A., 2001. Marine snow, organic solute plumes, and optimal chemosensory behavior of bacteria. Limnology and Oceanography 46 (6), 1309 – 1318.

Kiørboe, T., Lundsgaard, C., Olesen, M., Hansen, J. L., 1994. Aggregation and sedimentation processes during a spring phytoplankton bloom: A field experiment to test coagulation theory. Journal of Marine Research 52, 297 – 323.

Kiørboe, T., Ploug, H., Thygesen, U. H., 2001. Fluid motion and solute distribution around sinking aggregates. I. Small-scale fluxes and heterogeneity of

nutrients in the pelagic environment. Marine Ecology Progress Series 211, 1 – 13.

Klaas, C., Archer, D. E., 2002. Association of sinking organic matter with various types of mineral ballast in the deep sea: Implications for the rain ratio. Global Biogeochemical Cycles 16 (4), 1116, doi:10.1029/2001GB001765.

Kohlmeier, C., Ebenhöh, W., 2007. Modelling the ecosystem dynamics and nutrient cycling of the Spiekeroog back barrier system with a coupled Euler-Lagrange model on the base of ERSEM. Ecological Modelling 202, 297 – 310.

Kranenburg, C., 1994. The fractal structure of cohesive sediment aggregates. Estuarine, Coastal and Shelf Science 39, 451 – 460.

Kriest, I., Evans, G. T., 1999. Representing phytoplankton aggregates in biogeochemical models. Deep Sea Research Part I 46, 1841 – 1859.

Kriest, I., Evans, G. T., 2000. A vertically resolved model for phytoplankton aggregation. Journal of Earth System Science 109 (4), 453 – 469.

Krishnappan, B. G., 1991. Modelling of cohesive sediment transport. In: International Symposium on the transport of suspended sediments and its mathematical modelling.

Krishnappan, B. G., Marsalek, J., 2002. Transport characteristics of fine sediment from an on-stream stormwater management pond. Urban Water 4, 3 – 11.

Krivtsov, V., Howarth, M. J., Jones, S. E., Souza, A. J., Jago, C. F., 2008. Monitoring and modelling of the Irish Sea and Liverpool Bay: An overview and an SPM case study. Ecological Modelling 212, 37 – 52.

Krone, R. B., 1962. Flume studies of the transport of sediment in estuarine shoaling processes. Tech. rep., University of California.

Lanuru, M., 2004. The spatial and temporal patterns of erodibility of an intertidal flat in the East Frisian Wadden Sea, Germany. Ph.D. thesis, Christian-Albrechts-Universität Kiel.

Le Hir, P., Bassoullet, P., Jestin, H., 2001. Application of the continuous modeling concept to simulate high-concentration suspended sediment in a macrotidal estuary. In: Coastal and Estuarine Fine Sediment Processes. Elsevier, pp. 229–247.

Le Hir, P., Monbet, Y., Orvain, F., 2007. Sediment erodability in sediment transport modelling: Can we account for biota effects? Continental Shelf Research 27 (8), 1116 – 1142.

Lee, C., Schwab, D. J., Beletsky, D., Stroud, J., Lesht, B., 2007. Numerical modeling of mixed sediment resuspension, transport, and deposition during the March 1998 episodic events in southern Lake Michigan. Journal of Geophysical Research 112, C02018.

Lee, C., Wakeham, S., Arnosti, C., 2004. Particulate Organic Matter in the Sea: The Composition Conundrum. AMBIO: A Journal of the Human Environment 33 (8), 565 – 575.

Lee, D. G., Bonner, J. S., Garton, Laurie S. Ernest, A. N. S., Autenrieth, R. L., 2002a. Modeling coagulation kinetics incorporating fractal theories: comparison with data. Water Research 36, 1056 – 1066.

Lee, J.-Y., Tett, P., Jones, K., Jones, S., Luyten, P., Smith, C., Wild-Allen, K., 2002b. The PROWQM physical-biological model with benthic-pelagic coupling applied to the northern North Sea. Journal of Sea Research 48, 287 – 331.

Lemke, A., Lunau, M., Stone, J., Dellwig, O., Simon, M., 2009. Spatio-temporal dynamics of suspended matter properties and bacterial communities in the back-barrier tidal flat system of Spiekeroog Island. Ocean Dynamics 59, 277 – 290.

Leppard, G. G., Heissenberger, A., Herndl, G. J., 1996. Ultrastructure of marine snow. I. Transmission electron microscopy methodology. Marine Ecology Progress Series 135, 289 – 298.

Levich, V. G., 1962. Physicochemical Hydrodynamics. Prentice-Hall Inc., Englewood Cliffs, New Jersey, 700p.

Li, X.-Y., Logan, B. E., 2001. Permeability of fractal aggregates. Water Research 35 (14), 3373 – 3380.

Lick, W., Huang, H., Jepsen, R., 1993. Flocculation of fine-grained sediments due to differential settling. Journal of Geophysical Research 98 (C6), 10279 – 10288.

Lick, W., Lick, J., Ziegler, K., 1992. Flocculation and its effect on the vertical transport of fine-grained sediments. Hydrobiologia 235/236, 1 – 16.

Logan, B. E., 1986. Mass transfer models for microorganisms in aggregates and biofilms. Ph.D. thesis, University of California, Berkeley, 305p.

Logan, B. E., 1999. Environmental transport processes. John Wiley & Sons, Inc, New York / Chichester / Weinheim / Brisbane / Singapore / Toronto.

Logan, B. E., Alldredge, A. L., 1989. Potential for increased nurient uptake by flocculating diatoms. Marine Biology 101, 443 – 450.

Logan, B. E., Dettmer, J. W., 1990. Increased mass transfer to microorganisms with fluid motion. Biotechnology and Bioengineering 35, 1135 – 1144.

Logan, B. E., Hunt, J. R., 1987. Advantages to microbes of growth in permeable aggregates in marine systems. Limnology and Oceanography 32 (5), 1034 – 1048.

Logan, B. E., Hunt, J. R., 1988. Bioflocculation as a microbial response to substrate limitations. Biotechnology and Bioengineering 31, 91 – 101.

Logan, B. E., Kilps, J. R., 1995. Fractal dimensions of aggregates formed in different fluid mechanical environments. Water Research 29 (2), 443 – 453.

Logan, B. E., Passow, U., Alldredge, A. L., Grossart, H., Simon, M., 1995. Rapid formation and sedimentation of large aggregates is predictable from coagulation rates (half-lives) of transparent exopolymer particles (TEP). Deep Sea Research Part II 42 (1), 203 – 214.

Longhurst, A., Sathyendranath, S., Platt, T., Caverhill, C., 1995. An estimate of global primary production in the ocean from satellite radiometer data. Journal of Plankton Research 17 (6), 1245 – 1271.

Lumborg, U., Pejrup, M., 2005. Modelling of cohesive sediment transport in a tidal lagoon - an annual budget. Marine Geology 218, 1 – 16.

Luna, E., Domínguez-Zacarias, G., Ferreira, C. P., Velasco-Hernandez, J. X., 2004. Detachment and diffusive-convective transport in an evolving heterogeneous two-dimensional biofilm hybrid model. Physical Review E 70.

Lunau, M., Lemke, A., Dellwig, O., Simon, M., 2006. Physical and biogeochemical controls of microaggregate dynamics in a tidally affected coastal ecosystem. Limnology and Oceanography 51 (2), 847–859.

Lunau, M., Sommer, A., Lemke, A., Grossart, H., Simon, M., 2004. A new sampling device for microaggregates in turbid aquatic systems. Limnology and Oceanography Methods 2, 387 – 397.

Lundkvist, M., Grue, M., Friend, P., Flindt, M. R., 2007. The relative contribution of physical and microbiological factors to cohesive sediment stability. Continental Shelf Research 27, 1143–1152.

Maerz, J., Verney, R., Wirtz, K., Feudel, U., 2010. Modelling flocculation processes: intercomparison of a size class-based model and a distribution-based model. Continental Shelf Research doi:10.1016/j.csr.2010.05.011.

Maerz, J., Wirtz, K., 2009. Resolving physically and biologically driven suspended particulate matter dynamics in a tidal basin with a distribution-based model. Estuarine, Coastal and Shelf Science 84 (1), 128 – 138, doi:10.1016/j.ecss.2009.05.015.

Maggi, F., Mietta, F., Winterwerp, J., 2007. Effect of variable fractal dimension on the floc size distribution of suspended cohesive sediment. Journal of Hydrology 343 (1-2), 43 – 55.

Manning, A. J., Bass, S. J., 2006. Variability in cohesive sediment settling fluxes: Observations under different estuarine tidal conditions. Marine Geology 235, 177 – 192.

Manning, A. J., Dyer, K. R., 1999. A laboratory examination of floc characteristics with regard to turbulent shearing. Marine Geology 160, 147 – 170.

Manning, A. J., Dyer, K. R., 2007. Mass settling flux of fine sediments in Northern European estuaries: Measurements and predictions. Marine Geology, 107 – 122.

Martin, J. H., Knauer, G. A., Karl, D. M., Broenkow, W. W., 1987. VERTEX: carbon cycling in the northeast Pacific. Deep Sea Research Part A 34 (2), 267 – 285.

McAnally, W., Mehta, A. J., 2002. Significance of aggregation of fine sediment particles in their deposition. Estuarine, Coastal and Shelf Science 54, 643 – 653.

McCave, I. N., 1984. Size spectra and aggregation of suspended particles in the deep ocean. Deep Sea Research Part A 31 (4), 329 – 352.

Merico, A., Bruggemann, J., Wirtz, K., 2009. A trait-based approach for downscaling complexity in plankton ecosystem models. Ecological Modelling 220 (4), 3001 – 3010.

Mikes, D., Verney, R., Lafite, R., Belorgey, M., 2004. Controlling factors in estuarine flocculation processes: experimental results with material from the Seine estuary, Northwestern France. Journal of Coastal Research SI 41, 82 – 89.

Mikkelson, O. A., 2002. Examples of spatial and temporal variations of some fine-grained suspended particle characteristics in two Danish coastal water bodies / Variations spatiales et temporelles des matières fines en suspension dans deux masses d'eau des côtes danoises. Oceanologica Acta 25, 39 – 49.

Mikkelson, O. A., Pejrup, M., 2000. In situ particle size spectra and density of particle aggregates in a dredging plume. Marine Geology 170, 443 – 459.

Milligan, T. G., Loring, D. H., 1997. The effect of flocculation on the size distributions of bottom sediment in coastal inlets: implications for contaminant transport. Water, Air and Soil Pollution 99, 33 – 42.

Monin, A. S., Yaglom, A. M., 1975. Statistical fluid mechanis: mechanisms of turbulence. Vol. 1. Cambridge: The MIT Press.

Munk, W., Anderson, E., 1948. A note on the theory of the thermocline. Journal of Marine Research 7, 276 – 295.

Munk, W., Riley, G. A., 1952. Absorption of nutrients by aquatic plants. Journal of Marine Research 11, 215–240.

Murray, J. W., Jannash, H. W., Honjo, S., Anderson, R. F., Reeburgh, W. S., Top, Z., Friederich, G. E., Codispoti, L. A., Izdar, E., 1989. Unexpected changes in the oxic/anoxic interface in the Black Sea. Nature 338, 411 – 413.

Muschenheim, D. K., Kepkay, P. E., Kranck, K., 1989. Microbial growth in turbulent suspensions and its relation to marine aggregate formation. Netherlands Journal of Sea Research 23 (3), 283 – 292.

Myklestad, S., 2000. Marine Chemistry. Vol. 5D of The handbook of environmental chemistry. Springer Berlin/Heidelberg, Ch. Dissolved organic carbon from phytoplankton, pp. 111 – 148.

Paerl, H. W., 1974. Bacterial uptake of dissolved organic matter in relation to detrial aggregation in marine and freshwater systems. Limnology and Oceanography 19 (6), 966 – 972.

Partheniades, E., 1984. A fundamental framework for cohesive sediment deposits. In: Mehta, A. J. (Ed.), Lecture notes on Coastal and Estuarine Studies 14, Estuarine Cohesive Sediment Dynamics. Springer, Berlin, Heidelberg, New York, Tokyo, pp. 219 – 250.

Passow, U., 2002a. Formation of transparent exopolymer particles, TEP, from dissolved precursor material. Marine Ecology Progress Series 192, 1 – 11.

Passow, U., 2002b. Production of transparent exopolymer particles (TEP) by phyto- and bacterioplankton. Marine Ecology Progress Series 236, 1 – 12.

Passow, U., 2002c. Transparent exopolymer particles (TEP) in aquatic environments. Progress in Oceanography 55, 287 – 333.

Passow, U., 2004. Switching perspectives: Do mineral fluxes determine particulate organic carbon fluxes or vice versa? Geochemistry, Geophysics, Geosystems 5 (4).

Passow, U., Alldredge, A. L., 1995. A dye-binding assay for the spectrophotometric measurement of transparent exoploymer particles (TEP). Limnology and Oceanography 40, 1326 – 1335.

Passow, U., De La Rocha, C. L., 2006. Accumulation of mineral ballast on organic aggregates. Global Biogeochemical Cycles 20, doi:10.1029/2005GB002579.

Passow, U., Shipe, R. F., Murray, A., Pak, D. K., Brzezinski, M. A., Alldredge, A. L., 2001. The origin of transparent exopolymer particles (TEP) and their role in sedimentation of particulate matter. Continental Shelf Research 21, 327 – 346.

Pleskachevsky, A., Gayer, G., Horstmann, J., Rosenthal, W., 2005. Synergy of satellite remote sensing and numerical modelling for monitoring of suspended particulate matter. Ocean Dynamics 55, 2 – 9, doi:10.1007/s10236-004-0101-z.

Ploug, H., Grossart, H., 2000. Bacterial growth and grazing on diatom aggregates: Respiratory carbon turnover as a function of aggregate size and sinking velocity. Limnology and Oceanography 45, 1467 – 1475.

Ploug, H., Grossart, H., Azam, F., Jørgensen, B. B., 1999. Photosynthesis, respiration, and carbon turnover in sinking marine snow from surface waters of Southern California Bight: implications for the carbon cycle in the ocean. Marine Ecology Progress Series 179, 1 – 11.

Ploug, H., Hietanen, S., Kuparinen, J., 2002. Diffusion and advection within and around sinking, porous diatom aggregates. Limnology and Oceanography 47, 1129 – 1136.

Ploug, H., Kühl, M., Buchholz-Cleven, B., Jørgensen, B. B., 1997. Anoxic aggregates – an ephemeral phenomenon in the pelagic environment? Aquatic Microbial Ecology 13, 285 – 294.

Postma, H., 1954. Hydrography of the Dutch Wadden Sea. Archives Néerlandaises de Zoologie 10, 405 – 511.

Postma, H., 1961. Transport and accumulation of suspended matter in the Dutch Wadden Sea. Netherlands Journal of Sea Research 1, 148 – 190.

Postma, H., 1981. Exchange of materials between the North Sea and the Wadden Sea. Marine Geology 40, 199 – 213.

Prakash, A., Bapat, A. P., Zachariah, M. R., 2003. A simple numerical algorithm and software for solution of nucleation, surface growth, and coagulation problems. Aerosol Science and Technology 37, 892 – 898.

Prat, O. P., Ducoste, J. J., 2006. Modeling spatial distribution of floc size in turbulent processes using the quadrature method of moment and computational fluid dynamics. Chemical Engineering Science 61, 75 – 86.

Pruppacher, H. R., Klett, J. D., 1980. Microphysics of Clouds and Precipitation. Boston D. Riedel Publishing Co.

Riebesell, U., Wolf-Gladrow, D. A., 1992. The relationship between physical aggregation of phytoplankton and particle flux: a numerical model. Deep Sea Research Part A 39 (7/8), 1085 – 1102.

Rink, B., Seeberger, S., Martens, T., Duerselen, C.-D., Simon, M., Brinkhoff, T., 2007. Effects of phytoplankton bloom in a coastal ecosystem on the composition of bacterial communities. Aquatic Microbial Ecology 48, 47 – 60.

Ritzau, W., 1996. Microbial activity in the benthic boundary layer: small-scale distribution and its relationship to the hydrodynamic regime. Journal of Sea Research 36 (3/4), 171 – 180.

Ruiz, J., 1997. What generates daily cycles of marine snow? Deep Sea Research Part I 44, 1105 – 1126.

Ruiz, J., Izquierdo, A., 1997. A simple model for the break-up of marine aggregates by turbulent shear. Oceanologica Acta 20 (4), 597 – 605.

Saffman, P. G., Turner, J. S., 1956. On the Collision of Drops in Turbulent Clouds. Journal of Fluid Mechanics 1, 16 – 30.

Sala, M. M., Karner, M., Arin, L., Marrasé, C., 2001. Measurements of ectoenzyme activities as an indication of inorganic nutrient imbalance in microbial communities. Aquatic Microbial Ecology 23, 301 – 311.

Sanford, L. P., 2008. Modeling a dynamically varying mixed sediment bed with erosion, deposition, bioturbation, consolidation, and armoring. Computers and Geosciences 34, 1263 – 1283.

Santamarina Cuneo, P., Flemming, B. W., 2000. Quantifying concentration and flux of suspended particulate matter through a tidal inlet of the East Frisian Wadden Sea by acoustic doppler current profiling. Elsevier Science B. V., pp. 39 – 52.

Schartau, M., Engel, A., Völker, C., Thoms, S., Wolf-Gladrow, D., Schröter, J., 2007. Modelling carbon overconsumption and the formation of extracellular particulate organic carbon. Biogeosciences Discussions 4, 13 – 67.

Schuhmacher, J., 2007. Sub-Kolmogorov-scale fluctuations in fluid turbulence. Europhysics Letters 80, doi:10.1209/0295-5075/80/54001.

Serra, T., Casamitjana, X., 1998. Structure of the aggregates during the process of aggregation and breakup under a shear flow. Journal of Collod an Interface Science 206, 505 – 511.

Serra, T., Logan, B. E., 1999. Collision frequencies of fractal bacterial aggregates with small particles in a sheared fluid. Environmental Sciences and Technology 33, 2247 – 2251.

Shanks, A. L., Walters, K., 1997. Holoplankton, meroplankton, and meiofauna associated with marine snow. Marine Ecology Progress Series 156, 75 – 86.

Sherwood, T., Pigford, R., Wilke, C., 1975. Mass transfer. McGraw-Hill Inc., New York, US, 516p.

Simon, M., Grossart, H. P., Schweitzer, B., Ploug, H., 2002. Microbial ecology of organic aggregates in aquatic ecosystems. Aquatic Microbial Ecology 28 (2), 175–211.

Sintes, E., Stoderegger, K., Parada, V., Herndl, G., 2010. Seasonal dynamics of dissolved organic matter and microbial activity in the coastal North Sea. Aquatic Microbial Ecology 60, 85 – 95.

Smith, D. C., Simon, M., Alldredge, A. L., Azam, F., 1992. Intense hydrolytic enzyme activity on marine aggregates and implications for rapid particle dissolution. Nature 359, 139 – 142.

Son, M., Hsu, T., 2008. Flocculation model of cohesive sediment using variable fractal dimension. Environmental Fluid Mechanics 8 (1), 55 – 71, 10.1007/s10652-007-9050-7.

Staats, N., Stal, L. J., Mur, L. R., 2000. Exopolysaccharide production by the epipelic diatom *Cylindrotheca fusiformis*: effects of nutrient conditions. Journal of Experimental Marine Biology and Ecology 249, 13 – 27.

Stal, L. J., 2003. Microphytobenthos, their extracellular polymeric substances, and the morphogenesis of intertidal sediments. Geomicrobiology Journal 20, 463 – 478.

Stanev, E. V., Brink-Spalink, G., Wolff, J., 2007. Sediment dynamics in tidally dominated environments controlled by transport and turbulence: A case study for the East Frisian Wadden Sea. Journal of Geophysical Research 112.

Stanev, E. V., Flöser, G., Wolff, J.-O., 2003a. First- and higher-order dynamical controls on water exchanges between tidal basins and the open ocean. A case study for the East Frisian Wadden Sea. Ocean Dynamics 53, 146 – 165.

Stanev, E. V., Wolff, J.-O., Burchard, H., Bolding, K., Flöser, G., 2003b. On the circulation in the East Frisian Wadden Sea: numerical modeling and data analysis. Ocean Dynamics 53, 27 – 51.

Stemmann, L., Jackson, G. A., Ianson, D., 2004a. A vertical model of particle size distributions and fluxes in the midwater column that includes biological and physical processes - Part I: model formulation. Deep Sea Research Part I 51, 865 – 884.

Stemmann, L., Jackson, G. A., Ianson, D., 2004b. A vertical model of particle size distributions and fluxes in the midwater column that includes biological and physical processes - Part II: application to a three year survey in the NW Mediterranean Sea. Deep Sea Research Part I 51, 885 – 908.

Stevens, H., Brinkhoff, T., Simon, M., 2005. Composition of free-living, aggregate-associated and sediment surface-associated bacterial communities in the German Wadden Sea. Aquatic Microbial Ecology 38, 15 – 30.

Stoderegger, K. E., Herndl, G. J., 1999. Production of exopolymer particles by marine bacterioplankton under contrasting turbulence conditions. Marine Ecology Progress Series 189, 9 – 16.

Sundaram, S., Collins, L. R., 1997. Collision statistics in an isotropic particle-laden turbulent suspension. Part 1. Direct numerical simulations. Journal of Fluid Mechanics 335, 75 – 109.

Tanaka, T., 1992. Phase transitions of gels. Vol. 480 of A.C.S. Symposium Series. American Chemical Society, Washington, DC, pp. 1 – 20.

Tessier, C., Le Hir, P., Jourdin, F., Castaing, P., 2007. Measuring water turbidity dynamics with acoustic current profilers: experiments in Southern Brittany (France). In: 9th International Conference on Cohesive Sediment Transport Processes.

Thomas, D. N., Judd, S. J., Fawcett, N., 1999. Flocculation modelling: A review. Water Research 33 (7), 1579 – 1592.

Thornton, D., 2002. Diatom aggregation in the sea: mechanisms and ecological implications. European Journal of Phycology 37, 149–161.

Tian, T., Merico, A., Su, J., Staneva, J., Wiltshire, K., Wirtz, K., 2009. Importance of resuspended sediment dynamics for the phytoplankton spring bloom in a coastal marine ecosystem. Journal of Sea Research 62, 214 – 228.

Toorman, E. A., 2003. Validation of macroscopic modelling of particle-laden turbulent flows. In: Proceedings 6th Belgian National Congress on Theoretical and Applied Mechanics.

Tritton, D., 2005. Physical Fluid Dynamics. Oxford University Press.

Uncles, R. J., Stephans, J. A., Law, D. J., 2006. Turbidity maximum in the macrotidal, highly turbid Humber Estuary, UK: Flocs, fluid mud, stationary suspensions and tidal bores. Estuarine, Coastal and Shelf Science 67, 30 – 52.

Underwood, G. J. C., Boulcott, M., Raines, C. A., Waldron, K., 2004. Environmental effects on exopolymer production by marine benthic diatoms: dynamics, changes in composition, and pathways of production. Journal of Phycology 40, 293 – 304.

Van der Lee, E. M., Bowers, D. G., Kyte, E., 2009. Remote sensing of temporal and spatial patterns of suspended particle size in the Irish Sea in relation to the Kolmogorov microscale. Continental Shelf Research 29 (9), 1213 – 1225, doi:10.1016/j.csr.2009.01.016.

Van der Lee, W., 2000. The settling of mud flocs in the Dollard estuary, The Netherlands. Dissertation, Utrecht University.

Van Leussen, W., 1994. Estuarine macroflocs and their role in fine-grained sediment transport. Ph.d. thesis, University of Utrecht.

van Leussen, W., 1999. The variability of settling velocities of suspended fine-grained sediment in the Ems estuary. Journal of Sea Research 41, 109 – 118.

Van Santen, P., Aardoom, J., Maushake, C., 2007. Sediment transport measurements in the Elbe estuary, Germany, using ADCP backscatter. In: 9th International Conference on Cohesive Sediment Transport Processes.

Van Straaten, L. M. J. U., Kuenen, P. H., Aug. 1957. Accumulation of fine grained sediments in the Dutch Wadden Sea. Geologie en Mijnbouw, NW. Ser. 19e Jahrgang, 329 – 354.

Verdugo, P., Alldredge, A. L., Azam, F., Kirchman, D. L., Passow, U., Santschi, P. H., 2004. The oceanic gel phase: a bridge in the DOM-POM continuum. Marine Geochemistry 92, 67 – 85.

Verney, R., Brun-Cottan, J., Lafite, R., Deloffre, J., Taylor, J. A., 2006. Tidally-induced shear stress variability above intertidal mudflats. Case of the macrotidal Seine estuary. Estuaries and Coasts 29 (4), 653–664.

Verney, R., Lafite, R., Brun-Cottan, J., 2009. Flocculation potential of natural estuarine particles: The importance of environmental factors and of the spatial and seasonal variability of suspended particulate matter. Estuaries and Coasts 32, 678 – 693.

Verney, R., Lafite, R., Brun-Cottan, J., 2010. Behaviour of a floc population during a tidal cycle: laboratory experiments and numerical modelling. Continental Shelf Research.

Villermaux, E., 2007. Fragmentation. Annual Review of Fluid Mechanics 39, 419–446.

Visser, A., Jackson, G. A., 2004. Characteristics of the chemical plume behind a sinking particle in a turbulent water column. Marine Ecology Progress Series 283, 55 – 71.

von Smoluchowski, M., 1916. Drei Vorträge über Diffusion, Brownsche Molekularbewegung und Koagulation von Kolloidteilchen. Zeitschrift für physikalische Chemie, 530 – 599.

von Smoluchowski, M., 1917. Versuch einer mathematischen Theorie der Koagulationskinetik kolloidaler Lösungen. Zeitschrift für physikalische Chemie 92 (2), 129 – 168.

von Wachenfeldt, E., 2008. Flocculation of Allochthonous Dissolved Organic Matter – A Significant Pathway of Sedimentation and Carbon Burial in Lakes. Ph.d. thesis, University of Uppsala.

Warner, J. C., Sherwood, C. R., Signell, R. P., Harris, C. K., Arango, H. C., 2008. Development of a three-dimensional, regional, coupled wave, current, and sediment-transport model. Computers & Geosciences 34, 1284 – 1306.

Wells, M. L., Goldberg, E., 1994. The distribution of colloids in the North Atlantic and Southern Oceans. Limnology and Oceanography 39, 286 – 302.

Winter, C., Becker, M., Ernsten, V. B., Hebbeln, D., Port, A., Bartholomä, A., Flemming, B., Lunau, M., 2007a. In-situ observations of aggregate dynamics in a tidal channel using acoustics, laser diffraction and optics. Journal of Coastal Research Special Issue 50, 1173 – 1177.

Winter, C., Katoshevski, D., Bartholomä, A., Flemming, B. W., 2007b. Grouping dynamics of suspended particulate matter in tidal channels. Journal of Geophysical Research 112, doi:10.1029/2005JC003423.

Winterwerp, J. C., 1998. A simple model for turbulence induced flocculation of cohesive sediment. Journal of Hydraulic Research 36 (3), 309–326.

Winterwerp, J. C., 2002. On the flocculation and settling velocity of estuarine mud. Continental Shelf Research 22, 1339 – 1360.

Winterwerp, J. C., 2007. On the sedimentation rate of cohesive sediment. In: Maa, J. P. Y., Sandford, L. P. (Eds.), 7th International conference on Estuarine and coastal fine sediments dynamics. Proceedings in marine science. Vol. 8. pp. 209 – 226.

Winterwerp, J. C., Manning, A. J., Martens, C., de Mulder, T., Vanlede, J., 2006. A heuristic formula for turbulence-induced flocculation of cohesive sediment. Estuarine, Coastal and Shelf Science 68 (1-2), 195–207.

Wirtz, K., Eckhardt, B., 1996. Effective variables in ecosystem models with an application to phytoplankton succession. Ecological Modelling 92, 33 – 53.

Wirtz, K. W., 1998. Modellierung von Anpassungsvorgängen in der belebten Natur. Dissertation, Universität Kassel.

Wirtz, K. W., Wiltshire, K., 2005. Long-term shifts in marine ecosystem functioning detected by assimilation the Helgoland Roads time-series into a complex food-web model. Journal of Marine Systems 56, 262 – 282.

Xu, F., Wang, D.-P., Riemer, N., 2008. Modeling flocculation processes of fine-grained particles using a size-resolved method: Comparison with published laboratory experiments. Continental Shelf Research 28, 2668 – 2677.

Xue, Y., Wang, L.-P., Grabowski, W. W., 2008. Growth of cloud droplets by turbulent collision-coalescence. Journal of the Atmospheric Sciences 65 (2), 331 – 356.

Zahnow, J. C., Maerz, J., Feudel, U., 2009. Particle-based modelling of aggregation and fragmentation processes in chaotic advection: Fractal aggregates. arXiv http://arxiv.org/abs/0904.3418v1.

Ziervogel, K., Arnosti, C., 2008. Polysaccharide hydrolysis in aggregates and free enzyme activity in aggregate-free seawater from the north-eastern Gulf of Mexico. Environmental Microbiology 10 (2), 289 – 299.

Zimov, S. A., Schuur, E. A. G., Chapin III, F. S., 2006. Permafrost and the Global Carbon Budget. Science 312, 1612 – 1613.

Zwolsman, J. J. G., van Eck, B. T. M., van der Weijden, C. H., 1997. Geochemistry of dissolved trace metals (cadmium, copper, zinc) in the Scheldt estuary, southwestern Netherlands: Impact of seasonal variability. Geochemica et Cosmochimica Acta 61 (8), 1635 – 1652.

Curriculum Vitae

Jöran März
Tel. (dienstl.): 0441 – 798 – 3634
maerz@icbm.de

2004 Diplom der marinen Umweltwissenschaften; seitdem: Wissenschaflicher Mitarbeiter in der DFG Forschergruppe „BioGeoChemie des Watts“ am Institut für Chemie und Biologie des Meeres (ICBM), AG Theoretische Physik / Komplexe Systeme

2001 Vordiplom

1999 Beginn des Diplomstudiums der marinen Umweltwissenschaften an der Carl von Ossietzky Universität Oldenburg

1998 Gymnasialer Abschluß und Beginn des Zivildienstes

1989 Wechsel zum Gymnasium

1985 Einschulung

Danksagung

Der Abschluß einer solchen Arbeit ist eine gute Möglichkeit, vielen Menschen, die direkt oder indirekt daran Teil hatten, Danke zu sagen ...

Meinhard Simon möchte ich für die Ausrichtung des Schwebstoffpraktikums danken, mit dem alles anfing ...

Aber insbesondere möchte ich Ulrike Feudel für die unermüdliche Unterstützung, insbesondere beim Schreiben von Anträgen, und das Vertrauen danken, das sie mir entgegengebracht hat, wenn es um die Entwicklung eigener Ideen und Zielsetzungen ging. Danke insbesondere auch für die zahlreichen Möglichkeiten, die eigene Arbeit im Rahmen von Tagungen und Workshops präsentieren und dabei wichtige Kontakte, auch über die Zeit der Doktorarbeit hinaus, knüpfen zu können.

Kai Wirtz hat mich gerade in den Anfängen mit immer wieder neuen Ideen der Herangehensweise an die Modellierung sehr unterstützt und ich bin dankbar, von seinem kreativen, oft unverkrampften Umgang mit neuen modelltechnischen Herausforderungen umzugehen, gelernt zu haben.

Mirko möchte ich danken für die unermüdlichen Diskussion gerade in der Anfangszeit, als es um ein besseres Verständnis der biologischen Zusammenhänge ging.

Viele, gerade numerische Kniffe und Spitzfindigkeiten habe ich durch Cora kennenlernen können – Cora, Du hast mich wahrscheinlich vor so mancher Verzweiflung bewahrt, wenn es wieder einmal darum ging, Programmierfehler zu finden ... Das gleiche gilt für Knut, der so manches Programmierhindernis – gerade am Anfang – zu lösen half.

Stephan und Cora: Danke, daß ihr manchmal einfach da wart.

Ein großer Dank an meine Arbeitsgruppe – insbesondere Michael, mit dem ich lange das Büro teilte und darüber hinaus auch später noch manch' anregende Diskussion führen konnte. Jan für manche statistische Hilfe. Dirk, der einem gezeigt hat, wie es auch gehen kann ... Hier auch an Ulf für so manche gemeinsame Mittagspause. David – Du konntest einem in vielem helfen ... – einfach: Danke!!! Jens, der einem mit der eher rein physikalischen Herangehensweise an Aggregations- und Fragmentationsmechanismen eine neue, weite

Welt mindestens einen Türspalt breit (wenn nicht gar mehr) eröffnet hat – die Zusammenarbeit hat Freude bereitet! Nico – ich werde Deine Art so schnell nicht vergessen (– und das soll keine Drohung sein) – sie wird mir auch in Zukunft so manches Schmunzeln entlocken!

Romaric, it was a great experience to work with you! Thank you very much for all!

Allen ICBM'lern ein großes Danke! – es war schön, mit Euch zusammengearbeitet zu haben – allen voran Heike in ihrer unermüdlichen Schaffenskraft – und trotzdem immer ein Lachen parat – es hat insbesondere Spaß gemacht, mit Dir die Rolltanks neu zu entwerfen! Melanie – die biogeochemischen Exkurse haben so manchmal das Salz in der Suppe meiner Arbeit ausgemacht – Danke! Danke auch an die Praktikanten und Abschlußarbeitenschreiber (-Innen) – es hat mich viel gelehrt, mit Euch zusammenzuarbeiten.

Und last, but not least: Ich weiß nicht, wie ich mich für die viele Unterstützung aus der Familie und meinem engsten persönlichen Umkreis bedanken soll . . . – weshalb ich auch auf einen – immer unzureichenden – Versuch an dieser Stelle verzichte. Und dennoch: Danke! – insbesondere meinen Eltern und Großeltern.

Chris, ich habe mich gefreut und freue mich auf weitere zukünftige Unternehmungen! – Ich bin zu allen Schandtaten bereit! Florian, ich würde mich auch weiterhin über so manchen, mit Delikatessen zelebrierten Abend freuen!

Antje, auf dem Weg des Lebens sind wir dabei, uns das wahrscheinlich höchste Gut im Leben eines Menschen zu erarbeiten – manchmal mit Last, oftmals mit Freude – sich *wirklich* kennenzulernen – wohl wissend, daß das einem *wahrscheinlich* auf immer verwehrt bleibt.

Ce sont les microbes qui auront le dernière mot !

Louis Pasteur
(Dole, 1822 – † Paris, 1895)*

Hiermit versichere ich, dass ich die vorliegende Arbeit selbstständig verfasst und nur die angegebenen Hilfsmittel verwendet habe.

_____